COMPUTATIONAL CIVIL ENGINEERING
2015

**Proceedings of the 13th International Symposium
"Computational Civil Engineering"
Iasi, Romania - May 29th, 2015**
Scientific publication

THE 13th INTERNATIONAL SYMPOSIUM
"COMPUTATIONAL CIVIL ENGINEERING 2015"

ORGANIZERS

Faculty of Civil Engineering and Building Services - "Gheorghe Asachi" Echnical University from IASI, Romania
Academic Society "Matei - Teiu Botez", IASI, Romania
Spanish Association of Seismic Engineering, Spain

Co-ordination committee

Prof. Eng. Mihai Budescu, PhD
Prof. Eng. Constantin Ionescu, PhD
Prof. Eng. Alex. Horia Barbat, PhD

Scientific commission

Prof. Doina Ştefan, PhD
Prof. Elena Axinte , PhD
Assoc. prof. Mihai Petru, PhD
Prof. Daniela Manea, PhD –*Technical University of Cluj-Napoca*
Prof. Valeriu Stoian, PhD - *"Politehnica" University of Timisoara*
Prof. Radu Văcăreanu, PhD – *Technical University of Civil Engineering, Bucharest*
Gabriela Covatariu, PhD
Asist.prof. Mircea-Vasile Venghiac, PhD
Rodian Scînteie, PhD

Organizing commission

Eng. Maria Nicoleta Peşehonov

CONTENTS

Numerical Analysis of a Steel Wire Mesh Seismic Retrofitting Techniques for Masonry Structures

Adrian Dogariu

Department CMMC, University Politehnica Timisoara, Timisoara, 300244, Romania

Summary

Many masonry buildings located in prone seismic areas need structural interventions; therefore solutions which will increase the wall capacity and ductility, without a major influence on its stiffness is valuable. This article will present the experimental activities and numerical analysis of this technique efficiency. This technique applies a stainless or zinc coated steel wire mesh (SWM) bonded with epoxy resin to the masonry walls, on one or both sides.

The solution can be applied to internal shear walls and on façade either on piers or spandrel. In most of the cases old masonry buildings shown weaker piers than spandrel, so to obtain a maximum benefit effect of reinforcing technique this areas are to be retrofitted. Important advantage of this technique may be related to its reversibility - wire mesh fixed with epoxy resin can be removed from the masonry wall by heating the resin layer.

Steel wire mesh reinforced masonry walls have a complex behaviour and no analytic procedures for design are available; therefore, advanced numerical models confirmed by extended experimental tests are need. The experimental program is presented together with the finite element model adopted for retrofitted masonry specimens.

The numerical model is calibrated according to the contact-less and full-field measurements. The experimental tests, carried-out within the framework of a European research project, have included tests on steel wires, on steel meshes, on 500 by 500 mm retrofitted masonry elements (diagonal tensile tests) and 1500 by 1500 mm masonry walls.

The numerical calibration have been made using ABAQUS finite element software. The replacing of simple masonry with an equivalent material with improved behaviour, can be done following the experimental testing results. This kind of approach that considers the retrofitting steel wire mesh as an external reinforcing can really simplify the numerical effort.

KEYWORDS: masonry, seismic retrofit, finite element, ABAQUS, steel wire mesh.

1. INTRODUCTION

1.1. Masonry behaviour and anti-seismic retrofitting technique

Masonry material is one of the most wildly use material for construction of buildings in most part of the world. Brick masonry structures employing solid clay units and cement-mortar can be found in many urban and rural areas of Romania. Romanian territory is subjected to frequent earthquakes that induce shear stresses in the structural walls.

Many masonry buildings, located in prone seismic areas, present a high seismic vulnerability and require structural interventions. Retrofitting solutions which will increase capacity and ductility of the elements, without a major influence on its stiffness is valuable. Such a technique [14], investigated within the framework of FP6 EU PROHITECH [13], applies a stainless or zinc coated steel wire mesh bonded with epoxy resin to the masonry walls (see Figure 1), on one or both sides.

Figure 1. Retrofitting solution based on epoxy-glued steel wire mesh (SWM)

Masonry structures are mainly composed of transversal and longitudinal load bearing walls which withstand at both vertical and horizontal loads. A proper connection between walls and floors, inhibit out-of-plane associate failure modes and consequently the building resist lateral at earthquake actions by shear response of walls. Figure 2 shows typical in-plane damages of masonry walls subjected to earthquakes.

Sliding failure (a)   Flexural failure (b)   Shear failure (c)
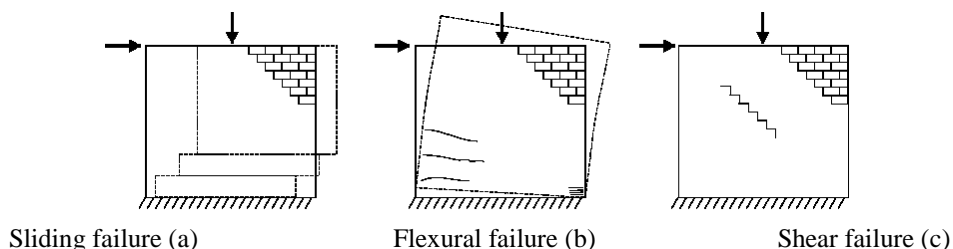
Figure 2. Retrofitting solution based on epoxy-glued steel wire mesh

The retrofitting solution can be applied to internal shear walls and on façade, either on piers or spandrel (see Figure 3). In most of the cases old masonry buildings shown weaker piers than spandrel, so to obtain a maximum beneficial effect of reinforcing technique, these areas are to be retrofitted. Important advantage of this technique may be related to its reversibility - wire mesh fixed with epoxy resin can be removed easily from the masonry wall by heating the resin layer.
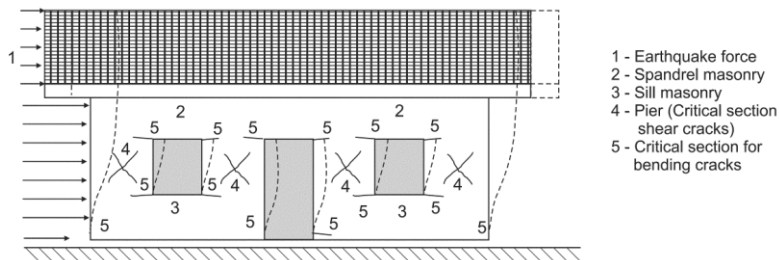
Figure 3. Critical failure modes in a masonry wall with openings [15]

All the available analytical models to estimate the in-plane strength require basic mechanical properties of masonry material. This fact makes the experimental investigation on masonry materials essential before the assessment of structures can be performed.

2. EXPERIMENTAL PROGRAMS

The behaviour of masonry material under lateral loading is highly different due to high non-homogeneity and composite nature of masonry components. The different mechanical properties of masonry units and mortar and their interface makes the masonry system behaviour difficult to predict using simple hypotheses as adopted for other construction materials. The masonry mechanical behaviour can establish through experimental tests, which can be used for calibration of numerical models used for development of analytical.

In addition to the pure masonry intricate response, steel wire mesh reinforced masonry walls have even a more complex behaviour and no analytic procedures for design are available; therefore, advanced numerical models confirmed by extended experimental tests are need. Is briefly presented the experimental program, carried out at Politehnica University Timisoara in the CESMAST laboratory. Mechanical characterization of a highly inhomogeneous material composed by solid clay-brick masonry glued by means of epoxy resin with steel wire layer material was aimed.

The experimental work included laboratory tests under monotonic loading on masonry prisms: for the estimation of masonry compressive strength (f_{mc}) and

elastic Young modulus (E), besides tests on constituent materials i.e. brick units: for unit compression strength, mortar: for compression strength (f_m) (see Figure 4). Most valuable are the test on wallets: for the estimation of diagonal tension strength (f_t) and shear modulus (G) (see Figure 7).

a) Compression brick   b) Elastic modulus masonry   c) Elastic modulus mortar

d) Tension mortar   e) Compression mortar
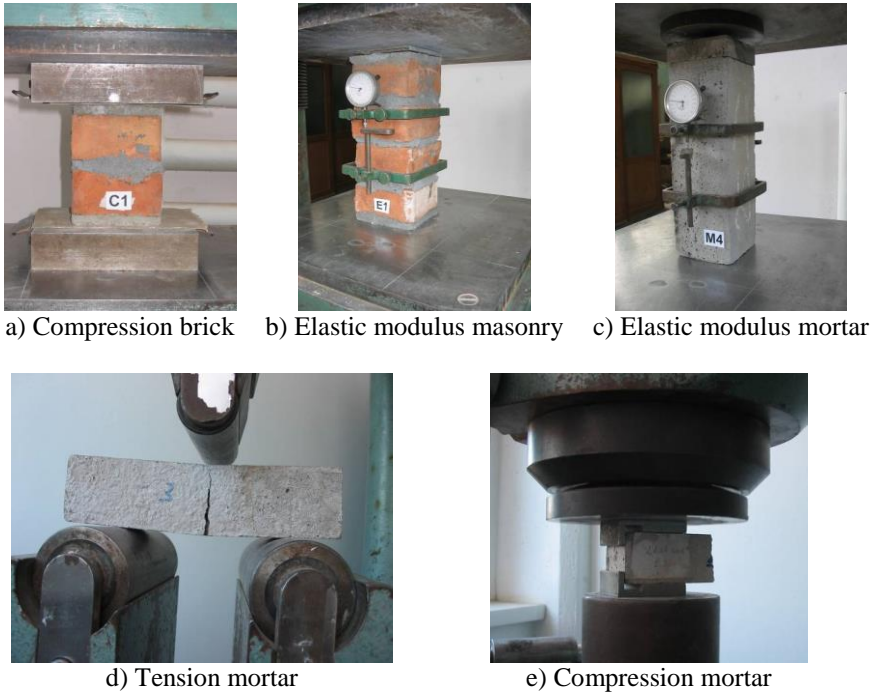
Figure 4. Tests on masonry and components (mortar and brick)

Six different types of steel wire and steel wire meshes have been tested (see Figure 5) (three zinc-coated (ZC) 0.25x0.40, 0.25x0.56, 0.4x1.0 and three made of stainless steel (SS) 0.3x1.25, 0.4x0.5, 0.4x1.0 – wire diameter – grid distance). The material behaviour is presented in Figure 6. Based on the experimental result from application on one side (Figure 9), three wire meshes were applied on both sides.

Figure 5. Tensile tests on individual steel wire and steel meshes
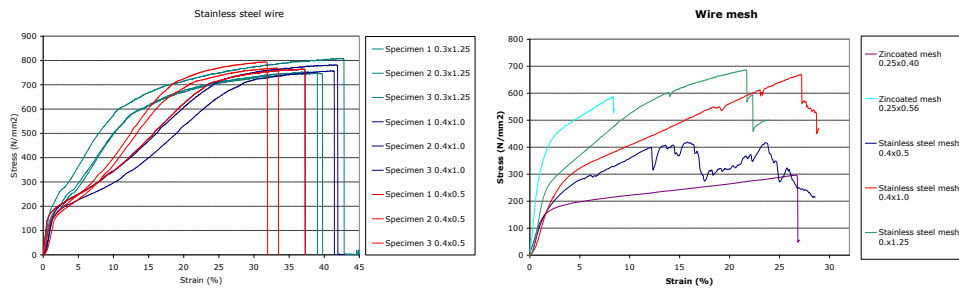
Figure 6. Material behaviour - steel wire and steel meshes [14]

2.1. Experimental tests – wallets tests

2.1.1. Description of the tests set-up and specimens

One of the most important masonry experimental tests is applied on wallets. This test offering diagonal tensile test and shear modulus. Tests on masonry panels (wallets) of size 500 mm x 500 mm with 250mm thickness were prepared in regular masonry bond pattern using solid clay bricks with dimensions 63x240x115 mm and unit strength $9.0 \div 10.0$ N/mm^2 and cement based mortar (cement : sand ratio was 1:1) with strength $30 \div 50$ N/mm^2. Tests were performed on panels, retrofitted on one side or in both sides, for the estimation of diagonal tension strength of masonry. The whole experimental program (on other retrofitting solution too [16]) included a total number of 27 retrofitted wallet samples, from which steel wire mesh (swm) was applied on one side in six specimens and on both side on nine specimens.

The testing setup is shown in Figure 7. Two displacement transducers were installed, on horizontal (D2) and vertical (D1) directions, to measure the total horizontal and vertical deformation of the specimen. During tests all the specimens' strain and movement were recorded with the use of non-contact optical system, Limess VIC-3D^{TM} from Correlated Solutions [17]. Strain gauges were also placed on the wallets surface.

The wallets test setup is for diagonal tensile strength based on the fact that the specimen is subjected to pure shear. The masonry element is cracked when the principal stress at the centre of the panel becomes equal to the tensile strength of masonry. However, based on numerical and analytical studies, the specimen is not subjected to uniform and homogenous state of stresses and is not subjected to pure shear.

Figure 7. Wallets

2.1.2. Experimental results

One can observed based on typical damage pattern that the masonry cracks developed upon failure follows mostly bed and head joints of masonry. This fact indicate that mortar and mortar-brick interface bond strength plays an important role in the masonry strength.

Figure 8. Damage pattern

Figure 9. Damage pattern of one side retrofitted elements with swm

2.1.3. *The benefit of the retrofitting solution*

In Table 1 are given the values of the maximum load and vertical and horizontal displacement for each of the experimental specimen. The following failure modes and capacity were observed (see Figure 10) for wallets retrofitted on both sides:

ZC 0.4x1.0 – sudden wire mesh rupture simultaneous with masonry crack – resistance improvement (weak wire mesh);

SS 0.4x0.5 – debonding of wire mesh, rupture in resin – strength improvement, energy dissipation due to the successive debonding (strong wire mesh);

SS 0.4x1.0 – wire mesh yield – improvement of resistance and ductility (optimal).

Table 1. Results of SWM applied on both side [14]

	Load (ton)			Vertical displacement (mm)			Horizontal displacement (mm)		
	1	2	3	1	2	3	1	2	3
ZC 0.4x1	31.2	27.3	27.1	0.8	5.5	1.3	0	0	0
SS 0.4x1.0	31.1	27.1	41.1	6.2	2.7	7.6	0.7	0	0.8
SS 0.4x0.5	31.1	22.8	39.4	4.5	8.9	4.6	0.4	0.8	0.4

2.1.4. *Digital deformation measurements*

In the Figure 10 are presented the internal deformation (i.e. principal tensile strain) at failure point for each of the specimens retrofitted with steel wire mesh on both sides, measured with Vic3D, based on digital image correlation (DIC) technique. The VIC-3D calculates the Lagrangian strain tensor on the specimen surface [17].
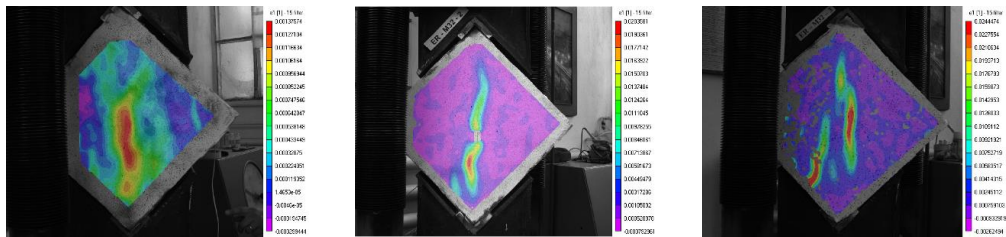
Zinc coated 0.4x1.0 (1, 2 and 3)
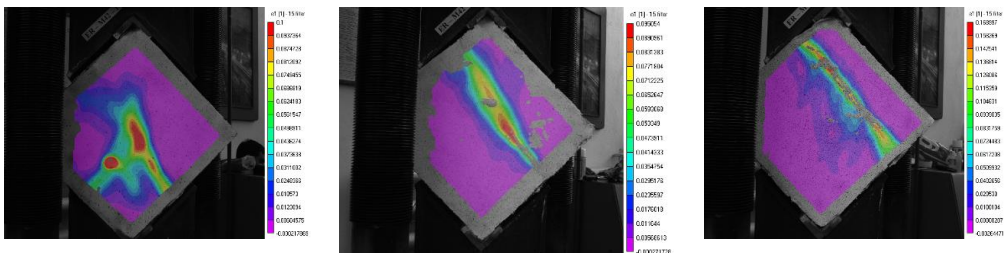
Stainless steel 0.4x0.5 (1, 2, and 3)
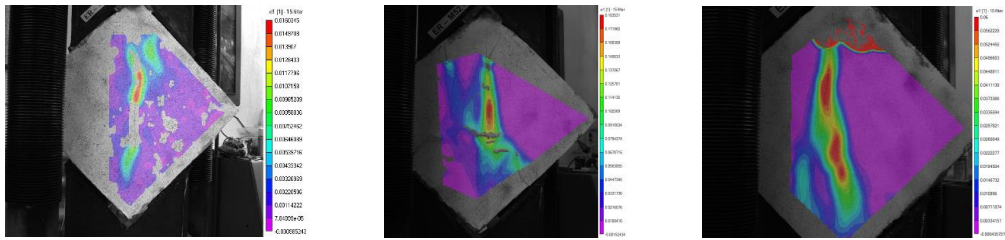
Stainless steel 0.4x1.0 (1, 2 and 3)

Figure 10. VIC-3D

Optical measurements' have shown an ultimate tensile strain of un-retrofitted masonry varying from 0.0016 – 0.004, after which, in post-cracking domain, the load capacity of specimens is suddenly and completely lost. The composite masonry-steel mesh system starts to record inelastic deformation at 0.002, but continues to maintain almost constant the load bearing capacity of specimen in the post-cracking domain, until reach a tensile strain of 0.121. Even after capacity decrease of the specimens, the steel wire mesh (swm) embedded in epoxy resin doesn't fail at strains larger than 0.175. If normally the ultimate horizontal deformation of a masonry wallet is less than 0.2 mm (see Figure 11), the retrofitted specimens easily exceeded 3 mm (see Figure 12).

(a)   (b)
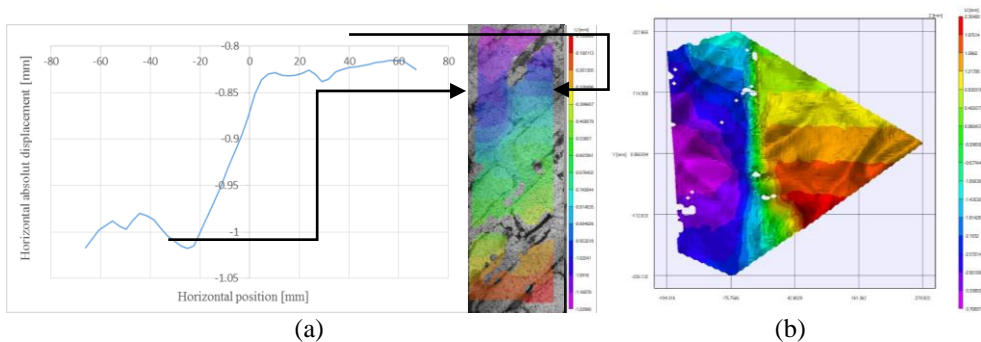
Figure 11. Horizontal crack opening masonry (a) vs. masonry-steel-wire-mesh (b) VIC-3D

Due to the high scattering of the masonry mechanical characteristics, in order to perform a statistical interpretation of the experimental results are needed many experimental specimens on the same techniques. In our case, three different retrofitting techniques for masonry walls and three specimen for each of these were experimentally studied. Based on previous observation, the experimental results have more an indicative character offering a qualitative results values for the ultimate strength and the ultimate displacement of the retrofitted walls (see Table 1). From this point of view it is difficult to assess clear values for the improved

mechanical characteristics. This fact makes it not so important to do a quantitative replication of experimental test, rather to point out the beneficial effects on global behaviour of elements.
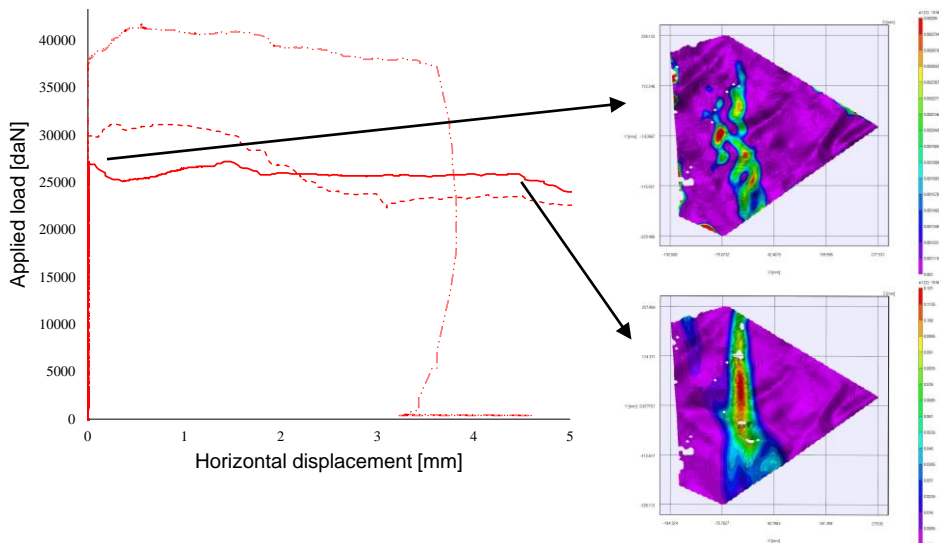
Figure 12. Total horizontal deformation of SS 0.4 x 1.0 retrofitted specimens

3. NUMERICAL ANALYSIS OF MASONRY ELEMENTS

3.1. Problem dimension and section types

Due to the fact that the wallets are not quite subjected to a uniform and homogeneous state of stress the problem dimensionality may become an issue. It is obvious, the three-dimensional solid elements defined in three-dimensional space solve all problems degree of difficulties. Because of the huge amount of computational resource and time involved, these elements are recommended only when the geometry and/or the loading and boundary conditions are too complex for any other element type with fewer spatial dimensions and degrees of freedom. Using solid 3D elements makes some global analysis on real scale structure impossible to be performed, so the user have to use one from several different types of two-dimensional elements [3].

Choosing the element's dimensionality combined with modelling space is one of the key aspect in finite element simulations. Modelling space refers to the space in which the elements are embedded and not to the topology of the element. For entire

structures with transversal and longitudinal walls a three-dimensional element must be used. In many cases, similar to the hand calculation approaches, the masonry buildings can be divided in planar shear walls and only a façade or internal wall could be model with a two-dimensional planar part using two-dimensional solid continuum elements. Are included plane stress elements and plane strain elements.

Material properties for masonry elements are obtained on solid elements with comparable size on all directions. The transition from 3d calibrated models to 2d models could introduce inherent differences due to the change in states of stress. For this reason 3D Shell elements are preferred for this study.

Solid sections includes the material type and, if the section is to be associated to a two-dimensional region, the section thickness must be specified by a plane stress or plane strain thickness. For a shell sections one must define the thickness, material type. Many commercial finite elements software [3] includes a special type of shell section, i.e. the composite shell sections. Composite shell sections consist of layers of materials, a section Poisson's ratio, and optional rebar layers.

3.2. Modelling issues

Few commercial finite element software have in their material library defined masonry materials behaviour laws. During the last forty years, an enormous growth in the development of numerical tools for structural analysis has been achieved. Nowadays, the finite element method is usually adopted in order to achieve sophisticated simulations of the structural behaviour. A description of the material behaviour, which yields the relation between the stress and strain tensor in a material point of the body, is necessary for this purpose. This mathematical description is commonly named a constitutive model and an important objective of today's research is to obtain robust numerical tools, capable of predicting the behaviour of the structure from the elastic domain until total failure, due to excessive cracking and rigidity degradation.

3.2.1. *Discontinuous modelling of masonry*

Lately, a considerable attention has been given to rational assessment methodologies, to be directly consistent with the discontinuous nature of structural masonry.

The discontinuities in continuous systems are in fact interfaces between dissimilar materials and joints or fractures in the material. A survey of the literature [12] on finite element modelling of cracks and joints shows that three main approaches are common for a representative analysis: the discrete crack and the smeared crack approach or the use of joint or interface elements.

Discrete crack approach represents the crack as a separation of nodes. When the stress or strain at a node, or the average in adjacent elements, exceeds a given value, the node is redefined as two nodes and the elements on either side are allowed to separate increasing the number of equations to be solved and extends the bandwidth of the stiffness matrix.

In the smeared crack approach, cracks and joints are modelled in an average sense by an appropriate modification of the material properties at the integration points of regular finite elements.

Smeared cracks are convenient when the crack orientations are not known beforehand, because the formation of a crack involves no re-meshing or new degrees of freedom. However, they have only limited ability to model sharp discontinuities and represent the topology or material behaviour in the vicinity of the crack.

The method is attractive if global analysis of large-scale masonry structures is required. It does not make a distinction between individual bricks and joints, but treats masonry as an anisotropic composite such that joints and cracks are smeared out. An inherent limitation of the smeared crack approach is that discrete cracks are smeared out over an entire element and the crack opening is modelled by the continuous displacement approximation functions of the conventional finite element approach. In view of this limitation, as well as other problems such as mesh-dependency due to tensile and compressive softening and difficulties of model calibration, smeared crack models should only be used with caution for the analysis of discontinuous structures.

The Interface smeared crack approach combines the advantages of the discrete and smeared approaches described above, treating cracks discretely like joint elements, but, like smeared crack elements.

Most of the crack models available have only limited ability to model sharp discontinuities present in many structural systems.

3.2.2. Continuous modelling of masonry

The first step toward carrying out such analyses is to develop adequate constitutive models. In the case of masonry, when using the continuum model approach, three levels of approximation might be applied: micro-models, simplified or detailed, and macro-models [1]:

• Micro-modelling – when units are represented by continuum elements whereas the behaviour of the mortar joints and unit-mortar interface is lumped in discontinuous or interface elements. A complete micro-model must include all the failure mechanisms of masonry, namely, cracking of joints, sliding over one head or bed joint, cracking of the units and crushing of masonry.

In the micro-model, each component of masonry – unit, mortar (simplified), and unit/mortar joint (detailed) – must be represented by different finite elements. The employment of a micro-model to analyse an entire building becomes prohibitive, since it would result in a large number of finite elements, and consequently require a lot of computer resources to run the analyses.

Two approaches can be used: the first one is the simplified or layer model, without taking into account the interface (friction law) between brick unit elements and mortar elements (Figure 13b), and the second one detailed or interface model, by introducing a normal and tangential contact surface instead of mortar layers (Figure 13c).

These kinds of detailed and simplified micro-models have very accurate results provided that there are suitable input data. This type of analysis is the most advanced level of numerical simulation for masonry elements. It is very appropriate for simulating out-of-plane behaviour of masonry, but for in-plane behaviour this type of approach is not justified due to the high complexity compared to similar results as in easier approaches.

However, if there is a high interest in observing local behaviour and interaction with other elements or material this technique may be the only one that leads to coherent results.

• Macro-modelling – use an anisotropic continuum model that establishes the relation between average stresses and average strains in masonry, considering composite masonry as a homogeneous material.

Units and joints are not represented anymore and the geometry of masonry constituents (units and joints) is lost (Figure 13d). An adequate macro-model must include anisotropic elastic and inelastic behaviour.
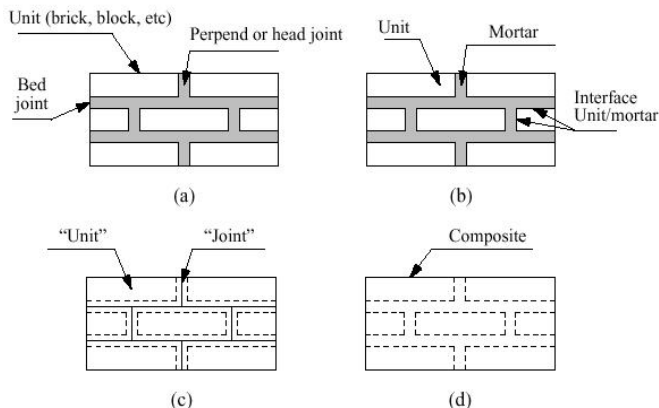

Figure 13. Advanced modelling approach (a) masonry sample; (b) detailed micro-modelling; (c) simplified micro-modelling; (d) macro-modelling [2]

3.2.3. Macro-modelling of masonry elements

This type of analysis is the most suitable from the point of view of balance between involved time and accuracy of the results. Macro-modelling requires an extra process, homogenization [6]. Homogenization of masonry is a step that has been widely treated in articles [7], [8], [9], [10], [11] proposing complicated energy and deformation compatibility equations. Even so, the obtained results must be seriously calibrated after this homogenization, in order to obtain a good correlation with the experimental tests.

The most convenient approach is to use o macro-model in which the material behaviour characteristic parameters to be borrowed from concrete models.

Because of the non-symmetrical behaviour in tension and compression, typically for a concrete material calibration at least uniaxial compression and uniaxial tension experimental tests are needed. Default values which consider the bi-axial behaviour of concrete are available in the scientific literature [3] based on large experimental campaigns. If an accurate post-failure/cracking behaviour is desired than other experiments may be required. Unlike concrete elements, due to their inherent inhomogeneous character masonry pose an anisotropic behaviour. At least theoretically the material mechanical properties should be defined taking into account their directionally dependent character.

The uniaxial compression test consist in compressing the material specimen. By recording the load and displacement, applying simple formulas one can extract the stress-strain curve. Uniaxial tension test is much more difficult to perform and only the pre-failure response can be obtain with enough confidence even for mortar specimens. In case of masonry specimens this kind of test is not available, and one can make only assumption about the tensile failure strength of the masonry material. The scientific literature recommends a value of 7%−10% of the compressive strength. The choice of tensile cracking stress is very important, because in almost all cases the failure mode is govern by tensile behaviour. Use of low cracking stresses will cause numerical problems.

In case of brittle material, calibration of the post-cracking behaviour depend on the reinforcement present. For masonry behaviour law, a stress-displacement tension stiffening model is recommended with typical values less than 0.05 mm. In case of reinforced masonry, if the reinforcing layer is strong enough, the stress-strain tension stiffening model is more appropriate. For numerical models with an acceptable mesh network could be assumed that the strain softening after cracking brings the stress to zero at a total strain 10 times the strain at failure. This results a zero stress at a total strain of about 0,001 or less [3].

To understand the post-cracking shear behaviour combined tension and shear experiments are used. Unfortunately these experiments are quite difficult to perform. Without experimental results one may assume with a good confidence

that the shear retention factor goes linearly to zero at the same crack opening strain used for the tension stiffening model.

For defining the failure ratios which gives the biaxial yield and flow parameters biaxial experiments are required to calibrate [4], [5].

High scattering of the masonry mechanical characteristics, impose for the statistical interpretation of the experimental results many experimental specimens on the same techniques. In our case were experimentally study three different techniques for masonry walls retrofitting and only three specimen for each of these. On this observation, the experimental results have more a qualitative values offering an indicative results values for the strength and displacement characteristics of the retrofitted walls.

3.2.4. Concrete smeared cracking model

This materials uses oriented damaged elasticity concepts (smeared cracking) to describe the reversible part of the material's response after cracking failure [3].

The concrete smeared cracking model was made for defining plain concrete elements (beams, trusses, shells, and solids) behaviour for monotonic loadings under low confining pressures with small consideration of the confining effect. The material use an isotropic hardening yield surface active when the stress is mainly compressive.

This material law assumes that cracking is the most important aspect of the behaviour of such a relatively brittle material, and representation of cracking and post-cracking behaviour prevail the model. An independent "crack detection surface" that determines if a point fails by cracking.

The compressive behaviour law must to be defined. One can model post-cracking behaviour for direct straining across cracks with tension stiffening, which allows to define the strain-softening behaviour or by means of a post-failure stress-strain relation or by applying a fracture energy cracking criterion giving a displacement at which gives zero stress along cracks.

The cracking phenomenon makes shear stiffness smaller. The shear modulus is define as a function of the opening strain across the crack. In case of wallets specimens the overall response is not strongly dependent on the amount of shear retention.

The shape of the failure surface is defined by means of four values [3]:
  - Ratio of the ultimate biaxial compressive stress to the uniaxial compressive ultimate stress – 1.16;
  - Absolute value of the ratio of uniaxial tensile stress at failure to the uniaxial compressive stress at failure – 0.625;

- Ratio of the magnitude of a principal component of plastic strain at ultimate stress in biaxial compression to the plastic strain at ultimate stress in uniaxial compression – 1.28;
- Ratio of the tensile principal stress value at cracking in plane stress, when the other nonzero principal stress component is at the ultimate compressive stress value, to the tensile cracking stress under uniaxial tension – 0.33;
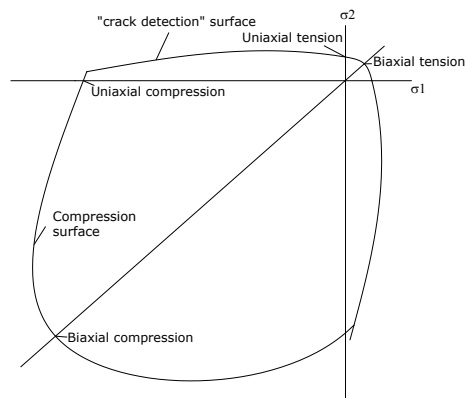
Figure 14. Theoretical interaction curves (ABAQUS – Concrete smeared cracking [3])

4. NUMERICAL RESULTS AND CONCLUSIONS

In present study a macro-model approach was adopted. Due to very complex mathematical procedure and experimental results need for the homogenisation process, the finite element model from this article used the masonry material properties, i.e. tensile strength ($f_{tm} = 0.45MPa$) and compressive strength ($f_{cm} = 7.5MPa$), taken from the wallets tests.

A 3D Shell element was chosen in order to reduce the computational effort and time and, more important, to be adequate for large models resulting in modelling real structures. Also a 3D Solid based model was built for validate the shell finite element model.

The concrete smeared cracking was used for both masonry (mas) and complex masonry-steel wire mesh (mas-swm) materials. Many empirical equations are suggested in scientific literature and design standards as constitutive laws for masonry elements as a homogenous material, subjected to compressive loading normal to the bed joints. Due to the fact that principal tensile stresses cause cracking and failure of the specimens, a very simple rectangular law was used for

uniaxial compression behaviour (elastic – perfect plastic). The following properties have been defined σ_k = *7.5 MPa* maximum allowable compression strength.

The only difference introduce at the definition of the two materials (i.e. mas and mas-swm) is the value for the tension stiffening. Even if for the complex mas-swm material a strain type definition could be more appropriate, for the sake of simplicity, for both cases the tension stiffening was define in terms of displacement, i.e. 0.2 mm for masonry and 3 mm for complex masonry-steel mesh material.

The mesh technique was structured, consisting in an 8 by 8 finite element square network, using 64 linear quadrilateral elements of type S4R [3].

In terms of global behaviour the masonry elements shown a sudden failure after reaching the maximum crack width. In case of retrofitted elements an important increase of capacity from approximate *16t* around *30t*. For retrofitted element after reaching the maximum force and important "inelastic plateaux" was observed and a major increase of crack opening have been obtained.

Unfortunately it is most difficult to obtain an almost rigid behaviour until crack and such a "yielding plateaux" behaviour for brittle material laws, therefore a compromise between the numerical and experimental results have to be accepted. Taking into account that this material calibration is intended to be used for global seismic retrofitting analysis of structures, the most important aspects are the energy dissipation, yield-point, ultimate displacement and stiffness. Complex nonlinear behaviour are subject to a linearization process. A bilinear idealization of the behaviour curve it is common practice in performance based evaluation in seismic engineering. In Figure 15 are shown the numerical results on the retrofitted material. The numerical model stops at 2 mm horizontal displacement. After this point the integrity of the element is compromised.
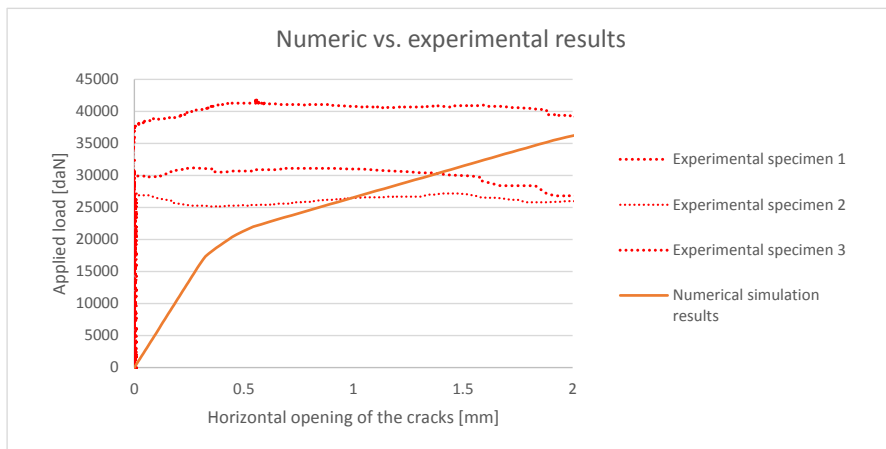
Figure 15. Horizontal deformation of masonry (MAS) and (MAS-SWM)

One may notice that the experimental results may be consider as bi-linear simplified behaviour of the numerical behavioral curve, keeping unaltered the energy dissipation and yield point.

The numerical simulation have proved that by modifying only one parameter from the material definition (i.e. the displacement in the tension stiffening definition), the numerical model is able to replicate the important increase of strength and deformation capacity. As was before mention, because of the high degree of experimental result scatter (see Table 1), is was not the aim of this study to calibrate in detail the material behaviour, but only to propose an equivalent material that easy to be apply in case of an performance based seismic assessment of an existing masonry wall bearing structure. If the energy dissipation, overall capacity and ultimate deformation are almost the same for the elements composed by complex material and the numerical model, then the global assessment is quite fair. It is true that because of the different rigidity of the real element and numerical model, the evaluation of the neighbouring elements, such as floors and foundations, should be perform applying other hypothesis.

In conclusion a simple material model assigned to 3d deformable shell elements could offer a reasonable preliminary estimation of overall benefits of such very complex anti-seismic retrofitting technique. But even so further detailed numerical investigation by means of either 2d composite shells or 3d solid elements used in a macro or micro-model taking into account the real interaction laws between its components it will be necessary to fully describe the real behaviour of the retrofitting solution.

Acknowledgements

References

1. Rots J.G. *Numerical simulation of cracking in structural masonry*, Heron, Vol. 36(2), pp. 49-63, 1991
2. Lourenço P.B., *Computational strategies for masonry structures*, Delft University Press, Stevinweg 1, 2628 CN Delft, The Netherlands, 1996
3. Dassault Systèmes *ABAQUS Documentation 6.10*, 2010
4. Dhanasekar M, Page, A.W. and Kleeman P.W. *The failure of brick masonry under biaxial stresses*. Proc. Intsn. Civ. Engrs., Part 2, 79 , p. 295-313, 1985
5. Page A.W. *The biaxial compressive strength of brick masonry*, Proc. Intsn. Civ. Engrs., Part 2, Vol. 71, pp. 893-906, 1981
6. Salamon M.D.G. *Elastic moduli of stratified rock mass*, Int. J. Rock. Mech. Min. Sci., 5, 519-527, 1968

7. Pande G. N., Liang J. X. and Middleton J. *Equivalent Elastic Moduli for Brick Masonry*; Computers and Geotechnics, 8, 243-265, 1989
8. Lourenço P.B., Zucchini A., *A homogenization model for stretcher bond masonry*, Computer Methods in Structural Masonry - 5, Eds. T.G. Hughes and G.N. Pande, Computers & Geothecnics, UK, p. 60-67, 2001
9. Lourenço P.B: *Experimental and numerical issues in the modelling of the mechanical behaviour of masonry*, Structural Analysis of historical constructions II - P. Roca, J.L. González, E. Oñate and P.B. Lourenço (Eds.) CIMNE, Barcelona ;1998
10. Pande G. N., Liang J. X. and Middleton J. *Equivalent Elastic Moduli for Brick Masonry*; Computers and Geotechnics, 8, 243-265, 1989
11. Wang Gang, Li Shaofan, Nguyen Hoang-Nam, Sita Nichloas: *Effective Elastic Stiffness for Periodic Masonry Structures via Eigenstrain Homogenization* , ASCE Journal of Materials in Civil Engineering, 2006
12. Tzamtzis A.D., 2003. *Finite Element Modeling of Cracks and Joints in Discontinuous Structural Systems*, 16th ASCE Engineering Mechanics Conference, July 16-18 2003, University of Washington, Seattle;
13. PROHITECH FP6 INCO-CT-2004-509119/2004 *Earthquake Protection of Historical Buildings by Reversible Mixed Technologies*
14. Adrian Dogariu *Seismic retrofitting techniques based on metallic materials of RC and/or masonry buildings (PhD thesis)* Ed. Politehnica, ISBN 978-973-625-846-7, 2009
15. IAEE/NICEE *Guidelines for Earthquake Resistant Non-Engineered Construction*. First printed by International Association for Earthquake Engineering, Tokyo, Japan. Reprinted by the National Information Center of Earthquake Engineering, IIT Kanpur, India, 2004
16. FP 6 PROHITECH - *Seismic protection of historical buildings: experimental activity vol. 3* – Ed. Polimerica, ISBN 978-88-7699-173-8, 2011
17. Correlated Solutions Inc. – www.correlatedsolutions.com

Modelling Methods for Large Masonry Structures

Lucian Soveja, Mihai Budescu and Vlad Lupasteanu

[1]*Faculty of Civil Engineering and Building Services, Gheorghe Asachi Technical University of Iaşi, 700050, Romania*

Summary

A large part of the built cultural heritage is affected by structural damages which may lead to infringements of the essential quality requirements of the buildings. Structural analysis contributes to the safety assessment and design of the necessary interventions, therefore accurate results are needed in order to avoid inappropriate rehabilitation solutions. This paper describes the modelling methods of masonry structures taking into consideration different strategies of analysis in correlation with the complexity of the investigated elements and with the type of the expected results. Advantages and disadvantages of different modelling techniques and the applicability of the latter in the field of old masonry structures assessment are presented. Also, a case study composed of different FEM analysis for a masonry monumental building is presented. Aspects resulted from modal and linear static analysis are discussed.

KEYWORDS: masonry monumental buildings, modelling strategies, modal and linear static analysis.

1. INTRODUCTION

From a structural point of view, masonry historical buildings are characterized by: high degree of static indetermination, complex geometry given by the overlapping elements, high variations of transversal cross section, and differences in rigidity or irregular mass concentrations.

In general, unreinforced masonry structures are characterized by complex structural system, being composed of massive walls on which, arches, vaults and domes rest. The structural over strength evaluation, especial to seismic action, is made by the identification of the areas with high stress concentration. Thus, a realistic modelling of the structural system is required.

Linear analyses are not always appropriate due to the complexity of historical masonry structures, which, besides the anisotropic character behave different in tension and compression. Moreover, because of the insignificant tension strength of the masonry, linear analysis can be considered inaccurate even at low levels of

loads. Masonry structures, especially those with arches and vaults, during the degradation process (which comes with local failures and dislocations), create numerous subsystems that are no longer subject to the initial conditions and therefore their shape and boundary conditions cannot be described anymore. However, the linear analysis is effective in identifying the global tendency of building behaviour, the modal characteristics and the areas in which the structure is subjected to stress concentrations which may lead to gaps in the continuity of the material. The required input data consists in the masonry specific weight and the modulus of elasticity. Despite all the restrictions, in recent decades, linear analyses were used to simulate the structural behaviour of a large number of masonry buildings with high cultural value [1].

1.1. Modelling strategies

Masonry is a composite material with direction-depended properties related to the geometry and to the mechanical properties of its constituents (brick or stone and mortar). Due to the low resistance of the mortar in both tension and compression, the masonry joints may lead to horizontal and vertical failure surfaces.

Depending on the complexity level corresponding to the structural analysis, three main strategies have been developed for masonry modelling: detailed micro-modelling, simplified micro-modelling and macro-modelling.

The decision of choosing a suitable modelling strategy depends on the expected analysis accuracy and on the size of the model (fig. 1). Micro-modelling provides a more realistic representation of the structural behaviour of masonry, but it has a prohibitive character due to the large number of degrees of freedom that are used, because of the increased volume of input data and also, due to the complexity in defining the failure criterions for masonry.

Thus, this method has proved suitable for studying the local behaviour of masonry structures, with a low level of complexity, especially for modelling masonry elements tested experimentally, being able to capture all possible failure modes of masonry.
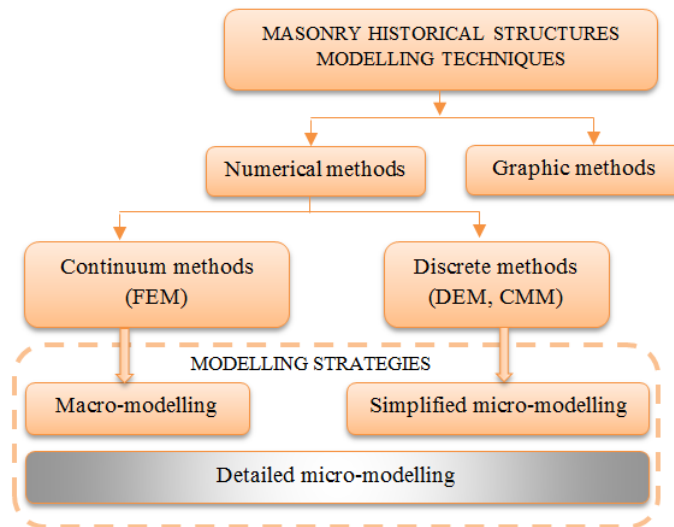
Figure 1. Masonry modelling techniques and strategies

Between micro-modelling and macro-modelling, the homogenization concept plays an important role in the analysis of masonry, referring to a unique continuous medium and aiming to determine the mechanical parameters of a fictitious homogeneous material which is able to simulate the real heterogeneous material.

Constitutive structural macro-models are relatively simple to use, they require less input data and the failure criterion for masonry is defined, in general, by a simplified law. Constitutive equations of the material, in this case, are suitable for studying the behaviour of the entire masonry structure because it reduces computation time and performance. The difficulties in macro-modelling consists in the formulation of quasi-brittle materials behaviour laws considering, in general, different failure criteria in tension and compression [2].

1.2. Shell and solid elements

Geometric representation of the structure can be made using two-dimensional elements (shell elements) or three-dimensional elements (solid elements). No element is superior to the other, the decision of choosing one depending entirely to the complexity of the problem (fig. 2).

For example, it would be unnecessary to use solid elements for the out of plane investigation of a masonry wall. Instead of solid elements, it would be enough to use shell elements for such a kind of investigation. When the concern is the investigation of a thick wall for in-plane loading, using shell elements (Fig. 2)

would be an inappropriate decision since it would be very difficult to investigate the stresses through the thickness of the wall.
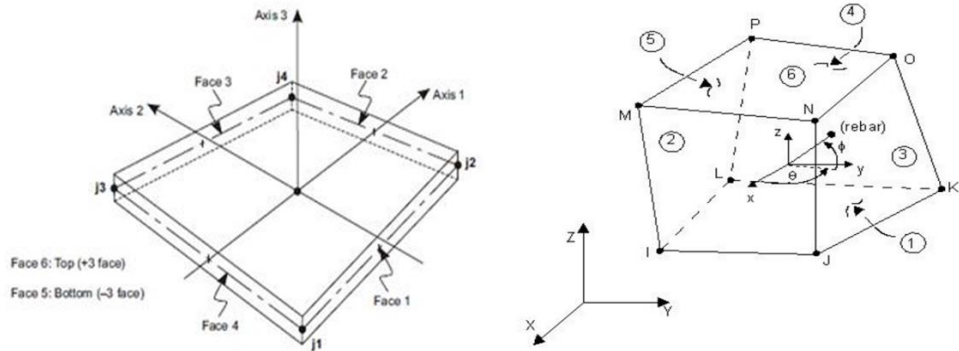
Figure 2. Shell and solid elements in masonry modelling

Because the two-dimensional elements are defined by a small number of nodal connections, their use in modelling masonry structures leads to efficient and practical analysis. In contrast, solid-type elements allow the control of the stress evolution within the structural elements, a necessary information regarding masonry structures with thick walls.

One of the basic principle of creating an analytical model is creating a geometrical model. However, it is difficult to distinguish between the structural and decorative elements in case of historic masonry structures. As a general rule, the geometric idealization should be as simple as possible.

In ETABS software, a shell is a three or four-node area object used to model membrane and plate-bending behaviour. Shell objects are useful for simulating floors, walls, 3D curved surfaces and components within structural members. Often, an eight-node solid brick element was used to model masonry.

These elements include a smeared crack analogy for cracking in tension zones and a plasticity algorithm to account for the possibility of concrete crushing in compression regions.

2. CASE STUDY

The "Al. I. Cuza" University of Iasi is an historical monument, and it was built between 1893 - 1897 on the site of the former Grand Theatre from Copou and School of Fine Arts, being designed by the Swiss architect, Louis Blanc.

The building has been further developed and strengthened in several stages, of which the most important after the Second World War and after the 1977 earthquake. The building is still used, serving as educational and research spaces.

In order to assess historical masonry buildings, linear and nonlinear dynamic analysis, based on FEM, offer important information and contributes to their classification in seismic risk classes and in the development of the intervention solution.

The finite element method (FEM) is a technique based on numerical analysis in order to obtain approximate solutions further used to determine the variation of parameters characterizing continuous media (field displacements, strains, stresses).

The basic idea of the FEM is based on the possibility of describing the real strain field through their values in a finite number of points. Usually finite elements are defined in the process of meshing, which occur as the result of decomposition of a domain into several compatible subdomains with disjunctive interior. The method was widely used in the evaluation of historic masonry buildings in linear and nonlinear analysis, offering good results in describing the structural response of the buildings [3].

2.1. Finite element model
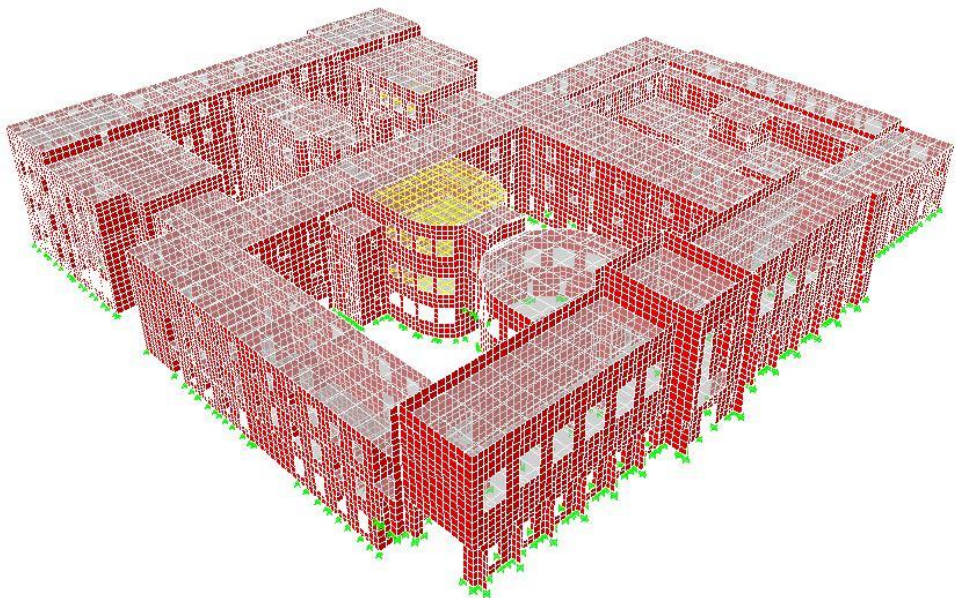
Figure 3. Structural analysis of "Al.I. Cuza" University, based on macro-modelling strategy

The analysis models were developed by using Etabs V9.7.2. software (fig. 3). The model has 90.000 shell elements both for walls and floors, with a meshing step of 0.4m and 1m. The difficulties in the modelling process consisted of simulating the geometry of the very large sized building, with curved walls and floors at different levels.

3. MODAL ANALYSIS

In the first step, a modal analysis has been carried out, revealing the characteristic deformed shapes and periods of the building for each vibration mode. After preliminary analysis, it has been observed that significant modal masses are present only for the modes with the vibration period of 0.48 to 0.16 s. outside this range, the vibration modes are insignificant in terms of deformations and tensions induced by seismic loads.

A number of 100 vibration modes were included in the analysis to obtain the sum of the participation mass factors over 90% on both directions. The first 4 vibration modes are presented in figures 4 to 7.
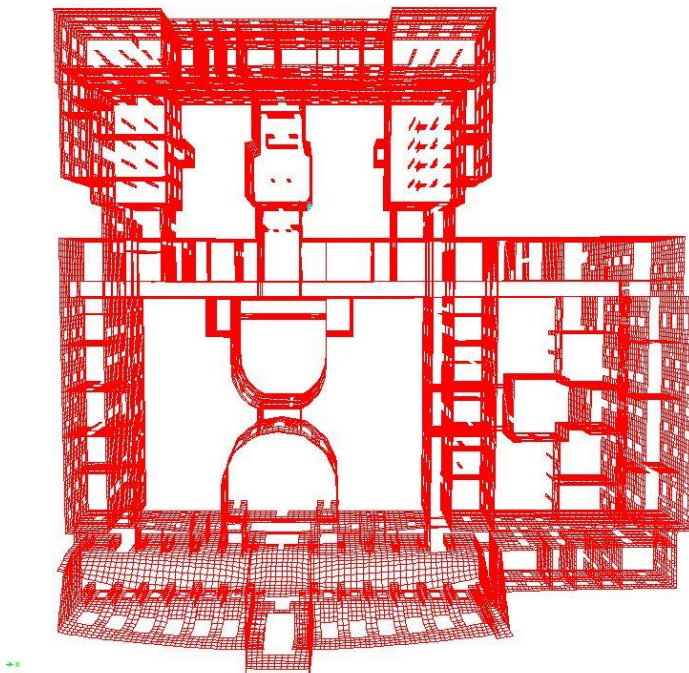
Figure 4. First vibration mode T=0.480s
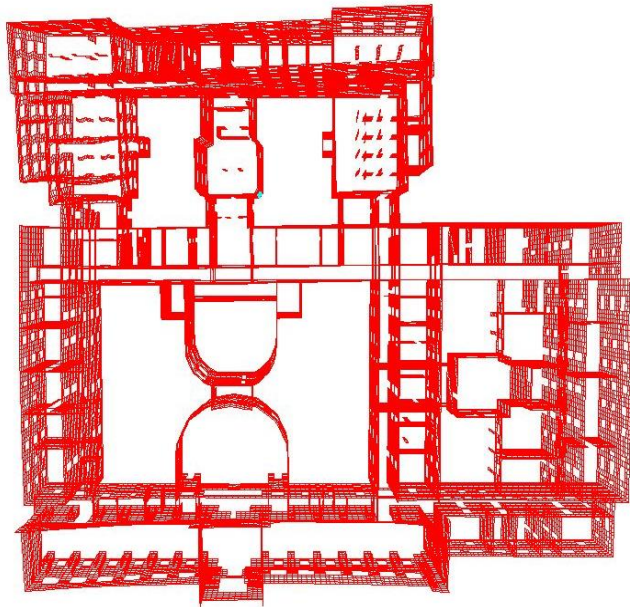
Figure 5. Second vibration mode T=0.409s
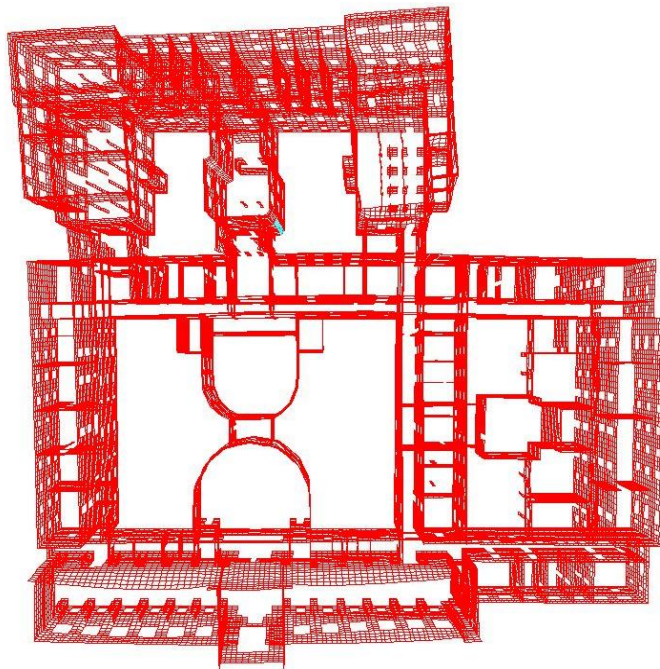
Figure 6. Third vibration mode T=0.395s
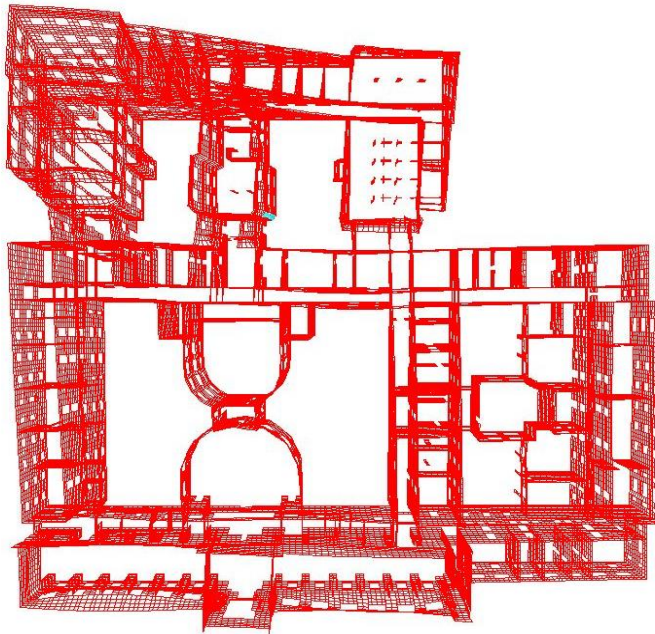
Figure 7. Forth vibration mode T=0.371s

Overall, the allure of the deformed shapes of the structure does not fit precisely in the main directions of the structure (transversal and longitudinal) but rather seems a mix of simultaneous translational and torsional modes in different parts of the buildings, mainly due to the in-plane shape.

Obviously, the modal analysis obtained by computer simulation has a degree of precision and detailing far superior to any manually approach, regardless of the used method.

4. LINEAR STATIC ANALYSIS

The structural analysis of the monumental building was performed by subjecting the finite element model to three types of actions: dead load, live loads and seismic loads. The actions were defined in accordance with Romanian standards, in agreement with Eurocode 8. Table 1 presents the load cases defined by the code.

Table 1. Load cases

The fundamental loading cases	$1.35 \sum\limits_{j=1} G_{k,j} + 1.5 Q_{k,i} + \sum\limits_{i>1} 1.5 \Psi_{Q,i} Q_{k,i}$
The special loading cases	$\sum\limits_{j=1} G_{k,j} + \gamma I A_{Ek} + \sum\limits_{i>1} \Psi_{2,i} Q_{k,i}$

Where: G_{kj} – the dead load; Q_{ki} – the live load; Q_{kj} – the predominant live load; $\Psi0,1$ – the live load factor equal to 0.7; A_{Ek} – the earthquake action for a recurrence interval of 100 years, P100 - 2006; $\Psi_{2,i}$ – the live load coefficient equal to 0.4; γ_I – the coefficient of importance equal to 1.20 for importance class 2.

The seismic actions have been introduced in the program in a response spectrum analysis using the design accelerations spectra (fig. 8) according to the national code P100/2006.
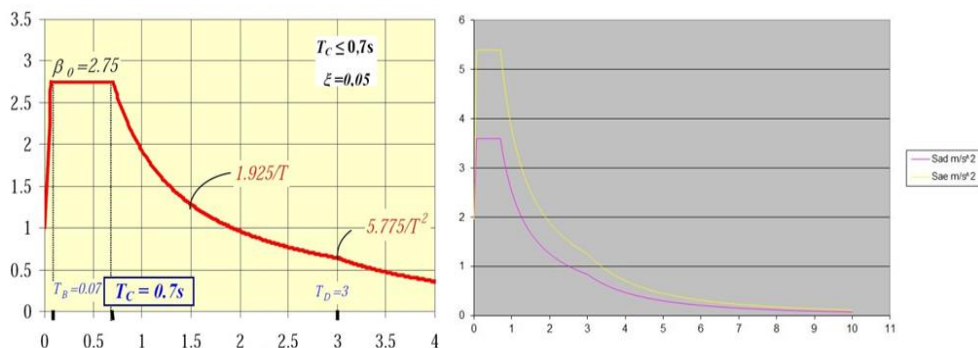
Figure 8. Elastic and design accelerations spectra

On the basis of modal analysis, further seismic analysis on the two main directions of the building was performed. The deformed shapes of the construction, in the two main directions, parallel and perpendicular to the central core, are shown in figures 9 and 10.

From the following figures it is clear that the seismic action parallel to the central body, leads to a state of deformation more pronounced on the secondary façade bodies, while an earthquake action on perpendicular direction tends to deform predominantly the central body.
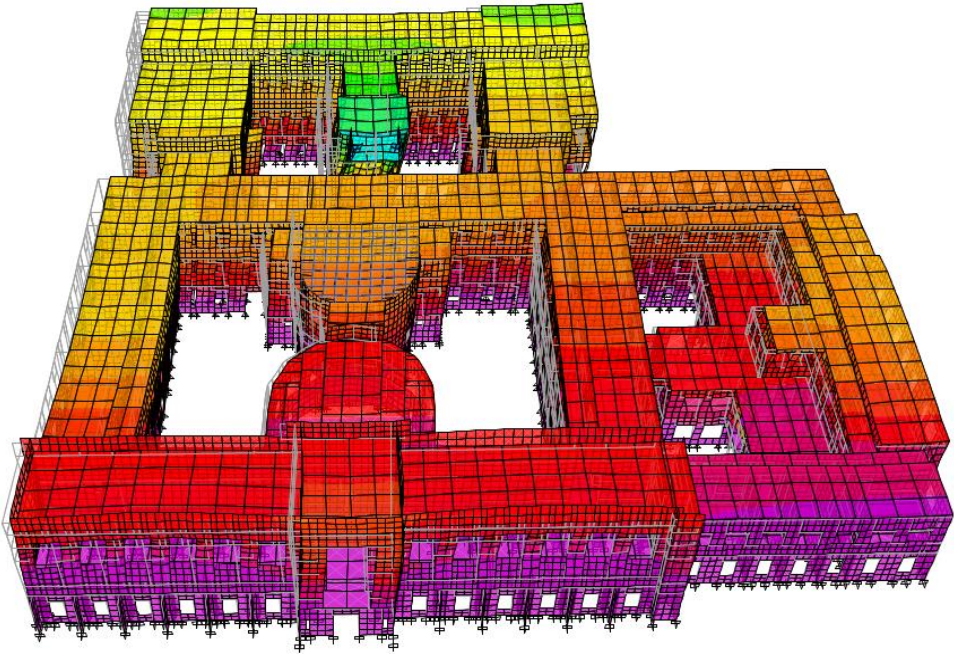
Figure 9. Deformed shape – seismic action on longitudinal direction
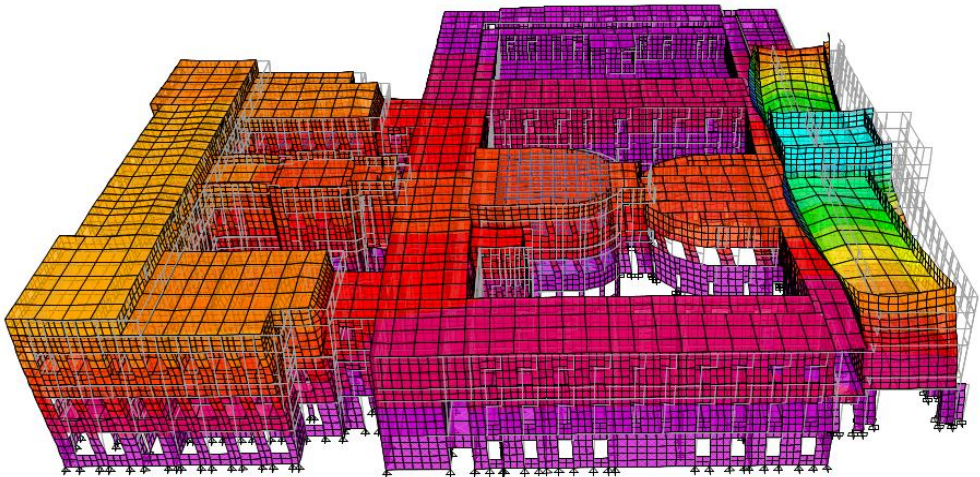
Figure 10. Deformed shape – seismic action on transversal direction

Obviously, the differences in stiffness of the bodies that compose the structure, in relation to the each direction of the earthquake, determines an almost different way of structural response for each individual body.

Analysing the stress state in the walls of the main and secondary façade (fig. 11), it has resulted that compression stresses are close to the masonry compression bearing capacity of 4.5N/mm², determined through experimental investigations.
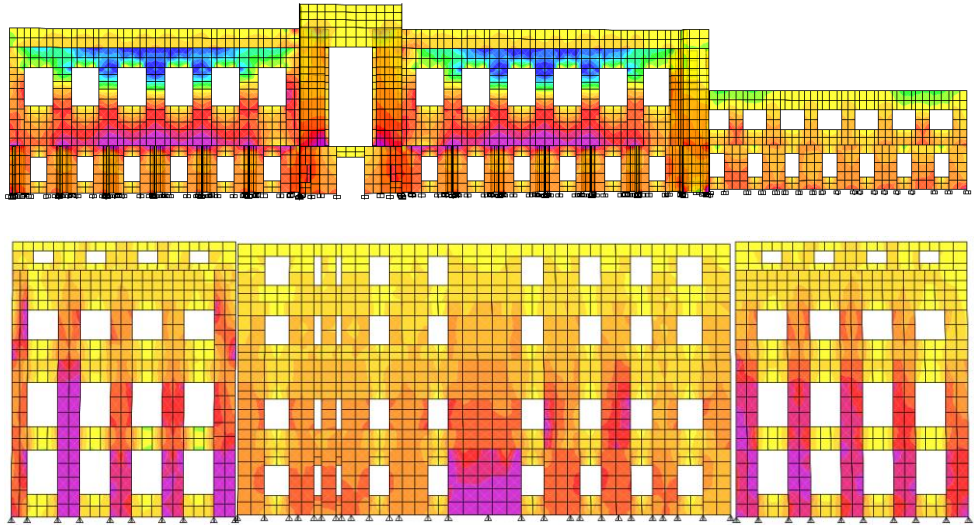
Figure 11. Compression stresses maps at main and secondary façade walls
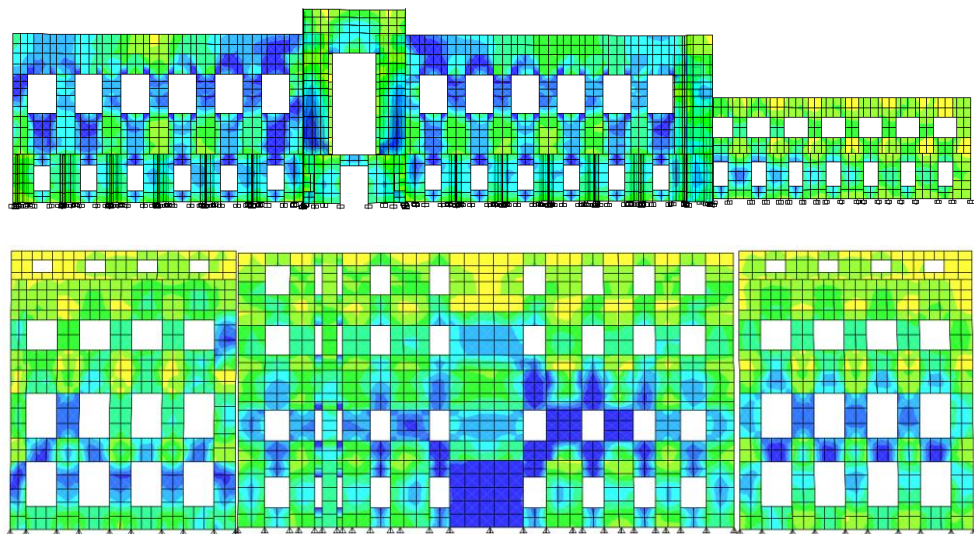
Figure 12. Tension stresses maps at main and secondary façade walls

At the secondary façade wall, the stresses in the central and marginal piers, at the ground level, are about 3.6N/mm^2. At the main façade, the maximum compression stresses are reached in the piers wich support the metallic girdes of the floors.

The tension stresses (fig. 12) are with maximum values of 1.6N/mm^2 at the secondary façade walls and 1.8N/mm^2 at the main façade walls, mainly in the zones that suffered most damage during the 1977 seismic action.

5. CONCLUSIONS

In the mechanical analysis of historical masonry buildings, the structural evaluation, especial to seismic action, is made by the identification of the areas with stress concentration therefore a realistic modelling of the structural system is required.

Constitutive structural macro-models are relatively simple to use, require less input data and are suitable for studying the behaviour of the entire masonry structures because it reduces computation time and performance. The difficulties in macro-modelling relates to the formulation of quasi-brittle materials behaviour laws considering, in general, different failure criteria in tension and compression.

The linear model is effective in identifying the global tendency of building behaviour, modal characteristics and areas in which the structure is subjected to stress concentrations able to interrupt the continuity of the masonry.

Linear analyses can be efficiently and successfully used to simulate the structural behaviour of masonry monumental buildings with realistic results in the process of their structural evaluation.

References

1. Pappas A., Calibration of the numerical material behaviour of multi-leaf stone masonry walls based on experimental results. *M. Sc. Diss.*, Univ. of Padova, 2012.
2. Roca P., Cervera M., Pela L., Clemente R., Chiumentini M., Continuum FE models for the analysis of Mallorca Cathedral, *Enging. Struct.*, 46, 653-670 (2013).
3. Varum H., Tarque N., Silveira D., Structural Behaviour and Retrofitting of Adobe Masonry Buildings, *Build. Pathol. a. Rehabil.,* 2, 37-75 (2014).

Comparative Study Regarding the Choice of Structural System for Buildings with Regular Plan Configurations in Seismic Areas

Marian Pruteanu, George Crețu and Maricica Vasilache

Department of Civil and Industrial Engineering, „Gheorghe Asachi" Technical University of Iași, Iași, 700050, Romania

Summary

The introduction of Eurocodes regulations imposed on masonry structure buildings the use of a large number of reinforcing elements, especially in areas with intense seismic activity. Thus, in the Moldavia area of Romania choosing the structural system for buildings with regular plan configuration, aiming for optimal price-performance ratio, is a current issue.

The paper presents an analysis of the behaviour of concrete frame structure and active masonry structure, for a building with regular plan configuration, placed on areas with different peak ground acceleration. Structural and architectural conformation of the building follows the current regulations, 2013 version. The study is conducted by using numerical modelling program ETABS, information on the properties of the used materials is obtained by tracking the sites of producers.

Finally, some conclusions and recommendations are mentioned regarding the choice of the structural system for buildings with regular plan configuration, as well as regarding structural conformation of active confined masonry walls.

1. INTRODUCTION

In our country, Vrancea seismic zone is characterized by an intense seismic activity caused by the intersection of at least three tectonic units: Eastern - European plate and Intra - Alpina and Moesica microplates. The seismic activity is concentrated at depths of 60-200 km intermediate in an old subduction plate, almost vertical, which leads to the generation of 1-6 events of magnitude Mw > 7.0 on century, in a very small focal volume [1].

This intense seismic activity requires as essential priority the compliance of the strength and stability requirements. Earthquake design aims to satisfy, with an adequate degree of safety, the two fundamental requirements (performance levels), namely life safety requirement and the requirement to limit damages. To this purpose, the structural strength will be designed to meet the seismic action by the design value shown in P100 [2], with a sufficient margin of safety compared to the deformation level whereat local or general collapse occurred, so that people's lives to be protected. Also, the structural systems will be designed to respond to seismic

actions with a higher probability of occurrence compared to the design value, without degradation of the building or taking of it out of service, whose costs are unreasonably high compared to the initial cost of the structure. In designing new buildings to meet the seismic action requirements, Romania is divided into seven seismic areas, characterized by the horizontal peak ground acceleration, "a_g" determined for a mean interval of recurrence of reference, value named hereinafter as „design ground acceleration". Considering this, the choice of the structural system is made by taking into consideration the design ground acceleration, aiming to obtain an optimal price-performance ratio.

The intention of both engineers and beneficiaries is to build as cheaply, as quickly and as less difficult as possible. Therefore, for buildings with regular plan configuration and reduced height regime (up to B + GF + 3F), placing them in different areas of Moldova, raised the issue of choosing the structural system, the most commonly used being reinforced concrete frames and confined masonry structural walls. According to the code governing the calculation of the strength structures with confined masonry walls CR6 - 2013 [3], in areas with $a_g \geq 0.30g$, the disposition of the tie-columns is thickened, their high number leading to a large volume of concrete and reinforcement.

This paper aims to examine the economic benefits of using confined masonry wall construction, in three different locations, $a_g \geq 0.30g$; $a_g = 0.20g$ - $0.25g$ and $a_g < 0.20g$. To this purpose, a building with regular plan configuration and height of B + GF + 2F was modelled in ETABS compute software, considering two structural systems - reinforced concrete frames and confined masonry structural walls. Next, were computed the materials quantities for the superstructure, namely for concrete, masonry and reinforcement, in order to obtain an estimate cost of the building, on the three locations and for the two different structural systems. Also, in the case of placing the building in areas where $a_g \geq 0.30g$, a number of solutions were analysed for the optimization of the structural strength with confined masonry walls in order to reduce the cost. Finally, there are noted a series of conclusions and recommendations.

2. STRUCTURAL AND ARCHITECTURAL CONFORMATION OF THE ANALYSED BUILDING

For the case study a condominium apartment building was analysed. The height regime of the building was B + GF + 2F. The research of the real estate market showed that lately these buildings are increasingly used, especially in suburban areas.

The analysed building has two apartments disposed on each floor with areas of 98.6 m^2 or 115.8 m^2 (Fig. 1).

Figure 1. Architectural conformation of the analysed building - confine masonry walls placed in seismic areas with $a_g = 0,35g$

The building was structurally conformed in two different solutions, namely with reinforced concrete structural frames and with confined masonry structural walls.

In the case with confine masonry structural walls, Fig. 2, the wall thickness is of 25 cm, in the area with $a_g > 0.25g$ being used bricks with dimensions of 240 x 115 x 63 mm, with a standardized compression strength of 30 N/mm^2, meanwhile in the areas with $a_g \leq 0.25g$ hollow ceramic blocks with dimensions of 240 x 290 x 138 mm, with a standard compressive strength of 15 N/mm^2 were used. Masonry mortar used an additive for increasing the plasticity which does not attack the seismic anchors placed in mortar joints, with the mean compressive strength of 5 N/mm^2. Confinement elements, as tie-beams (250 x 250 mm) and tie-columns (250 x 250 mm), are made of concrete of C16/20 class. The reinforcement of the tie-column is made with PC52 bar with a diameter of 16 mm, while the tie-beams reinforcing bars are made of Ø14 mm. Coupling girders are with low rigidity, made of reinforced concrete lintels with dimensions 250 x 150 mm, two bricks layers and the tie-beams. It is noted that in areas with $a_g = 0.20 - 0.25g$, which requires an active wall density of at least 5%, the walls on the axes B', compassed between the axes 2-3 and 4-5, and C axis, compassed between the axes 3-4 are replaced with non-structural walls. Also, in the case of placing the buildings in areas where $a_g < 0.20g$, where the minimum required active wall density is 4% in the longitudinal direction, the walls on the axes C and B 'are replaced by non-structural walls.
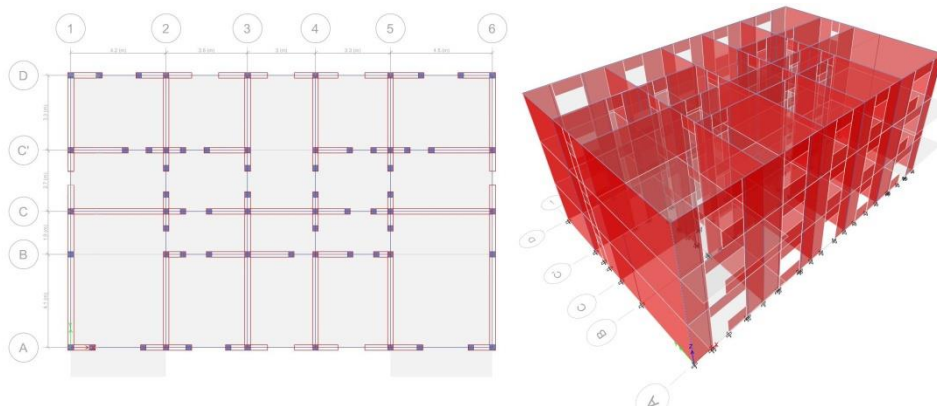
Figure 2.Building with confined masonry structural walls
Horizontal section. ETABS 3D model

In the second version of structural conformation, figure 3, the structure is a three-dimensional reinforced concrete frame, consisting of 3 longitudinal plane frames and 6 transverse plane frames. Structural elements are made of reinforced concrete, class C 20/25. The columns sections are 35 x 35 cm, for areas with ground acceleration $a_g \geq 0.30g$ and 30 x 30 cm for areas with $a_g < 0.30g$. The beams sections are 30 x 50. Reinforcement of columns and beams is made according to current regulations. The framed masonry walls are made of hollow ceramic light blocks, with low standard compression resistance, of around 5 N/mm^2. The mortar used is lime and cement mortar, M5. Characteristic compressive strength of the panels was 2 N/mm^2.

The slabs are similar in both structure variants, with 13 cm thickness and made of concrete class C16/20.
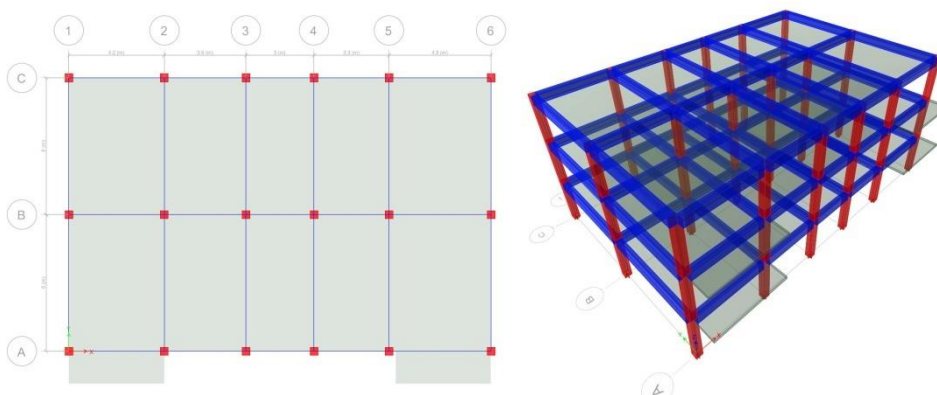
Figure 3. Building with reinforced concrete structural frames
Horizontal section. ETABS model

3. NUMERICAL ANALYSIS OF THE BUILDING ON VERTICAL AND SEISMIC ACTION

Numerical analysis was performed in ETABS software. Load combinations are modelled according to in force regulation [4]. With the intention of pointing out that analyzed resistance structures successfully takes and transmits to the foundation ground both vertical loads and seismic loads, in tables 1 and 2 are presented the values of their periods of vibration and maximal drift and the borderline values. It is noted that all six buildings have their vibration periods beyond the limits and the maximum drift below the value imposed by the regulations.

Table1. Dynamic characteristics of the building with confined masonry structural walls, obtained from modelling

Nr. Crt.	Building's emplacement	Modes of vibration	Period of vibration	Borderline values	Maximal drift (ETABS)	Maximum allowable values P100 (SLS)
1	$a_g = 0,35g$	Mode 1	0,0711	<0,7 >1,2	0,52 mm	42 mm
		Mode 2	0,0621			
		Mode 3	0,0558			
2	$a_g = 0,25g$	Mode 1	0,0919	<0,7 >1,2	0,56 mm	42 mm
		Mode 2	0,0717			
		Mode 3	0,0651			
3	$a_g = 0,15g$	Mode 1	0,0978	<0,7 >1,2	0,53 mm	42 mm
		Mode 2	0,0706			
		Mode 3	0,0646			

Table 2. Dynamic characteristics of the building with reinforced concrete frames, obtained from modelling

Nr. Crt.	Building's emplacement	Modes of vibration	Period of vibration	Borderline values	Maximal drift (ETABS)	Maximum allowable values P100 (SLS)
1	$a_g = 0,35g$	Mode 1	0,4397	<0,7 >1,2	8,61 mm	42 mm
		Mode 2	0,3661			
		Mode 3	0,3513			
2	$a_g = 0,25g$	Mode 1	0,4397	<0,7 >1,2	8,79 mm	42 mm
		Mode 2	0,3661			
		Mode 3	0,3513			
3	$a_g = 0,15g$	Mode 1	0,5144	<0,7 >1,2	7,98 mm	42 mm
		Mode 2	0,4472			
		Mode 3	0,4194			

4. ESTIMATED ECONOMICAL ANALYSIS FOR THE SUPERSTRUCTURE COST

The purpose of the paper is to analyse the economic advantages of choosing confined masonry wall structures for buildings with regular plan configuration. Therefore, they have been calculated for the 6 fictitious buildings material consumption necessary to construct the superstructure namely those of concrete, masonry and reinforcement. To determine the estimated costs, the materials prices were obtained from researching building materials market in Iasi area.

In Tables 3 and 4 are presented the material consumptions for buildings located in the area with $a_g = 0.35g$. For building with structural masonry walls (table 4) were used bricks in order to achieve greater resistance and to avoid using horizontal reinforcement in the mortar joints. In this case it is noted that the estimated cost is higher than for building with reinforced concrete frames. This is mainly due to the high cost of bricks. Consumption of reinforcement and concrete for tie-columns are higher than the one necessary for the columns of the frame, but surpluses are balanced by consumption of material needed for the beams, much higher than those needed for the tie-beams. When using hollow ceramic blocks for structural walls, the estimated cost is 31366.27 Euros still higher than the frame structure.

Table 3. Estimated consume for the reinforced concrete frames building placed in areas with ag=0.35g

Element name	Material	Quantity/ Volume	Units of measurement	Cost [Lei]
Beams	Concrete C20/25	57.51		280
Columns	Concrete C20/25	15.21		280
Slabs	Concrete C16/20	81.55	mc	240
Masonry walls	Hollow bricks	231.2		226.84
Beams reinforcement	PC 52	5607.37		
Beams reinforcement	OB 37	3649.8	kg	2.97
Columns reinforcement	PC 52	1687.38	kg	2.97
Columns reinforcement	OB 37	1382		
	Total weight of concrete C20/25	72.72	mc	20361.6
	Total weight of concrete C16/20	81.55	mc	19572
	Total weight of masonry	231.2	mc	52445.4
	Total weight of reinforcement	12326.55	kg	36609.9
TOTAL COST [RON]			128988.86	
TOTAL COST [EURO]			29997.41	

Table 4. Estimated consume for the building with confined masonry structural walls placed in areas with a_g=0.35g

Element name	Material	Quantity/ Volume	Units of measurement	Cost [Lei]
Tie-beams	Concrete C16/20	29.82	mc	240
Tie-columns	Concrete C16/20	32.51		
Slabs	Concrete C16/20	81		
Masonry wall	Bricks	242.76		735.6
Tie-beams reinforcement	PC 52	3014	kg	2.97
	OB 37	1808		
Tie-columns reinforcement	PC 52	3610		
	OB 37	1857		
	Total volume of concrete	143.33	mc	34399.2
	Total volume of masonry	242.76	mc	178574.3
	Total weight of reinforcement	10289	kg	30558.33
	TOTAL COST [RON]		243531.79	
	TOTAL COST [EURO]		57968.60	

In tables 5 and 6 are presented consumption of material for buildings located in the area with a_g = 0.25g. It is noted that estimated cost of reinforced concrete frames building is higher than the one for masonry building due to the reducing of tie-columns number required for confinement of masonry walls. Also, for this areas can be used hollow ceramic blocks for the structural masonry wall, without the need for reinforcement in the horizontal joints.

Table 5. Estimated consume for the building with confined masonry structural walls placed in areas with ag=0.25g

Element name	Material	Quantity / Volume	Units of measurement	Cost [Lei]
Tie-beams	Concrete C16/20	27.22	mc	240
Tie-columns	Concrete C16/20	16.25		
Slabs	Concrete C16/20	83.16		
Masonry wall	Bricks	232.62		236.67
Tie-beams reinforcement	PC 52	2135	kg	2.97
	OB 37	1478		
Tie-columns reinforcement	PC 52	1382.3		
	OB 37	928.28		
	Total volume of concrete	126.63	mc	30391.2
	Total volume of masonry	232.62	mc	55054.18
	Total weight of reinforcement	5923.58	kg	17593.03
	TOTAL COST [RON]		103038.41	
	TOTAL COST [EURO]		23962.42	

Table 6. Estimated consume for the reinforced concrete frames building placed in areas with ag = 0.25g

Element name	Material	Quantity/ Volume	Units of measurement	Cost [Lei]
Beams	Concrete C20/25	57.51	mc	280
Columns	Concrete C20/25	15.21		
Slabs	Concrete C16/20	81.55		240
Masonry walls	Hollow bricks	231.2		226.84
Beams reinforcement	PC 52	4582.89	kg	2.97
	OB 37	3649.8		
Columns reinforcement	PC 52	1492.64		
	OB 37	1382		
	Total weight of concrete C20/25	72.72	mc	20361.6
	Total weight of concrete C16/20	81.55	mc	19572
	Total weight of masonry	231.2	mc	52445.41
	Total weight of reinforcement	11107.33	kg	32988.77
	TOTAL COST [RON]		125367.78	
	TOTAL COST [EURO]		29155.30	

In the tables 7 and 8 are shown consumption of material for buildings located in the area with a_g = 0.15g. It is noted that the difference between the estimated costs is maintained, with decreasing intensity seismic action, structural elements of the concrete frame are more slender and less reinforced.

Table 7. Estimated consume for the building with confined masonry structural walls placed in areas with ag=0.15g

Element name	Material	Quantity/ Volume	Units of measurement	Cost [Lei]
Tie-beams	Concrete C16/20	25.02	mc	240
Tie-columns	Concrete C16/20	16.25		
Slabs	Concrete C16/20	84.21		
Masonry wall	Bricks	210.25		236.67
Tie-beams reinforcement	PC 52	1855.6	kg	2.97
	OB 37	1365		
Tie-columns reinforcement	PC 52	1014.4		
	OB 37	928.28		
	Total volume of concrete	125.48	mc	30115.2
	Total volume of masonry	210.25	mc	49759.87
	Total weight of reinforcement	5163.28	kg	15334.94
	TOTAL COST [RON]		95210.01	
	TOTAL COST [EURO]		22141.86	

Table 8. Estimated consume for the reinforced concrete frames building placed in areas with ag=0.15g

Element name	Material	Quantity/ Volume	Units of measurement	Cost [Lei]
Beams	Concrete C20/25	57.65		280
Columns	Concrete C20/25	12.15	mc	
Slabs	Concrete C16/20	81.55		240
Masonry walls	Hollow bricks	231,8		226.84
Beams reinforcement	PC 52	3685.04		
	OB 37	3649.8	kg	2.97
Columns reinforcement	PC 52	1268.86		
	OB 37	1382		
Total weight of concrete C20/25		69,8	mc	19544
Total weight of concrete C16/20		81,55	mc	19572
Total weight of masonry		231.8	mc	52581.51
Total weight of reinforcement		9985.7	kg	29657.53
TOTAL COST [RON]			121355.04	
TOTAL COST [EURO]			28222.10	

4. CONCLUSION AND RECOMANDATION

The above analysis argues that in areas with low and medium seismicity, peak ground acceleration $a_g \leq 0.35g$, it is economically advantageous to use confined masonry structural walls. In addition to lower material consumption, another argument is the more accessible implementing technology. It was noted that in these areas the estimated cost is lower for buildings with masonry walls, 22141.86 euro to 28222.10 euro in areas with $a_g = 0.15g$ and 23962.42 euro to 29150.30 euro in areas with $a_g = 0.25g$.

In areas with $a_g > 0.25g$, by thickening the tie-columns, the material consumption increased. If masonry walls are made of bricks, the estimated cost is much higher than the cost for reinforced concrete frames, 57968.60 euro to 29997.41 euro. If ceramic hollow blocks are used, estimated cost decreases but still remains higher than the reinforced concrete frame structure, due to the need to use reinforcement in horizontal mortar joints.

In the future, the authors intend to continue the research and to use numerical analysis to optimize confined masonry structural walls for buildings located in areas with $a_g = 0.35g$, in terms of material consumption.

The authors noted that the numerical modelling of the specific structural strength was one specific to current design.

REFERENCES

1. http://www.infp.ro/despre-cutremure/#ch_6;
2. Seismic Design Code, Part 1 - P100-1/2013, Earthquake Resistant Design of buildings;
3. CR6/2013 – Masonry structures design code;
4. CR 0/2012 – Basis of structural design;
5. CR 1-1-3/2012 - "Design **code**: Assessment of **snow action** on structures";
6. SR EN 1991-1/2006 – Actions on structures - Part 1-4: General actions Wind actions. National Annex;
7. https://wiki.csiamerica.com/display/etabs/Home;
8. Neophytou, V., *Etabs Modelling,* 2013;
9. Vasilache, M., Pruteanu M., *Construcții din zidărie. Curs. Îndrumător de proiectare*, Ed. Soc. Acad. „Matei – Teiu Botez", 2014. (in Romanian)

Analysis and Design of a Base Isolation System for an Old Church with Masonry Structure

Lucian Soveja, Mihai Budescu

Faculty of Civil Engineering and Building Services,Gheorghe Asachi Technical University of Iaşi, 700050, Romania

Summary

The studies that consider the evaluation and the rehabilitation processes of historical masonry structures consist of structural analysis, aiming to better understand the seismic behaviour of these buildings, and also, may refer to the assessment of the safety level with respect to different rehabilitation strategies. This paper present the case of an old historical masonry church for which a base isolation system has been developed. Aspects regarding the modelling process, finite element method analysis, modal and static linear analysis are presented. The efficiency of the base isolation system that has been designed for this specific structure is also verified using a time history analysis.

KEYWORDS: FEM, base isolation, masonry church, time history analysis.

1. INTRODUCTION

Historic buildings provide the most tangible legacy of our past civilization and in some cases they speak clearer than any remaining manuscripts. Historic masonry structures have low ductility, and, due to their stiff and brittle structural components, are usually severely damaged during strong earthquakes. The main reason for damage is a lack of ductility that prevents a structure from being able to sustain the displacements and distortions caused by severe earthquakes. Damage caused by earthquakes to historic buildings is irreversible and these lost documents cannot be retrieved. The goal should then be to strengthen these structures in a manner that requires the least intervention and the greatest care to preserve authenticity. This goal, reflected in such conventions as the Venice Charter, poses real challenges with traditional masonry structures subjected to earthquakes [1].

Seismic isolation systems work by decoupling the building or structure from the horizontal components of earthquake ground motion by interposing a layer of low horizontal stiffness between the structure and its foundation. This layer prevents the transmission of accelerations from the ground to the building. This decoupling action is affected by mounting the building on a system of bearings that are stiff in the vertical direction (in order to support the building weight) but soft in the horizontal direction [2].

With base isolation, the earthquake energy that would have been transferred to the structure gets absorbed at the base level. In addition, the period of the isolated structure is increased which typically results in a reduction in seismic demands.

In these ways, ductility demand to the structure is greatly reduced. Displacement across the isolation system can be somewhat controlled by the addition of damping.

Seismic base isolation has so far been applied mainly in newly designed structures but has shown great promise in the improvement of existing structures with stiff and brittle structural systems. The advantage of this method is in the minimal intervention on the existing structure and the protection of architectural integrity. A disadvantage is the loss of the cultural layer and any archaeological remains as part of the base isolation installation. In the case of compact and exceptionally valuable historic structures of smaller proportions, base isolation becomes an acceptable, although expensive solution [1].

2. STUDY CASE

The studied church is dedicated to St. Nicholas and was built in Iasi, in 1592 on the site of an older church, erected by Alexandru Lăpuşneanu. Over time, the church was damaged and repaired several times.

The design objective for seismic strengthening of the church was to provide global and local performances that exceeded the requirements of P100-3/2008. The enhanced global performance targets at design earthquake (DE) and maximum considered earthquake (MCE) were:
  - - DE (475 year): Performance of between immediate occupancy (IO) and life safety (LS)
  - - MCE (2475 year): Performance of between LS and collapse prevention (CP)

These performance targets exceed the current common seismic retrofit requirements of LS and CP at DE and MCE, respectively P100-3/2008. Accelerations and drift ratios were reduced to level below the limiting values that initiate either in-plane or out-of-plane failure of vulnerable URSM walls.
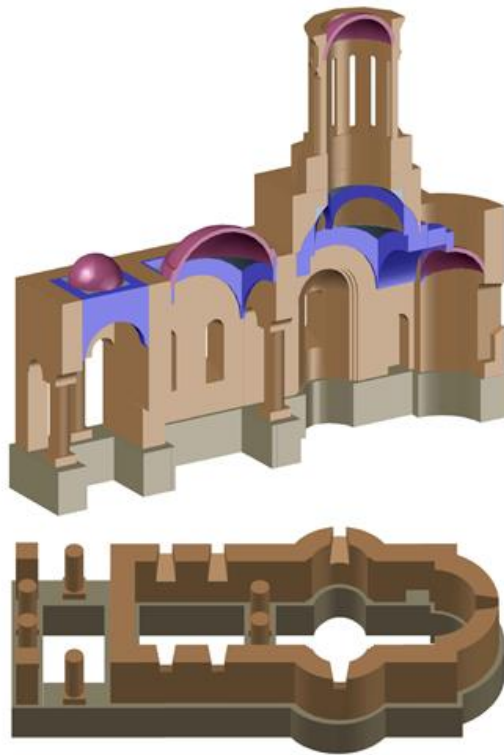
Figure 1. Isometric view of Aroneanu Church

Due to economic advantages (reduced prices) and the specific behaviour of friction pendulum isolators (the mass centre coincides with the centre of stiffness), they were chosen as the optimal solution.
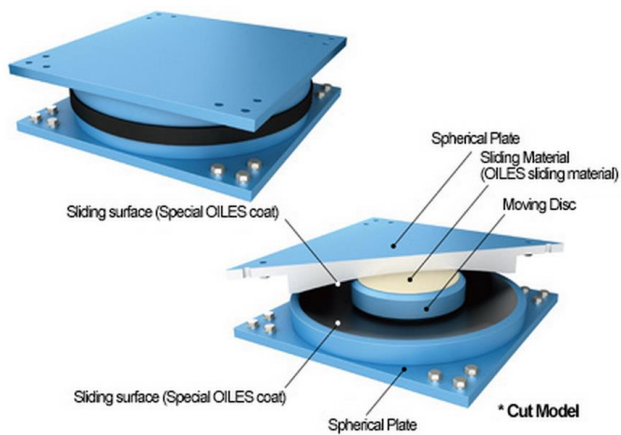

Figure 2. Spherical seismic isolators

The sliding isolation devices presented in figure 3 are consisting of three main steel parts with inner sliding surfaces. The shape of the internal part is always spherical and allowing rotations and horizontal sliding displacements as well. The device is transmitting the vertical loads and is providing free horizontal flexibility, while dissipating energy.

The proposal of the seismic isolators in plan layout, in accordance with geometrical considerations, stability and vertical loads balancing, is presented in figure 3.
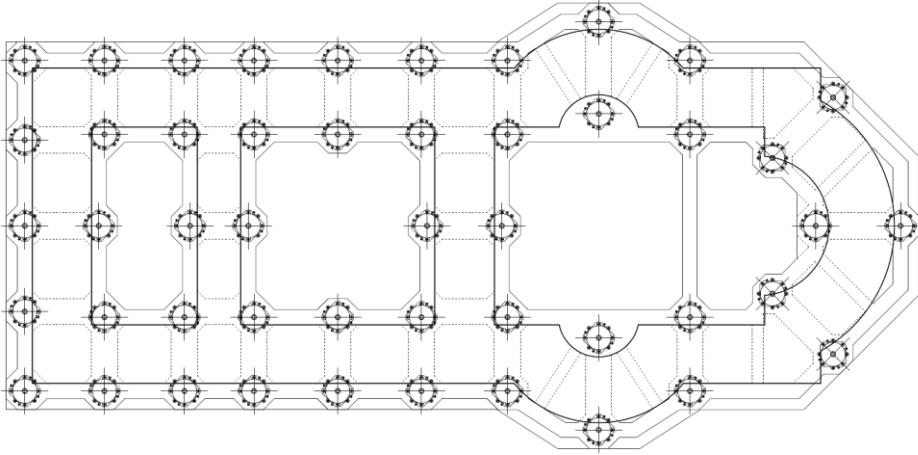
Figure 3. In plan layout of the seismic isolators

The seismic isolators were chosen (radius and friction coefficient) by iterative computation proposing a target period of isolated system and a maximum displacement, based on the following relationships [3]:

$$R = g * \sqrt{T/2\pi} \qquad (1)$$

where:

- R is the curvature radius of the seismic isolators;

- T the period of the isolated system;

$$\xi = \frac{2}{\pi} * \left(\frac{\mu}{\mu + \frac{D}{R}} \right) \qquad (2)$$

where:

- ξ is the equivalent damping of the isolated system;

- μ isolator friction coefficient;

- D maximum displacement of the isolators;

$$k_{eff} = V * \left(\frac{1}{R} + \frac{\mu}{D}\right) \qquad (3)$$

where:

- k_{eff} effective stiffness of the isolators;

- V is the total weight of the isolated structure;

$$T_{eff} = 2\pi * \sqrt{\frac{V}{k_{eff}*g}} \qquad (4)$$

where:

- T_{eff} is the effective period of the isolated system;

3. MODAL AND LINEAR STATIC ANALYSIS

The analysis models were developed by using Etabs V9.7.2. software (fig. 4). The model contains 1500 shell elements both for walls and vaults, with a meshing step of 0.4m. The difficulties in the modelling process consisted of simulating the geometry of the church, with curved walls and vaults at different levels.
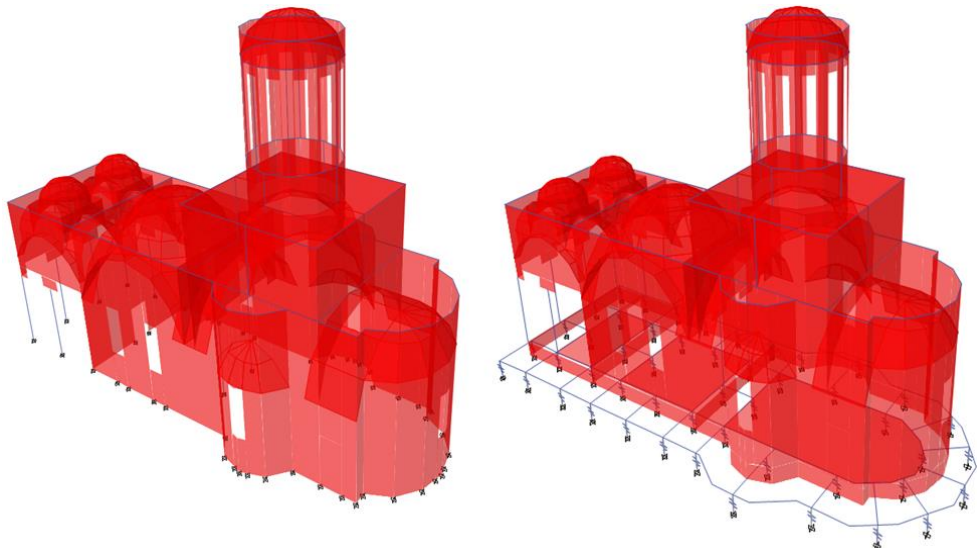

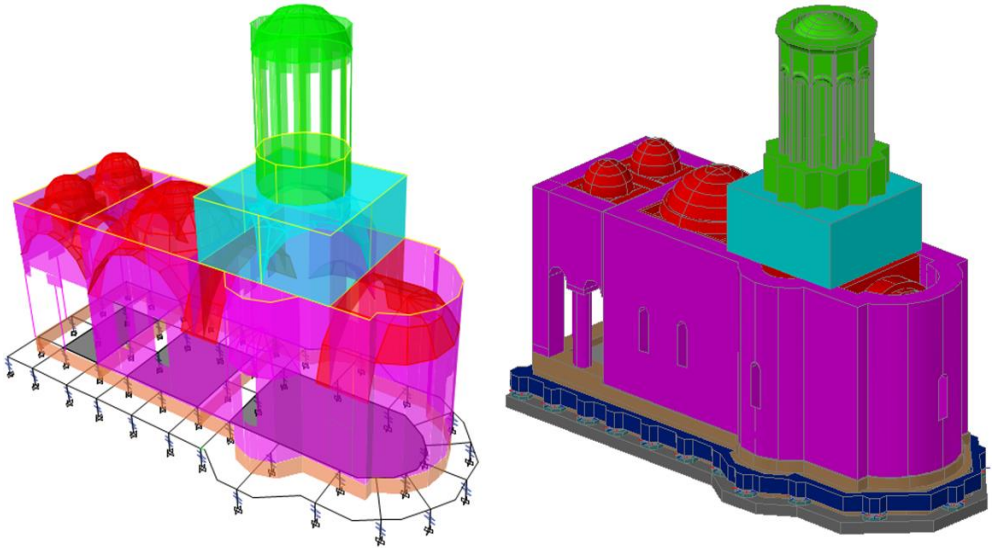Figure 4. Structural analysis of Aroneanu Church

Figure 5. Model calibration

The calibration of the structural model was done by gradual correlation of the own weight loads with the three-dimensional survey of the structure (fig. 5).

$d_{x\text{-}max}=10.2mm$

$d_{y\text{-}max}=34.1mm$
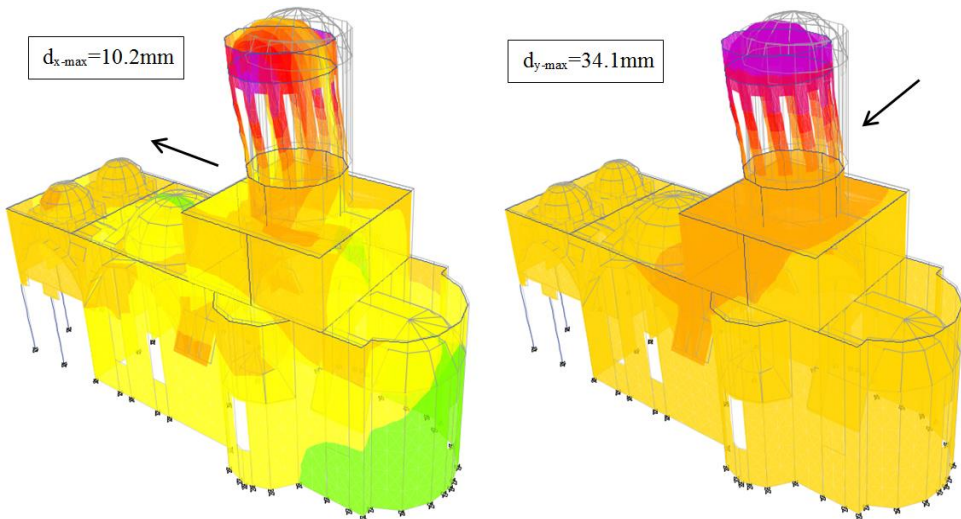
Figure 6. Maximum displacements from linear static analysis of Aroneanu Church with fixed base

The maximum displacement of the structure in the fixed base analysis have resulted at the upper level of the tower, with values of $d_{x-max} = 10.2mm$ in the longitudinal direction and $d_{y-max} = 34.1mm$ in the transversal direction (fig. 6).

In the case of the isolated base analysis, the maximum displacements have been recorded at the base level, with values of $d_{x-max} = 193.5mm$ in the longitudinal direction and $d_{y-max} = 197.6mm$ in the transversal direction, lower than the allowable maximum displacement of the isolators ($d_{max}=250mm$) (fig. 7).
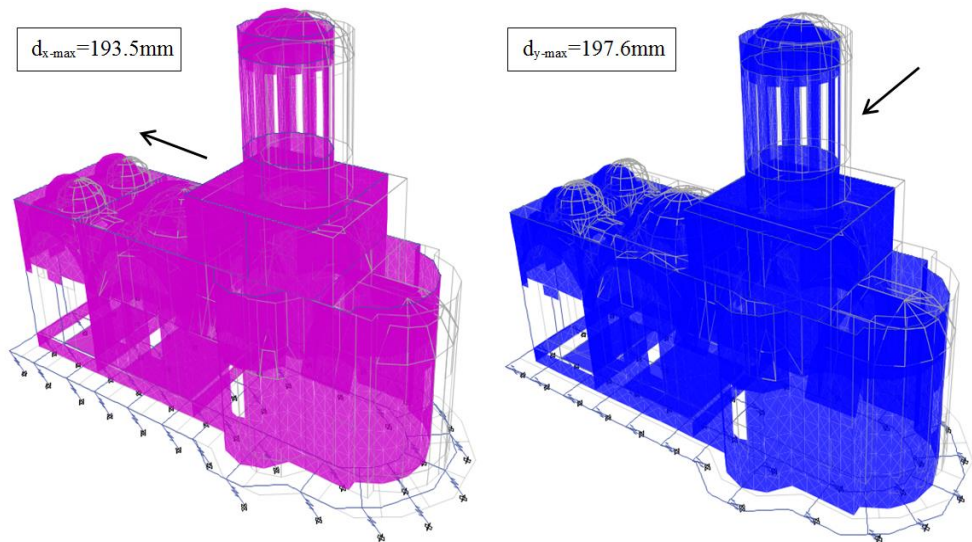
Figure 7. Maximum displacements from linear static analysis of Aroneanu Church with isolated base

2. CONCLUSIONS

Analysing the results from both fixed and isolated base analysis has been observed that modal participation factors for first 2 vibration modes in the case of the isolated base structure is 99% on both directions, whilst in the fixed base case, for the first 4 vibration modes, the sum of the modal participation factors is 51% on longitudinal direction and 70% on transversal direction.

The base shear force is reduced by 45% in the case of the base isolated structure.

The maximum displacements of the structure due to seismic action, modifies from 10.2mm and 34.1mm at upper level of the tower (fixed base) to 193mm and 197mm at the base level (isolated base).

Table 1. Result from both fixed and isolated base structure analysis

Comparison criteria	Direction	Structure	
		Fixed base structure	Isolated base structure
Vibration mode / Period/ modal participation factors	x	2 / 0.22s / 7% 4 / 0.10s / 41%	2 / 2.78s / 99%
	y	1 / 0.26s / 14% 3 / 0.16s / 52%	1 / 2.82s / 99%
Sum of the modal participation factors (first 4 vibration modes)	x	51%	99%
	y	70%	99%
Base shear force	x	2221.64 kN	1165.39 kN
	y	2133.12 kN	1158.10 kN
Relative displacements (base-tower)	x	10.2 mm	0 mm
	y	34.1 mm	0 mm
Base displacements	x	0 mm	193.5 mm
	y	0 mm	197.6 mm

References

1. Stephen J. K., Sendova V., Predrag G., *Seismic Protection of Byzantine Churches*, *5th National Conference on Earthquake*, Chicago, USA (2009).
2. Kelly, James M., *The Application of Seismic Isolation for the Retrofit of Historic Buildings*, *Earthquake Engineering Research Center*, University of California at Berkeley, (2011).
3. Iancu D., Florea I. M., Nicolau M., *Clădire rezidenţială protejată seismic cu izolatori de tip pendul cu frecare*, AICPS Review 1-2/2013.

Seismic Analysis of a Base Isolated Structure

Daniela Oanea (Fediuc), Mihai Budescu

Faculty of Civil Engineering and Building Services, "Gheorghe Asachi" Technical University, Iasi, 700050, Romania

Summary

This paper presents the seismic analysis of a structural model with fixed base and isolated with a multi-stage system made up of four layers of elastomeric bearings.

The steel structure has an opening of 1.4 m, a span of 1 m and a height of 1.5 m. The seismic analysis of structure was performed in SAP2000 program.

The aim of this paper is to study the behavior of the base isolated structure with a multi-stage system, in the case of some artificial accelerograms compatible with the elastic response spectrum for the horizontal components of ground acceleration, in areas characterized by the corner period T_c=0.7s, as recommended by the P100-2013 design norm.

The artificial accelerograms were generated using the ANCO SPECTIME program. The accelerograms are characterized by a peak ground acceleration of 0.3g, a duration of 45 seconds, 2250 steps at equal time intervals of 0.02 seconds.

Following the numerical analyses of the structural model, it was noticed that the effect of seismic actions was reduced for each accelerogram and the multi-stage isolation system can take over large displacements safely.

KEYWORDS: time-history analysis, artificial accelerogram, seismic base isolation, multi-stage system, elastomeric bearing with holes.

1. INTRODUCTION

In literature, many experimental tests regarding multilayer elastomeric bearings are presented (Barbat, et al., 1997), (Connor, 2002). These bearings have high vertical stiffness, a large deformation capacity and are stable. The main characteristic of the multilayer elastomeric bearings consists in obtaining a high isolation period compared to conventional bearings.

The multi-stage system design is more flexible compared to conventional bearings due to the possibility of choosing the bearing dimensions and the number of layers of the isolation system in order to take over the vertical force and to obtain the necessary horizontal frequency. The design displacement is equal to the product

between the displacement of an elastomeric bearing and the number of layers (JNES-RC-2013-1002, 2014), (Murota, et al., 2005).

The aim of this paper is to determine the dynamic characteristics of a base isolated structure with a system consisting of four layers of elastomeric bearings, at different seismic actions corresponding to three artificial accelerograms compatible with the elastic response spectrum for the horizontal components of ground acceleration, in areas characterized by the corner period $T_c= 0.7$ s, according to P100-2013.

2. EXPERIMENTAL MODEL

The experimental model has an opening of 1.4 m, a span of 1 m and a height of 1.5 m. The columns and the beams of the structure are made of INP 80 steel profiles. The steel type is S235JR. The structure is recessed at the base.

The base isolated structure will be unidirectional tested in the opening direction, on the shaking table of the Faculty of Civil Engineering and Building Services of Iasi, fig. 1.

Figure 1. The base isolated structure on the shaking table

The additional mass consists of concrete slabs with dimensions of 1500x700x100 mm, each of them having a weight of 360 kg.

The multi-stage isolation system consists of a metal frame made of HEB 180 steel profiles, with a length of 150 cm respectively 121.5 cm in the other direction, fig. 2.

Figure 2. Multi-stage isolation system with elastomeric bearings

The seismic analysis of the structure was performed for the multi-stage system with elastomeric bearings with nine holes with a diameter of 20 mm. The bearing dimensions are shown in fig. 3.
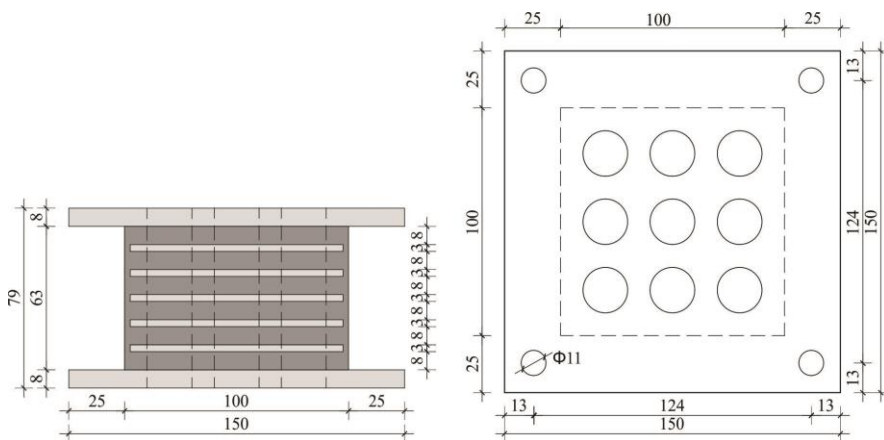

Figure 3. Elastomeric bearings with nine holes

3. TIME-HISTORY ANALYSIS

Time-history analysis is to determine the accelerations and displacements recorded at the isolation system level and at the top of the structure and to evaluate the shear force recorded in the structural elements.

Time-history analysis helps to check and eventually to optimize the chosen bearings after the design process. Time-history for a seismic isolated structure can be achieved in any program that has implemented this type of analysis.

The artificial accelerograms were generated using the ANCO SPECTIME program. In the program, the target response spectrum, the fraction of critical damping $\xi = 5$ %, the duration and the time step that define the accelerogram were introduced.

The imposed elastic response spectrum (red color) and the resulted response spectrum (green color) can be seen in fig. 4
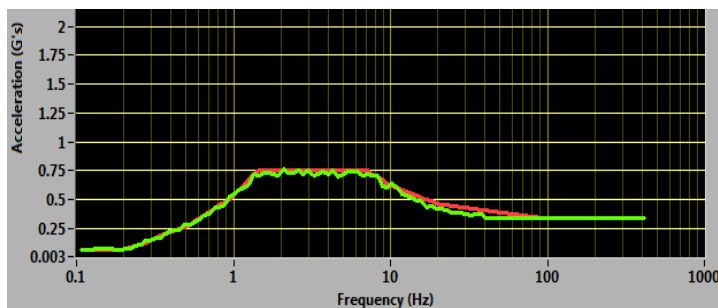
Figure 4. The imposed and resulted response spectrum

According to design standards, a minimum number of three accelerograms were imposed, figs. 5, 6, 7. The accelerograms are characterized by a peak ground acceleration of 0.3g, a duration of 45 seconds, 2250 steps at equal time intervals of 0.02 seconds.

The elastic response spectrum for the critical damping fraction of 0.05 was generated using the PRISM program.

Modal and time-history analyses of the structure were performed in SAP2000 program.

For the modal analysis, three concrete slabs on the top floor of the fixed base structure were considered. A fundamental vibration period of 0.2 seconds was obtained for the fixed base structure.

In the case of seismic isolation, an additional mass (four concrete slabs) was introduced at the base of the structure using beams of UNP 260 steel profiles.
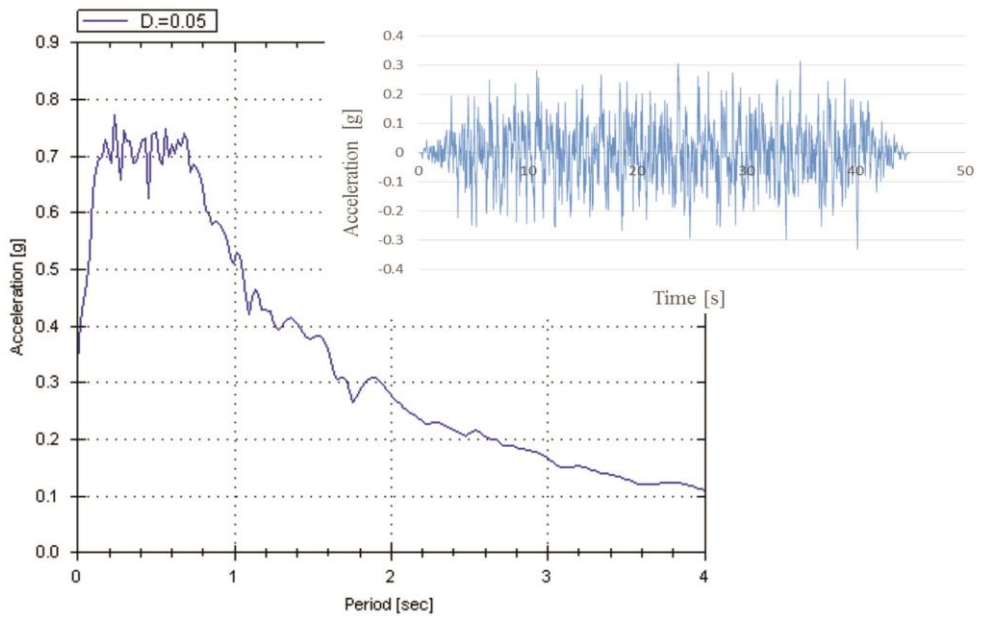
Figure 5. Artificial accelerogram 1 and the response spectrum
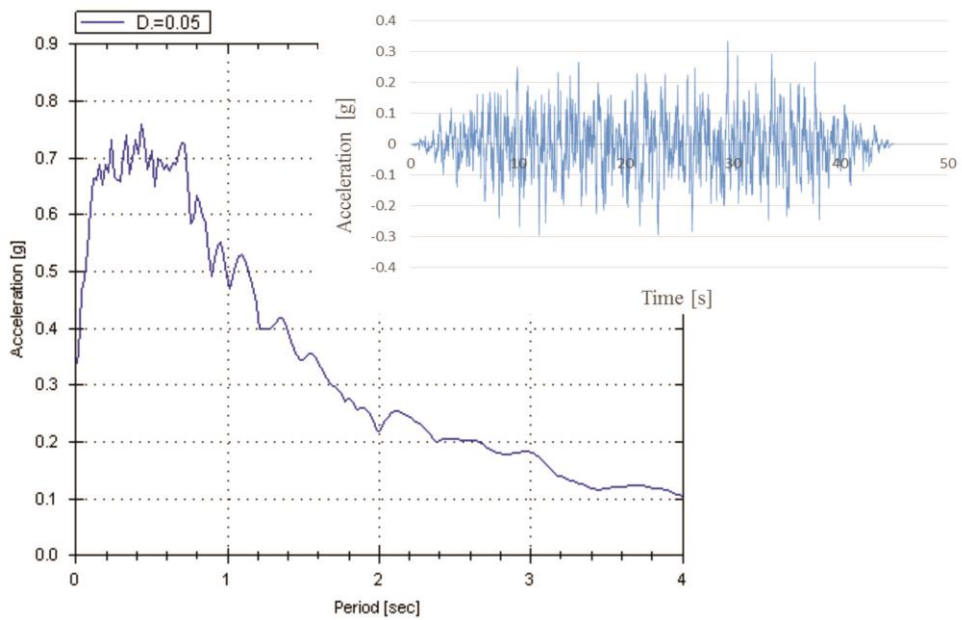
Figure 6. Artificial accelerogram 2 and the response spectrum
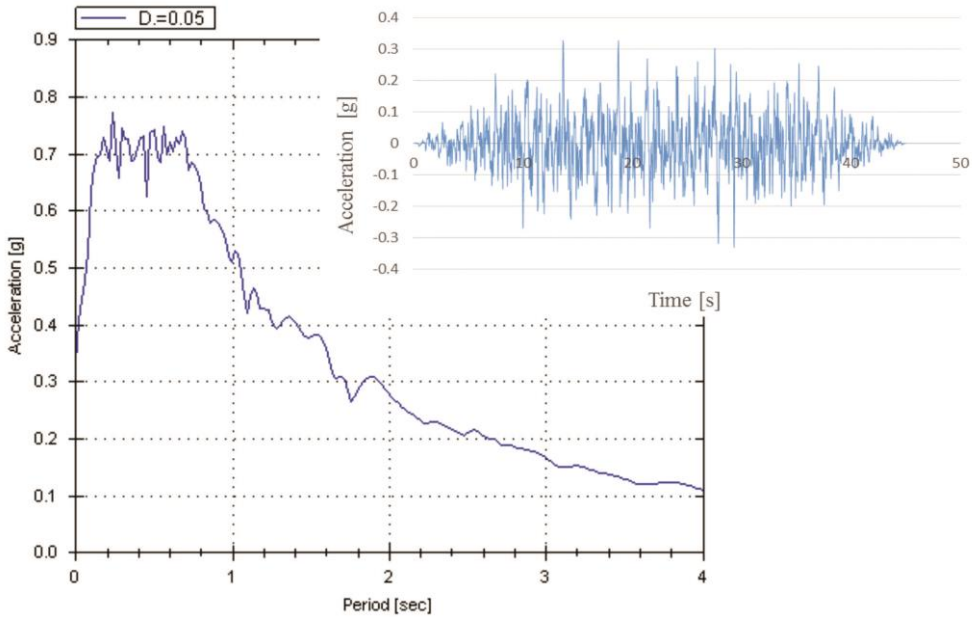
Figure 7. Artificial accelerogram 3 and the response spectrum

A multi-stage system was used for the seismic isolation of steel structure in order to obtain a high vibration period of the isolation system. The elastomeric bearings properties were defined with a Rubber Isolator link provided in SAP2000 program.

A fundamental vibration period of 2 seconds was obtained for the base isolated structure with multi-stage system made up four layers of elastomeric bearings with nine holes. The first three vibration modes of the base isolated structure are shown in fig. 8.
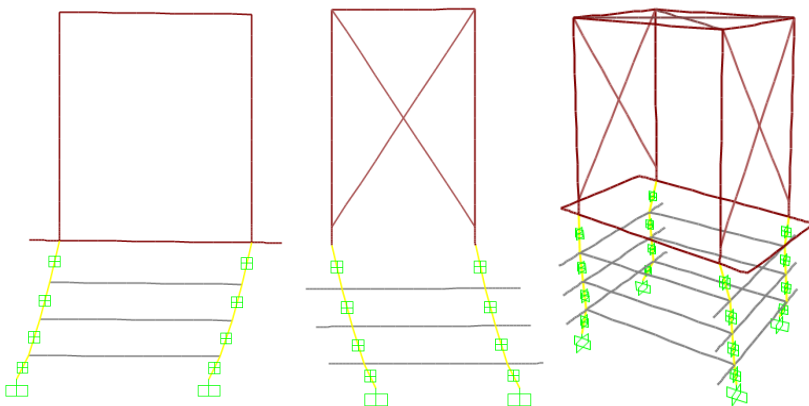
Figure 8. Vibration modes of the base isolated structure

The displacements and accelerations recorded at the top floor of the structure with fixed and isolated base, obtained for the artificial accelerogram 3, are presented in figs. 9 – 12.
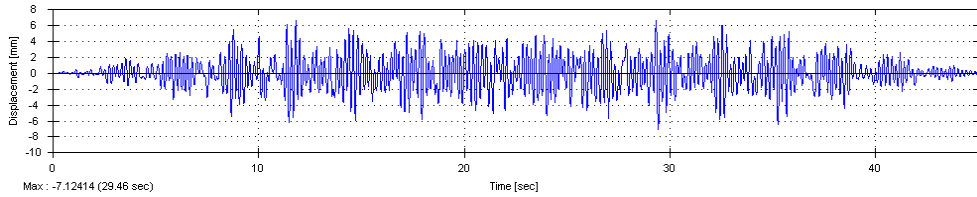
Figure 9. Displacements recorded at the top floor of the fixed base structure
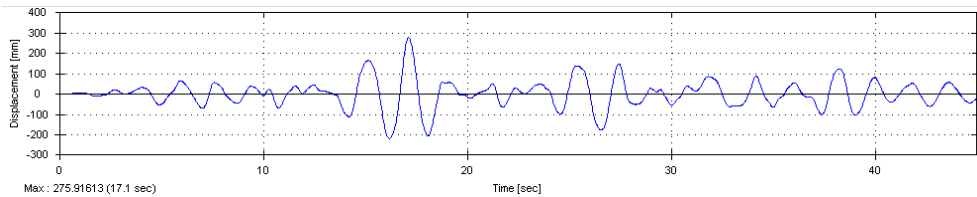
Figure 10. Displacements recorded at the top floor of the base isolated structure
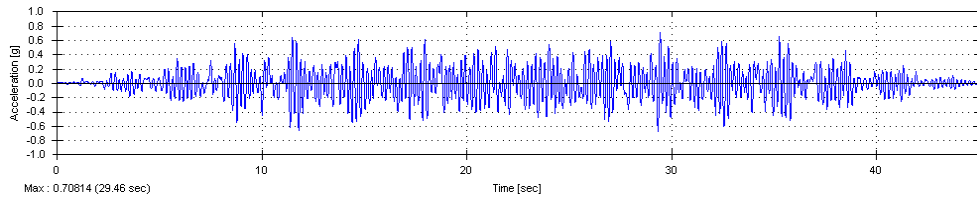
Figure 11. Accelerations recorded at the top floor of the fixed base structure
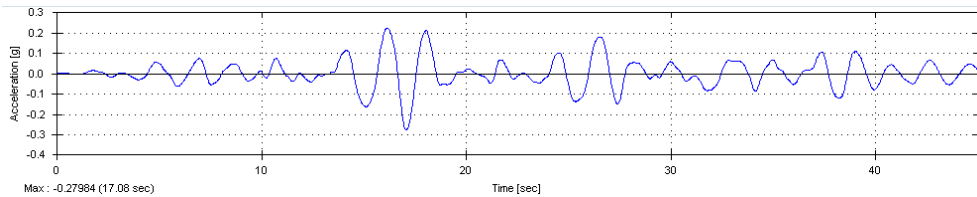
Figure 12. Accelerations recorded at the top floor of the base isolated structure

4. CONCLUSIONS

The paper presents the determination of dynamic characteristics of a base isolated structure with multi-stage system, at different seismic actions.

The multi-stage isolation system was used in order to prevent the stability loss of elastomeric bearings at large displacements and to make the system more flexible.

Three artificial accelerograms compatible with the elastic response spectrum for the horizontal components of ground acceleration, in areas characterized by the corner period $T_c= 0.7$ s, were generated.

Following the numerical analyses of the structural model, the accelerations recorded at the top of the fixed and isolated base structure were compared. In the seismic isolation case, the values of accelerations resulted by 2.5 times lower for accelerograms 1, 3 and 3 times lower for accelerograms 3.

The displacement and acceleration values at each level of the seismic isolated structure resulted approximately equal, the structure having a rigid body displacement.

In the case of base isolated structure with multi-stage system with four layers of bearings, a vibration period of ten times higher was obtained compared to the fixed base structure.

Considering the obtained results, the multi-stage isolation system can take over large displacements safely and is stable compared with the classical system.

References

1. Barbat, A.H., Bozzo, L.M., Seismic analysis of base isolated buildings, *Archives of Computational Methods in Engineering,* vol. 4, 2, 1997.
2. Connor, J.J., *Introduction to Structural Motion Control*, Pearson Education Inc., New Jersey, 2002.
3. JNES-RC-2013-1002, *Proposal of Technical Review Guidelines for Structures with Seismic Isolation*, Japan Nuclear Energy Safety Organization, Japonia, 2014.
4. Murota, N., Feng, M.Q., Liu, G.Y., *Experimental and Analytical Studies of Base Isolation Systems for Seismic Protection of Power Transformers*, Multidisciplinary Center for Earthquake Engineering Research, California, 2005.
5. P100-2013, *Cod de proiectare seismică, Partea I: Prevederi de proiectare pentru clădiri*, Universitatea Tehnică de Construcții București, 2013. (in Romanian)

Parametric Study for Seismic Response of Dual Steel Frames with Dissipative Steel Panels

Calin Neagu[1], Florea Dinu[1] and Dan Dubina[1]

[1] *Department of Steel Structure and Structural Mechanics, Politehnica University Timisoara, Romania*

Summary

Present study investigates the parametric response of dual steel frames that consist of steel plate shear walls and moment resisting frames.

The parametric study was carried out using numerical models which were validated against experimental tests. Sap2000 was used to replicate the test results in order to validate the numerical models. The numerical model was applied to conduct incremental dynamic analyses on a 6 story SPSW frame in order to determine its seismic response. In the analysis two types of soil conditions and seven different ground motion records were taken into account. The main objective was to estimate the behaviour factor q, which is used in seismic design of such structures. Summary of investigations and main results will be presented

KEYWORDS: dual frames, dissipative panels, nonlinear dynamic analysis, q factor.

1. INTRODUCTION

The structural system using steel plate shear walls (SPSW) for lateral resistance had a major development worldwide with the introduction of design rules in North American and Japanese codes. The lack of design provisions in European seismic code EN 1998-1 [1] made difficult the application of the system. In the absence of such design provisions, other design codes (e.g. AISC 2010 [2]) could be used as reference, but this is not very straightforward.

The economic cost and construction efficiency of the system represent two advantages of such structural systems. The detailing of the infill panel to bordering elements can be done using fillet welds or bolted connections. When bolted connections are used, the construction time may be reduced and there is a possibility of plate replacement after an earthquake. This represents a recent development in the field, where dissipative elements may be designed and detailed to be replaced after an earthquake [3]. This requires special design and detailing conditions and may reduce the cost of intervention for low to moderate

earthquakes. In most cases, replacement is conditioned by the re-centering capacity of the dual system.

In order to address the issues presented above with regard to the performances of SPSW systems, a research program, including experimental and numerical studies, was developed at Politehnica University Timisoara, Laboratory of Steel Structures. The experimental study was performed on dual SPSW systems in order to quantify the behavior factor q and to evaluate the re-centering capacity of the system. The numerical studies were performed on dual SPSW structures designed according to Eurocodes. Where necessary, AISC 2010 [2] provisions were employed, also.

The study reported in this paper investigated the performance of a six story SPSW dual structure. The dual structural system used is composed of a moment resisting frame (MRF), two infill panels which are connected to the boundary elements with bolts, and two additional stanchions that are placed as interior vertical boundary elements (Figure 1). This system allows the concentration of damage mainly in the plates. If the flexible MR frames are designed to remain elastic during the earthquake, they provide the restoring force that is necessary to re-center the structure and to allow the replacement of the damaged infill plates.
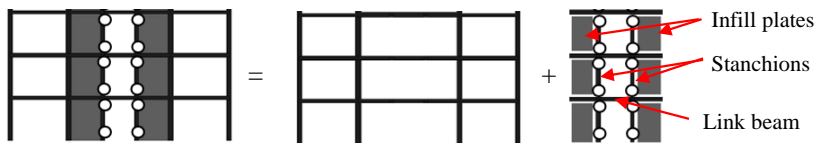
Figure 1. Dual SPSW with MRF, infill plates and stanchions

Non-linear dynamic analyses were employed taking into account two sets of ground motions scaled for two types of spectra corresponding to soft and stiff soil conditions given in EN1998-1 [1]. The numerical models were calibrated and validated against experimental data [3].

2. PARAMETRIC STUDY

2.1. Design of structures

Design of the structure was done according to Eurocodes ([1], [5], [6]) and AISC [2]. According to EN1998 [1], the building site is characterized by a peak ground acceleration of 0.4 g, with a corner period T_C of 0.8 s (Type 1 response spectra and ground type D). A behavior factor of 5 was used for preliminary design of structure. The structure has the configuration presented in Figure 2.a. According to

AISC Seismic Provisions [2], SPSW is first approximated by a vertical truss with equivalent tension braces (Figure 2.b). The cross sections of the equivalent braces need to be designed to meet the lateral drift requirements.

Figure 2. a) SPSW structure; b) equivalent structure with tension diagonals

According to the capacity design principles from AISC [2], the horizontal and vertical boundary elements (HBE and VBE) are designed to resist the maximum forces developed under the tension field action of the fully yielded panels. Axial forces, shear forces, and bending moments develop in the SPSW boundary elements because of the overall overturning, shear, and tension field action in the panels. VBEs and HBEs should remain essentially elastic under the forces generated by fully yielded plates, but flexural hinges are allowed at the ends of HBEs. To prevent excessive deformation, leading to premature buckling under the pulling action of the plates, the minimum moment of inertia of the columns was calculated. After the equivalent structure with the vertical truss was designed and configured, the braces were replaced by steel panels. For an assumed angle of inclination α of the tension field (taken as 45°) and using the area of the equivalent braces, the thickness of the plates was calculated (see [3]).

The geometry and section of frame members are shown in Figure 3. The exterior bays measure 6 m, the interior bay measure 8 m and has two braced spans of 2.8 m long. The story height is 3.5 m. The beams, stanchions and columns were designed using S355 steel, which has a nominal yield strength f_y of 355 N/mm^2. The plates were designed using S235 steel, which has a nominal yield strength f_y of 235 N/mm^2. European IPE and HEB hot rolled profiles were used for beams, columns and stanchions (see Figure 3).
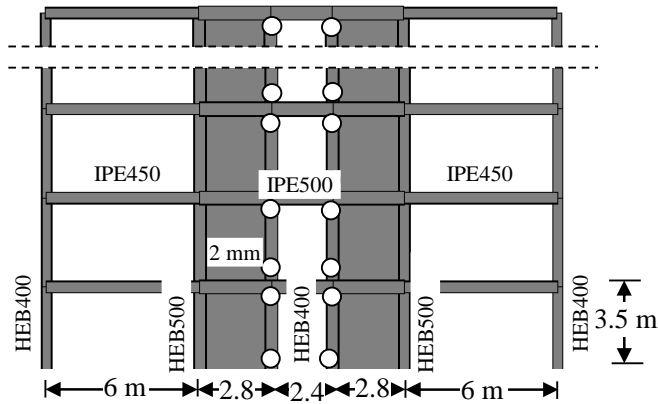
Figure 3. Six story building frame

2.2. Analysis procedure

A non-linear incremental dynamic analysis (IDA) was employed in order to estimate the seismic response of the SPSW system. Two type of soils were taken into account, i.e. soft soil (type D) and stiff soil (type A) (Figure 4), and seven different ground motion records for each type of soil.

Each ground motion record was scaled to the linear-elastic 5%-damped spectral acceleration between $0,2T_1$ and T_1 (where T_1 is the fundamental period of the structure) to match the target spectrum (Type A and D spectra, see Figure 5). Note that the first three periods of the structure are $T_1=0.61$ sec, $T_2=0.18$ sec and $T_3=0.08$ sec. In the incremental dynamic analysis, the ground motion records were scaled to several intensities (using factor λ) until the attainment of numerical non-convergence (dynamic instability, DI) or other limiting criteria are attained (e.g. exhaustion of plastic deformation capacity in elements). Three performance levels were considered, i.e. serviceability limit state (SLS), where the intensity of ground motion is scaled by $\lambda =0.5$, ultimate limit state (ULS) with intensity factor $\lambda=1.0$ and collapse prevention limit state (CPLS) with intensity factor of $\lambda=1.0$.
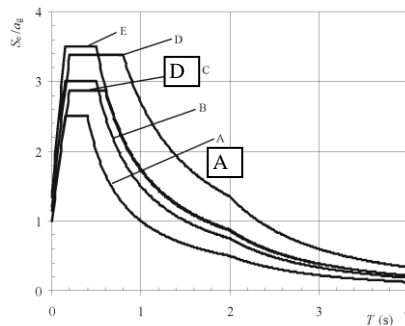
Figure 4. Type 1 elastic spectrum according to EN1998 [1]

(a)   (b)
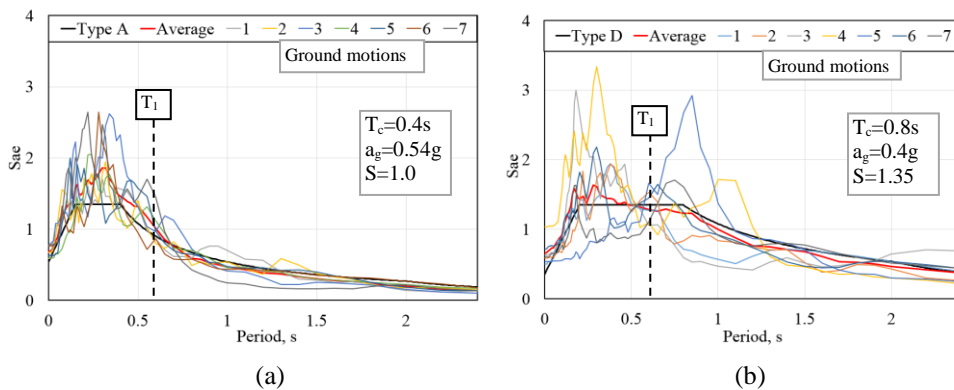
Figure 5. Scaled records: a) type A elastic spectrum; b) type D elastic spectrum

2.3. Validation of numerical model

The Finite Element Model used for the IDA analysis is detailed in [3] and [8]. The numerical model was validated against experimental test results. The test specimens were isolated from the second and third story of a 6 story dual SPSW frame structure with the configuration presented in Figure 1. Because of laboratory restrictions, the specimens were downscaled. The experimental frame was 3500 mm height and 4200 mm wide (distances measured between elements centerlines, Figure 6.a). Slender steel panels, with plate thickness of 2 mm, ratio L/t_w amounting 595 and aspect ratio L/h of 0.8, were used. Typical connections used for the experimental specimens are presented in Figure 6. Extended end plate bolted connections were used to join beams and columns. The joint was considered rigid and partial strength ($M_{j,Rd}=0.9M_{b,Rd}$) (according to EN1993-1-8 classification [6]) (Figure 6.b). For the connection of the plates to the boundary elements, 8.8 class preloaded bolts and 6 mm fish plates were used. Additional fishplates of 4 mm

were added in order to strengthen the plate and reduce the number of bolts (Figure 6.c).

(a)   (b)   (c)
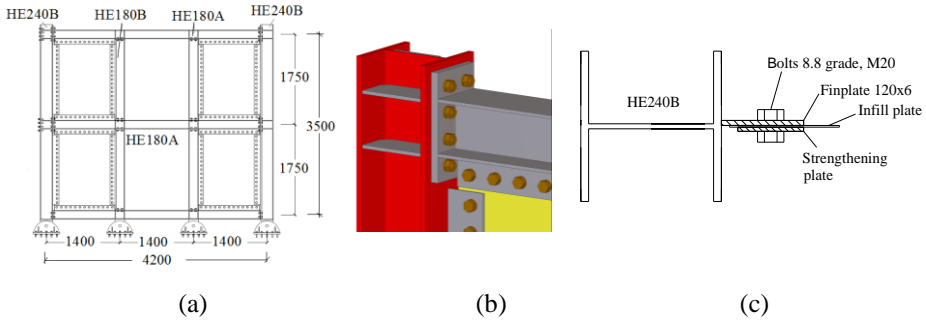
Figure 6. a) Experimental specimen; b) beam-to-column joint; c) plate to boundary elements connection

The specimen was subjected to increasing cyclic loading until failure, according to ECCS loading protocol [Figure 7.b] [9]. Two actuators with 360 mm stroke and 1000 kN and 500 kN capacity, respectively, were used, one at each story [Figure 7.b]. To note that a monotonic test is first required for evaluating the yielding displacement that is used as loading parameter in the cyclic test.

(a)   (b)
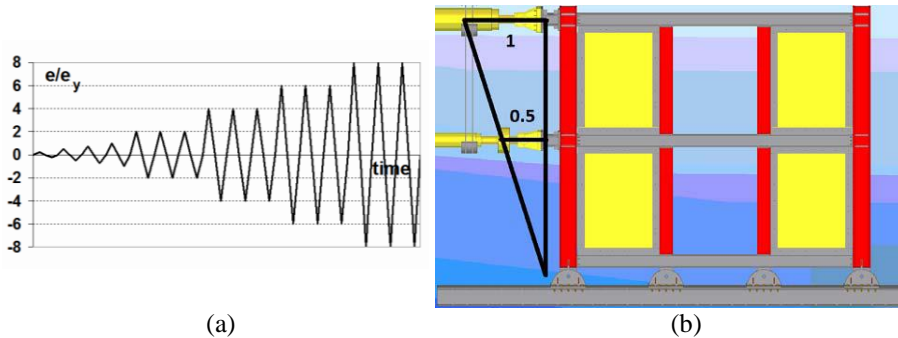
Figure 7. a) Loading protocol; b) Test set-up

Figure 8 shows the monotonic (a) and cyclic (b) response of the specimen in terms of base shear force versus top displacement. Due to the high plate slenderness (2 mm thickness), the shear buckling occurred at relatively low levels of drifts, at approximately 0.4%. After buckling, the lateral load was carried through the tension field developed in the panel. The infill plates yielded first at 0.9% inter-storey drift (Figure 8, point a). The specimen could withstand drifts of almost 6% before the drop in strength (point b).

The numerical models have been validated against the monotonic and cyclic tests. The numerical model for monotonic analysis predicted with good accuracy the entire behaviour of the system, including the softening branch, see Figure 8.a. The small differences can be attributed to imperfections in testing set-up and contribution of beam to column connections (gusset plate effect). Using pivot hysteretic type hinges for strips, it was possible to predict the overall cyclic behaviour also, including the degradation of the plates and pinching effect, Figure 8.b.

(a)   (b)
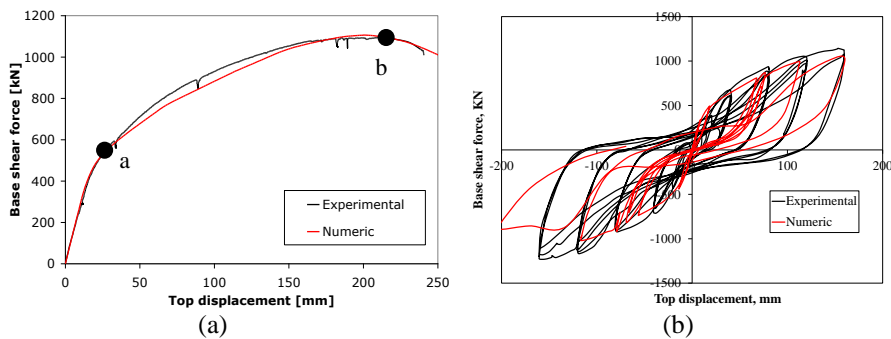
Figure 8. Numeric vs experimental results

2.4. Results

One of the main parameters associated with the global performance of the SPSW systems is the behaviour factor q. The behaviour factor q can be expressed as a product of the ductility reduction factor, q_μ, and the over-strength factor, q_s. The over-strength may vary significantly and is affected by the contribution of gravity loads, material over-strength, structural redundancy, etc. The ductility component q_μ is defined as the ratio between the acceleration multiplier leading to collapse, λ_u, and the acceleration multiplier leading to first yielding, λ_1. The ductility factor is more important when the dissipation capacity is of concern, and will be further investigated.

Figure 9 to Figure 12 show the development of plastic hinges and the inter-story drift ratios for the 6 story structure. In this paper is presented only the plastic mechanisms for the 2nd and 4th ground motions (see Figure 5), while the corresponding inter-story drifts are shown in comparison for the two types of soil conditions.

In case of 2nd ground motion, at ultimate limit state the plastic hinges are mainly developed in plates, with very small damage in moment resisting frame for soft soil conditions. This indicates that the frames remained in elastic domain and poses the restoring force that is required to re-center the structure and to replace the damaged

panels. At collapse prevention limit state, the damage is initiated in the frame also for both type of soils, and is larger for soft soil conditions (see Figure 9).

(a)

(b)
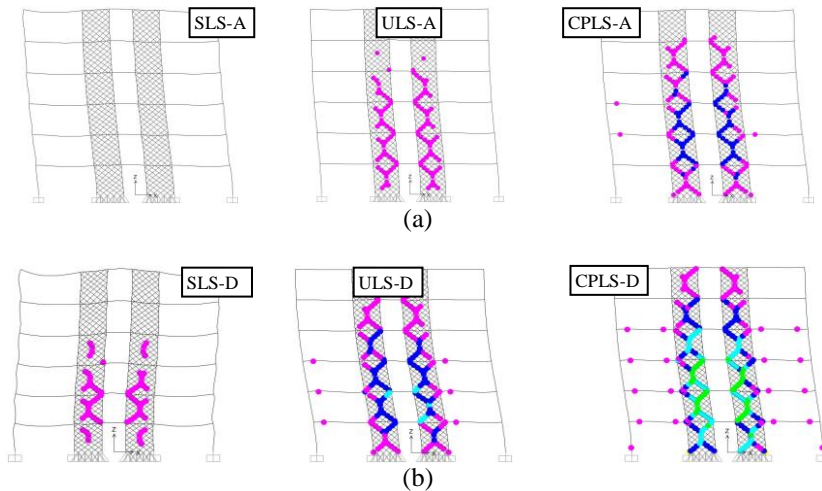
Figure 9. Plastic mechanism for 2nd ground motion: a) stiff soil; b) soft soil
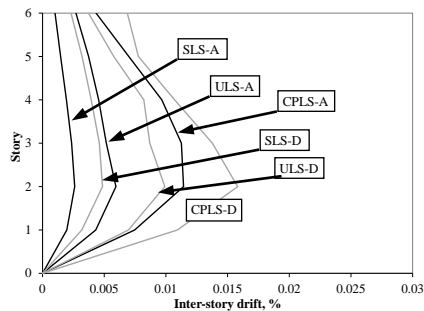
Figure 10. Inter-story drift ratio for the two types of soils

In case of 4th ground motion, for stiff soil conditions the damage is concentrated mainly in plates, frame does not present any damage until CPLS, indicating that the structure has re-centering capacity (Figure 11.a).

(a)

(b)
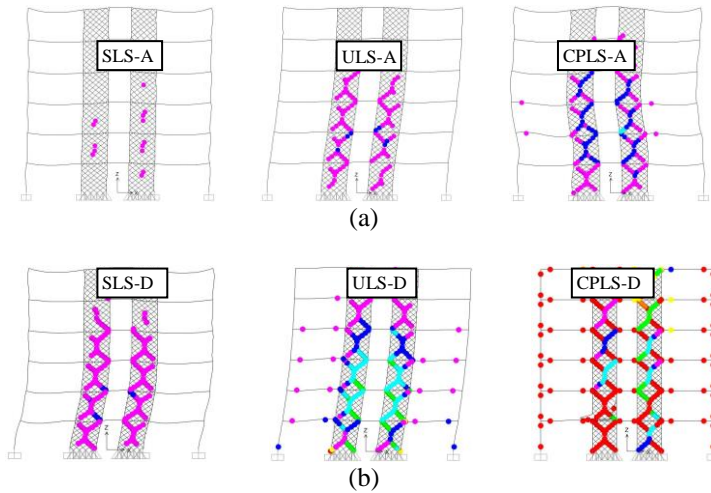
Figure 11. Plastic mechanism for 4th ground motion: a) stiff soil; b) soft soil

In case of soft soil conditions, plastic hinges are developed at ULS in plates and frame elements (beam and columns), which show that the frame does not have enough re-centering capacity. (Figure 11.b).
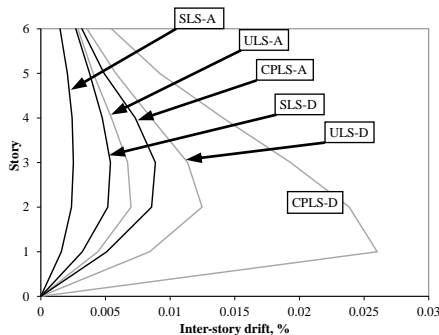
Figure 12. Inter-story drift ratio for the two types of spectra

For soft soil condition, the structure exhibits larger drifts compared to stiff soil conditions (see Figure 10 and Figure 12). One can observe an amplification of effects in case of soft soil conditions (Type D spectrum), and concentration of damages in the lower half of the structure (Figure 10 and Figure 12).

Table 1 present the plastic rotations in hinges developed in beams (B) and columns (C) at the three limit states for the seven ground motion.

Table 1. Plastic hinges values for the 7 ground motions scaled to type A spectrum

Soil	Level	1st		2nd		3rd		4th		5th		6th		7th	
		B	C	B	C	B	C	B	C	B	C	B	C	B	C
A	SLS	-	-	-	-	-	-	-	-	-	-	-	-	-	-
	ULS	-	-	-	-	-	-	-	-	-	-	-	-	-	-
	CPLS	-	0.002	0.002	0.001	0.001	-	0.003	0.001	0.001	-	0.001	-	0.001	0.001
D	SLS	-	-	-	-	-	-	-	-	-	-	-	-	-	-
	ULS	-	-	0.004	0.002	-	-	-	0.016	-	-	-	-	-	0.005
	CPLS	-	-	DI	DI	0.003	0.002	DI	DI	0.004	0.003	-	-	DI	DI

Note: B – beams; C- column; DI – dynamic instability;

Figure 13 shows the incremental dynamic analysis curves in terms of inter-story drift ratios and acceleration multipliers for the structure for the two types of soil conditions considered in this study. In case of ground motions scaled to type D spectrum, the structure attains the collapse criteria before reaching collapse prevention limit state for 3 ground motions (2nd, 4th and 7th). In case of ground motions scaled to type A spectrum, the structures attain the collapse criteria well after collapse prevention limit state.
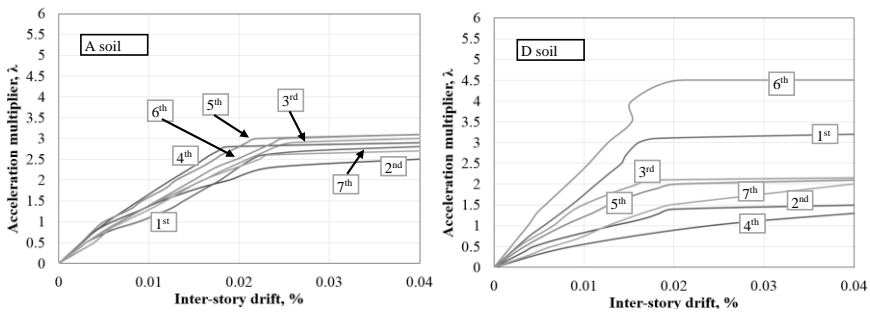
Figure 13. IDA curves for ground motions scaled to type A and D spectra

Table 2 shows the individual values for each ground motion and the average value of the ductility component, q_μ, per type of spectrum. For stiff soil conditions (type A spectrum), the average value of the ductility factor is 4.0, while for soft soil conditions (type D spectrum), q_μ amounts 3.6. The type of ground motion influences the yielding and the ultimate value of the acceleration but the effect on q_μ factor is not very significant.

Table 2. q_μ values

Soil.	Parameter	1st	2nd	3rd	4th	5th	6th	7th	Average
A	λ_l	0.7	0.6	0.8	0.7	0.7	0.8	0.6	**0.7**
	λ_u	2.7	2.3	3.0	2.8	3.0	3.0	2.7	**2.8**
	q_μ	3.9	3.8	3.8	4.0	4.3	3.8	4.5	**4.0**
D	λ_l	0.8	0.4	0.6	0.3	0.6	1.2	0.4	**0.6**
	λ_u	3.1	1.5	2.2	1.0	2.0	4.6	1.3	**2.2**
	q_μ	3.9	3.8	3.7	3.3	3.3	3.8	3.3	**3.6**

To note that, if the average values of the ductility factor are multiplied with the over-strength factor q_s=1.2 used in design, the resulting value of behaviour factor q is around 5, which indicates that the SPSW system has a good ductility and may be designed considering the high dissipation concept.

3. CONCLUSIONS

An extensive numerical simulation program using incremental nonlinear dynamic analysis was employed on 6 story dual SPSW structure with link beams and rigid beam-to-column connection, in order to evaluate the behaviour factor q. A set of seven ground motions and two types of soil (i.e. stiff and soft soil) were taken into account.

The results of the numerical analyses showed that the type of ground motion affects the response of SPSW structures. The damage in structure is more severe in case of soft soil conditions.

The values of q factor obtained in the numerical study are closed to those reported experimentally (see [3]) and confirm that SPSW structures can be classified as highly dissipative structures.

However, further studies are required for a complete validation of behaviour factor q.

Acknowledgements

References

1. EN 1998-1, "Eurocode 8: Design of structures for earthquake resistance - Part 1: General rules, seismic actions and rules for buildings", CEN, 2004.
2. ANSI/AISC 341-10, "Seismic provisions for structural steel buildings", American Institute for Steel Construction, 2010.
3. Dubina Dan, Dinu Florea, "Experimental evaluation of dual frame structures with thin walled, steel panels", Thin Walled Structures, 78, 2014.
4. Neagu C., "Multi-storey building frames stiffened with dissipative shear walls", PHD Thesis, Ed. Politehnica, pp 193, University Politehnica Timisoara, Romania, 2011.
5. EN 1993-1-1, "Eurocode 3: Design of steel structures - Part 1-1: General rules and rules for buildings", CEN, 2005.
6. EN1993-1-8, "Eurocode 3: Design of steel structures, Part 1-8: Design of joints", CEN, 2005.

7. Vamvatsikos, D. and Cornell, C.A. "Incremental Dynamic Analysis", Earthquake Engineering and Structural Dynamics, 31(3): 491-514. 2002.
8. Dubina D., Dinu F., "Experimental evaluation of dual frame structures with thin-walled steel panels", Thin-Walled Structures, Vol. 78, pp 57-69, 2013.
9. ECCS 1985. Recommended Testing Procedures for Assessing the Behavior of Structural Elements under Cyclic Loads. *European Convention for Constructional Steelwork*. Technical Committee 1, TWG 1.3 – Seismic Design, No.45, 1985.

On Energy Dissipative Columns

Vasile-Mircea Venghiac[1] and Mihai Budescu[1]

[1] Department of Structural Mechanics, "Gheorghe Asachi" Technical University of Iaşi, 700050, România

Summary

Taking into consideration the devastating effect of earthquakes on human lives, the problem regarding the anti-seismic protection of buildings has become a very important and of interest subject in Civil Engineering. In this paper a series of innovative energy dissipation devices is presented. These devices are yielding metallic dampers and friction dampers, proposed by the author to be used for the anti-seismic protection of steel frame buildings with Slimdek composite floors or with flat slabs. The devices are called "energy dissipative columns" or EDC. The EDC absorbs the seismic energy through the plastic deformation of steel dissipative elements. The numerical analyses and the experimental tests carried on the shaking table outline their advantages and increased protection against big earthquakes.

KEYWORDS: yielding metallic dampers; friction dampers; composite floor; anti-seismic design.

1. INTRODUCTION

Earthquakes are among the most destructive phenomena on earth. The great destruction potential is due to the energy released by the earthquake, energy which can be thousands or tens of thousands larger than the energy released by an atomic bomb. Annually human lives and material assets are lost, activities and services for maintaining social relations are disturbed due to these phenomena. Thereby, seismic protection is a very important aspect in structural design and is a subject studied worldwide.

Seismic design of structures provides certain performance criteria relating to the capacity of buildings to dissipate the seismic energy in a steady state and for as many motion cycles as possible. The current design theory is based on the acceptance of plastic zones occurrence in structural elements, but the design should be oriented so as to avoid structural collapse. Plastic zones, which in the case of bars become plastic hinges, have the ability to dissipate energy through various phenomena, such as friction and plastic deformation of steel. Plastic hinges are

designed to develop only in the main beams, avoiding their occurrence in columns which obviously would facilitate the creation of collapse mechanisms within the structure.

In recent years many methods for energy dissipation appeared by placing special devices within the structure. These devices can be designed to take over the motion given by the wind and also the seismic action. Their use eliminates the need for repair and strengthening of structures damaged after a major earthquake. Due to their beneficial effects of energy dissipation these devices quickly spread worldwide, becoming an essential solution for seismic protection of structures.

There are types of buildings whose structure eliminates the occurrence of plastic hinges in beams. Frame structures with Slimdek composite floors or with flat slabs are such cases. The special design of Slimdek floors is described in chapter 2. Since these floors increase the risk of developing plastic hinges in columns, the necessity for energy dissipation devices appears.

2. SLIMDEK COMPOSITE FLOORS

Composite floors are widely used for offices, leisure and recreation, airport terminals, hotels, schools, residential, retail, renovation and hospitals mainly for their advantages.

In recent years, a new type of composite floor has been introduced by Tata Steel (the former Corus Ltd). It is called Slimdek and it comprises the following components: Asymmetric Section Beams (ASB) [1] and SD Decking. For example, the 225 mm deep and 1.25 mm thick galvanised cold rolled steel deck profile is capable of spanning up to 6.5 m un-propped and up to 9 m propped [2, 3]. The decking rests on the bottom flange of the beam [4] as shown in Figure 1.

Slimdek has several features that offer significant advantages:
- ▪ service integration. A continuous horizontal service duct 160 mm deep and 320 mm wide can be accommodated within the depth of the slab;
- ▪ composite action without shear stud connectors;
- ▪ savings in fabrication costs;
- ▪ fire resistance. Slimdek can eliminate the need for passive fire protection;
- ▪ thermal capacity. The profile of the deck and thermal capacity of Slimdek provide simple options for natural ventilation, night time cooling and air circulation within the ribs of the profile [2, 5].
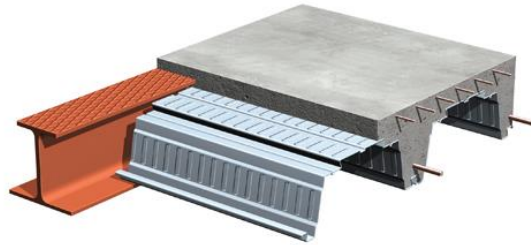
Fig. 1. Slimdek composite flooring system. [5]

The problem when adopting this system in seismic areas is that plastic hinges cannot develop in the beams of the Slimdek composite floor, making this system similar to flat slabs. The seismic energy must be absorbed by using damping devices. The author proposes a new type of damper called "energy dissipative column".

3. ENERGY DISSIPATIVE COLUMNS

The main purpose of installing energy dissipation devices in structures is to control the structural seismic response in order to increase the safety and to reduce structural damage. The effectiveness of damping devices in improving the seismic performance of a structure is a function of several variables including their number, their location in the structure and their physical parameters. This is clearly outlined in the equation of motion of an N degree of freedom structure with supplemental energy dissipation devices subjected to ground excitations at its base during an interval of time t between 0 and t_f. This equation is written as Equation 1:

$$\mathbf{M}\ddot{\mathbf{u}}(t) + \mathbf{C}_s\dot{\mathbf{u}}(t) + \mathbf{K}_s\mathbf{u}(t) + \sum_{k=1}^{n_l} \mathbf{r}_k n_k P_k(t) = -\mathbf{M}\,\mathbf{E}\,\mathbf{f}(t); \ \ t \in \left[0, t_f\right] \quad (1)$$

where:
   $\mathbf{M}$ is the $N{\times}N$ mass;
   $\mathbf{K}_s$ – structural stiffness;
   $\mathbf{C}_s$ – inherent structural damping matrices;
   $\mathbf{f}(t)$ – a k dimensional vector representing the seismic excitation;
   $\mathbf{E}$ – a $N{\times}k$ matrix of ground motion influence coefficients;
   $\mathbf{u}(t)$ – the N dimensional relative displacement vector with respect to the base;
   $P_k(t)$ – the local force due to a passive damper installed at the kth location. This force is considered through the N dimensional influence vector $\mathbf{r}_k$, with n_k being the number of identical dampers and n_l the number of possible locations for a device in the structure [6].

The concept of "energy dissipative column" is new in Civil Engineering, where columns are designed to be acted in the elastic domain and the energy dissipation occurs in secondary elements especially designed for this purpose. One disadvantage of most seismic dampers is that they are visible inside the structure. Energy dissipative columns solve this problem by absorbing the seismic energy within the column itself, through different mechanisms: either by plastic deformation of steel (metallic yielding) or by dry friction.

These devices are presented in the following sub-chapters.

3.1. Yielding metallic energy dissipative columns

The first yielding steel energy dissipative column, proposed by the author is the unidirectional energy dissipative column or UDC. It consists of two euro profiles placed at a certain distance from each other. The connection between the two profiles is achieved by means of specially shaped metallic plates. These plates are designed to dissipate the seismic energy through inelastic deformations. The shape follows an optimized curve in order to ensure a good distribution of plastic deformations in the entire element. The curved shape is close to a linear curve, which is why some models were created using plates with linear variation section in order to simplify the model and to simplify the manufacturing process of these plates. Several models were created. The models differ by the number and the distribution method of the dissipative plate pairs on the height of the column, as shown in Figure 2.

The performed analyses show that these columns are a good solution for seismic energy dissipation. However, there are some disadvantages, such as:
- the system requires a large amount of material,
- certain construction difficulties may arise,
- these columns do not have equal stiffness on all directions,
- the energy dissipation occurs on one direction.

In order to improve the energy dissipation capacity of these columns, some optimization methods were taken into consideration, such as: increase the dissipative plate number and increase the dissipative plate rigidity [7].

Another energy dissipative column is the multidirectional energy dissipative column, or MDC. MDC, are an improved version of the UDC models. The improvement consists in the use of profiles having the same inertia on all directions. Such sections are the circular hollow sections. Energy dissipation is achieved at the ends of the column, where a weakened cross-section is adopted [8]. The weakening of the cross-section was achieved by drilling holes of different shapes and sizes as shown in Figure 3.
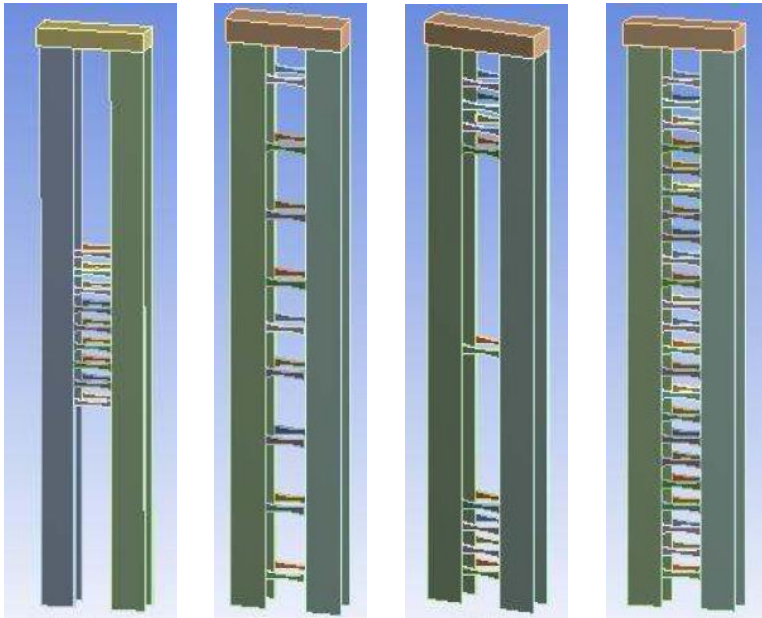
Fig. 2. Unidirectional energy dissipative columns.

a)

b)
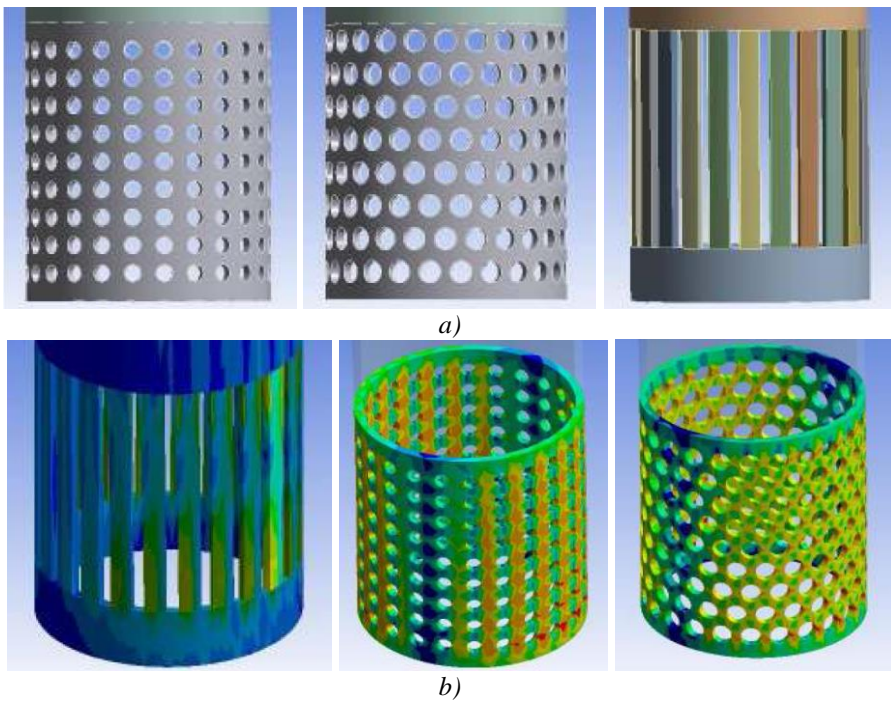
Fig. 3. MDC models: a) geometry, b) von-Mises equivalent stresses maps [8].

The MDC columns solve the problem of unidirectional energy dissipation of the UDC columns, although, due to the weakened sections at the ends of the columns, the MDC cannot overtake gravitational loads. In this case, multidirectional energy dissipative columns with the overtaking of gravitational loads or MDOG have been created. They are provided with special elements at the ends, elements designed to overtake the axial loads and which create the double hinged supports of the column as shown in Fig. 4. The aim is to focus the plastic hinges at the ends of the column, while the central element of the column remains intact [8].

a)

b)
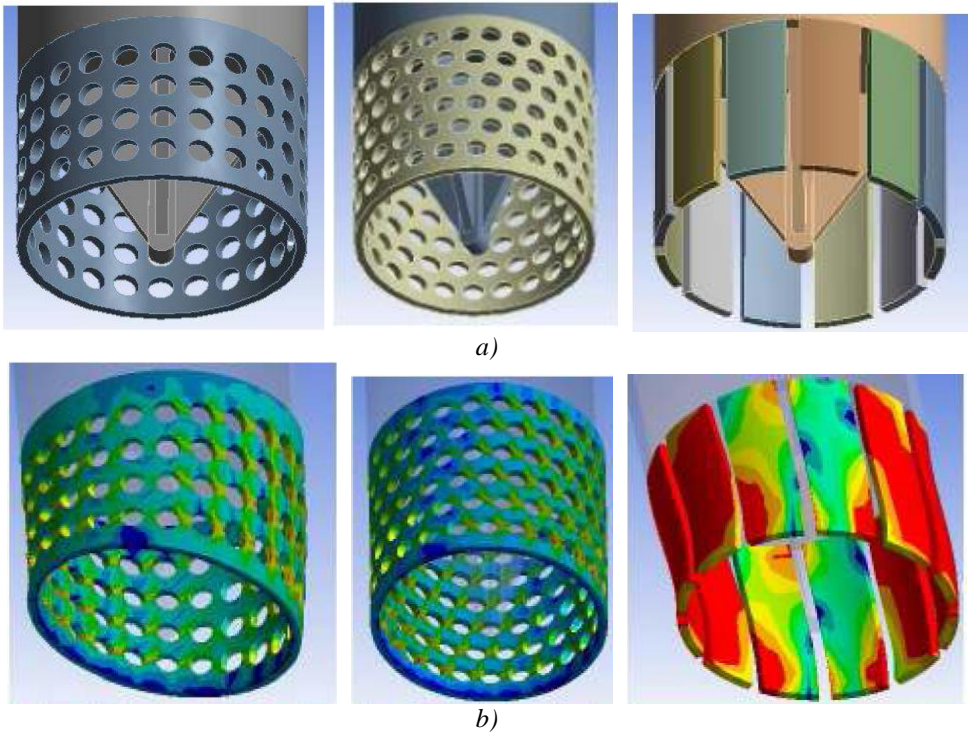
Fig. 4. SDMG models: a) geometry, b) von-Mises equivalent stresses maps [8].

3.2. Dry friction energy dissipative columns

Dry friction energy dissipative columns, or SDF, have a compound section consisting of two euro profiles jointed together with bolts, as shown in Fig. 5. The seismic energy dissipation is realized through the dry friction phenomenon at the interface between the two profiles. The normal force to the slip surface is provided by the pre-stressed bolts.
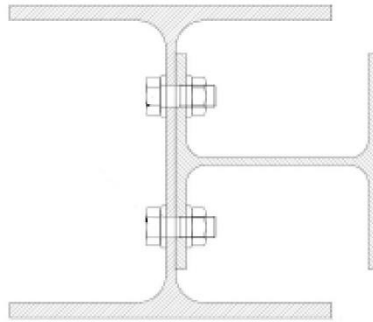
Fig. 5. Dry friction energy dissipative column.

Several analyses were carried out, first taking into consideration the thicknesses of the steel plates that come into contact (the flanges of the euro profiles) and second the finishing of the contact surfaces. This was accomplished by using different values for the friction coefficient, μ, between 0.15 and 0.45 according to SR ENV 1090-1/2003 [9].

An important aspect of the analysis is the influence area created by the pre-stressed bolts, which differs from one model to another due to changes of the plate thickness. The maximum normal stresses increase by up to 67% if the thickness of one plate is halved. In the case of small thicknesses, the influence area is small, but the stresses are high, and in the case of large thicknesses, the influence area is large, but the stresses are much smaller. This makes the dissipated energies to be close in value [10].

3. CONCLUSIONS

Among the yielding metallic energy dissipative columns the SDMG column is the best type. These columns have the best energy dissipation capacity, they can absorb the seismic energy on all directions and have the capacity to overtake the gravitational loads when the dissipating elements lose their structural integrity after a major earthquake. Also, the central element is acted by elastic deformations and the overall stability is satisfied.

In the case of dry friction energy dissipative columns the thickness of the contact elements has no influence on the energy dissipation. However, the stresses that appear at the interface of the contacting plates have large variations depending on the values of the plate thicknesses. If the thickness is small the stresses are large, reaching values in the plastic domain.

In conclusion, the energy dissipative columns are a good solution for the anti-seismic protection of structures with Slimdek composite floors or with flat slabs. The advantages of these devices are: high seismic energy dissipation capacity, capacity of overtaking the gravitational loads when the dissipative elements have lost their structural integrity, the damaged dissipative elements can be replaced after a major earthquake and these devices have the capacity of restricting level displacements.

References

1. Structural Sections to BS4: Part 1: 1993 and BS EN10056:1999, Corus Construction & Industrial, Scunthorpe, United Kingdom, 2005.
2. Slimdek: Engineered Flooring Solution, Corus, 2001.
3. www.corusconstruction.com/en/about_us/panels_profiles/structural_products_systems/comflor/comflor_range/comflor225/ (May 17th 2015).
4. Tsavdaridis, K. D., Agathoklis, G., Derivation of dynamic properties of steel asymetric perforated Ultra Shallow Floor Beams (USFB™) via finite element modal analysis and experimental verification, *7th National Conference on Steel Structures*, 2011.
5. Slimdek Manual, http://www.corusconstruction.com.
6. Moreschi, L.M., *Seismic Design of Energy Dissipation Systems for Optimal Structural Performance*, Dissertation submitted to the Faculty of the Virginia Polytechnic Institute and State University in partial fulfillment of the requirements for the degree of Doctor of Philosophy in Engineering Mechanics, 2000.
7. Venghiac, V.M., Budescu, M. Optimization methods of energy dissipative columns, *Buletinul Institutului Politehnic din Iaşi, Secţia Construcţii. Arhitectură*, Tomul LVII, Fasc. 4, ISSN 1224-3884, 2012, pp. 33-41.
8. Venghiac, V.M. Multidirectional energy dissipative columns, *Proceedings of The 10th International Symposium Computational Civil Engineering – CCE2012*, Editura Societăţii Academice „Matei – Teiu Botez", ISSN 2285-2735, 2012, pp. 402-409, Iaşi.
9. SR ENV 1090-1, Executarea structurilor de oţel. Partea 1: Reguli generale şi reguli pentru construcţii, *Asociaţia de standardizare din România* (ASRO), Bucureşti, 2003 (in Romanian).
10. Venghiac, V.M., Melenciuc, S.C., Ciongradi, I.P., Budescu, M. The influence of solid dry friction damping at columns with compound sections, *Buletinul Institutului Politehnic din Iaşi, Secţia Construcţii. Arhitectură*, Tomul LVII, Fasc. 1, ISSN 1224-3884, 2011, pp. 47-54.

Behavior Factors: a Proposal for RC Framed Buildings Designed According to Current Seismic Codes

Juan Vielma[1], William Lobo[2] and Maria Mulder[1]

[1]Structural Engineering Department, Lisandrro Alvarado University, Barquisimeto, 3001, Venezuela
[2]Civil Engineering Faculty, Los Andes University, Merida, 5101, Venezuela

Summary

Nowadays the seismic design is based on the results of elastic analysis of structures (indeed of the growth of the non-linear based procedures). In order to perform the analysis of structures which are modeled with elastic behavior, although the engineer knows that they could reach plastic behavior, seismic design codes prescribe the reduction of elastic design spectra using response reduction factors. These factors have been formulated based on engineering judgement. In this article it is proposed a new methodology in order to determine these response reduction factors by means of the results of the non-linear response of soils representative of the profiles of the Venezuelan seismic code simultaneously with reinforced concrete structures modeled as multi-degree of freedom systems. Computed values are greater than those the seismic code prescribes, then the design of buildings is controlled by displacements rather strength.

KEYWORDS: Design spectrum, response reduction factor, non-linear analysis, ductility, redundancy, overstrength.

1. INTRODUCTION

The procedure performed to obtain the design equivalent forces is based on the response spectra, which represent the geotechnical characteristics of the buildings' locations. Those spectra are reduced in order to take into consideration the inelastic behavior the structures may reach when are subjected to the action of a strong ground motion. The reduction is obtained using response reduction factors (R), named behavior factors (q) according the Eurocode-8 [1], which were proposed by Veletsos and Newmark [2] in the format that they are applied in most of the worldwide seismic codes.

In the past two decades a large number of works dealing with the study of the response reduction factors were presented [3], some of them were focused into

determinate the components of R. In sake of the brevity, in this work only the ATC-19 [4] approach is referenced among other relevant works:

$$R = \left(R_S \cdot R_\mu \right) \cdot R_R \tag{1}$$

Where R_S is the strength-based reduction component, R_μ is the ductility-based component and R_R is the redundancy-based reduction component. The first two components are time-dependent, while the values of are used to assume a fix value, depending on the structural type. It is important to mention that obtaining values of is a difficult task, so they are usually associated with the strength-based component, in a single factor called overstrength-based component, defined according to:

$$R_\Omega = R_S \cdot R_R \tag{2}$$

2. METHODOLOGY

The new procedure to obtain the response reduction factors is performed in two steps. The first one consists into determine the ductility-based component by means of the procedure formulated by [5, 6, 7], see Equation 3:

$$R_\mu = 1 + \frac{T}{T_g}\left(\frac{\mu}{\beta} - 1 \right) \quad T \le T_g$$
$$R_\mu = \frac{\mu}{\beta} \qquad\qquad T > T_g \tag{3}$$

In this equation T is the period (in sec.), T_g is the characteristic soil period, μ is the design assumed ductility and is a coefficient which depends on ductility and the dynamic non-linear response of the soil. Values of and can be seen in Table 1 and Table 2, respectively.

Table 1. Values of the characteristic period T_g

Soil type	μ=2	μ=4	μ=6
S1	0,12	0,19	0,25
S2	0,22	0,29	0,38
S3	0,34	0,47	0,74
S4	0,60	0,71	0,82

Table 2. Values of the coefficient β

Soil type	$\mu=2$	$\mu=4$	$\mu=6$
S1	1,16	1,29	2,02
S2	1,24	1,35	1,50
S3	1,26	1,27	1,38
S4	1,28	1,27	1,38

Those values are used in Equation 3 for the determination of R_μ for the soil where the building is located. Note in Tables 1 and 2 that the soil profiles correspond to the spectral shapes the Venezuelan seismic code [8] prescribe. Results are shown in Figures 1 to 4 for those soil profiles.
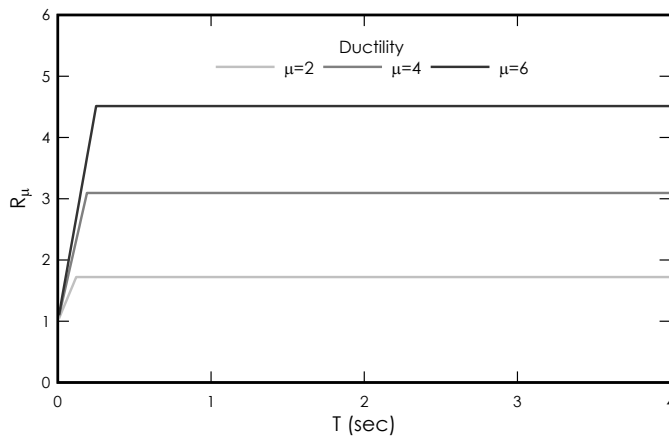
Figure 1. Ductility reduction component for soil S1
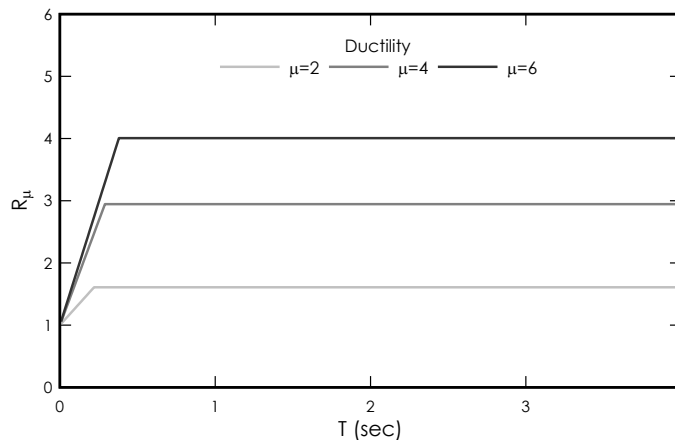
Figure 2. Ductility reduction component for soil S2
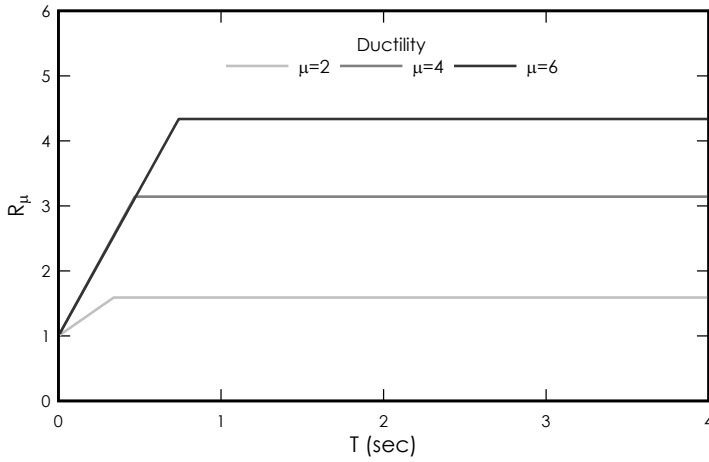
Figure 3. Ductility reduction component for soil S3
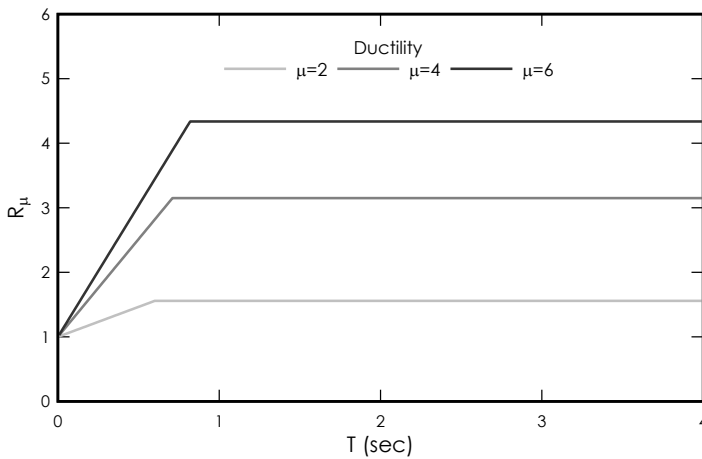
Figure 4. Ductility reduction component for soil S4

The next step consists in to obtain a reliable value for the overstrength component defined according to Equation (2). This goal is matched using the results proposed in , which were computed from non-linear analysis of RC framed buildings with various numbers of spans and stories, designed for high ductility according current codes [9]. Figure 5 shown the resulting values of R_μ plotted vs. the level numbers of the buildings; note the convenience to calculate the mean value in order to apply a unique value for the case studies that are presented in next section.
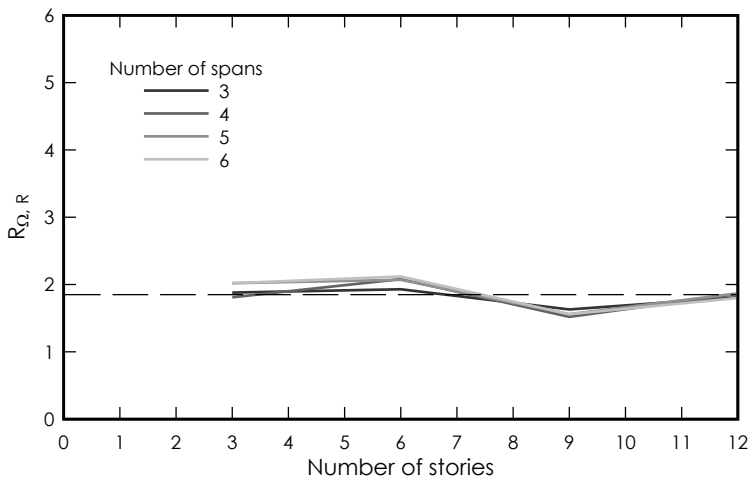
Figure 4. Ductility reduction component for soil S4

2. CASE STUDIED

In order to know how suitably the proposed methodology is, a set of RC regular framed buildings have been designed following the standard procedures the current Venezuelan seismic prescribes and the new methodology. The set consist in four buildings with different number of stories: 3, 6, 9 and 12. Columns and beams have square and rectangular shapes, the floors are two-way 15cm thick solid slabs. Members have been detailing and dimensioning using 25 MPa concrete and 420MPa reinforcement steel (longitudinal and transversal).

Figures 5 and 6 showed the lateral view of the 3 stories building and a typical plan view of the buildings, respectively. Note that the spans are 6,00m long, equispaced in both directions. Seismic parameters specific for a high-level hazard site selected for the analysis are shown in Table 3.

Analysis process requires an initial value for the structural fundamental period. The approximate formulae let to calculate this period using the building total height h_n (in m) and an empirical coefficient C_t which depends on the main material that constitutes the structure:
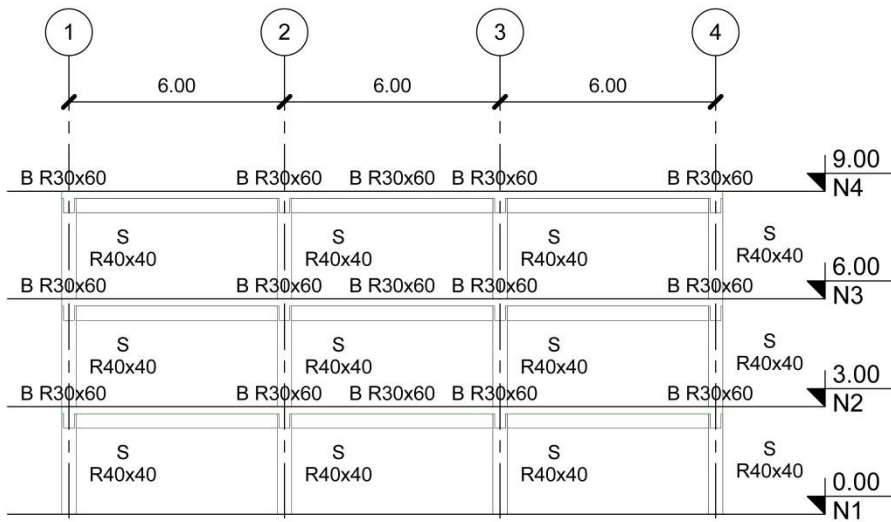
Figure 5. Lateral view of the 3 stories building
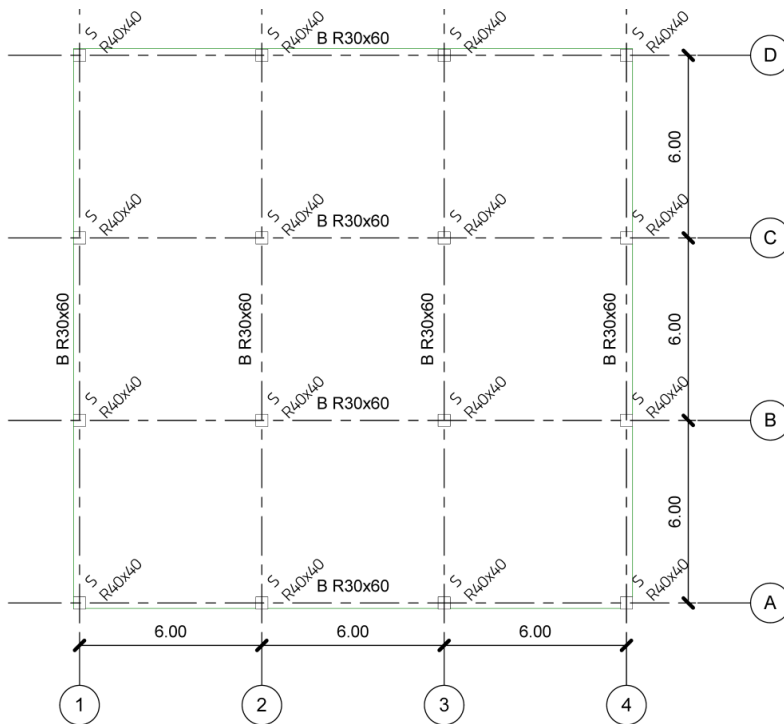
Figure 6. Typical plan view of the buildings

Table 3. Seismic parameters selected for the analysis

Parameter	value
Seismic zone	3
Design acceleration	0,3g
Design level	DL-3
Response reduction factor	6

$$T = C_t h_n^{3/4} \tag{3}$$

Values of the approximate fundamental period are used with the parameters contained in Tables 1 and 2 in order to determine the values of R_μ via Equation (3). Results are summarized in Table 4.

Table 4. Values of the coefficient β

Number of levels	T (sec)	R
3	0,36	7,12
6	0,61	7,42
9	0,83	7,42
12	1,03	7,42

Inelastic spectra are then obtained using those values jointly with the value corresponding to the standard procedure. Figure 7 shows the elastic and inelastic spectra computed according the guidance of the Venezuelan seismic code.
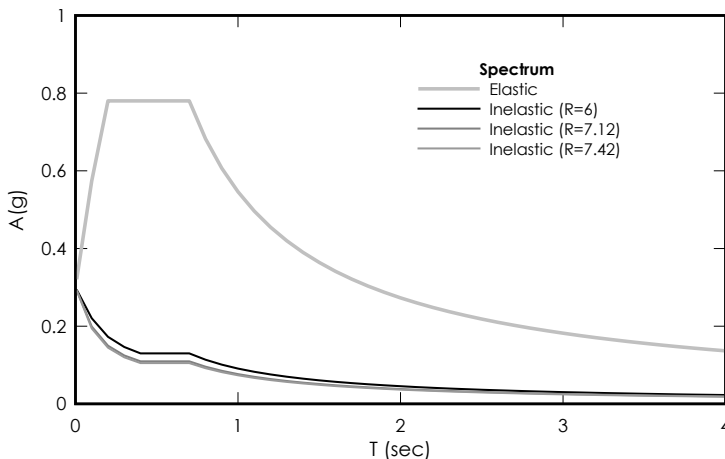
Figure 6. Elastic and inelastic design spectra

Elastic analysis of the models is performed using the forces resulting for modal-spectral analysis for the case of the buildings designed by the code's prescribed procedure and the alternative procedure described above. Derived displacements of

the gravity centers in each floor computed from elastic analysis are then used to compute the inelastic displacements. Note that most of the seismic codes prescribe the amplification of the elastic displacements times R. In the case of the alternative procedure, those displacements are computed using amplification factors derived from energy-based relationships obtained from non-linear response of similar buildings [10, 11]. For buildings whose dynamic response is velocity-dependent, the displacement amplification factor is calculated trough:

$$C_\mu = \frac{\left(R_\mu^2 + R_\Omega^2\right)}{2R_\Omega} \tag{4}$$

While for buildings whose dynamic response is displacement-dependent, displacement amplification factor must be calculated using:

$$C_\mu = R_\mu R_\Omega \tag{5}$$

All the terms in Equation (4) and (5) are the same defined in past section. Inelastic displacements allowing calculating inter-story drifts, in order to check the dimensioning of the whole structure by comparing against a maximum inter-story drift that the code prescribes, 1,8% according to the Venezuelan seismic code. In Figure 7 are shown the inters-story drifts calculated vs. the height, for the three levels building, using standard procedure (Figure 7a) and alternative procedure (Figure 7b).
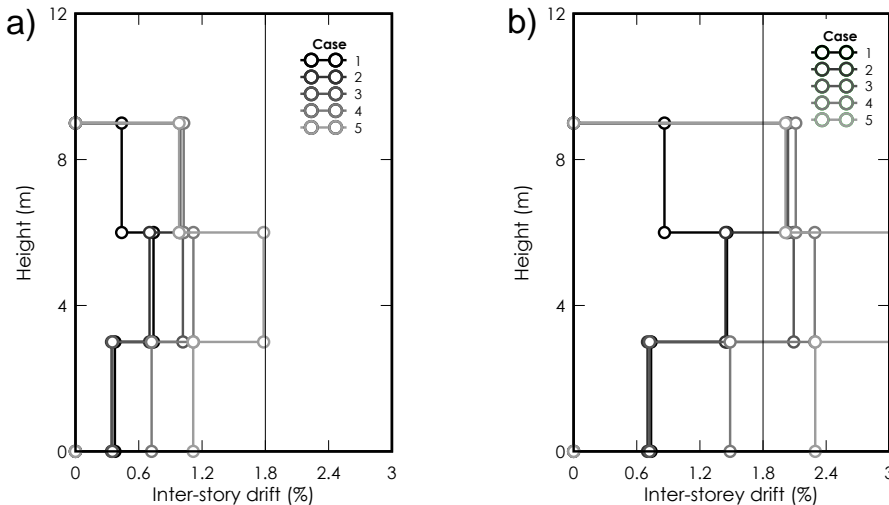
Figure 7. Inter-story drifts of the three levels building

The reader may note that for each procedure five cases have been plotted. Those cases correspond to different building's configurations in which the cross sections

of the columns have been modified in order to satisfy that their interstorey drifts are not greater than the maximum value of 1,8%. Selected configurations received a numeration that range from the most flexible (case 1) to the stiffer (case 5). It is evident the difference between the results obtained with the standard procedure and the alternative one, because in Figure 7a all the cases have interstorey drifts lesser than 1,8%, while from Figure 7b only the case 5 fulfill the adopted criterion.
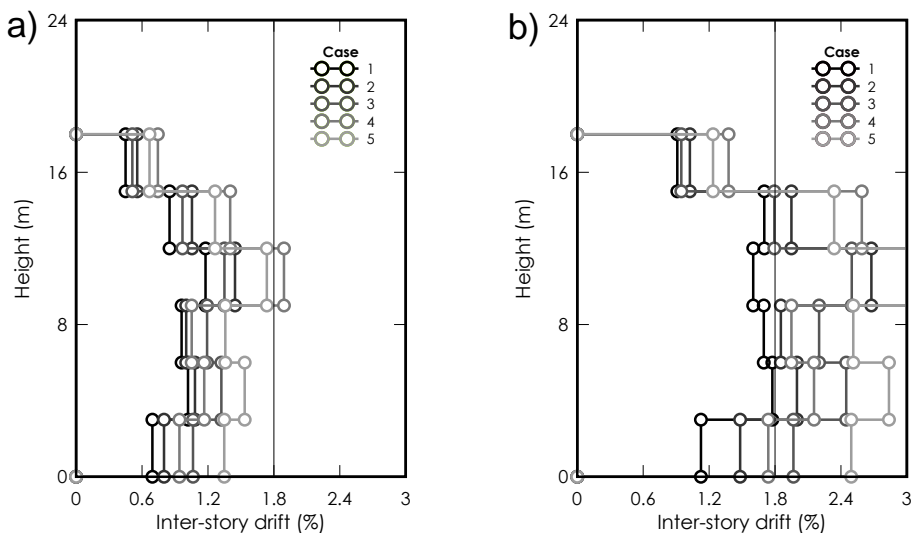
Figure 8. Inter-story drifts of the six levels building
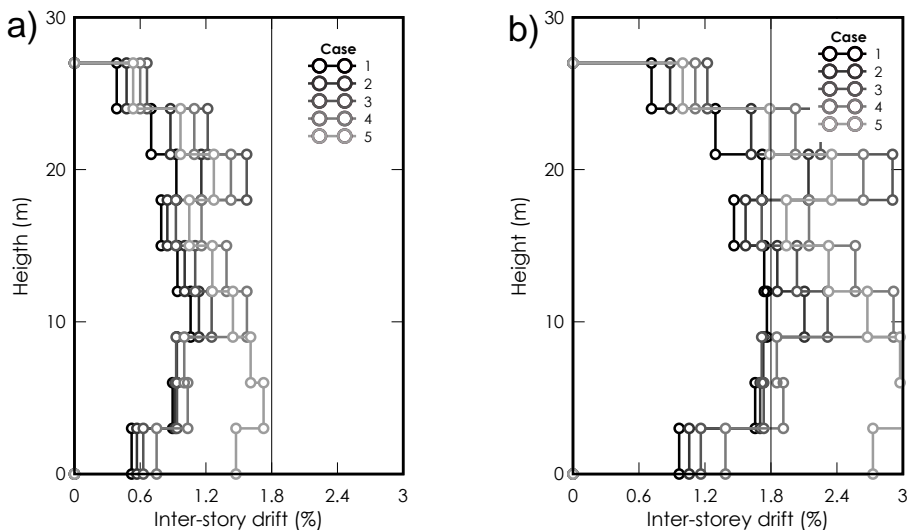
Figure 9. Inter-story drifts of the nine levels building
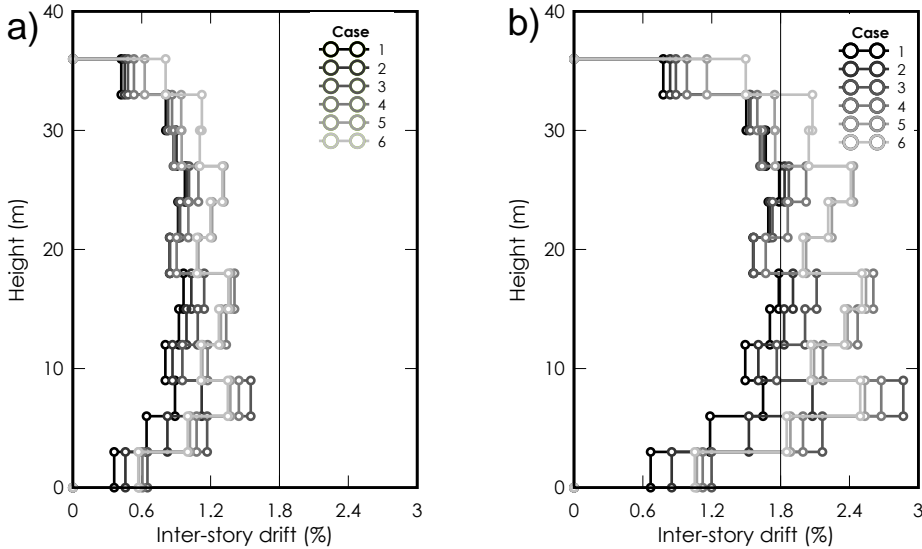
Figure 10. Inter-story drifts of the twelve levels building

Results for 6, 9 and 12 stories buildings can be seen in Figures 8, 9 and 10, respectively. Those figures reveal that according to standard procedure every configuration can be considered for the next stage in the design process: the detailing of structural members. But the resulting longitudinal reinforcement ratio exceed the maximum value that the Venezuelan RC design code [12] prescribes for columns (6%) or have values too large which are technically impossible to place in cross sections. Only case 5 is able to satisfy both the maximum interstorey drift and reinforcement ratio. In contrast, the cases calculated using the alternative procedure, exhibit results which demonstrate that only the stiffer case (case 5) satisfy the maximum inter-story drift criteria, and also satisfy the reinforcement ratio requirement.

According to obtained results, it can be concluded that standard procedure is strength-controlled, while alternative procedure is displacement-controlled, this last feature produce more realistic designs with a desirable performance when buildings are under the effect of strong ground-motions [13, 14, 15, 16]. By the other hand, it is evident that the design process will demand less computational effort if the alternative process is applied, because it reduce the number of iterations for determine the appropriate configuration.

3. CONCLUSIONS

In this paper an alternative procedure has been presented. The procedure wants to present a rational approach in order to determine the response reduction factors for RC framed buildings in a compatible format with the factors used in the current version of the Venezuelan Seismic Code.

The procedure can be extended to other structural typologies used for seismic design.

The procedure is suitably and easy to apply in order to let seismic engineers to obtain inelastic response design spectra they need to perform the analysis and design of new buildings. The procedure includes determining inelastic displacements using equations derived from energetic-based methods, whose components are the same than the used for conduct the analysis.

Dimensioning of buildings using the alternative procedure led to reach a configuration which not only satisfy the maximum inter-story drift that the Venezuelan seismic code prescribes (displacement-controlled design) but also satisfy the maximum reinforcement ratio for structural elements (strength-controlled design). This feature led to reduce the computational effort, because it requires less iteration to find an adequate solution for the structural dimensioning.

References

1. CEN, European Standard EN1998-1:2004 Eurocode 8: Design of structures for earthquake resistance, Part 1: general rules seismic actions and rules for buildings. Comitee Europeen de Normalization, Brusells.
2. Veletsos, A. S. and Newmark, N. M., Effect of inelastic behavior on the response of simple systems to earthquake motions. *Proceedings of 2nd World Conference on Earthquake Engineering*, Tokyo, Japan, 1960.
3. Vielma, J. C., Barbat, A. H.y Oller, S., Factores de reducción de respuesta: estado del arte and estudio comparativo entre códigos. *Revista internacional de ingeniería de estructuras,* vol. 11, nº 1, pp. 79-106, 2006. (in Spanish)
4. ATC, Structural response modification factors. Applied Technology Center, Redwood City, 1995.
5. Lobo, W., Rivero, P. and Vielma, J. C., Hysteretic determination of the response factors Rμ according to structural types. *Proceedings of 13th World Conference on Earthquake Engineering* Vancouver, 2004.
6. Vielma, J. C., Lobo, W. and Rivero, P., Factores de reducción de respuesta por ductilidad de estructuras con comportamiento no lineal. *Revista Ingeniería UC,* vol. 12, nº 2, pp. 1-25, 2005.

7. Vielma, J. C., Lobo, W. and Rivero, P., Factores de reducción de respuesta por ductilidad de estructuras con comportamiento histerético. *Revista Sul-Americana de Engenharia Estrutural*, vol. 3, nº 2, pp. 45-65, 2007. (in Spanish)

8. Fondonorma, *Norma Venezolana COVENIN 1756:2001. Edificaciones sismorresistentes Fondonorma*, Caracas, 2001. (in Spanish)

9. Vielma, J. C., *Caracterización de la respuesta sísmica de edificios de hormigón armado mediante la respuesta no lineal*, 1a ed., Barcelona: Universitat Politécnica de Catalunya, 2008. (in Spanish)

10. Vielma, J. C., Barbat, A. H. and Oller, S., *Proyecto sismo-resistente de estructuras porticadas*, 1a ed., Barcelona: Centro Internacional de Métodos Numéricos en Ingeniería CIMNE, 2011. (in Spanish)

11. Vielma, J. C., Barbat, A. H. and Oller, S., Dimensionado sísmico de edificios de hormigón armado mediante factores de amplificación de desplazamientos con base en el balance de energía. *Hormigón y Acero,* vol. 63, nº 263, pp. 83-96, 2011. (in Spanish)

12. Fondonorma, *Norma Venezolana 1753:2001. Proyecto and construcción de obras en concreto estructural*. Fondonorma, Caracas, 2006. (in Spanish)

13. Vielma, J. C., Barbat, A. H. and Oller, S., Seismic safety of low ductility structures used in Spain. *Bulletin of Earthquake Engineering*, vol. 8, nº 1, pp. 135-155, 2010.

14. Vielma, J. C., Barbat, A. H. and Oller, S., Seismic response of the RC framed buildings designed according to Eurocodes. *In Computational methods in Earthquake Engineering*, M. Papadrakakis, M. Fragiadakis and N. Lagaros, Edits., Heidelberg, Springer, 2010, pp. 201-220

15. Vielma, J. C., Barbat, A. H. and Martinez Y., The Quadrants Method: A procedure to evaluate the seismic performance of existing buildings. *Proceedings of 15th World Conference on Earthquake Engineering* Lisboa, 2012

16. Vielma, J. C., Barbat, A. H. and Oller, S., Seismic performance of buildings with waffled-slab floors. *Proceedings of the ICE - Structures and Buildings*, vol. 162, nº 3, pp. 169-182, 2009.

The First Order Shear Deformation Theory for Sandwich Plates

Radu Chiriac and Mihai Vrabie

Department of Structural Mechanics, Technical University "Gheorghe Asachi", Iaşi,
700050, Romania

Summary

This paper presents the specifics of applying the First Order Shear Deformation Theory (FSDT) for determining the bending response parameters of sandwich plates. The classical lamination theory (CLT) is used to establish the stiffness matrices of the element, the significance and importance of the shear correction factor, and finally, different methods (analytical and numerical) for implementing the theory are presented.

KEYWORDS: sandwich plates, first order shear deformation theory, bending

1. INTRODUCTION

Sandwich plates are frequently used because of their ability to provide high bending stiffness while being light weight. A sandwich panel can be assimilated with a I-beam in which the faces act as the flanges who carry the normal stresses caused by bending moments and the core as the web supporting the shear stresses caused by transverse forces. However, typically the core is made of materials with reduced stiffness, which results in the appearance of shear effects that need to be accounted for.

The first order shear deformation theory (FSDT), commonly referred to as the Mindlin-Reissner theory, is the most basic tool available to take into account such effects. The theory is based on the following displacement field:

$$u(x, y, z) = z\phi_x(x, y)$$
$$v(x, y, z) = z\phi_y(x, y) \tag{1}$$
$$w(x, y, z) = w_0(x, y)$$

where Φ_x and Φ_y denote rotations about the x and y axes, respectively. The rotations Φ_x and Φ_y are no longer explicit functions of the derivatives of the deflection w_0, as for the classical plate theory.

From the displacement field (1), the components of the linear strains are (fig. 1):

$$\varepsilon_x = z\frac{\partial \phi_x}{\partial x}; \quad \varepsilon_y = z\frac{\partial \phi_y}{\partial y}; \quad \gamma_{xy} = z\left(\frac{\partial \phi_x}{\partial y} + \frac{\partial \phi_y}{\partial x}\right)$$

$$\gamma_{xz} = \phi_x + \frac{\partial w_0}{\partial x}; \quad \gamma_{yz} = \phi_y + \frac{\partial w_0}{\partial y} \tag{2}$$
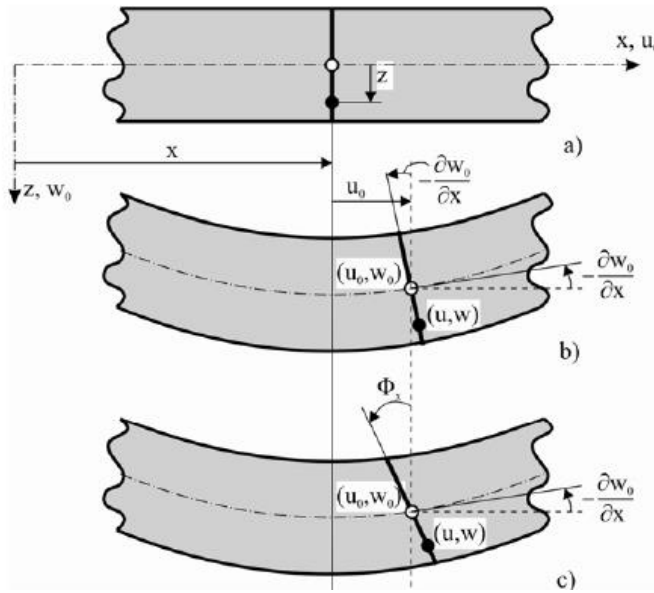
Figure 1. Undeformed and deformed geometries of an edge plate:
a) undeformed; b) Kirchoff plate theory; c) Mindlin-Reissner plate theory

The kinematics of FSDT assume a global transverse shear strain considered constant on the plate thickness. To compensate for this assumption, a shear correction factor is required, which appears as a coefficient in the expression for the transverse shear stress resultant. The accuracy with which this factor is computed is paramount for the validation of the results.

2. ANALYSIS OF SANDWICH PLATES USING FSDT

2.1. Laminate stiffness's

In order to establish the constitutive equations for sandwich plates and determine the necessary parameters to accurately estimate the bending behaviour of said plates, it is necessary to employ the Classical Lamination Theory (CLT) to determine the stiffness matrices (extensional stiffness matrix – [A], coupling matrix [B] and

bending stiffness matrix – [D]). For simplicity, this papers strictly refers to rectangular isotropic sandwich plates with equal face sheets, hence the [B] matrix will be null. According to [3], a sandwich plate is isotropic when the core is made of an isotropic (such as foam) or transversely isotropic (such as honeycomb) material and the top and bottom facesheets are made of identical isotropic materials or are identical quasi-isotropic laminates.

There are two ways to approach the problem:

1) If the core is made of a material with a much lower modulus of elasticity than that of the faces, then its influence on the overall stiffness of the plate can be completely neglected, and the method presented in 2.1.1 can be used;

2) If the core material and that of the faces both have comparable moduli of elasticity, then the method presented in 2.1.2 must be used.

2.1.1. The stiffness matrices for the case when $E_c << E_f$

First, the face stiffness's are determined as follows [3]:

$$A_f = 2 \cdot h_f \cdot \frac{E_f}{1 - v_f^2} \quad ; \quad D_f = E_f \cdot \frac{2 \cdot \left(d^2 \cdot h_f + \frac{h_f^3}{12} \right)}{1 - v_f^2} \tag{3}$$

where, according to Figure 2:

- d represents the distance from the centre of the plate to the mid-plane of the faces;

- h_f and h_c are the thickness of the faces and of the core;

- E_f and v_f are the Young modulus and Poisson ratio for the facesheets material.

Next, the stiffness matrices for the whole panel can be determined [3]:

$$A = A_f \cdot \begin{bmatrix} 1 & v_f & 0 \\ v_f & 1 & 0 \\ 0 & 0 & \frac{1 - v_f}{2} \end{bmatrix} \quad ; \quad D = D_f \cdot \begin{bmatrix} 1 & v_f & 0 \\ v_f & 1 & 0 \\ 0 & 0 & \frac{1 - v_f}{2} \end{bmatrix} \tag{4}$$

2.1.2. The stiffness matrices for the case when E_c is comparable to E_f

In this situation, the components of the stiffness matrices can be determined as follows:

$$A_{ij} = \sum_{k=1}^{3} (Q_{ij})_k (z_k - z_{k-1}) \quad D_{ij} = \sum_{k=1}^{3} (Q_{ij})_k (z_k^3 - z_{k-1}^3)$$

$$; \qquad\qquad\qquad\qquad ; \quad i,j = 1,2,6 \qquad (5)$$

$$A_{44} = A_{55} = 2 \cdot G_f \cdot h_f + G_c \cdot h_c \qquad (6)$$

where $(Q_{ij})_k$ are terms of the plane stress-reduced elastic coefficient matrices for the materials of the core and faces of the plate and can be determined like so:

$$Q_{11} = Q_{22} = \frac{E}{1-v^2} \; ; \quad Q_{12} = Q_{21} = \frac{v \cdot E}{1-v^2} \quad Q_{66} = G \qquad (7)$$

with E, G and v - the Young modulus, shear modulus and Poisson's ratio of the materials of the core (c index) and faces (f index) of the sandwich panel.
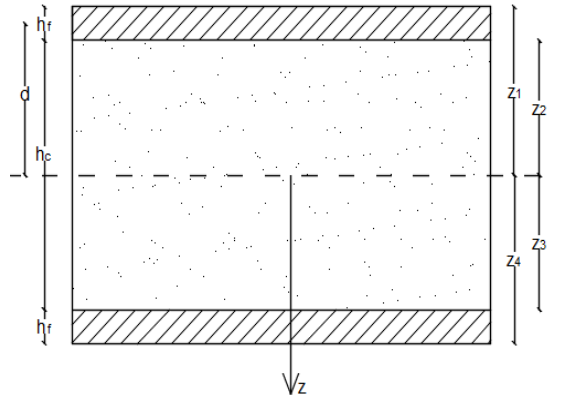
Figure 2. Distances required for determining the stiffness matrices

2.2. The shear correction factor

Since the transverse shear strains are represented as constant through the laminate thickness, consequently, the transverse shear stresses will also be constant. It is well known that the transverse shear stresses vary parabolically. The discrepancy between the actual stress state and the constant stress state predicted by FSDT is corrected by multiplying the transverse shear forces with a coefficient K_s, called *shear correction factor*.

For elements with homogenous cross-sections, the value for the shear correction factor, accepted in the literature [6], is 5/6. However, for composite laminates, this value is no longer suitable. In [4, 8], the authors present a series of methods to determine this factor.

The most widely used method for computing the shear correction factor is the so called energy equivalence method. The strain energy due to transverse shear stresses predicted by FSDT is equalled with that from the three-dimensional elasticity theory.

For example, for a symmetric sandwich beam, the shear correction factor can be determined like so:

$$K_s = \frac{D^2}{A_{55} \cdot (2 \cdot b_1 + b_2)} \tag{8}$$

where:

$$D = \frac{E_f \cdot (h^3 - h_c^3) + E_c \cdot h_c^3}{12}$$

$$b_1 = \frac{E_f^2}{4G_f} \cdot \left[\left(\frac{8}{15}\right)\left(\frac{h}{2}\right)^5 - \left(\frac{h}{2}\right)^4\left(\frac{h_c}{2}\right) + \left(\frac{2}{3}\right)\left(\frac{h}{2}\right)^2\left(\frac{h_c}{2}\right)^3 - \left(\frac{h_c^5}{2^5 \cdot 5}\right) \right] \tag{9}$$

$$b_2 = \frac{\left\{ E_c^2 \cdot \frac{h_c^5}{2^5 \cdot 5} + E_c \cdot \left(\frac{h_c}{2}\right)^3 \frac{E_f(h_c^2 - h^2) - E_c h_c^2}{6} + \left[E_f(h_c^2 - h^2) - E_c h_c^2\right]^2 \frac{h_c}{32} \right\}}{2 \cdot G_c}$$

In [4], Birmann and Bert concludes that this method is not reliable if the modular ratio for the materials of the faces and core is extremely high, in which case the values predicted for the shear correction factor are close to zero. This statement has also been proven in [9], where the authors studied the bending behaviour of a sandwich plate with the core made of extruded polystyrene and aluminium faces. Because of the low values of K_s, the plate deflections predicted by FSDT were several orders of magnitude greater than those of CLPT.

Birmann and Bert suggests that for the design of sandwich plates, the shear correction value should be taken equal to unity.

2.3. Bending analysis of sandwich plates using FSDT

2.3.1. The governing differential equations

The governing differential equations for a laminated composite plate subjected to a transverse load (Figure 3) are [7]:

$$D_{11} \frac{\partial^2 \phi_x}{\partial x^2} + D_{66} \frac{\partial^2 \phi_x}{\partial y^2} + (D_{12} + D_{66}) \frac{\partial^2 \phi_y}{\partial x \partial y} - K_s A_{55}\left(\phi_x + \frac{\partial w}{\partial x}\right) = 0$$

$$(D_{12} + D_{66}) \frac{\partial^2 \phi_x}{\partial x \partial y} + D_{66} \frac{\partial^2 \phi_y}{\partial y^2} + D_{22} \frac{\partial^2 \phi_y}{\partial y^2} - K_s A_{44}\left(\phi_y + \frac{\partial w}{\partial y}\right) = 0 \tag{10}$$

$$K_s A_{55}\left(\frac{\partial \phi_x}{\partial x} + \frac{\partial^2 w}{\partial x^2}\right) + K_s A_{44}\left(\frac{\partial \phi_y}{\partial y} + \frac{\partial^2 w}{\partial y^2}\right) + q(x, y) = 0 \tag{*}$$
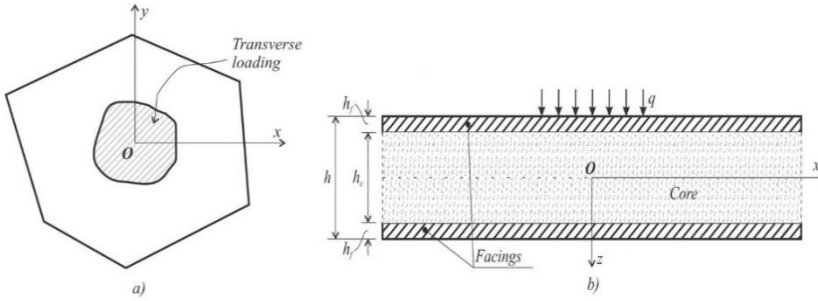
Figure 3. Geometry and loading of a sandwich plate: a) general polygonal shape; b) plate cross section

The inclusion of transverse shear deformation effects results in three coupled partial differential equations with three unknowns, Φ_x, Φ_y and w, as opposed to having one partial differential equation with one unknown, w, in classical plate theory.

The plate constitutive equations for the classical or first-order shear deformation theories are:

$$\begin{Bmatrix} M_x \\ M_y \\ M_{xy} \end{Bmatrix} = \begin{bmatrix} D_{11} & D_{12} & 0 \\ D_{12} & D_{11} & 0 \\ 0 & 0 & D_{66} \end{bmatrix} \begin{Bmatrix} \dfrac{\partial \phi_x}{\partial x} \\ \dfrac{\partial \phi_y}{\partial y} \\ \dfrac{\partial \phi_x}{\partial y} + \dfrac{\partial \phi_y}{\partial x} \end{Bmatrix} \tag{11}$$

$$\begin{Bmatrix} V_y \\ V_x \end{Bmatrix} = K_s \begin{bmatrix} A_{44} & 0 \\ 0 & A_{55} \end{bmatrix} \begin{Bmatrix} \phi_y + \dfrac{\partial w_0}{\partial y} \\ \phi_x + \dfrac{\partial w_0}{\partial x} \end{Bmatrix} \tag{12}$$

where the laminate stiffness's D_{ij} and A_{ij} are defined in [1, 2, 5, 7] for symmetric laminates with multiple isotropic layers.

2.3.2. The Navier Solution for FSDT

The boundary conditions for a simply supported plate (Figure 4), in FSDT, are:

- for the edge parallel to the y-axis: $v_0 = w_0 = \phi_y = M_x = 0$
- for the edge parallel to the x-axis: $u_0 = w_0 = \phi_x = M_y = 0$
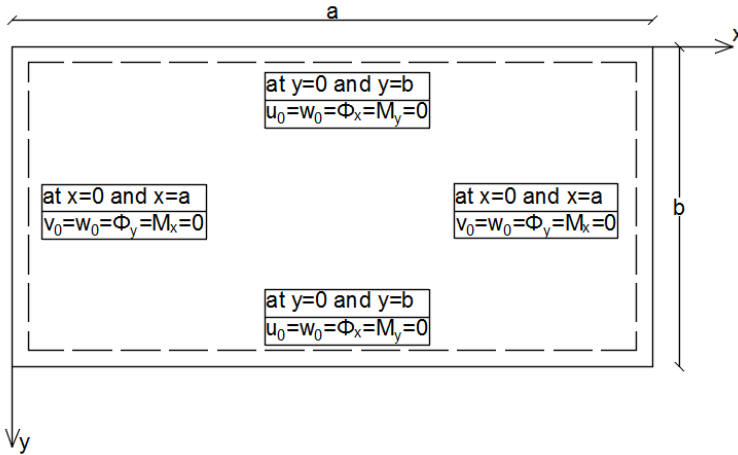
Figure 4. Boundary conditions on a simply supported plate for the Mindlin theory

The boundary conditions are satisfied by the following expressions:

$$w_0(x, y) = \sum_{n=1}^{\infty}\sum_{m=1}^{\infty} W_{mn} \sin\alpha x \sin\beta y$$

$$\phi_x(x, y) = \sum_{n=1}^{\infty}\sum_{m=1}^{\infty} X_{mn} \cos\alpha x \sin\beta y \tag{13}$$

$$\phi_y(x, y) = \sum_{n=1}^{\infty}\sum_{m=1}^{\infty} Y_{mn} \sin\alpha x \cos\beta y$$

where $\alpha = m\pi/a$, $\beta = n\pi/b$ and m, n are the steps of the series.

The transverse load is also transcribed in double Fourier series:

$$q(x, y) = \sum_{n=1}^{\infty}\sum_{m=1}^{\infty} Q_{mn} \sin\alpha x \sin\beta y \tag{14}$$

$$Q_{mn} = \frac{4}{ab}\int_0^a\int_0^b q(x, y) \cdot \sin\alpha x \cdot \sin\beta y \cdot dxdy \tag{15}$$

The coefficients W_{mn}, X_{mn} and Y_{mn} have the following expressions:

$$W_{mn} = \frac{b_0}{b_{mn}} Q_{mn} \quad ; \quad X_{mn} = \frac{b_1}{b_{mn}} Q_{mn} \quad ; \quad Y_{mn} = \frac{b_2}{b_{mn}} Q_{mn}$$

(16)

where:

$$b_0 = s_{22} \cdot s_{33} - s_{23} \cdot s_{23} \; ; \quad b_1 = s_{23} \cdot s_{13} - s_{12} \cdot s_{33} \; ; \quad b_2 = s_{12} \cdot s_{23} - s_{22} \cdot s_{13}$$
$$b_{mn} = s_{11} \cdot b_0 + s_{12} \cdot b_1 + s_{13} \cdot b_2$$

(17)

and

$$s_{11} = K_s (A_{55} \cdot \alpha^2 + A_{44} \cdot \beta^2) \; ; \quad s_{22} = (D_{11} \cdot \alpha^2 + D_{66} \cdot \beta^2 + K_s A_{55})$$
$$s_{12} = K_s \cdot A_{55} \cdot \alpha \; ; \quad s_{23} = (D_{12} + D_{66}) \cdot \alpha \cdot \beta$$
$$s_{13} = K_s \cdot A_{44} \cdot \beta \; ; \quad s_{33} = (D_{66} \cdot \alpha^2 + D_{22} \cdot \beta^2 + K_s A_{44})$$

(18)

Once the displacements and rotations are determined, the bending and twisting moments can be computed:

$$M_x = \sum_{n=1}^{\infty} \sum_{m=1}^{\infty} (D_{11} \cdot \alpha \cdot X_{mn} + D_{12} \cdot \beta \cdot Y_{mn}) \cdot \sin \alpha x \sin \beta y$$

$$M_y = \sum_{n=1}^{\infty} \sum_{m=1}^{\infty} (D_{12} \cdot \alpha \cdot X_{mn} + D_{22} \cdot \beta \cdot Y_{mn}) \cdot \sin \alpha x \sin \beta y$$

(19)

$$M_{xy} = D_{66} \sum_{n=1}^{\infty} \sum_{m=1}^{\infty} (\beta \cdot X_{mn} + \alpha \cdot Y_{mn}) \cdot \cos \alpha x \cos \beta y$$

and the stresses:

$$\sigma_x = -z \sum_{n=1}^{\infty} \sum_{m=1}^{\infty} (Q_{11} \cdot \alpha \cdot X_{mn} + Q_{12} \cdot \beta \cdot Y_{mn}) \cdot \sin \alpha x \sin \beta y$$

$$\sigma_y = -z \sum_{n=1}^{\infty} \sum_{m=1}^{\infty} (Q_{12} \cdot \alpha \cdot X_{mn} + Q_{22} \cdot \beta \cdot Y_{mn}) \cdot \sin \alpha x \sin \beta y$$

$$\tau_{xy} = -z \sum_{n=1}^{\infty} \sum_{m=1}^{\infty} -Q_{66} (\beta \cdot X_{mn} + \alpha \cdot Y_{mn}) \cdot \cos \alpha x \cos \beta y$$

(20)

$$\tau_{yz} = \sum_{n=1}^{\infty} \sum_{m=1}^{\infty} G_c (Y_{mn} + \beta \cdot W_{mn}) \cdot \sin \alpha x \cos \beta y$$

$$\tau_{xz} = \sum_{n=1}^{\infty} \sum_{m=1}^{\infty} G_c (X_{mn} + \alpha \cdot Y_{mn}) \cdot \cos \alpha x \sin \beta y$$

2.3.3. Numerical methods

2.3.3.1. Finite difference method

The finite difference method can easily be used to determine the bending behaviour of isotropic sandwich plates for the first order shear deformation theory.

The first step consists in determining the moment sum and deflections for an equivalent homogenous plate, composed of the two face sheets glued together, using the well-known Poisson equations of the Classical Plate Theory:

$$\nabla^2 M^K = -q ; \quad \nabla^2 w^K = -\frac{M^K}{D} \tag{21}$$

After which the deflections of the real sandwich plate are computed using the relationship that connects the two theories [5]:

$$w^M = \frac{D}{D_c + D_f} w^K + \frac{M^K}{K_s (G_c h_c + 2G_f h_f)} \tag{22}$$

where:
- - ∇^2 - the Laplacian operator, approximated by the finite difference method;
- - q is the transverse load;
- - "M" and "K" superscripts denote quantities of the Kirchoff and Mindlin plate theories;
- - D is the bending stiffness of the equivalent homogenous plate:

$$D = \frac{E_f \cdot (2h_f)^3}{12 \cdot (1 - v_f^2)} \tag{23}$$

- - M^K is the moment sum for the homogenous equivalent Kirchoff plate;
- - D_c and D_f are the bending stiffnesses of the core and faces for the real plate;
- - G_c, G_f - the shear moduli of the materials for the core and faces;
- - h_c and h_f - the thickness of the core and that of the faces;
- - K_s – the shear correction factor, as discussed in section 2.2.

The stiffnesses D_c and D_f are:

$$D_c = \frac{E_c h_c^3}{12(1 - v_c^2)} ; \quad D_f = \frac{2E_f h_f \left(\frac{3h_c^2}{4} + \frac{3h_c h_f}{2} + h_f^2 \right)}{3(1 - v_f^2)} \tag{24}$$

2.3.3.2. Finite elements method

Almost all commercial finite element analysis codes (Abaqus, Ansys) use Mindlin type plate elements.

For example, the most common type of element used by Ansys to model layered plates is SHELL181. The following is from the Ansys Workbench Help [10]:

"SHELL181 is a four-node element with six degrees of freedom at each node: translations in the x, y and z directions, and rotations about the x, y and z-axes. SHELL181 can be used for layered applications for modelling composite shells or sandwich construction. The accuracy in modelling composite shells is governed by the first-order shear-deformation theory.(usually referred to as Mindlin-Reissner theory).

Transverse shear stiffness of the shell section is estimated by an energy equivalence procedure. The accuracy of this calculation may be adversely affected if the ratio of material stiffness's (Young's moduli) between adjacent layers is very high."

3. CONCLUSIONS

The first-order shear-deformation theory is widely used for the bending analysis of sandwich plates. It relaxes the normal segment hypothesis and takes into account a constant shear strain on the plate thickness. In order to correct the discrepancy between this constant distribution and the real parabolic distribution, the theory uses a shear correction factor. As has been shown, the accuracy with which this factor is computed is critical for the validity of the results. The Mindlin plate model is implemented in all major finite element analysis software and the shear correction factors are determined using the energy equivalence method.

References

1. Reddy J.N., *Mechanics of laminated composite plates and shells. Theory and analysis*, 2nd edition, CRC Press, 2004.
2. Reddy J.N., *Theory and analysis of elastic plates and shells,* 2nd edition, CRC Press, 2007.
3. Kollar L.P., Springer G.S., *Mechanics of composite structures*, Cambridge University Press, 2003.
4. Birman V., Bert C.W., *On the choice of shear correction factor in sandwich structures,* Journal of sandwich structures and materials, vol. 4, pp. 83-95, 2002.
5. Wang C.M., Reddy J.N., Lee K.H., *Shear Deformable Beams and Plates,* Elsevier Sc. Ltd., 2000.
6. Timoshenko St., Woinowski-Krieger S., *Teoria plăcilor plane şi curbe,* Ed. Tehnică, Bucureşti, 1968.
7. Vinson R.J., Sierakowski R.L., *The Behavior of Structures Composed of Composite Materials,* Second Edition, Kluwer Academic Publishers, 2004.
8. Dube G.P., Kapuria S., Dumir P.C., Pramod J.P., *Effect of Shear Correction Factor on Response of Cross-ply Laminated Plates Using FSDT*, Defence Science Journal, Indian Institute of Technology, 2005.
9. Vrabie M., Chiriac R., *Theoretical and numerical investigation regarding the bending behavior of sandwich plates*, Bul. Inst. Polit. Iaşi, t. LX (LXIV), f. 4, 2014.
10. ANSYS 12 Structural Analysis Guide, Ansys Workbench Help, 2009.

Performance Evaluation of Dual-eccentrically Braced Frames

Gabriel-Alexandru Sabau, Aurel Stratan

*Department of Steel Structures and Structural Mechanics, Politehnica University Timisoara,
200224, Romania*

Summary

The later force resistance in dual-eccentrically braced frames is provided by two structural system: eccentrically braced frames (the primary sub-system) and moment-resisting frames (the secondary sub-system). Eccentrically braced frames dissipates most of the seismic energy through plastic deformations in links, while moment-resisting frames represent a back-up system, increases the redundancy of the overall system. This paper presents the modelling approach of steel dual-eccentrically braced frames using the OpenSees software framework. Ten different structural configurations were used to evaluate their performance given two levels of seismic hazard. The analyses of the frames is part of the ongoing European pre-QUALified steel JOINTS project, concerned with the pre-qualification of all-steel Beam-to-Column joints in steel structures. The designed frames were evaluated in terms of seismic performance by means of non-linear static (pushover) analyses, with a modal and uniform distribution of forces, time history and incremental dynamic analyses. The eccentrically braced frame contains short links, for which the shear force - shear deformation (V-γ) curve was calibrated based on experimental results. The physical theory models were used for columns and braces in the numerical model. The model was built in a 3D environment and extra nodes were added at each column and brace midpoint to account for initial imperfections. The midpoints were without restraints so that buckling could occur about the weak axis.

KEYWORDS: steel dual-eccentrically braced frames, short links, OpenSees, IDA analysis, performance evaluation, FEM modelling, physical theory models

1.   INTRODUCTION

An inverted "V" (Chevron) configuration was chosen for the dual eccentrically-braced frames. The braces are located at the central bay of each frame and are assumed to have out-of-plane pinned ends and rigid in-plane connections. The seismic links are horizontal, located at the beam where the braces converge and have a uniform length of 0.7m, which leads to a "short" link design, for the specific range of selected member sizes. The section of the link is the same as the section of the adjacent beam (using full-depth web stiffeners to ensure ductile cyclic

behaviour, per EN 1998-1 [5], Section 6.8.2). The exterior bays are modelled as moment resisting frames. Square hollow sections (i.e. SHHF or SHS) are selected for the braces and HEA sections are selected for the seismic links/beams. The beam-column joints are considered to be full strength and fully rigid connections. The structures analysed are presented in Table 1 .

Table 1 Designed dual-eccentrically braced frames

Frame Name	Structural Configuration
DEBF-6-3-6-MH	D-EBF, 6-storey, 3-bay, 6m span, PGA=0.25g
DEBF-6-3-6-HH	D-EBF, 6-storey, 3-bay, 6m span, PGA=0.35g
DEBF-6-3-8-MH	D-EBF, 6-storey, 3-bay, 8m span, PGA=0.25g
DEBF-6-3-8-HH	D-EBF, 6-storey, 3-bay, 8m span, PGA=0.35g
DEBF-6-5-6-HH	D-EBF, 6-storey, 5-bay, 6m span, PGA=0.35g
DEBF-12-3-6-MH	D-EBF, 12-storey, 3-bay, 6m span, PGA=0.25g
DEBF-12-3-6-HH	D-EBF, 12-storey, 3-bay, 6m span, PGA=0.35g
DEBF-12-3-8-MH	D-EBF, 12-storey, 3-bay, 8m span, PGA=0.25g
DEBF-12-3-8-HH	D-EBF, 12-storey, 3-bay, 8m span, PGA=0.35g
DEBF-12-5-6-HH	D-EBF, 12-storey, 5-bay, 6m span, PGA=0.35g

2.   BASIC MODELLING ASSUMPTIONS FOR DEBFS

The OpenSees model of the structure was defined in a 3D environment. Out of plane degrees of freedom were blocked for the nodes connecting beams, columns and braces. The 3D model allows for imperfections to be introduced in the columns and braces. The imperfections were added by inserting off-plane mid-points with an offset of L/1000 [9]. These nodes have 6 degrees of freedom allowing the elements to gain out-of-plane deformations. Except for the braces which have pinned out-of-plane connections and rigid in-plane connections, all the other elements have rigid connections. The columns' web panel was considered to be fully rigid. To model the rigid web panel nodes were added at the beams and columns flange positions as seen in Figure 4. These nodes were connected to the central node through rigid elements. The second order effects were taken into

account by modelling a leaning column with the additional loads of the rest of the structure. The masses were assigned to the leaning-column nodes. A typical structural scheme showing element connectivity is shown in Figure 1.
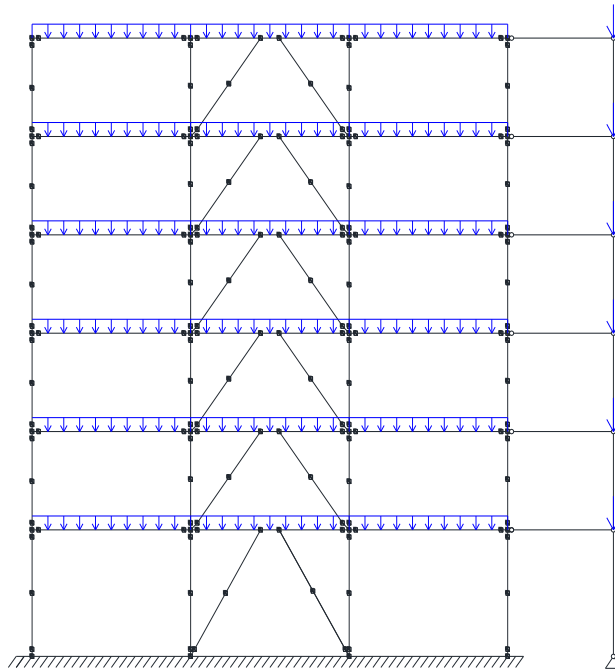
Figure 1. Structural model with nodes position

Beams, columns and braces were modelled as fiber sections with 20 fibres along the flange and web length, and 2 fibers along the flange and web thicknesses respectively. The sections were attributed to force controlled elements with distributed plasticity (forceBeamColumn). Three integration points were attributed to each half length of the columns and braces, five integration points for the beams and three for the links.

The link was modelled by aggregating the shear force-deformation response with a forceBeamColumn element accounting for flexural deformations. The shear response was modelled with a Steel4 [1] hysteretic relationship material with the yielding strength equal to the yielding force of the link element in shear calculated with Equation (1) and the initial stiffness of the link accounting only for shear Equation (2) (disregarding the contribution of the flexural stiffness). The stiffness was inserted as the ratio between shear force and shear deformation (V-γ). The modelling parameters for links values are shown in Table 2.

$$V_y = \frac{A_{vz} \cdot f_y}{\sqrt{3} \cdot \gamma_{MI}} \tag{1}$$

$$K_s = \frac{G \cdot A_{vz}}{e} \tag{2}$$

$$\gamma_y = \frac{V_y}{K_s \cdot e} \tag{3}$$

Table 2. Links shear modelling parameters

Link Section	V_y [kN]	K_s [kN/rad]	γ_y [rad]	γ_u [rad]
HE450A	1218.6	370737		
HE400A	1030.9	313632		
HE360A	922.5	280665		
HE340A	751.2	228541		
HE320A	668.5	203391		
HE300A	592.4	180387		
HE280A	519.7	158112	0.00329	0.15
HE260A	449.3	136687		
HE240A	411.3	125145		
HE220A	350.4	106596		
HE200A	294.2	89505		
HE180A	242.8	73872		

*V_y = force at yield; θy = link rotation at yield; θu = link rotation at failure;

The shear behaviour of the link was calibrated based on the experimental results from Okazaki and Engelhardt 2006 [11] on short links. The model used for the calibration consisted in a 2D beam element with all the degrees of freedom blocked at one end and rotation blocked at the other end. Fiber sections were used to define the cross-section of the element, just as in the large structural model. The material parameters determined for the link response are presented in Table 3.

Table 3. Steel4 material parameters

Parameter	Parameter description	Value
b_k	Kinematic hardening ratio	0.018
R_0		15
r_1	Controls the exponential transition from elastic to plastic asymptote	0.82
r_2		0.2
b_i	Isotropic hardening ratio	0.0032
b_l	Isotropic saturated hardening ratio	0.0014
rho_i	Position of intersection point between initial and saturated asymptote	0.24
R_i	Controls the exponential transition from initial to saturated isotropic hardening	50
l_yp	Length of the yielding plateau	0
f_u	Ultimate strength	$1.5 \cdot V_y$
R_u	Controls the transition from kinematic hardening to perfectly plastic asymptote	1.8

*V_y = force at yield as described in Table 2 taken for each link according to its cross-section properties

The calibrated link used from Okazaki and Engelhardt 2006 [11] was a W10x33 with the length of 584 mm subjected to a revised loading protocol according to 2005 AISC Seismic Provisions [3]. The static scheme used for the analyses can be seen in Figure 2.
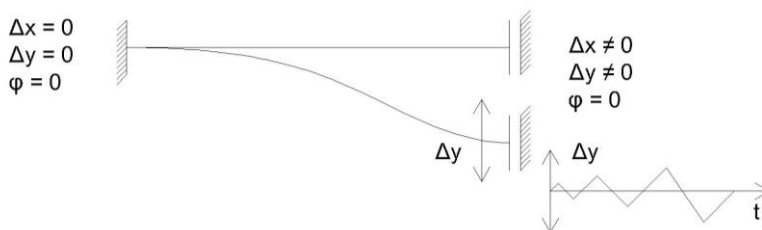
Figure 2. Link calibration static scheme

The comparison between the numerical and experimental results are displayed in Figure 3 in terms of shear force – element rotation.
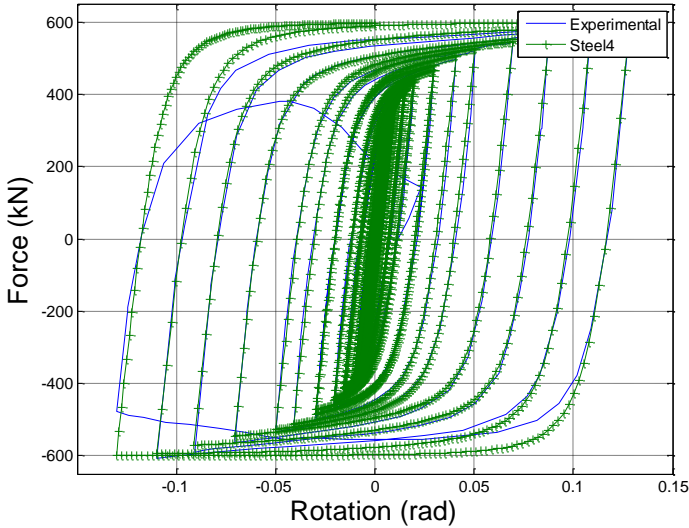
Figure 3. Numerical validation of shear link element

The leaning column was modelled using elastic elements (elasticBeamColumn) with the cross-section properties of the 4 central columns for the 3-bay model and 6 columns for the 5-bay model. The transformation methods assigned to each type of element can be seen in Table 4.

Table 4 Element modelling parameters

Structural element	Finite element type	Section	Transformation
Beam	forceBeamColumn	Fibre section	Linear
Brace	forceBeamColumn	Fibre section	Corotational
Column	forceBeamColumn	Fibre section	Corotational
Seismic link	forceBeamColumn	Fibre section	Linear
Leaning column	elasticBeamColumn	Elastic section	P-Delta
Rigid link element	elasticBeamColumn	Elastic section	Linear

The elements go from node to node with a rigid offset to account for the height of the beams and columns as seen in Figure 4. This is to model the panel zone as a fully rigid part of the structure. The nodes are considered to be full strength and fully rigid.
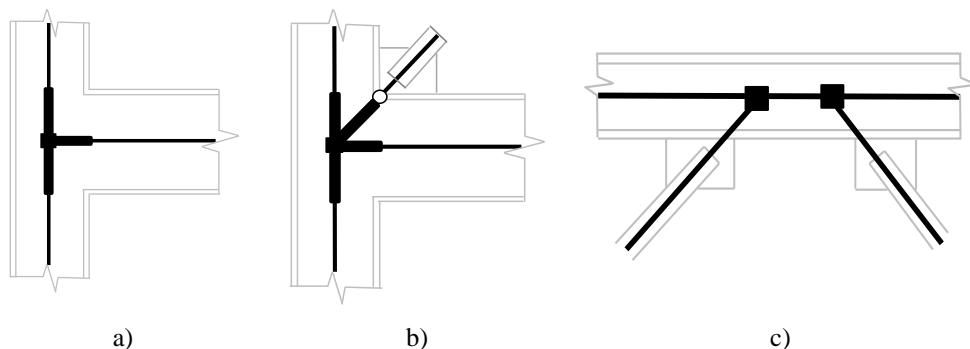
Figure 4. Model of connection types: beam-column joint (a), beam-brace column (b), brace link (c)

The material for all frame elements is S355 steel with an over-strength factor $\gamma_{ov}=$ 1.25. The chosen member sections are standard metric sections. The materials used for the fibre sections was Steel02 [12] (Giuffré-Menegotto-Pinto Model with Isotropic Strain Hardening) with the parameters values specified in Table 5.

Table 5. Steel02 modelling parameters

f_y, [N/mm^2]	E, [N/mm^2]	b	R0	cR1	cR2
443.5	210000	0.02	18	0.925	0.15

*f_y = steel yield stress; E = steel modulus of elasticity; b = strain hardening ratio; $R0$, $cR1$, $cR2$ = control the transition from elastic to plastic branches

3.   ANALYSIS RESULTS

3.1   Modal analysis

The results of the eigenvalue analysis in terms of 1st and 2nd modal periods of the moment moment frames are summarized in

Table 6. The range of the fundamental natural periods of vibration is from 0.93 to 1.14s for the 6-storey typologies and from 1.60s to 1.86s for the 12-storey typologies.

Table 6. Natural periods of vibration of DEBFs

Frame	T_1 (s)	T_2 (s)	Frame Typology	T_1 (s)	T_2 (s)
DEBF-6-3-6-MH	1.00	0.35	DEBF-12-3-6-MH	1.78	0.60
DEBF-6-3-6-HH	0.93	0.33	DEBF-12-3-6-HH	1.60	0.54
DEBF-6-3-8-MH	1.14	0.41	DEBF-12-3-8-MH	1.86	0.62
DEBF-6-3-8-HH	1.00	0.36	DEBF-12-3-8-HH	1.67	0.56
DEBF-6-5-6-HH	0.97	0.35	DEBF-12-5-6-HH	1.59	0.55

3.2   Pushover analysis

The frame typologies presented in Table 1 were subjected to pushover analyses, using both a uniform lateral load distribution and a modal lateral load distribution [10]. The control parameter is the top floor horizontal displacement. The computed pushover curves are presented in Figure 5 for the 6-storey frames and in Figure 6 for the 12-storey frames. The pushover curves for the structures with 6 m bays and 6 storeys show an increase of shear force over the plastic plateau mainly due to the overstrength [8] of the seismic links. Structures with larger spans and more storeys show a local failure mechanism due to the buckling of the compressed braces from the lower storeys. After the buckling occurs, an increased sensitivity to second order effects can be noticed in the structure. This happens at very large roof displacements (approx. 6% drift). The post-yielding plateau of the pushover curve is decreasing, response generated by a storey failure mechanism in addition to the second order effect, leading to a fragile failure mechanism. The 5 bays frames show ductility and an increase in the post-yielding stiffness, regardless of the number of storeys. On the other hand, it can be observed that the uniform load pattern leads to larger base shear force.
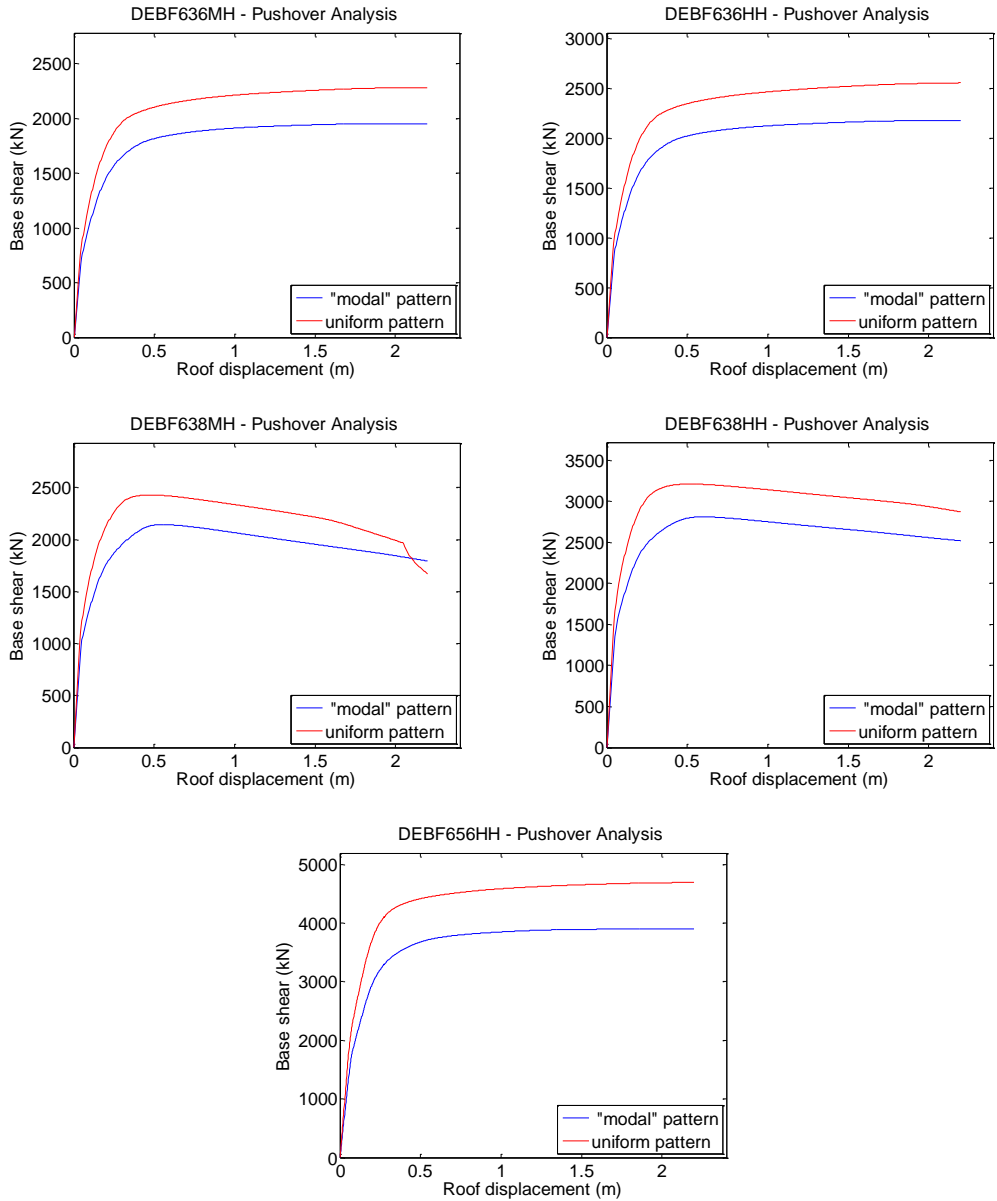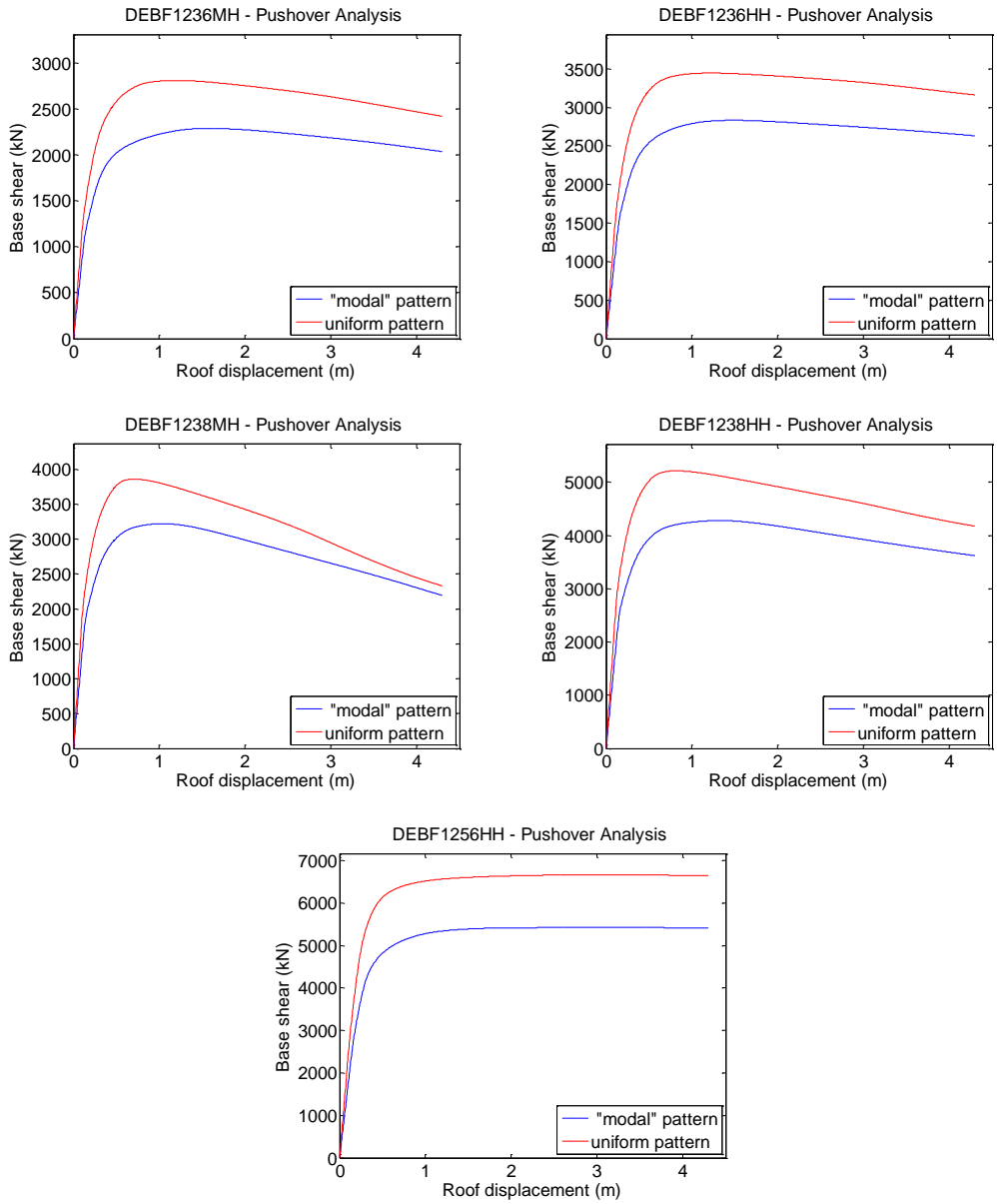
Figure 5. Pushover curves for 6-storey DEBFs

Figure 6. Pushover curves for 12-storey DEBFs

3.3 Non-linear dynamic analysis

The set of dual eccentrically braced frames was used for performing dynamic analyses, using as ground acceleration input two ground motion suites, for high seismic hazard (HH) and medium seismic hazard (MH) [1]. Rayleigh damping was used for a ratio $\xi_i = 2\%$ at the first and third natural frequencies of vibration. To monitor the residual displacements and deformations, additional 10 seconds were added to each accelerogram with 0 acceleration input. For the last 10 seconds the damping ratio was increased to $\xi_r = 20\%$. Three performance objectives (limit states) were considered, according to EN 1998-3 (CEN 2005b) [5]: damage limitation (DL), significant damage (SD), near collapse (NC). The corresponding seismic intensity levels were, respectively 50%, 100% and 175%, of the design one. The basic parameters monitored were the maximum and residual inter-storey drift ratios, link and beam rotations.

3.3.1. Inter-storey drift ratios

As seen in Figure 7 for the 6-storey frames the peak inter-storey drifts occur at the 2nd and 3rd storey and range from 0.014 rad for the MH cases up to 0.019 rad for the HH cases. The residual inter-storey drifts keep the same profile as the maximum values with the peaks at the 2nd and 3rd storey. The values range from 0.0011 rad for the MH cases to 0.0074 rad for the HH cases .In the case of the 12-storey frames, peak inter-storey drifts occur at the 3rd and 4th storeys of the frames and vary from 0.019 rad to 0.029 rad for the HH cases. The peak inter-storey drift for the MH frames occur at mid-height between the 5th and 6th storey. The values range between 0.0093 rad and 0.0095 rad, showing a reduced influence of the span's length. Same as for the 6-storey frame the residual inter-storey drift has the peaks were the maximum value for drift occurred. It can be seen that the values for residual inter-storey drift ranges from 0.0012 rad for MH frames to up to 0.0075 rad for HH frames.
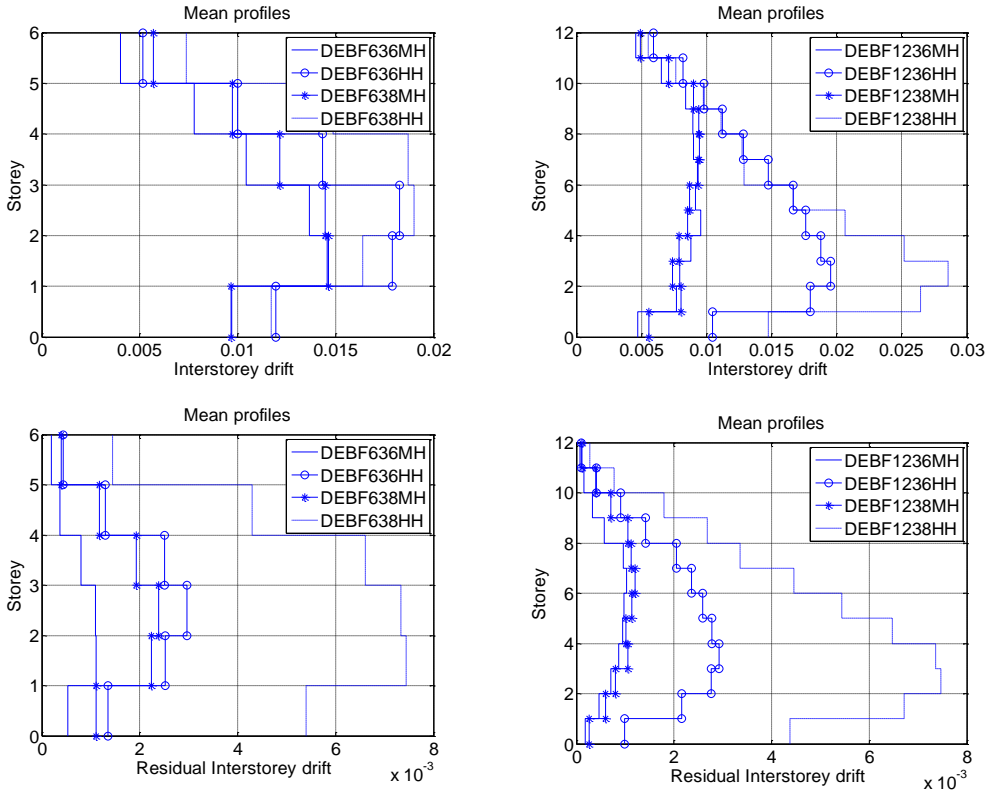
Figure 7. Mean profiles of max. and residual inter-storey drift ratios for the near collapse
performance level

3.3.2. Link deformations

The acceptance criteria for link deformations in terms of plastic rotation for the 3
limit states considered are taken from ASCE/SEI 41-13 [120], were the
corresponding limit states are immediate occupancy (IO), life safety (LS) and
collapse prevention (CP). The structures were verified that the elements
requirements are within the accepted limits as seen in Table 7. For the DL limit
state, the links rotations exceed the acceptance criteria in all the frames considered
as opposed to the SD limit state. The link rotations for the SD limit state are much
lower than the accepted ones (the lowest being 5 times less in the DEBF-12-3-6-
MH frame). At the CP limit state the links that exceed the acceptance criteria are
the ones from the 8 m spans frames designed for high seismic hazard. Comparing
the link rotation from the 6 m span and the 8 m span frames, it can be seen that the
link has a higher contribution when wider spans are implied.

Table 7. Performance evaluation of link elements

Frame	Mean profile of link max rotation			Acceptance criteria		
	DL (IO)	SD (LS)	NC (CP)	IO	LS	CP
DEBF-6-3-6-MH	0.0156*	0.0375	0.073			
DEBF-6-3-6-HH	0.0231*	0.0598	0.134			
DEBF-6-3-8-MH	0.0193*	0.0514	0.102			
DEBF-6-3-8-HH	0.0345*	0.0763	0.186*	0.005	0.14	0.16
DEBF-12-3-6-MH	0.0127*	0.0294	0.059			
DEBF-12-3-6-HH	0.0160*	0.0464	0.072			
DEBF-12-3-8-MH	0.0158*	0.0356	0.098			
DEBF-12-3-8-HH	0.0206*	0.0580	0.166*			

*the deformation requirement exceeds the acceptance criteria

3.3.3. Beam deformations

As described in paragraph 3.3.2 the same checks were made for the beam rotations. As seen in Table 8 the mean profile of beam rotations does not exceed the acceptance for none of the limit states considered. The values are much lower than the accepted ones by almost 5 times, even at DL limit state. This shows that the MRF beams do not suffer large deformations even at high seismic intensities. The MRF could serve this way as a backup for the failure of the EBF.

Table 8. Performance evaluation of beams

Frame	Mean profile of beam max rotation			Acceptance criteria		
	DL (IO)	SD (LS)	NC (CP)	IO	LS	CP
DEBF-6-3-6-MH	0.0047	0.0080	0.0151	0.0247	0.117	0.143
DEBF-6-3-6-HH	0.0063	0.0114	0.0242	0.0247	0.117	0.143
DEBF-6-3-8-MH	0.0054	0.0094	0.0171	0.0342	0.162	0.198
DEBF-6-3-8-HH	0.0081	0.0127	0.0266	0.0342	0.162	0.198
DEBF-12-3-6-MH	0.0058	0.0083	0.0129	0.0228	0.108	0.132
DEBF-12-3-6-HH	0.0073	0.0116	0.0224	0.0228	0.108	0.132
DEBF-12-3-8-MH	0.0060	0.0091	0.0126	0.0304	0.144	0.176
DEBF-12-3-8-HH	0.0080	0.0123	0.0328	0.0304	0.144	0.176

3.4   Incremental dynamic analysis

For performing incremental dynamic analyses (IDA) [7], the same ground acceleration input as for the time-history analyses was used. The parameters were kept unmodified. The ground motions were scaled by factors ranging from 0.25% to 400% at a constant step of 0.25%. The basic parameters monitored are the maximum inter-storey drift ratios (directly related to the rotation demands on connections) and the absolute storey accelerations (related to non-structural damage). Representative IDA curve sets in terms of maximum inter-storey drift ratio vs. ground motion intensity are presented in the plots of Figure 8. From the inter-storey drift IDA curve sets most of the frames considered, exhibit a hardening behaviour, with increasing ground motion intensity. However for the HH frames at higher seismic intensities, above 200% a soft storey mechanism begins to show. The IDA curves show a hardening mean response for all the considered frames. In the case of the 00293T accelerogram for HH frames, a softening behaviour can be observed, together with an intermediate collapse area followed by a structural resurrection. At different seismic intensities the global response of the structure changes, due to different failure mechanisms.

At the Damage Limitation (DL) performance level (corresponding to ground motion intensity 100%), the inter-storey drifts range approximately between 0.0075 rad and 0.012 rad, on average, which is much lower than the generally accepted ultimate drift levels for connections (0.035-0.040 rad). The latter levels of deformation are attained at intensities close to 350% (corresponding to two times the NC performance level) for the MH frames and around 175% for the HH frames.
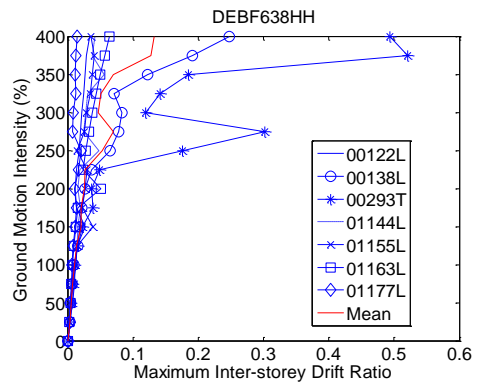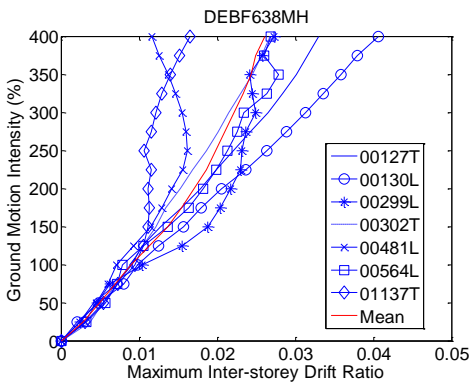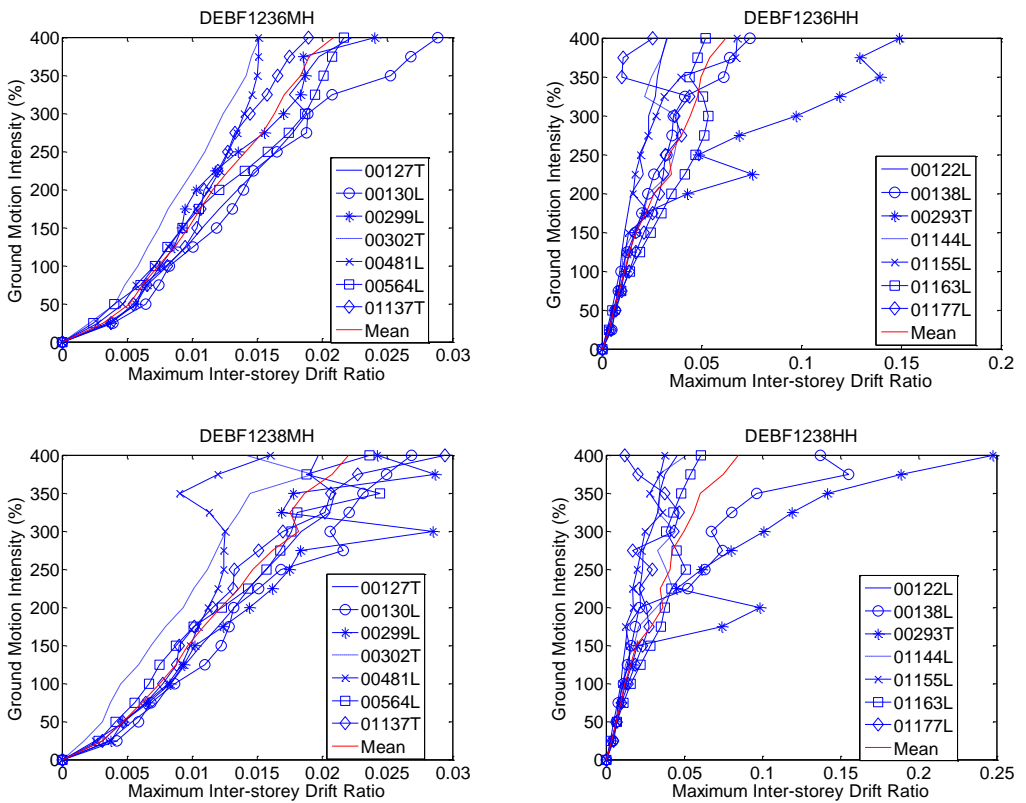
Figure 8. IDA curves maximum inter-storey drift ratio

IDA curve sets for maximum floor accelerations (absolute) vs. ground motion intensity for the 6-storey frame typology MRF636 (MH and HH) are presented in Figure 9. The peak recorded absolute accelerations are systematically recorded at the top floor of the frames. The dynamic amplification with respect to the peak ground acceleration is of the order of 400%.
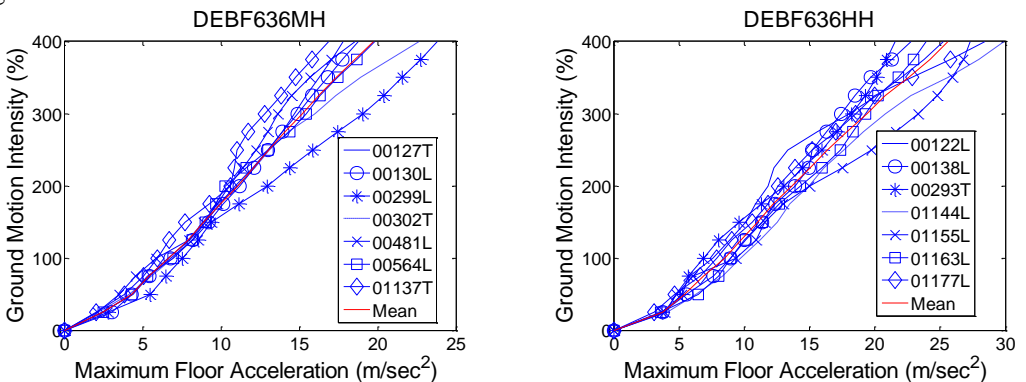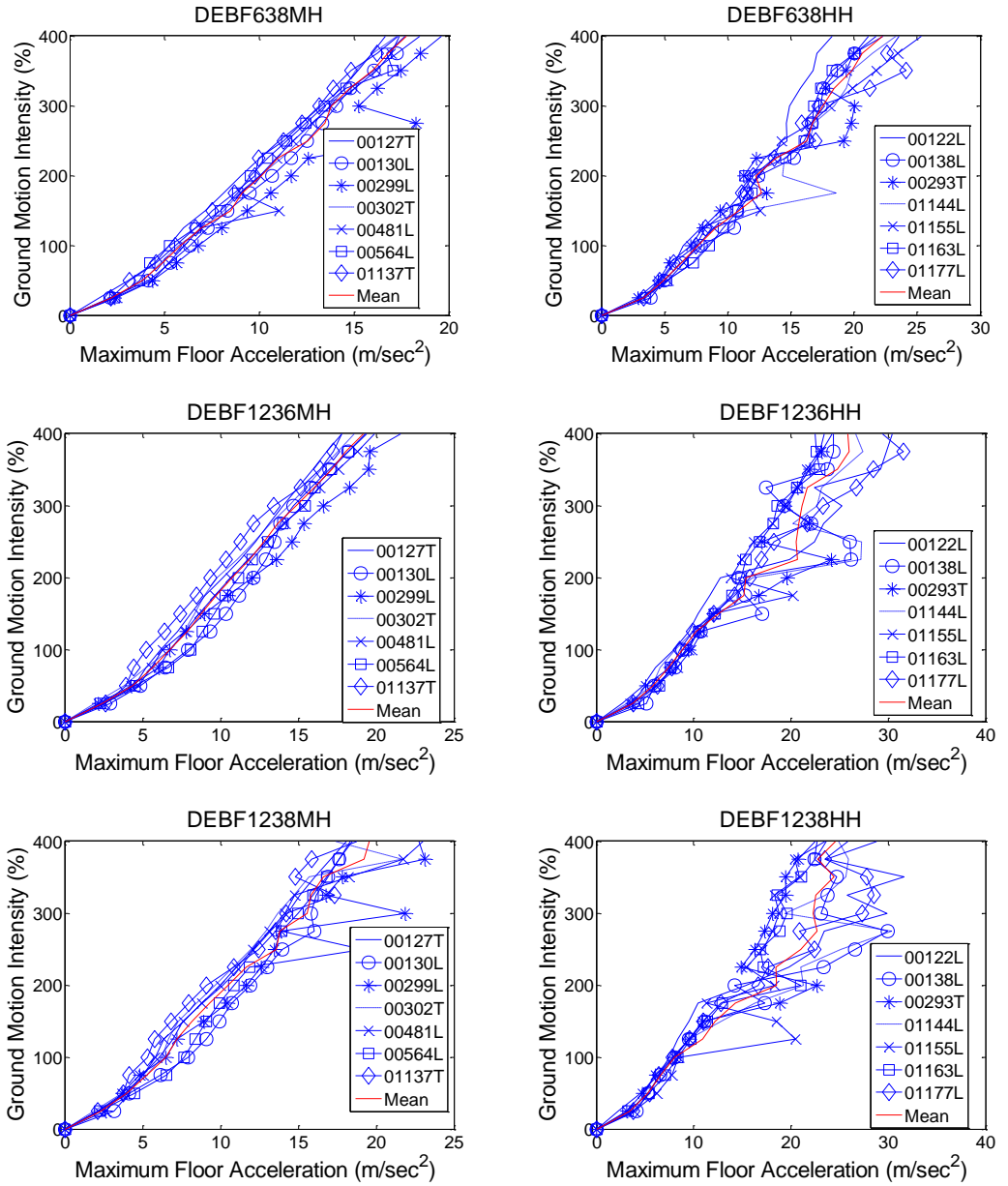
Figure 9. IDA curves maximum floor acceleration

4.   CONCLUSIONS

The 3D modelling approach allows the designer to check the structure's response including the buckling of compressed elements. This type of modelling gives a more realistic feedback of the structural behaviour. At the same the analysis and the results processing requires more resources and time.

As presented in the previous chapters the pushover results give valuable insights of the general behaviour of the considered frames. Different failure modes can be observed, varying from global failure of the frame through hardening behaviour to local failure of elements through a softening plateau. It can be seen that the P-delta effects have a large impact on the response of the structure, especially when imperfection are included in the model.

The time history analysis shows that for medium seismic hazard, the length of the bays has a negligible influence on the response of the structures (in terms of inter-storey drift), even at the near collapse limit state. For structures subjected to high seismic hazard, the span has a big influence on the response of the structure, leading to an absolute inter-storey drift increase of almost 50% from a 6 m span to an 8 meter span. The residual inter-storey drift is also increased by 2.5 times.

At element level, the two monitored deformations show that for the first limit state (DL) all the links exceed the acceptance criteria, whereas the beams have minor deformations. For the SD limit state neither of the two exceed the accepted values. At the CP limit state only links from 2 of the HH frames, with 8 m span length exceed the accepted rotation.

The performance of the structures can be further analysed in terms of elements behaviour to identify if the non-dissipative elements requirements are within the acceptance criteria; their design strength is not exceeded.

References

1. A. Tsitos, A. Elghazouli, *European pre-QUALified steel JOINTS: Provisional design of protype building and selection of strong motions records, Rev.02*. Imperial College London. July 2014
2. A. Zsarnóczay, L.G. Vigh, *Experimental and Numerical Investigation of Buckling Restrained Braced Frames for Eurocode Conform Design Procedure Development*, Budapest University of Technology and Economic, Budapest, 2013.

3. American Institute of Steel Construction, Inc. (AISC) (2010). *Seismic provisions for structural steel buildings*. Standard ANSI/AISC 341-10. Chicago (IL, USA).
4. ASCE/SEI 41-13: American Society of Civil Engineers: seismic evaluation and retrofit of existing buildings. ASCE standard. ISBN 978-0-7844-1285-5
5. CEN (2004). Eurocode 8: Design of structures for earthquake resistance – Part 1: General rules, seismic actions and rules for buildings. European Standard EN 1998-1:2004, Brussels.Eurocode 8
6. CEN (2004a). Eurocode 3: Design of steel structures – Part 1-1: General rules and rules for buildings. European Standard EN 1993-1-1:2004, Brussels.
7. D. Vamvatsikos and C. Allin Cornell. *Incremental dynamic analysis* Department of Civil and Environmental Engineering; Stanford University; CA 94305-4020; U.S.A.
8. G. Della Corte, M. D'Aniello, F.M. Mazzolani, (2008). *Overstrength of Shear Links in Eccentric Braces*. 15th World Conference on Earthquake Engineering, Lisbon.
9. EN 10034: 1993. "Structural steel I and H sections. Tolerances on shape and dimensions".
10. FEMA 356 (2000). "Prestandard and commentary for the seismic rehabilitation of buildings". Federal Emergency Management Agency;
11. Okazaki T., Engelhardt M. D. (2007). *Cyclic loading behaviour of EBF links constructed of ASTM A992 steel*. Journal of constructional Steel Research, 63, 751-765.
12. OpenSees (2015). *Open System for Earthquake Engineering Simulation*, Pacific Earthquake Engineering Research Center, University of California at Berkeley, California USA (opensees.berkeley.edu as of March 10th 2015).

Appendix

λ	Hazard level amplification factor
f_y	Steel yield stress
A_{vz}	Effective shear area of steel section
G	Shear elastic modulus
γ_{MI}	Material safety factor
e	Link length
E	Steel modulus of elasticity
b	Strain hardening ratio
γ_{ov}	Steel overstrength coefficient
V_y	Shear yield force
V_u	Shear ultimate force
K_s	Link shear elastic stiffness of element
γ_y	Link yield shear deformation
γ_u	Link ultimate shear deformation

Numerical Modelling of Beam-to-Column Connections Under Column Loss Scenarios

Ioan Mărginean, Dan Dubină and Florea Dinu

Department of Steel Structures and Structural Mechanics, Faculty of Civil Engineering, Politehnica University Timisoara, 200224, Romania

Summary

When steel moment frames are properly designed and detailed, additional capacity of carrying loads by catenary action can secure the resistance against progressive collapse in case of extreme load events. This may be accomplished by providing beam-to-column connections with improved ductility and strength properties. In order to achieve this aim, the connections should be designed for the combined effects of flexure and axial tension. This requirement is more demanding for partial-strength connections, where the plastic deformations are designed to develop within the connection components.

The paper presents the results of a research program that aimed at evaluating the capacity of typical beam-to-column connections to allow the development of the catenary action following the loss of a column. Two types of connections have been studied, i.e. end plate bolted connection and reduced beam section welded connection. Finite Element Method numerical models were used to design the test specimens and optimize the testing procedure. Using the FEM model, the evolution of bending moment and axial force at different cross sections with important plastic deformations has been monitored. These parameters give valuable information about the redistribution of stresses when connections are loaded beyond flexural capacity.

KEYWORDS: end-plate bolted connection, reduced beam section, catenary action, robustness, column loss scenario, FEM modelling, M-N interaction

1. INTRODUCTION

Moment resisting connections are widely used in the steel frame constructions. They can be designed to range from flexible and partial resistant connections to stiff and strong connections. Past research focused on earthquake type loading and gravity loading associated to permanent design situations. However, there are specific problems which need to be considered when localized failures, particularly of columns, occur, i.e. development of the catenary forces in the beams and admissibility criteria to be considered in the design considering the interaction between axial loads and bending moments. It is therefore of interest to study the

capacity of actual design procedures to provide enough robustness for connections under extreme loading conditions [1].

A large experimental program on connection components and assemblies with different connection configurations was developed within the framework of the CODEC research program at PU Timisoara [2]. The scope of the investigations was to evaluate the influence of initial design conditions of connections (i.e. capacity, failure mode) in case of extreme events, like column loss scenarios. The paper presents the results of the numerical simulations on joint specimens with reduced beam section connections (RBS) and extended end-plate bolted connections (EP) subjected to central column loss scenarios. The RBS and EP connections were designed for permanent and seismic design situations. The characteristics of materials used for the numerical models were obtained from coupon tests on the same material that were used to manufacture the specimens.

2. TEST SET-UP AND JOINT SPECIMENS

A case-study building with three bays, four spans and six storeys steel structure with moment frames in both directions was used as reference structure (Figure 1). The bays and spans each measured 8.0 m, and each story was 4.0 m high. The structure was design for permanent and design situations. Dead and live loads amounted 4.0 kN/m2 each and design acceleration was ag = 0.08 g (low-seismicity area). The details of the structure are presented in [3].

A perimeter frame with two bays and one story (Figure 1) was extracted from the reference building structure and downscaled. This scaling resulted in a 6.0 m long specimen, with two equal bays of 3.0 m and 1.2 m height columns. The beams were made from IPE 220 hot rolled profiles and the columns were HEB 260 profiles with the flange chamfered to reduce the width to 160 mm. The marginal columns were pinned at the base and the central column was removed.

The vertical displacement on the central column was introduced with a hydraulic actuator, as presented in Figure 1. The actuator acts also as a vertical support for the missing central column in the initial stage, before starting the test.

Double-pinned horizontal elements connected to the marginal columns and reaction structures serve as boundary conditions to simulate the continuity of the frame in the reference structure. A lateral restraining system was used to prevent out of plane displacements of the specimen.

The two types of connections are presented in Figure 2. The beam to end-plate weld is a full penetration weld. The nominal thickness of the end-plate is 16 mm. The 16 mm 10.9 class bolts are disposed in 5 rows (90mm, 60mm, 60 mm and 90

mm distances between rows). The horizontal distance between bolts is 70 mm. The bolts were not pre-loaded.

In case of RBS, the weld between the beam and the column is a full penetration weld. The cut outs from each flange were 22 mm within a 140 mm radius circle.
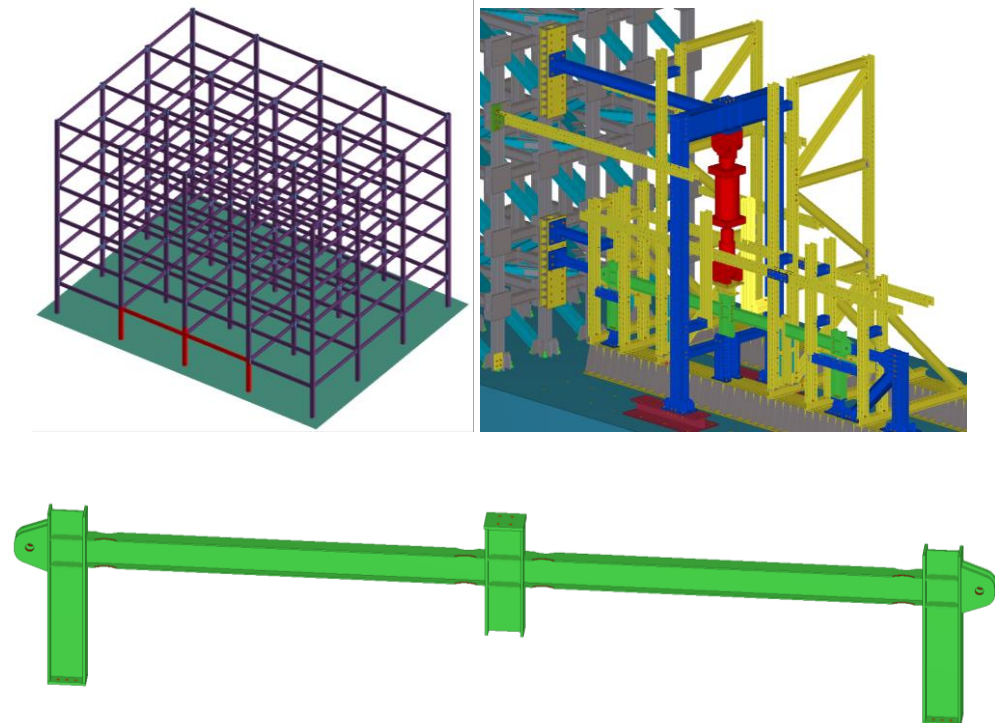

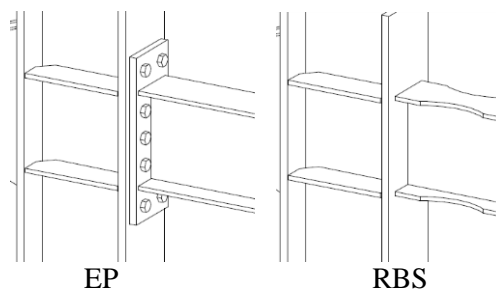Figure 1. Case study structure (top left); test set-up (top right); specimen (bottom)

Figure 2 View of connections: extended end-plate connections (left);
reduced beam section connection (right)

3. CALIBRATION OF MATERIAL

The material model is based on experimental tensile tests performed on coupons extracted from the same steel plates and steel profiles that were used to manufacture the specimens. The tensile tests were performed in the *Research Center for Mechanics of Materials and Structural Safety* – CEMSIG Laboratory of Politehnica University Timisoara, Romania on an INSTRON universal testing machine and the elongations were measured using a video-extensimeter module. Two points at each end of the calibrated length of the coupons were visually monitored during the tensile test (see Figure 3) in order to get an accurate relative displacement, avoiding errors such as grip slippage and influence of the elasticity of the machine itself.

Figure 3. Tensile test in progress (left); coupons with monitored white dots (right)

Three tensile tests were performed for each material category. Since the engineering stress-strain curves for coupons in the same batch were very similar, only one curve for each material was selected and processed. The engineering stress-strain curve extracted from the test was transformed in a true stress - true strain curve up to the ultimate force with equations (1) and (2) from EN 1993-1-5 [5]. When the necking occurs after the maximum load, the material seems to soften, while it is actually hardening [6]. After the attainment of maximum engineering strain, the material law in the true stress - true strain curve was considered ascending with a parabolic shape that was obtained through iterations by comparing the model results with the experimental results (Figure 4).

$$\sigma_{true} = \sigma(1 + \varepsilon) \tag{1}$$

$$\sigma_{true} = \ln(1 + \varepsilon) \tag{2}$$

Finite element models were constructed in Abaqus [4] for the tensile test on coupons, with the actual dimensions of the specimens. Only the coupon outside the grip was modelled, assigning kinematic restraints (highlighted in red in Figure 4 left) to the ends of the coupon by linking them to reference points. One reference point was fixed in all degrees of freedom, while to the other a vertical displacement was imposed in a dynamic explicit step. The monitored displacement in the FEM analysis was between points located in the same zone as the points monitored with

the video extensimeter (highlighted points in Figure 4 right). The mesh considered for this specimen was the equivalent size for the mesh in the joint models in the important plastic zones.

Apart from the true stress-plastic strain curve, material density (7.85 10^{-9} tons/mm^3), Young's modulus (210000N/mm^2) and the 0.3 Poisson's ratio, the IPE 220 web material model consists also of a ductile damage characterised by 0.4 fracture strain and 0.8 stress triaxiality. Also the sub-option of damage evolution was introduced – displacement type, linear softening and maximum degradation with 0.4 displacement at failure.
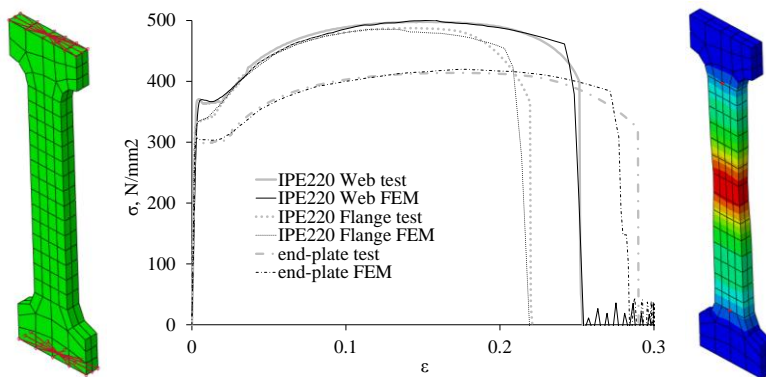
Figure 4. FEM model of coupon and its constraints (left); test and FEM engineering stress-strain curve (middle); strain and deformed shape of coupon with monitored points (right)
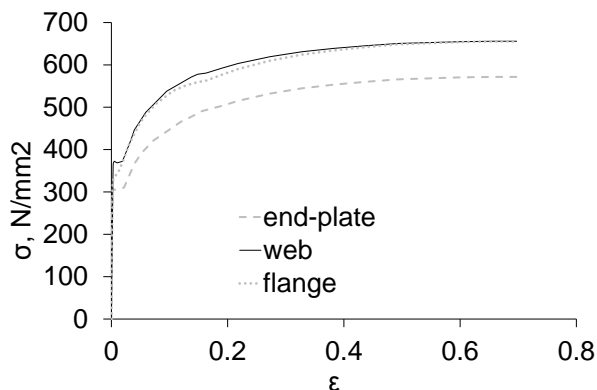

Figure 5. True stress-strain material curves

For the other materials, changes of fracture strain and elongation at failure have been done in order to comply with the breaking point. Also, changes to the polynomial parameters for the true stress - true strain relationship after the

maximum force were made in order to match the descending shape of the engineering stress-strain curve. Figure 5 plots the stress - true strain curves for materials. With the same procedure, the bolt material has been calibrated using experimental tensile tests on similar bolts that were used in the experimental tests.

4. NUMERICAL MODEL OF JOINTS

The analysis was performed in dynamic explicit step, using mass scaling in order to obtain a reasonable computational time. Thus, the ratio of kinematic energy and external work was monitored and maintained less than 1%. Nominal geometry was used to create the model (Figure 6). The lateral restraining system was modelled as in the test set-up. A general contact "all with self" has been defined with a "hard" contact interaction allowing all external surfaces to create contact reaction forces when the surfaces are close.

The horizontal links and reaction structures were modelled as beam parts meshed with B31 elements (2-node linear beam in space). C3D8R (8-node linear brick, reduced integration, hourglass control) finite elements were used to mesh solid parts in sweep or structural tehnique using local seed constraints for refined meshes in important zones (see Figure 7). The mesh size of the plastic zones has the same shape and size as the mesh of FEM models for material calibration of coupon tests.

Interaction between nodes was also modelled (some are presented in Figure 8). Welds were either modelled as ties on all degrees of freedom between points of two different solid parts, or directly modelled as material in the solid part. Kinematic constraints connected nodes from a surface to a reference point to which boundary conditions are imposed (the hinge under the edge columns, or the loading point above the central column). A smooth step amplitude displacement controlled load was applied. Small imperfections were asummed by the asymmetry of the mesh and vibrations in the dynamic loading.
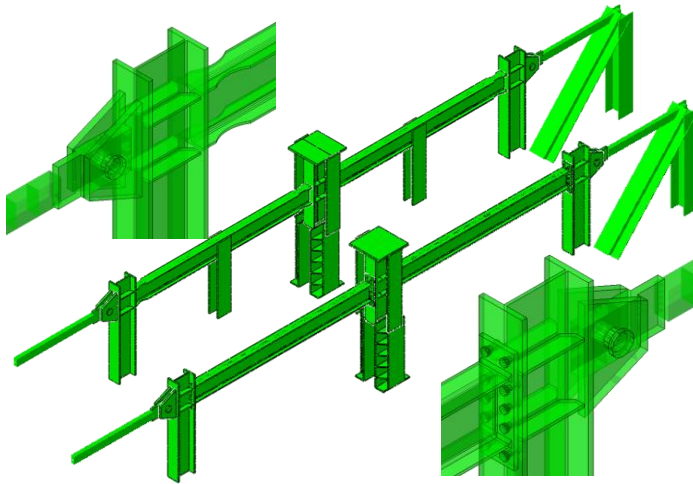
Figure 6. FEM model of joints: left connection of RBS joint (top-left); FEM model of RBS connection joint (top-middle); FEM model of EP connection joint (bottom-middle); right connection of RBS joint (bottom-right)
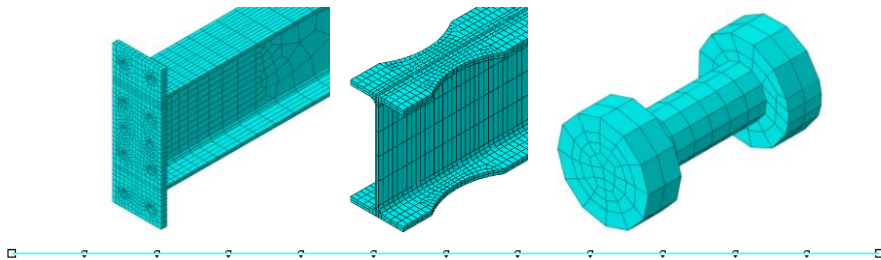

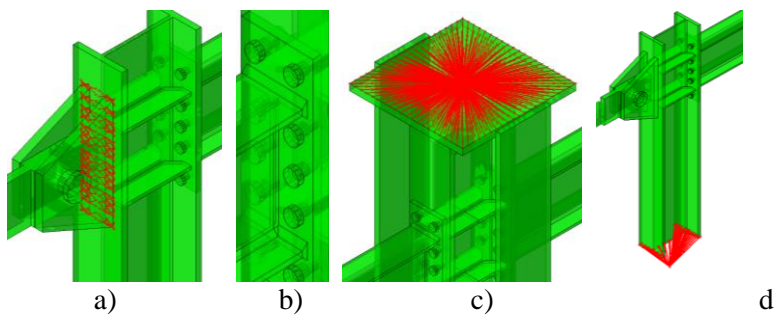Figure 7. Mesh of solids parts: (top), and beam elements (bottom)

a)   b)   c)   d

Figure 8. FEM constraints weld - by ties (a) or direct modelling, couplings (b)– on the surface (c), or with offset (d)

5. ANALYSIS RESULTS

The vertical force - vertical displacement curves for the two specimens are presented in Figure 9. In the initial elastic stage, it may be seen that the EP specimen is more flexible than RBS specimen, due to the flexibility of the end-plate and the tolerances for the bolt holes. The lower level of yield force for the RBS can be explained by the cross-section reduction near the edges of the beam, where plastic deformations develop first. Figure 10 and Figure 11 show the deformed shape of the specimens and Von Misses stresses/PEEQ for some details. The failure mode of the EP specimen is caused by the fracture of the bolts in bending and tension. Tension in bolts is due to the bending moment component, the axial force component and the prying effect, which can amplify the axial force in bolts with respect to the axial force imposed directly on the T-stub (Dinu et all 2015 STESSA). Plastic deformations were isolated in the end-plate near the tensioned flange (the upper flange for the marginal connections and the bottom flange for the central connections) and in the beam, near the connections. The maximum force was 185 kN at 196 mm vertical displacement until the last row of bolts from the central connection fractured. As the deformation increased, other bolt rows successively fractured in other locations and the same connection. The force has vibrations due to these sudden losses of capacity, but if these vibrations are neglected, the capacity seems to have an increasing trend between the points of bolt fracture.
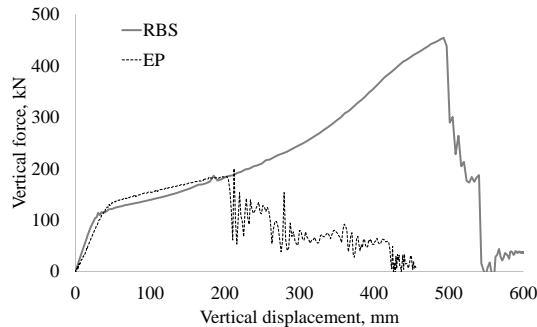
Figure 9. Vertical force-vertical displacement cures for EP and RBS
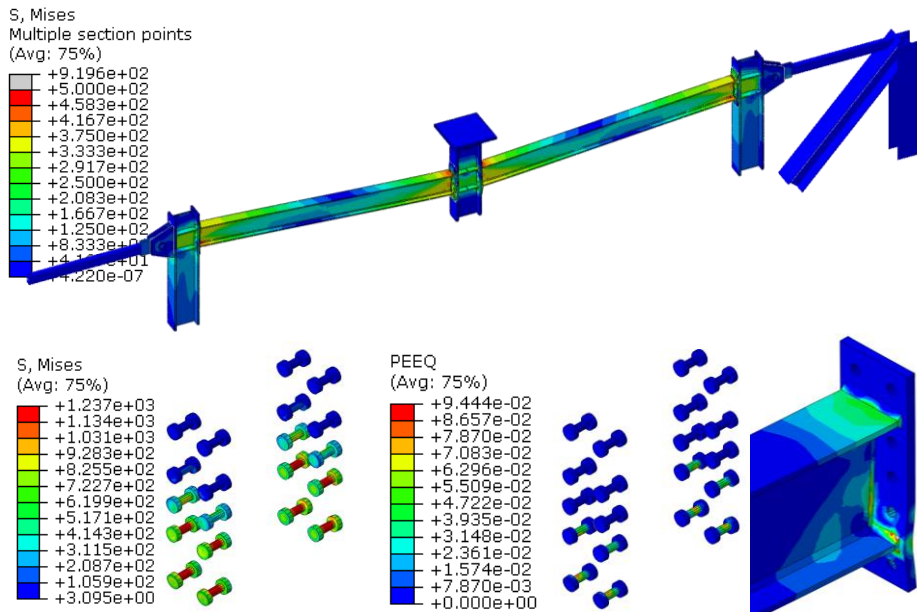
Figure 10. Deformed shape of EP at maximum load: Von Misses stress on beams and columns (top); Von Misses stress on bolts (bottom-left); PEEQ deformation for bolts and end-plate (bottom-right)
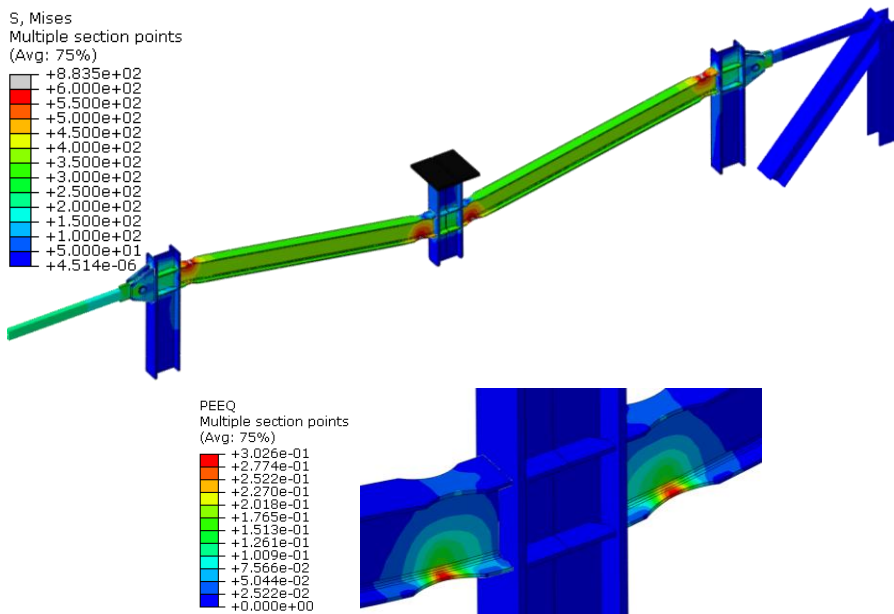
Figure 11. Deformed shape of RBS at maximum load: Von Misses stress (top); PEEQ deformation (bottom)
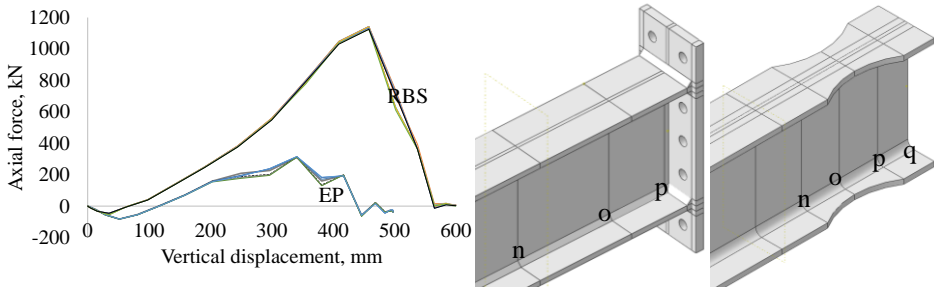
Figure 12. Axial loads in several sections of the beam vs vertical displacement for RBS and EP (left); beam end position of sections and notations (right)

(a)

(b)
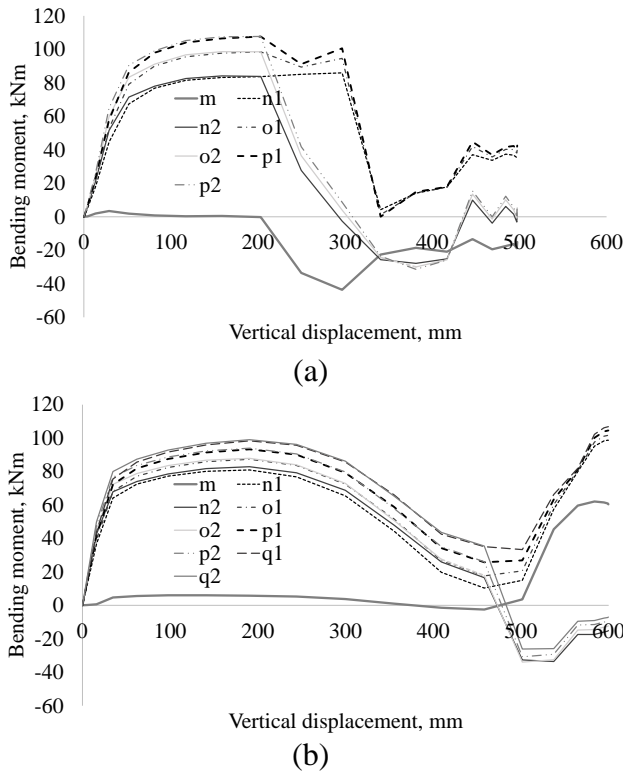
Figure 13. Bending moment in beam at different locations vs vertical displacement for EP (a) and RBS (b)

The plastic deformations of the RBS specimen were concentrated in the reduced sections, mostly on the tensioned flanges. The failure is cause by fracture of a flange in tension in the reduced zone at a vertical force of 455 kN and respectively 493 mm. The bending moment and axial force were monitored in several locations along the beam length: middle (noted as m) and n-p for EP and respectively n-r for

RBS (see Figure 12). The notations 1 and 2 represent the left and respectively right position of the cross sections on the beam. At a vertical deformation of 300 mm, an increase of axial force rigidity can be identified for the RBS specimen. This change is also indicated by a stiffness increase at 300 mm vertical displacement related to the vertical force and is directly related to the capacity increase due to catenary action. The axial force developed in the EP specimen (Figure 12) is significantly lower than in the RBS, due to a higher flexibility and also due to early failure of bolts. Bending moments in several locations of the beam are presented in Figure 13. As the bolts fracture in the EP specimen, the bending moment in the beam decreases. Fracture of bolts in the central connections of the EP specimen changed the static equilibrium, introducing moments in the middle of the beam. In the case of the RBS specimen, the bending moments significantly decreased after a vertical displacement of 300 mm, as a result of the increase of the axial force.

3. CONCLUSIONS

The paper presents the results of a numerical study on assemblies with RBS and EP connections subjected to column loss scenario. Material should be calibrated for each mesh size, as the for the higher plastic strain levels the material behaviour depends on the size of the mesh, even if in a continuous steel element, but with different mesh size. The bending moment and vertical force for the RBS specimen are directly linked to the axial force developed in catenary action, showed by the change of the curvature of all these parameters at 300 mm vertical displacement. The ductility and ultimate capacity of the RBS specimen are 2.5 times greater than the one of the EP specimen. The EP specimen does not develop catenary action due to bolt failure in tension. The premature failure of bolts in the EP connection develops, and suggests that such connections should be designed according to acceptance criteria developed specifically for column loss scenarios.

References

1. Dinu, F., Dubina, D., Marginean, I, Neagu C., Petran I., *Axial strength and deformation demands for t-stub connection components at catenary stage in the beams,* 8th International Conference on Behavior of Steel Structures in Seismic Areas, 2015

2. CODEC. *Structural conception and collapse control performance based design of multistory structures under accidental actions, 2012–2016.* Executive Agency for Higher Education, Research, Development and Innovation Funding, Romania, grant PNII PCCA 55/2012, the Partnerships Program Joint Applied Research Projects, 2012.

3. Dinu, F., Dubina, D., Marginean, I., *Improving the structural robustness of multi-story steel-frame buildings,* Structure and Infrastructure Engineering, Vol. 11, Issue 8, 2015 DOI: 10.1080/15732479.2014.927509.

4. ABAQUS *User's Manual, Version 6.9 (2007).* D. Hibbit, B. Karlson & P. Sorenson, Inc.

5. EN 1993-1-5, *Eurocode 3: Design of steel structures - Part 1-5: General rules - Plated structural elements,* CEN, 2006.

6. Arasaratnam P., Sivakumaran K. S., Tait M. J., *True Stress-True Strain Models for Structural Steel Elements, I*SRN Civil Engineering Volume 2011, 2011

Material Calibration for Static Cyclic Analyses

Andrei Crișan[1]

[1]Department of Steel Structures and Structural Mechanics,
Politehnica University of Timisoara, Timisoara, 300224, Romania

Summary

The material behaviour constitutive laws play a central role in the analysis of engineering components. With the focus to improve the representation of stress-strain response under non-monotonic loadings, several models for cyclic plastic deformation have been developed in recent years. Present FE commercial packages provide models for the analysis of plastic deformation of metallic materials, even though the most recent models are yet to be implemented. A combined isotropic/kinematic hardening model can be used as an extension of simple linear models. This approach provides a more accurate approximation to the stress-strain relation than the linear model. It also models other phenomena, such as ratchetting, relaxation of the mean stress and cyclic hardening, which are typical of materials subjected to cyclic loading.

Present paper presents the calibration and validation of the numerical model as part of a research project that was performed to check the validity of the moment frame connections of an 18-story steel structure. The finite element models were calibrated using experimental tests performed on four full-scale specimens at the CEMSIG Laboratory, Politehnica University Timisoara, Romania. Based on experimental test results, multiple cyclic material behavioural models were employed in order to obtain the best fitting curve.

KEYWORDS: isotropic hardening, kinematic hardening, cyclic loading, FEA

1. INTRODUCTION

Modelling the real elastic–plastic stress–strain response plays a central role in the design and failure analyses of engineering components. With the focus to improve the representation of stress-strain response under non-monotonic loadings, several models for cyclic plastic deformation have been developed in recent years. The need of different material models arises due to the fact that for modelling cyclic loading, uniaxial test information is not sufficient to describe the material behaviour. Experiments show that the cyclic plastic characteristics of a metallic

material are different from the monotonic. Using monotonic data to analyse cyclic behaviour of a steel component may lead to significant errors.

Reliable results on the yield limit and hardening behaviour can be obtained with one rather simple experiment (i.e. uniaxial tensile test), while undertaking experiments to determine the cyclic plastic behaviour of metals is very complex procedure. One aspect to be monitored is the cyclic hardening/softening of the material. The hardening behaviour will change as the load cycles and the stress-strain behaviour may become very different from the monotonic.

Following extensive research, a large variety of constitutive models is available to describe the material behaviour of metals under cyclic loading. The theories are based on the observation of some of the characteristic experimental behaviour in cyclic plasticity. Magnus and Segle [1] examined the capabilities and limitations of some of the most commonly used models in cyclic plastic deformation.

Reviewing some of the existing material models for cyclic material behaviour, present paper presents the calibration and validation of the numerical model, as part of a research project that was performed to check the validity of the moment frame connections of an 18-story structure. The finite element models were calibrated using experimental tests performed on four full-scale specimens at the CEMSIG Laboratory, Politehnica University Timisoara, Romania.

2. MATERIAL MODELS

Araujo [2] presents the comprehensive description of existing material models together with the mathematical and mechanical background. A brief description is presented hereafter.

In order to describe the work-hardening material behaviour, an initial yielding condition, a flow rule, and a hardening rule is required. The purpose of initial hardening rule is to specify the state of stress for which plasticity will first occur.

Plastic materials have an elastic range within which they respond in a purely elastic manner. The boundary of this range, in either stress or strain space, is called the yield surface. The shape of the yield surface depends on the entire history of deformation from the reference state. The yield surface can change its size and shape in the stress space. When the yield surface expands it is said that material hardens and when it contracts it is said that material softens. If the material under consideration strain-hardens, the yield surface will change in accordance with the hardening rule (i.e. isotropic, kinematic, combined) for values of stress values beyond the initial yield point, where the yield point will rise to the new value of the stress state in the work-hardened material.

Since it is difficult to determine the exact locus of the yield surface, many yield criteria have been proposed. The most commonly used type of surfaces for steels is the von Mises kind, where two state variables are used: the kinematic and the isotropic hardening variables. The kinematic variable accounts for the translation of the yield surface, while the isotropic variable accounts for its change in size or expansion. After the elastic limit is reached, the state of stress lies on the yield surface. If loading continues, hardening can be manifested in one of these two forms (or both): isotropic and kinematic. Isotropic hardening accounts for the expansion of the yield surface and kinematic hardening accounts for its translation in the deviatoric stress space.

2.1. Cyclic material models

Vast majority of cyclic material models rely on the two types of hardening rules described before i.e. isotropic and kinematic. Figure 1, a) presents the difference between isotropic and kinematic hardening for a uniaxial cycle loaded steel sample. For isotropic hardening, the yield surface remains the same shape, but expands with increasing stress (see Figure 1, b). The shape of the yield function is specified by the initial yield function and its size changes as the hardening parameter changes. The isotropic hardening rule cannot model the Bauschinger effect, nor similar responses, where a hardening in tension will lead to softening in a subsequent compression. This model implies that an initial yield surface symmetric about the stress axes will remain symmetric as the yield surface develops with plastic strains. In order to be able to account for such effects, a kinematic hardening rule must be implied. For this model, the yield surface remains the same shape and size but translates in stress space. The distance between the centres of the surfaces is defined as the back-stress or shift-stress.
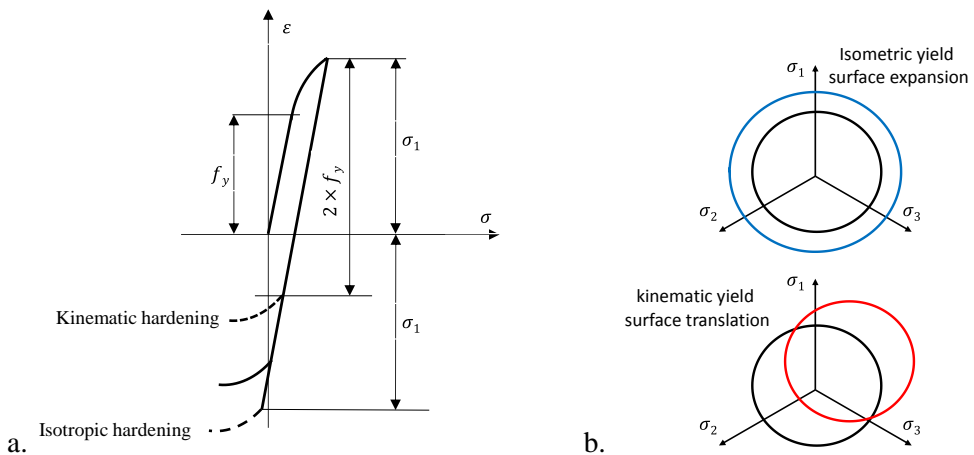

Figure 1. Isotropic/Kinematic hardening

Following, a short review of cyclic models evolution is given.

Initially, Prager [3] proposed a simple kinematic hardening rule, to simulate plastic response of materials under cyclic loading. For a prescribed uniaxial stress cycle with a mean stress, the model fails to distinguish between shapes of the loading and reverse loading hysteresis curves and consequently produces a closed loop with no ratcheting. Following, Mroz [4] proposed an improvement of the linear kinematic hardening model as a multisurface model, where each surface represents a constant work hardening modulus in the stress space. Earlier, in 1958, Basseling [5], introduced a multilayer model without any notion of surfaces. Unfortunately, like the linear kinematic hardening model, multi-linear models also predict a closed loop.

Following the pioneering work of Mroz [4], new concepts of uncoupled models have been introduced by Dafalias and Popov [6]. In this model, the plastic modulus calculation is not directly dependent on the yield surface kinematic hardening rule. The kinematic hardening rule specifies the direction of movement of the yield surface centre. During a uniaxial stress cycle, the yield surface moves along the stress direction only.

Probably, the best known nonlinear kinematic hardening model has been proposed by Armstrong and Frederick [7]. The model introduces a kinematic hardening rule that contains a 'recall' term. It incorporates the fading memory effect of the strain path and essentially makes the nonlinear rule. Several improved models which are based on the Armstrong-Frederick kinematic hardening rule have been developed.

Chaboche et. al. [8], [9] proposed a 'decomposed' nonlinear kinematic hardening rule. The Chaboche rule is, in fact, a superposition of several Armstrong-Frederick hardening rules, each with its specific purpose. Ohno and Wang [10] proposed a piecewise linear kinematic hardening rule. In his thesis, Bari [11] explains that a stable hysteresis curve can be divided into three critical segments where the Armstrong-Frederick model fails and explain in detail the functionality of above mentioned models.

2.2. Kinematic models in commercial FE program, ABAQUS [12]

For numerical simulations that contains metal elements subjected to cyclic loading Abaqus [12] offers a series of kinematic hardening models. The basic concept of these models is that the yield surface shifts in stress space so that straining in one direction reduces the yield stress in the opposite direction, thus simulating the Bauschinger effect and anisotropy induced by work hardening.

The linear kinematic hardening model is the simpler of the two kinematic hardening models available in Abaqus. The evolution law of this model consists of a linear kinematic hardening component that describes the translation of the yield

surface in stress space through the back-stress. It can describe stable loops in cyclic loading, including the Bauschinger effect. However, the linearity makes the approximation of the Bauschinger effect rather crude. One special case of the model is the one with zero tangent modulus, which will be identical to the perfectly plastic model.

The non-linear kinematic hardening model is based on the work of Lemaitre and Chaboche [13]. The evolution law of this model consists of two components: a nonlinear kinematic hardening component, which describes the translation of the yield surface in stress space (through the back-stress) and an isotropic hardening component, which describes the change of the equivalent stress defining the size of the yield stress, as a function of the plastic deformation. In this model, the kinematic hardening component is defined to be an additive combination of a purely kinematic term and a relaxation term (the recall term), which introduces the nonlinearity.

3. CASE STUDY

3.1. Experimental tests

In order to be able to calibrate and validate the numerical model, the results of an extended experimental program were used. The experimental work presented hereafter is connected with the design of a high-rise office building, located in a high seismic area. The lateral force-resisting system was intended to create a tube-in-tube structural layout with both perimeter and core framings steel framing composed of closely spaced columns and short beams. The central core is also made of steel framing with closely spaced columns and short beams. The ratio of beam length-to-beam height, L/h, varies from 3.2 to 7.4, which results in seven different types of beams. Some beams are below the general accepted inferior limit (L/h=4). The moment frame connections employee reduced beam section (RBS) connections that are generally used for beams loaded mainly in bending.

Detailed information regarding the experimental study is presented in [15], while a brief description is presented hereafter. The columns have a cruciform cross-section made from two hot-rolled profiles of HEA800 and HEA400 section. Both beams and columns are made from S355 grade steel. The base material characteristics have been determined experimentally. The measured yield strength and tensile stress of the plates and profiles were larger than the nominal values.

Figure 2 presents the test setup. Specimens were tested under cyclic loading. The cyclic loading sequence was taken from the ECCS Recommendations [16]. Further, in Figure 5 are presented the experimental test curve used for calibration, together

with the associated failure mechanism for the specimen with the RSB-S3 denomination [15].

The material properties (see Table 1) were determined using a uniaxial tensile test.

Table 1. Material properties based on uniaxial tensile tests

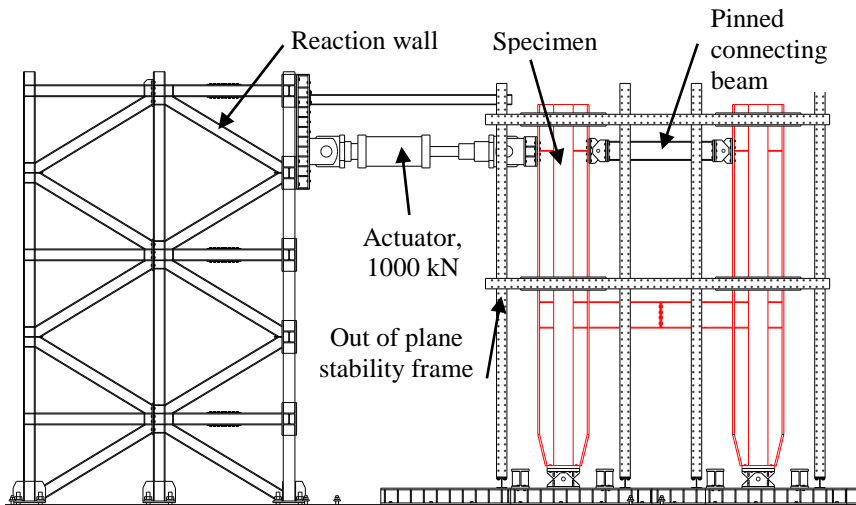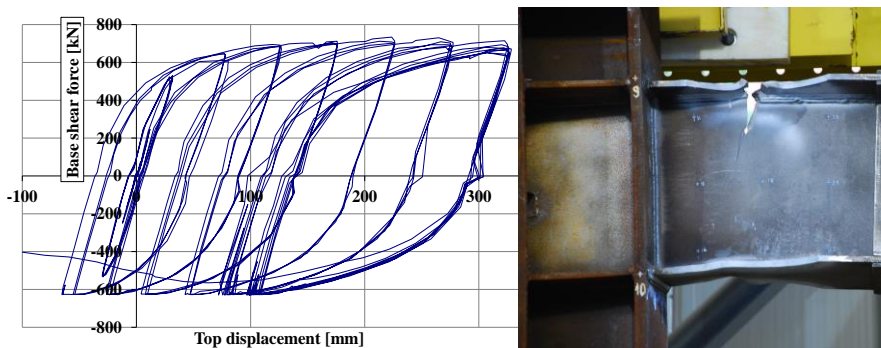| Section	Steel grade	Element	f_y [MPa]	f_u [MPa]	A_u [%]
HEA800	S355	Flange	410.5	618.5	15.0
		Web	479.0	671.2	13.0
HEA400	S355	Flange	428.0	592.0	15.1
		Web	461.0	614.0	12.8
14 mm	S355	Beam flange	373.0	643.0	17.0
20 mm	S355	Beam web	403.0	599.0	16.5

Figure 2. Test setup

Figure 3. Experimental behaviour curve and associated failure mode

3.2. Model definition

The geometric details of the numerical model were defined using the experimental tests as reference. Considering that the stress gradient within the elements thickness (i.e. flanges, web panels, etc.) is small enough, all components were modelled as shells and discretized using a quadratic 4-node doubly-curved "S4R" shell elements. It has to be noted that the S4R shell elements can capture the expected severe local buckling within the cross section. These elements also use reduced integration and hourglass control. The column edges at the top and bottom end are tied to the reference point using a "RIGID BODY" constraint in order to avoid local stress concentrations. At the bottom, the all three translations were blocked together with the rotation about the element axis. At the top, the rotation about element axis was blocked together with the out-of-plane translations. The axial shortening and the in-plane translations was allowed. In order to simulate pinned top connecting beam (see Figure 2), the reference points of top column constraints were tied together using a "TIE" constraint. Figure 4 presents the numerical model geometry, defined constraints, loading point and the load protocol.
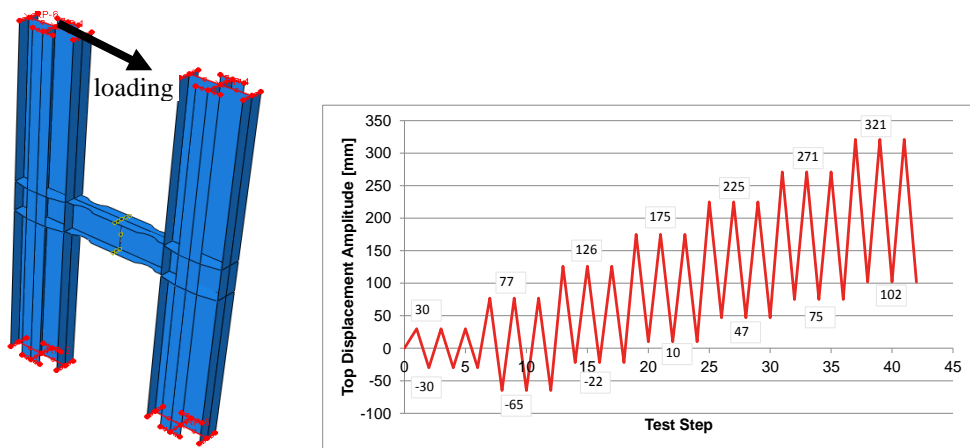
Figure 4. Geometry of numerical model and loading protocol

The load was applied at the top of left column according to the protocol presented in Figure 4.

3.3. Material calibration

Depending on the accuracy and the allowable strain required for the analysis, according to Annex C.6 of Eurocode 3 [17], the following assumptions may be used to model the material behaviour: a) elastic-plastic without strain hardening; b) elastic-plastic with a nominal plateau slope (E/10000 or similar small slope); c)

elastic-plastic with linear strain hardening (E/100); d) true stress-strain curve modified from the test results as follows:

$$\sigma_{true} = \sigma(1 + \varepsilon) \qquad (1)$$

$$\varepsilon_{true} = \ln(1 + \varepsilon) \qquad (2)$$

Based on the literature review presented before, multiple material modes were used to calibrate the numerical model. The elastic behaviour is modelled using the E, elastic modulus and ν, the Poisson's ratio.

3.3.1. Elastic – perfect plastic model

Usually, in structural analysis an elastic-perfect plastic model is accurate enough to model the behaviour of steel structures under monotonic loading. The parameters for an elastic-perfect plastic model are E, the elastic modulus, and the f_y yielding stress. The values used to define the elastic perfect plastic model are presented in Table 1 and in the Eurocode 3 [17]. The results of the numerical simulation, using the elastic-perfect plastic material model are presented in Figure 5.
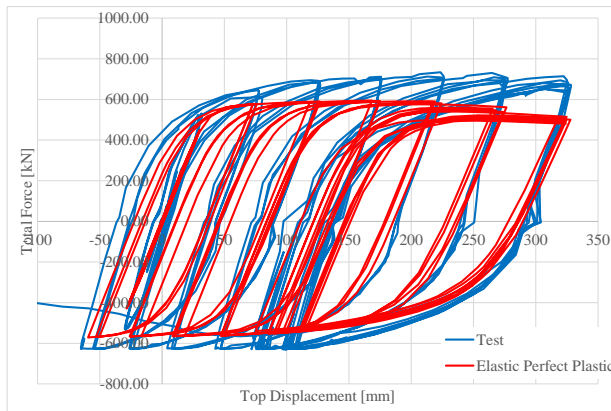
Figure 5. Experimental and numerical behaviour curves

3.3.2. Isotropic hardening model

When hardening is expected, this material model is very commonly used for metal plasticity calculations. The plasticity requires that the material satisfies a uniaxial-stress plastic-strain relationship. It use Mises yield surface with associated plastic flow, which allow for isotropic yield (increase of yield surface). This model is useful for cases involving gross plastic straining or for cases where the straining at each point is essentially in the same direction in strain space throughout the analysis.

For this model, the true stress – plastic strain was used to model the plastic material behaviour. In Figure 6 are presented the result using the isotropic hardening material model.

Figure 6. Experimental and numerical behaviour curves

3.3.3. Kinematic hardening model

As observed in Figure 6, the accumulation of plastic strain coupled with the inability to model the Bauschinger effect, lead to an overestimated of structural capacity. In order to solve this, a kinematic hardening model must be implied.

The true stress – plastic strain was used to model the plastic material behaviour. In Figure 7 are presented the results of the numerical simulation obtained using the kinematic hardening material model.
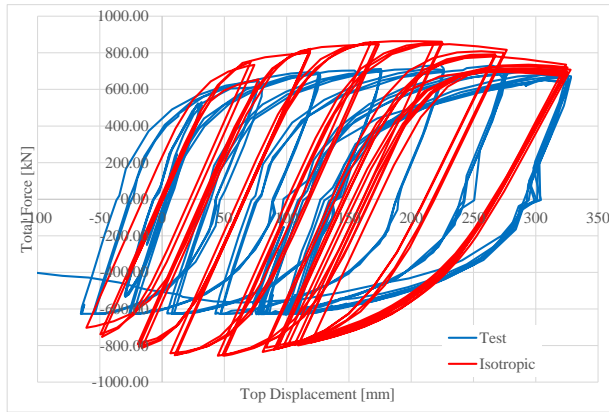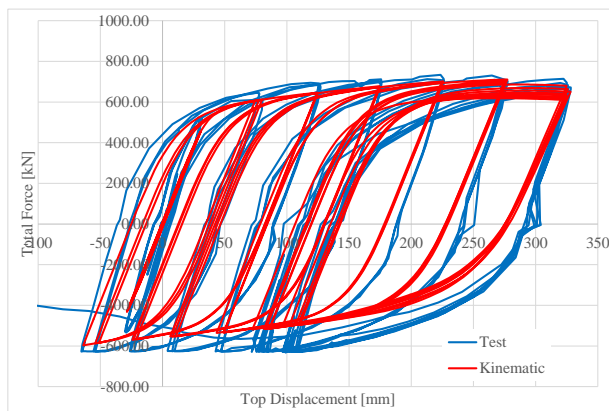

Figure 7. Experimental and numerical behaviour curves

3.3.4. Combined hardening models

Even if, the maximum load is achieved, the inability to correctly model the material hardening, resulted into underestimation of the minimum load. This nonlinear isotropic/kinematic hardening material model uses an evolution law that consists of two components: (i) a nonlinear kinematic hardening component, which describes the translation of the yield surface in stress space through the back-stress, and (ii) an isotropic hardening component, which describes the change of the equivalent stress defining the size of the yield surface as a function of plastic deformation.

Parametric

This material model simulates the cyclic strain hardening. In addition to the modulus of elasticity (E) and the yield stress (f_y), the nonlinear kinematic and isotropic hardening components are defined. C_γ is the initial kinematic hardening modulus, γ is the rate at which C_γ decreases with cumulative plastic deformation ε_{pl}. These two parameters can be determined using the uniaxial tensile test and the values for C_γ (linear kinematic hardening modulus) and γ were determined using the formulas presented below:

$$C_\gamma = \frac{\sigma - f_y}{\varepsilon_{pl}} \tag{3}$$

$$f_u = f_y + \frac{C}{\gamma} \tag{4}$$

In Figure 8 is presented the numerical results obtained using the combined parametric hardening material model.
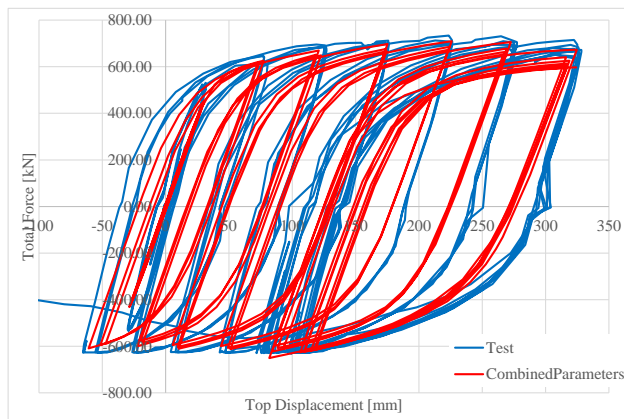
Figure 8. Experimental and numerical behaviour curves

Parametric with cyclic hardening

This material model simulates the cyclic strain hardening. In addition to the modulus of elasticity (E) and the yield stress (f_y), the nonlinear kinematic and isotropic hardening components are defined. C_γ is the initial kinematic hardening modulus, γ is the rate at which C_γ decreases with cumulative plastic deformation ε_{pl}. In addition to simple parametric model describer before, an isotropic hardening component can be defined. In Abaqus, this is defined by selecting Cyclic Hardening from the Suboptions menu. For this, the following two parameters are required: Q_∞ – the maximum change in the size of the yield surface and b – the rate at which the size of the yield surface changes as plastic deformation develops.

Since no cyclic data for the material was available, the cyclic plastic behaviour parameters were taken from the literature. In Table 2 are presented the values considered for each model. It has to be mentioned that all considered aterial parameters were determined for carbon-steels materials.

Table2. Material properties for combined hardening material model

No.	C [MPa]	γ	Q_∞ [MPa]	b	Reference	Results
1	25500	81	2000	0.26	[12]	Figure 11
2	2500	20	180	20	Unknown	Figure 12
3	6895	25	172	2	[18]	Figure 13
4	500000	50	20000	10	[19]	Figure 14
5	108939	2.5	-250	30	[20]	Figure 15
6	264156 20973	873 1.0	-320	30	[20]	Figure 16
7	16000	43	44	11	[21]	Figure 17

In Figure 9 to Figure 15 present the results obtained using the combined parametric hardening with cyclic hardening material model.

Figure 9. Experimental and numerical behaviour curves

Figure 10. Experimental and numerical behaviour curves

Figure 11. Experimental and numerical behaviour curves
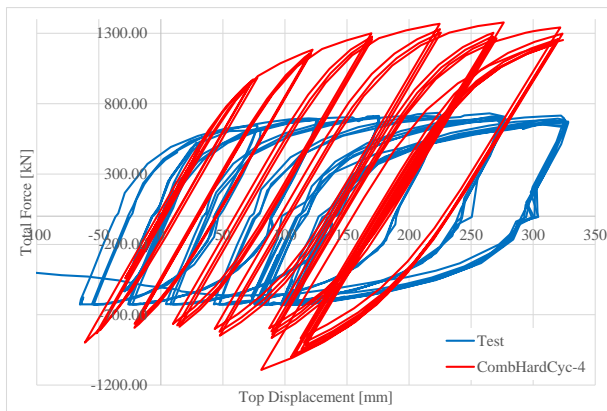
Figure 12. Experimental and numerical behaviour curves
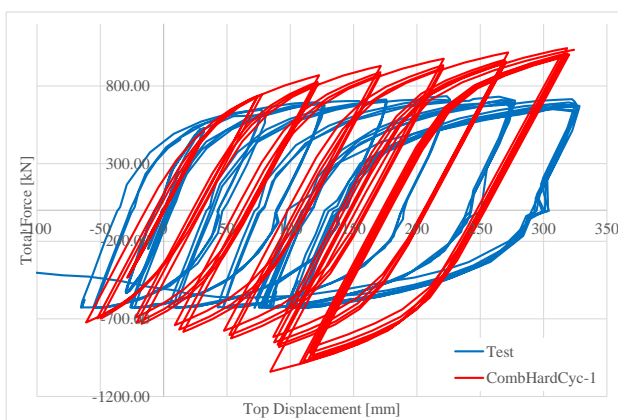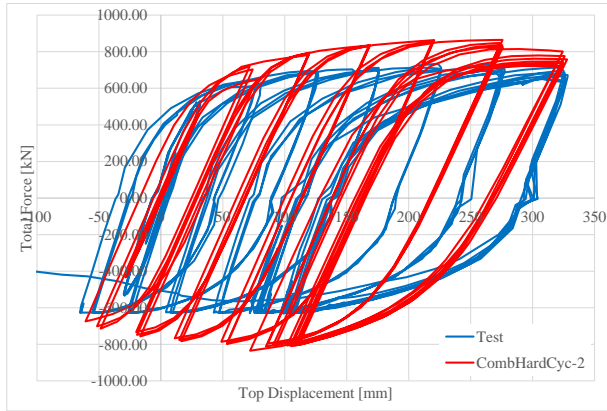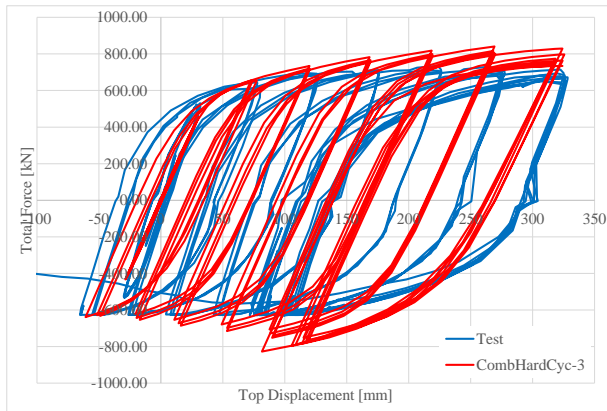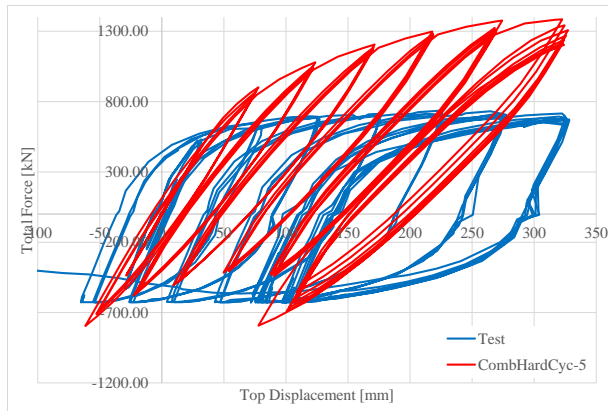
Figure 13. Experimental and numerical behaviour curves
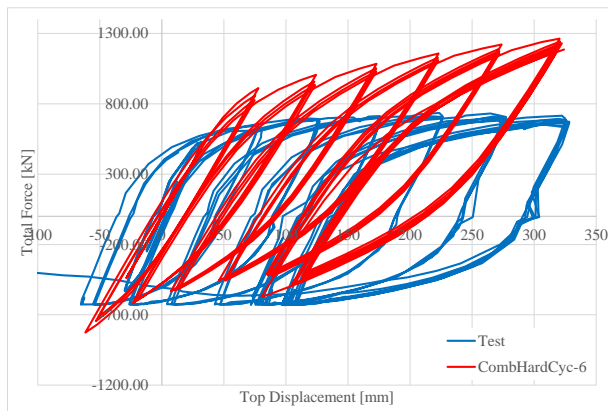
Figure 14. Experimental and numerical behaviour curves
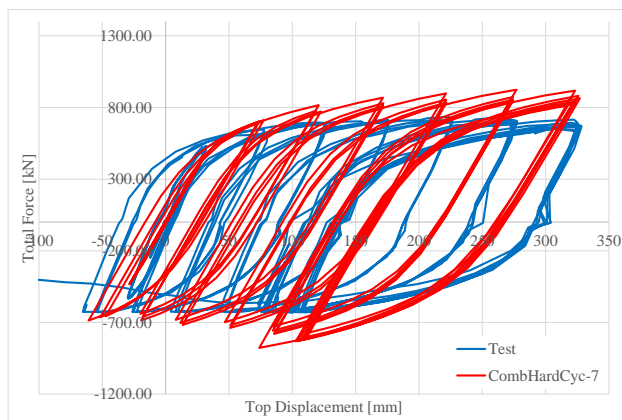
Figure 15. Experimental and numerical behaviour curves

Half-Cycle

When limited test data are available, C_γ and γ can be based on the stress-strain data obtained from the first half cycle of a unidirectional tension or compression experiment. Using this option, Abaqus determines the values of material parameters C_γ and γ. The data used for this material model was taken from the stress – strain curve obtained for the uniaxial tensile test. This option is suitable to be used if a limited number of cycles is performed. It has to be mentioned that only the plastic component was considered and that the yielding plateau was ignored due to the fact that, during plastic cyclic loading, the yielding plateau disappear.

In Figure 18 are presented the result using the combined parametric hardening defined using the half cyclic material model.
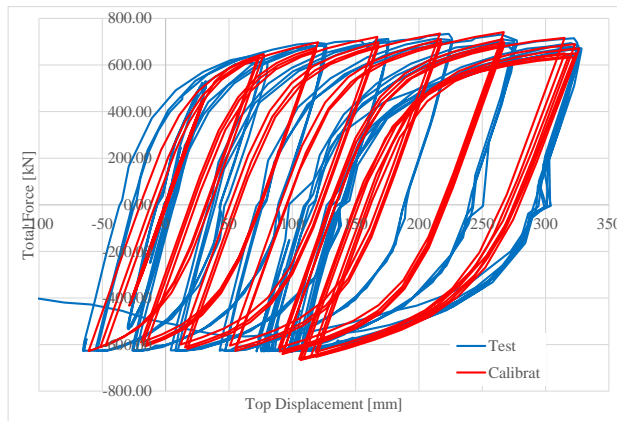
Figure 16. Experimental and numerical behaviour curves

3.3.5. Discussions

Considering the behaviour curves presented in Figure 7 – 16 it can be observed that a correct definition of material behaviour is of paramount importance when considering cyclic loading in steel structures. A simple elastic – perfect plastic material behaviour can produce very conservative results, severely underestimating the structural capacity (see Figure 5). On the other hand, considering the material isotropic hardening (Figure 6) the structural capacity is overestimated, while in case of kinematic hardening (Figure 7), the dissipated energy is underestimated.

Considering a material model that includes a combined isometric/kinematic hardening gives a very good approximation of structural behaviour. For this, two approaches can be considered, as presented in Figure 8 and Figure 16. It has to be underlined the importance of correct determination for all parameters included in material definition.

As presented in Figure 9 to Figure 15, the use of material parameters calibrated by other researchers can give unsatisfactory results for a given structure.

4. CONCLUDING REMARKS

Eurocode [17] present four basic types of material behaviour to be used for FE analyses. However, no reference is made to cyclic loading and the document do not offer information regarding the cyclic behaviour of steel. The use of these material models with isotropic and/or kinematic hardening rules alone can give unsatisfactory results. Moreover, the use of uniaxial test raw results i.e. engineering or true stress-strain data might not be suitable for modelling of cyclically loaded structures.

Even if various formulations are available for modelling the cyclic behaviour of ductile steels, the behaviour of specific structures cannot always be modelled by using data provided by other researchers. It was shown that using material data that was used to calibrate other models, do not give satisfactory results in this particular case. It has to be stressed that the numerical model have to be calibrated and validated against experimental results before it can be used for numerical simulations, sensitivity and parametric studies, etc.

The author have shown that the uniaxial test data might be sufficient for calibrating a cyclic behaviour material model that implies a combined kinematic/isotropic hardening.

Acknowledgements

References

1. Dahlberg M., Segle, P., Evaluation of models for cyclic plastic deformation – A literature study, *Report number: 2010:45*, 2010
2. Araujo, M., C., Non-Linear Kinematic Hardening Model for Multiaxial Cyclic Plasticity, *Thesis within Louisiana State University and Agricultural and Mechanical College*, 2002
3. Prager, W. *A New Method of Analyzing Stresses and Strains in Work Hardening Plastic Solids.* Journal of Applied Mechanics, Vol 23, pp. 493-496, 1956
4. Mroz, Z. On the Description of Anisotropic Work Hardening. *Journal of the Mechanics and Physics of Solids*, Vol 15, pp. 163-175, 1967

5.   Besseling, J.F. A Theory of Elastic, Plastic and Creep Deformations of an Initially Isotropic Material. *Journal of Applied Mechanics*, Vol 25, pp. 529-536, 1958
6.   Dafalias, Y.F. and Popov, E.P. Plastic Internal Variables Formalism of Cyclic Plasticity. *Journal of Applied Mechanics*, Vol 43, pp. 645-650, 1976
7.   Armstrong, P.J. and Frederick, C.O. A Mathematical Representation of the Multiaxial Bauscinger Effect. *CEGB Report No. RD/B/N 731*, 1966
8.   Chaboche, J.L. Time-Independent Constitutive Theories For Cyclic Plasticity. *International Journal of Plasticity*, Vol 2, pp. 149-188, 1986
9.   Chaboche, J.L. On Some Modifications of Kinematic Hardening to Improve the Description of Ratcheting Effects. *International Journal of Plasticity*, Vol 7, pp. 661-678, 1991
10. Ohno, N. and Wang, J.-D. Kinematic Hardening Rules with Critical State of Dynamic Recovery, Part I: Formulations and Basic Features for Ratcheting Behavior. *International Journal of Plasticity*, Vol 9, pp. 375-390, 1993
11. Bari, S., Constitutive Modeling for Cyclic Plasticity and Ratcheting, PhD thesis within the Department of Civil Engineering North Carolina State University, 2001
12. Hibbit. D., Karlson, B. and Sorenso, P (2007), ABAQUS User's Manual, Version 6.9
13. Lemaitre, J., and Chaboche J.-L., Mechanics of Solid Materials, *Cambridge University Press*, 1990.
14. Charles S., W., A Combined Isotropic-Kinematic Hardening Model for Large Deformation Metal Plasticity, U.S. Army Materials Technology Laboratory, Watertown, Massachusetts 02172-0001, 1988
15. Dinu F., Dubina, D., Neagu C., Vulcu C., Both, I., Herban S., Marcu D., Experimental and Numerical Evaluation of a RBS Coupling Beam For Moment Steel Frames in Seismic Areas, *Steel Construction Volume 6, Issue 1*, 27–33, 2013
16. European Convention for Constructional Steelwork, Technical Com-mittee 1, Structural Safety and Loadings; Working Group 1.3, Seismic Design. *Recommended Testing Procedure for Assessing the Behavior of Structural Steel Elements under Cyclic Loads*, First Edition, ECCS 1986
17. EN 1993-1-5: Eurocode 3: Design of steel structures - Part 1-5: General rules - Plated structural elements
18. Elkady, A., Lignos, G., D., Analytical investigation of the cyclic behavior and plastic hinge formation in deep wide-flange steel beam-columns, DOI 10.1007/s10518-014-9640-y, published online 2014
19. Terry P., Nonlinear response of steel beams, National Technical Information Service, *Operations Division, 5285 Port Royal Road, Springfield, Virginia 22161 - DSO-00-01*, 2000
20. Halama, R., Sedlák, J., & Šofer, M. Phenomenological Modelling of Cyclic Plasticity. Intech International, 1, 2012
21. Collin, J. M., Parenteau, T., Mauvoisin, G., & Pilvin, P. Material parameters identification using experimental continuous spherical indentation for cyclic hardening. Computational Materials Science, 46(2), 333-338, 2009

Numerical Evaluation of Reinforced Concrete Beams Loaded in Bending

Petru Mihai[1], Mihai Budescu[2], Nicolae Țăranu[3], Rareș-George Țăran[2] and Ionuț-Ovidiu Toma[2]

[1]Department of Concrete Structures, Building Materials, Technology and Management, "Gheorghe Asachi" Technical University of Iasi, 700050, Romania
[2]Department of Structural Mechanics,"Gheorghe Asachi" Technical University of Iasi, 700050, Romania
[3]Department of Civil and Industrial Buildings,"Gheorghe Asachi" Technical University of Iasi, 700050, Romania

Summary

In this paper, the behaviour of reinforced concrete beams is estimated with the Finite Element Method and improvements to the method are proposed. Because the reinforced concrete elements work in conjunction with the material cracking behaviour, the behaviour is very complex and depends on the shape of the reinforcement, mechanical characteristics of the materials and the intensity of loads.

In general, the Finite Element Method cannot emulate this complex process because the connection between elements at the node is fixed and slip behaviour of reinforcement is not allowed. For this reason, the results obtained with the Finite Element Method do not correctly describe the phenomenon. To address this, the authors propose an improvement on the Finite Element Method to eliminate the deficiency and describe the process with more accuracy.

KEYWORDS: concrete, reinforcement, finite element, numerical analysis.

1. INTRODUCTION

The numerical analysis is presented in the majority of engineering sciences, from aero spatial industry to electronics. Many programs are developed for civil engineering and almost all use Finite Element Method. The main goal consist in establishing of the structural behaviour under a various types of loads [1].

Reinforced concrete is a particularly material in civil engineering because it is a double composite material. First concrete is a composite material formed by cement and aggregates and with reinforcement is obtained a second-degree composite material. From this reason, the behaviour of reinforced concrete element is very complex and difficult to describe with simple mathematical relations [2].

Mathematical algorithms were developed in civil engineering for composite materials and the behaviour of such kind of materials can be numerically established [3]. These relations cannot be used for reinforced concrete elements because the reinforcement is not scattered on the entire volume of the element and is provided only in tensioned zone. This condition makes the analysis process very difficult especially when two different materials are combined together.

First programs that can study the behaviour of reinforced concrete elements was applied with limited success. The studies revealed important differences between numerical and experimental results as follow:

a) in numerical analysis the cracking are presented in all tensioned nodes; if the mesh is refined to 10 mm, the cracks appear at this distance and the correspondence with experimental results is no longer achieved;

b) in numerical analysis the stresses for the reinforced concrete element appear like in a plain concrete one and the tensile stresses are similar in and between the cracks; experimental results revealed large differences between tensile stresses, according with the crack pattern [4];

c) the reinforcement stresses have a continuous development in numerical analysis (according with the bending moment diagram) but in the experimental tests the reinforcement stresses have a number of relative maximum values (according with the crack pattern) [5].

In conclusion, the Finite Element Method can be successfully used for steel structures but in case of reinforced concrete elements this method can't provide accurate results, mainly due to poor bond implementation [6]. The bond between concrete and reinforcement is a very complex phenomenon and a simple combination of concrete and reinforcement in meshing process is not enough.

2. PROPOSED MODEL

A regular simply supported beam was considered to evaluate the behaviour of reinforced concrete elements using the Finite Element Method (Figure 1). The used concrete grade is C30/37 and the longitudinal reinforcement is made from steel BSt500 class C. Stirrups are provided at the ends of the beam to carry shear but in the middle area no stirrups were provided to avoid influences from confining. Steel grade 250 are used for transversal reinforcements.

The test is a classical 4 point test, using two concentrated forces to eliminate the shear force effect in the middle part of the element.
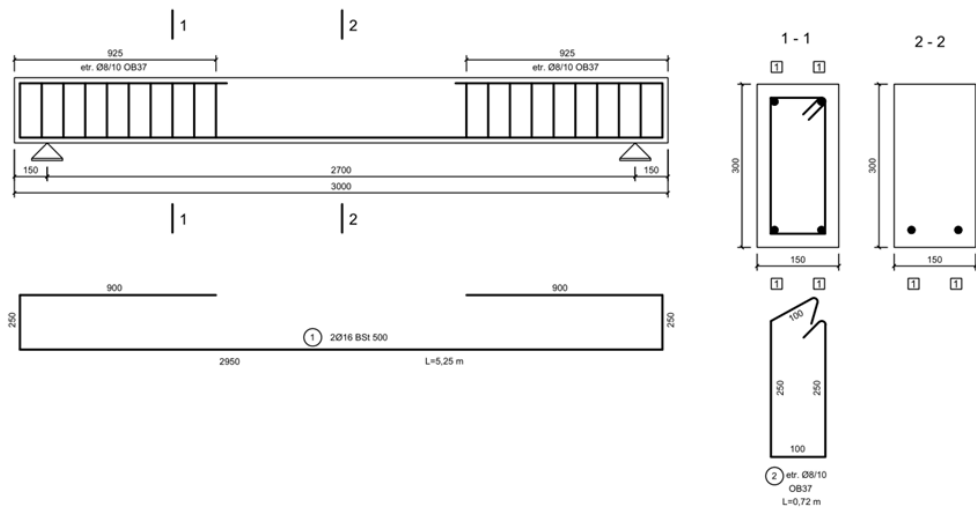
Figure 1. Making-up of reinforced concrete beam

To calibrate the Finite Element Method, the real bond between concrete and reinforcements must be included in the analytical model, according with the stress-slip diagram obtained from experimental tests (Figure 2).
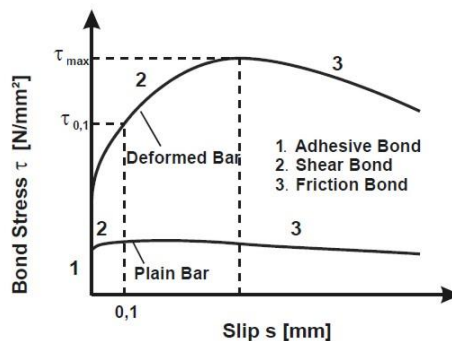
Figure 2. Making-up of reinforced concrete beam

In the Finite Element Method, the influence of the bond between concrete and reinforcement must be included. To do this, the external load must be applied in individual steps and the numerical model will be adapted according with intermediate results.

The initial loading step will determine the stresses and displacement for the perfect bond case with the finite element Equation (1):

$$\{F(t)\} = [k]^e \cdot \{u(t)\} \tag{1}$$

where $\{F(t)\}$ is the vector of external forces from the finite element nodes, $[k]^e$ is the stiffness matrix for the elastic stage and $\{u(t)\}$ is the nodal displacement vector

The algorithm will check for crack appearance in all nodes. If a crack appears, the bond between concrete and reinforcement must be re-evaluated around the crack area. Thus, the stiffness matrix for all of the concrete elements near the crack will be modified according with the Equation (2):

$$[k] = [k]^e - [k]^d \tag{2}$$

where $[k]$ is the revised stiffness matrix and $[k]^d$ is a damaged stiffness matrix. In the $[k]^d$ matrix, all of the concrete elements located inside of the broken bond area will have a reduced stiffness value. All of the finite elements unaffected by cracks will have a zero value in the $[k]^d$ matrix.

Next, the new stresses and displacements are established with the Equation (3):

$$\{F(t)\} = [k] \cdot \{u(t)\} \tag{3}$$

If new cracks appear in this stage, the stiffness matrix will be revised again and the process will be repeated until no new cracks appear. Finally, if failure does not occur, then external loads can be increased to the next step and the process will continue until failure (Figure 3).
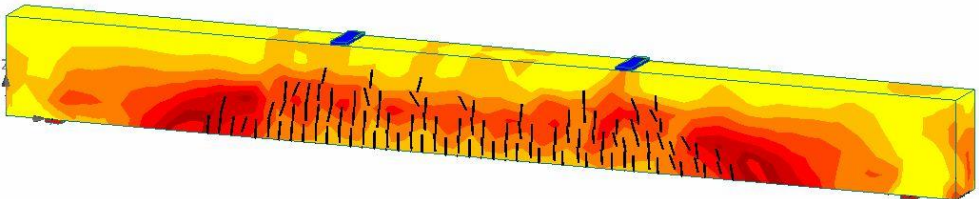
Figure 3. Numerical results on RC beam: stresses and crack pattern

The main problem of the proposed algorithm is the value of the loading step. If the loading step is very large, too many cracks appear at the same time and the results will be affected by errors.

To avoid this situation, a satisfactory solution is to diminish the loading step. In this case, accurate results will be obtained, but the computation time will increase substantially and many small useless steps will be processed.

The bisection algorithm can also be used to avoid this situation, but the convergence of the solution is still achieved quite slowly. Another faster method that establishes the optimum loading step and obtains accurate results in less time is proposed in [7].

3. EXPERIMENTAL RESULTS

Checking the accuracy of the proposed numerical algorithm was realised on three experimental beams (Figure 4) with characteristics described in Figure 1. The beams were equipped with one load cell and six resistive transducers for measurement of displacements on bottom side.

Figure 4. Experimental test

The force-displacement diagram was established for each tested element and the final results obtained with numerical analysis and experimental tests are presented in Figure 5.
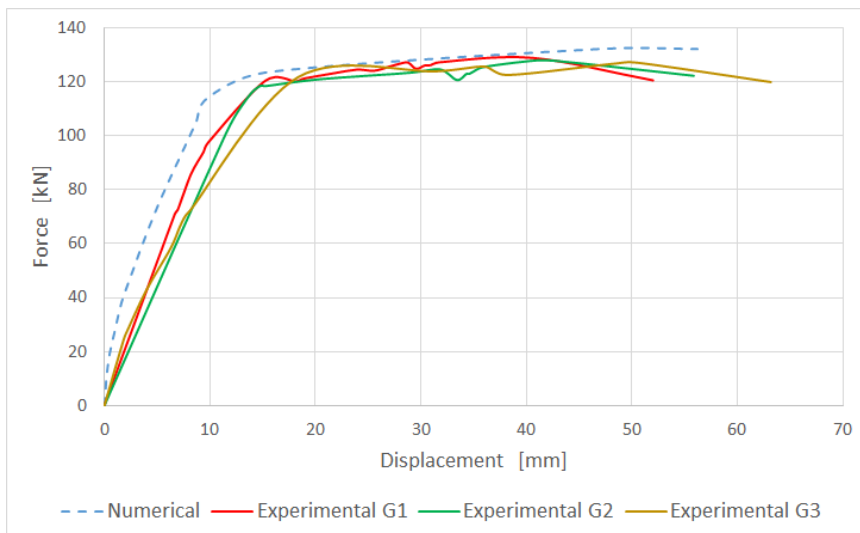
Figure 5. Force-displacement diagram

The comparison between numerical and experimental results revealed a good approach of the proposed method. The bearing capacity and the maximum displacement estimated with numerical analysis are very close to those obtained experimentally.

3. CONCLUSIONS

The non-elastic behaviour of the concrete and the cracking stage developed in service for the reinforced concrete elements impose a new approach of the finite element method. Because the regular Finite Element Method cannot describe the behaviour of the reinforced concrete structures, a new method was proposed by the authors.

The modified algorithm can be successfully applied to evaluate bond characteristics between concrete and reinforcement in reinforced concrete elements.

The main disadvantage of the proposed model is the requirement of a fine mesh. Thus, analysis time can increase significantly for large elements and structures. To overcome this inconvenient, a coarse mesh can be used to decrease the number of elements, but in this case, the results can be affected by bigger errors.

References

1. Mihai, P., Florea, N., Lepădatu, D., *New algorithm for establishing the behavior of reinforced concrete elements*, Buletinul Institutului Politehnic din Iaşi, Tomul LII (LVI), fasc. 3-4, 2006, 59-67.
2. Małecki, T., Marzec, I., Bobiński J., Tejchman, J., *Effect of a characteristic length on crack spacing in a reinforced concrete bar under tension*, Mechanics Research Communications, Volume 34, Issues 5-6, July-September 2007, 460-465.
3. Carter, B.J., Wawrzynek, P.A., and Ingraffea, A.R., *An Automatic 3-D Crack Growth Simulation*, International Journal for Numerical Methods in Engineering, Vol. 47, 2000, 229-253.
4. Yankelevsky, D.Z., Jabareen, M., Abutbul, A.D., *One-dimensional analysis of tension stiffening in reinforced concrete with discrete cracks*, Engineering Structures, Volume 30, Issue 1, January 2008, 206-217.
5. Barros, M.H.F.M., Martins, R.A.F., Ferreira, C.C., *Tension stiffening model with increasing damage for reinforced concrete*, Journal of Engineering Computations, Volume 18, Issue 5/6, 759-785.
6. Barnes, R.A., Mays, G.C. *The transfer of stress through a steel to concrete adhesive bond*, International Journal of Adhesion and Adhesives, Volume 21, Issue 6, 2001, 495-502.
7. Mihai, P., Hirhui, I., Roşca, B., *Numerical analysis of bond between concrete and reinforcement using the Finite Element Method*, Journal of Applied Sciences, vol. 10, issue 9, 2010, 738-744.

Checking the Homogeneity of Concrete Using Artificial Neural Network

Alexandrina-Elena Pandelea, Mihai Budescu,
Gabriela Covatariu and Rareş George Ţăran

"Gheorghe Asachi" Technical University of Iaşi, Faculty of Civil Engineering and Building Services,
1 prof. Dimitrie Mangeron street, 700050, Iaşi, Romania

Summary

This paper proposes a manner to verify the concrete samples homogeneity using artificial neural networks. This method determines the percentages of different areas of component materials visible at top and bottom of a concrete cylinder having 20 cm diameter and 20 cm height. The materials that have been achieved are rubber grains, aggregates and mineral matrix.

The training of the neural network was realise by using backpropagation algorithm and then, in order to separate the regions of interest was used Levenberg-Marquardt algorithm. As a neural network input data were used photos having 258 x170 pixels resolution achieved both on the both sides of the cylinder.

KEYWORDS: neural network, backpropagation algorithm, Levenberg Marquardt algorithm, concrete, rubber, computing percentage

1. INTRODUCTION

Artificial neural networks (ANN) have been used in Civil Engineering since 1989. They are applicable in practice as a result of testing older model biological neurons and brain activities. Compared with biological support which is largely unknown, the operation support of neural networks is specific mathematic having an artificial intelligence heuristics.

ANN phrase suggest that their function is inspired by biological neural networks and represent an informational processing device, with advantages / disadvantages common with any other device projected by human being for knowing purposes. It must avoid any confusion to correct understand of the role and limits of use of neural networks, which would create the impression that neural networks can be substitutes whenever and wherever a human brain [1].

Nowadays, networks application in construction is a very studied because its allow solving problems in a limited time and with fewer resources.

Engineering problem solving involves:

- Analysis of the problem, establishing network architecture, data input and output thereof.
- Choosing training algorithm (supervised learning, reinforcement learning and self-organizing).
- Data sets collected for problem sets are divided into training and test sets.
- Correctness network operations, by introducing input data not contained in the training set but the correct answer is known [3].

2. PERCENTAGE CALCULATION USING ANN WITH BACKPROPAGATION ALGORITHM

2.1 Introduction in neural networks for classification problem

In order to build a neural networks are used as input a set of images. For this, there are use images that can be taken from the satellite [4] or performed under a microscope [5], depending on the issue. The images consist of a number of pixels, each pixel of the colour image p being characterized by:

- a vector with two components, denoted $g(p)$ which contains the geometric coordinates of the pixel
- a three-component vector, $c(p)$ expressing the colour coordinates of the RGB cube.

Using the geometric coordinates we can define the set of pixel G_k, disjoint sets that correspond to the regions occupied by the colour e_k, k = 1, 2, 3, 4, where: e_1 - means black, e_2 - signifies red, e_3 – means green and e_4 - signifies blue. In the RGB cube scaled to [0, 1] x [0, 1] x [0, 1] defines the set of colours associated with each element e_k, k = 1, 2, 3 or 4.

Consider the set (1)

$$C_k = \{U_k c(p) | g(p) \in G_K\} \tag{1}$$

Select colour samples representative of the three types of regions and defined sets of samples C_1^*, C_2^*, C_3^* and C_4^*. They are the best way to get partial information about colour sets C_1, C_2, C_3 and C_4 which are unknown as concrete values into RGB cube. After that, delete identical vectors in each lot of colour. In considered working assumption $C_1^*, \subseteq C_K$, k = 1, 2, 3, 4, sets C_1^*, C_2^*, C_3^* and C_4^* are disjoint. Fulfilment of this hypothesis depends on the sharpness of image.

Its training the neural network with an appropriate architecture to classify colours into three classes of sets of samples C_1^*, C_2^*, C_3^* and C_4^*. It is used backpropagation algorithm for network training, information is processed in the opposite direction from output to input of the network.

The trained network is used to classify all pixels in the image in three classes, corresponding to C_1^*, C_2^*, C_3^* and C_4^*. It builds a new digital image that defines four regions which estimates ideal areas of interest G_k.

It uses three colours to represent different regions G_1^*, G_2^*, G_3^* and G_4^* expected to provide a better view. Estimate ideal regions will get by segmentation of image. Separating the region of interest is performed using a neural network trained by Levenberg Marquardt algorithm.

Levenberg-Marquardt algorithm is one of the fastest methods used in practice, it ensures numerical solutions in minimization problems of nonlinear functions. The algorithm is an interpolation between Gauss-Newton algorithm and the method of gradient descent.

It brings improvements Newton's method through an approximation of the Hessian with a singular and symmetrical matrix (2)

$$[\nabla^2 \varepsilon(w) + \vartheta I] \qquad (2)$$

where:

ϑ = positive parameter that provides rapid convergence of the algorithm

I = the identity matrix

E(w) = cost function

Finally, measure the area of estimated regions G_1^*, G_2^*, G_3^* and G_4^* and calculate the percentage held by each [6].

2.2. Case Study

It is considered as test sample a cylinder having 10 cm diameter and 20 cm height. The materials used to manufacture the test sample was rubber grains, aggregate and mineral matrix.

The rubber grains was obtained by recycling the used tires through a grinding process. The size of the aggregates are 0 - 4 mm and 4 – 8 mm and type of cement used is C30/37. For better workability of the composition were used SIKA 20HE additives. Reinforced concrete with recycled rubber mixes includes a 30% rubber.

After casting composition in a cylindrical shape, a vibrating procedure was achieved in order to eliminate the air from concrete sample and also to ensure uniformity, to increase the strength and eliminate segregation. It was obtained through vibration on concrete`s shaking table.

A neural network was designed in order to determine the percentage of the mineral matrix's area, aggregate and rubber on both sides of the element.

Figure 1. Cylinders made of concrete and rubber

To obtain the rates matrix, rubber and aggregate following steps:

1. Enter the initial image in neural network (figure 1.a, figure 6);

2. Select in image the following regions: black for rubber, red for aggregate, green for cement and blue for background;

3. The network generates a new image with that 4 chosen colours (figure 2.7);

4. Choose the colour samples of image representative regions;

5. Placing colours in sample sets C_1^*, C_2^*, C_3^* and C_4^* in RGB cube, scaled to [0, 1] x [0, 1] x [0, 1] (figure 3)

6. The network generates as output data that the regions of interest (Figure 4).
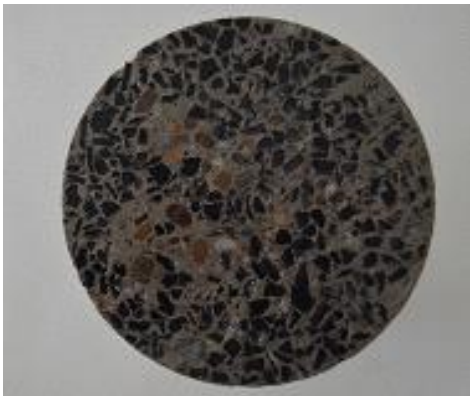
Figure 1. Initial image (upperside)   Figure 2. The image segmented in 4 colors
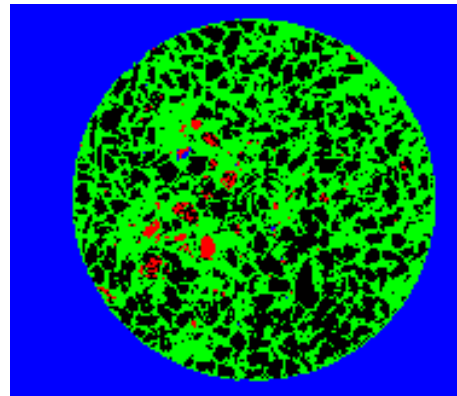
7. Train the network using multiple neurons and a large number of periods (figure 5 a, b, c, d, e and figure 10 a, b, c, d, e).

8. Using a program developed in MATLAB [2] to determine all the percentages of areas of interest, a program that has as main parameters resulting matrix as output date and number of colours (table 1, 2).

The following are the results generated by neural networks for studied cylinder.
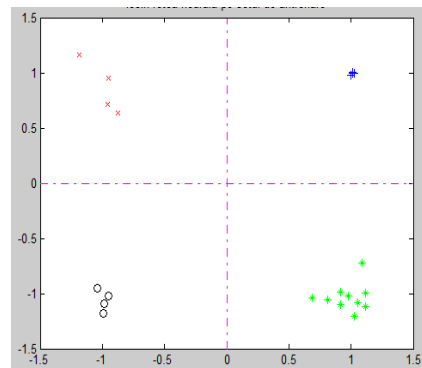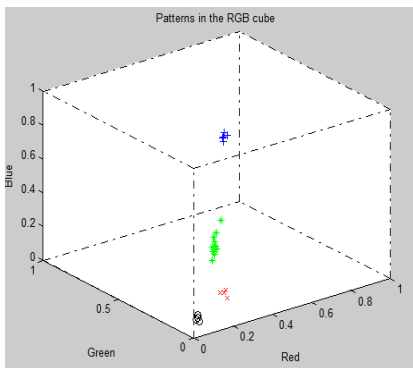
Figure 3. Placing colours in the cube RGB

Figure 4. Output networks with the training set
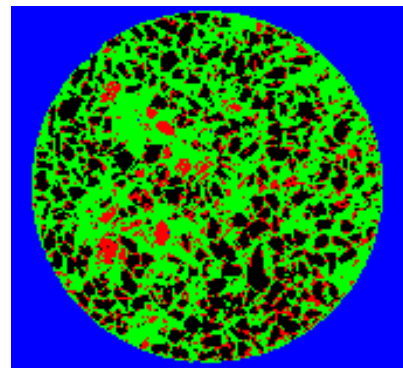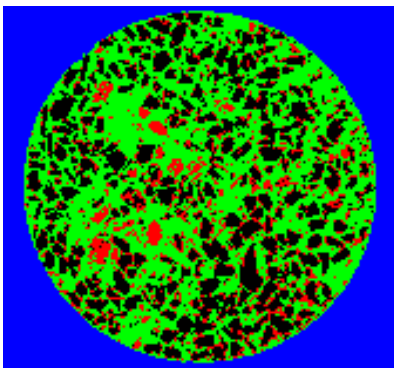
Figure 5.a. 20 neurons 20, 10 epochs

Figure 5.b. 20 neurons 20, 100 epochs

Table 1. Determining the percentage of material in various cases of training of neural network on the upperside of the cylinder

Number of neurons	No. of training epochs	Rubber (%)	Aggregate (%)	Matrix (%)	No of. figure
10	10	54.45	1.89	43.57	2
20	10	33.4593	13.8812	52.6595	5.a
20	100	33.0249	14.3236	52.6515	5.b
25	250	41.1319	14.3236	52.6515	5.c
30	1000	40.8866	4.7264	52.6515	5.d
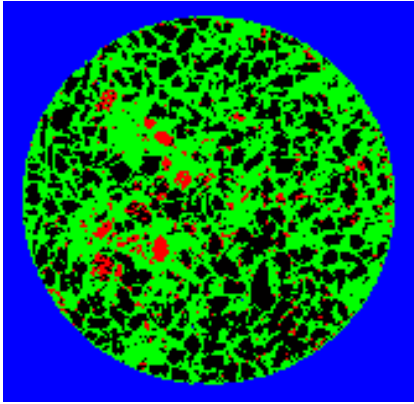
Figure 5.c. 25 neurons, 250 epochs
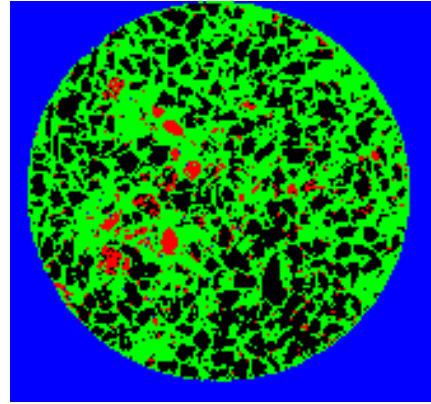
Figure 5.d. 30 neurons, 1000 epochs
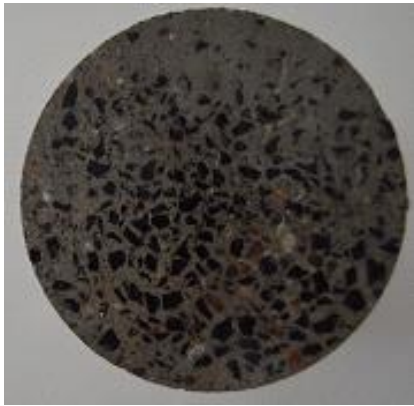
Figure 6. Initial image (underside)
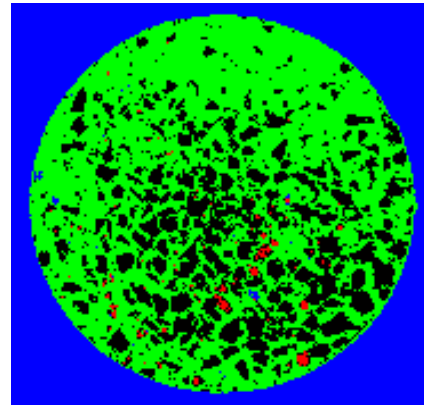
Figure 7. The image segmented in 4 colors
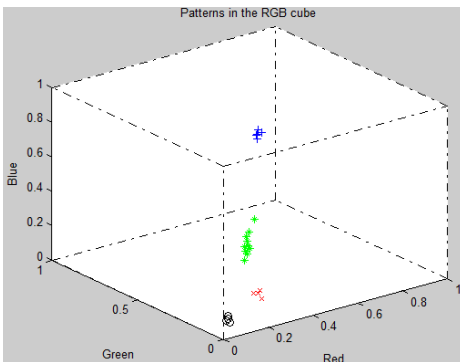
Figure 8. Placing colours in the cube RGB
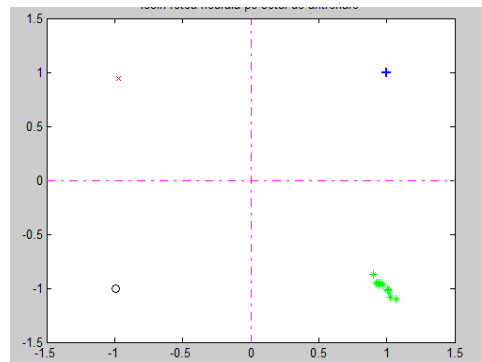
Figure 9. Output networks with the training set

Table 2. Determining the percentage of material in various cases of training of neural network on the underside of the cylinder

Number of neurons	No. of training epochs	Rubber (%)	Aggregate (%)	Matrix (%)	No of. figure
10	10	31.1863	0.9878	67.82589	7
20	10	29.245	0.9882	69.7668	10.a
20	100	28.0683	0.9768	70.9549	10.b
25	100	27.487	3.8728	68.6402	10.c
30	1000	28.5572	4.1619	67.2809	10.d
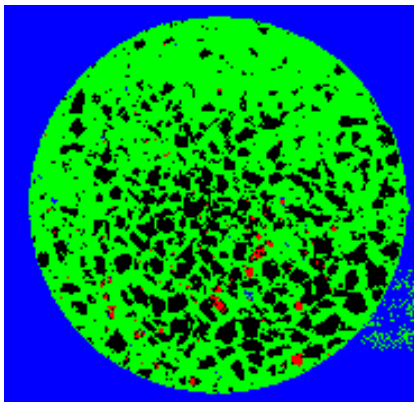
Figure 10.a 10 neurons, 10 epochs
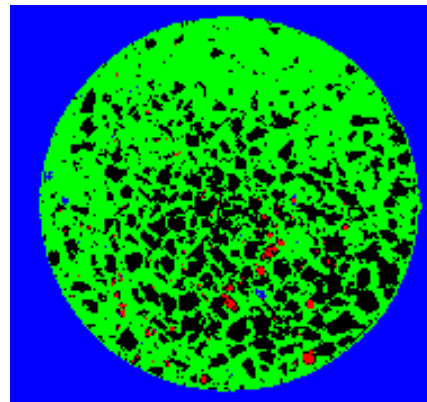
Figure 10.b. 20 neurons, 100 epochs
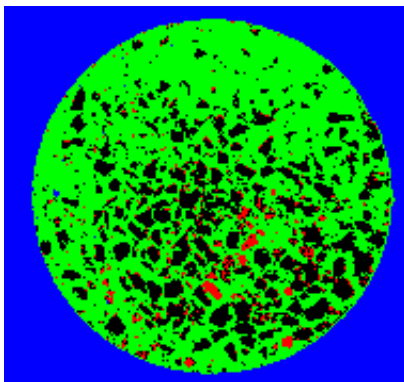
Figure 10.c. 25 neurons, 100 epochs
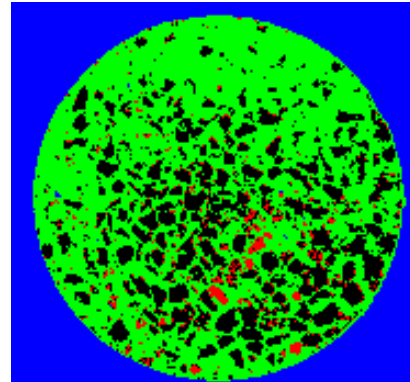
Figure 10.d. 30 neurons 30, 1000 epochs

3. CONCLUSIONS

After the network training with a number of neurons that varies between 10 to 30 and 10 to 1,000 iterations were obtained different percentages of component

materials. For the upperside of the cylinder, neural network with 30 neurons and 1000 iterations generated a percentage of 40.8866% rubber, 4.7264% aggregate and 52.6515% matrix.

To the underside of the cylinder network with the same number of neurons and iterations like upperside generated the results: 28.5572% rubber, 4.1619% aggregate and 67.2809% matrix.

The percentage is different between the both sides, 12.3294% for rubber, 0.5645% for aggregate and 14.6294% for matrix.

So, on the upperside is about 12% more rubber than underside. The cause of these differences in percentages between the two sides is caused by the improper vibration procedure.

Vibration for a longer period of time than that provided led to the creation of a less homogeneous concrete, the rubber is present in a greater amount on the upperside. Theoretically vibration range is 5-30 seconds.

In practice, regarding this period must be taken into account the following factors: the thickness layer of vibrated materials, concrete consistency and performance of vibrating device. Although vibration was terminated when the element surface became horizontal, without air bubbles and when the grout has appeared on the surface, and it wasn't taken into account the thickness of layer to vibrate.

Uniformity is an important parameter for increasing the element's strength.

References

1. Flood I., Kartam N., Garrett J.H., *Artificial Neural Network for Civil Engineering: Fundamentals and Applications*, American Society of Civil Engineers, 1997
2. Beale M.H., Hagan M.T., Demuth H.B., *Matlab - Neural Networks Toolbox – user guide*, Mathworks Inc, 2015
3. Covatariu G., *Aplicatii ale reţelelor neuronale în ingineria civilă*, PhD thesis, "Gheorghe Asachi" Technical University of Iaşi, (in romanian) 2010
4. Iounousse J. el al., *Using an Unsupervised Approach of Probabilistic Neural Network (PNN) for Land Use Classification from Multitemporal Satellite Images*, Applied Soft Computing, 2015.
5. Hage S., Hamade R., *Micro-FEM Orthogonal Cutting Model For Bone using Microscope Images Enhanced via Artificial Intelligence*, Procedia CEIRP, vol.8, pag.385-390, 2013
6. Matcovschi M., Păstrăvanu O., *Aplicatii ale retelelor neuronale in automatică*, Ed. Politehnium, Iasi, (in romanian) 2008

FEM Analysis of a Platform Framing Timber Structure

Ion Florenţa[1], Marian Pruteanu[1] and Ciprian-Ionuţ Zub[2]

[1]Department of Civil and Industrial Engineering, "Gheorghe Asachi" Technical University, Iaşi, Zip code: 700050, Romania

[2] Department of Steel Structures and Structural Mechanics, "Politehnica" University, Timişoara, Zip code: 300224, Romania

Summary

Due to climate changes of the last years, in Europe, there is a tendency of using ecological materials in building constructions. Therefore, timber structures represent a very good solution in reducing the negative environment impacts.

The Platform Framing structural system offers the possibility of constructing new multi-storey buildings. In order to increase the quality of execution and to reduce the time of constructing the building, it can be used prefabricated wood panels as structural walls.

This paper presents a numerical analysis of a multi-storey Platform Framing timber structure by using finite element method. The structure consisting of prefabricated panels is located in Iaşi City and it has 3 levels: Ground floor Level + 2 Levels. The numerical analysis of the structure was done by using the commercial structural program Axis VM 12.

KEYWORDS: timber, platform framing, prefabricated panels, Finite Element Method, Axis VM 12.

1. INTRODUCTION

Climate changes are already happening and their effects becoming more and more obvious. The humanity efforts to reduce them have resulted in a set of principles of sustainable development, which aims to put the society on a trajectory required to maintain a favourable climate for life on Earth. In addition to social and political components of these principles, the environmental component is also very important [1-2].

The latest norms from environmental and construction sector reduced both the amount of energy consumed during operation of the building and the one embedded in them. Therefore, in recent years, timber structures were imposed, the energy embedded in this material being inferior to the one embodied in the materials of classic structures, like concrete, metal or masonry [3]. The structure of the building is cover in various materials to meet the essential performance

requirements. To this purpose, the most often are used thermal and acoustic insulations made from mineral wool [4], but recently began to use low embedded energy materials as straw bales, cellulose, sheep wool insulation and hemp or flax insulation. Also, it is desired that the buildings to be more economical from the point of view of material consumption and also to have a cost as low as possible [5].

In order to fulfils these requirements, the best solution can be the timber framing structures. This system can be classified in two different structures: Balloon Framing and Platform Framing. The main advantages of this system when comparing with other systems made of reinforced concrete or masonry are the following [6]:
   • 30 % cost reduction;
   • fast and not season dependent execution;
   • reduced weight;
   • good seismic behaviour;
   • height thermal comfort;
   • ecological, with a positive environment impact.

The proposed building for the case study is a Platform Framing system. This system offers the possibility of constructing multi-storey buildings. The recommended maximum height regime for constructions located in seismic areas with peak ground accelerations values greater than 0.15 g is 7.00 m. The height is considered from the ±0.00 level of the building to the cornice (eaves). It can be allowed buildings with regime height greater than 10.00 m, but it is necessary that the structural capacity to be evaluated on 1/1, 1/2 or 1/4 scale models [7].

So, the paper presents the study of the structural behaviour of a multi-storey Platform Framing building, located in Iaşi City (a_g = 0.25 g), having a height regime G + 2 L (8.40 m). The building's layout is 18.60 m by 10.80 m. The analysis is performed on a 3D model, represented in Axis VM 12, with the scale of 1/1.

2. CASE STUDY

2.1. Description of the structural system

The Platform Framing structural system is specific for one-family houses. This structural system consists of structural walls (vertical and horizontal load-bearing elements), bearing walls (carrying only vertical loads), light frames (also carrying only vertical loads) and of rigid floors and roof, which have the role of transmitting the vertical and horizontal loads to the structural walls. Within this paper a

different approach was proposed, because the structure is a multi-family building, it was proposed that all the walls to be structural walls. In order to increase the quality of execution and to considerably decrease the time for erecting the building, prefabricated structural panels were used. The connection of the panels to the foundation is done by using anchors: bolt type anchors for shear connections and hold-down anchors for moment connections. The connection of the panels to the slabs is done by using straps and hold-down anchors [6].

The structure of the prefabricated panel is presented in Figure 1.
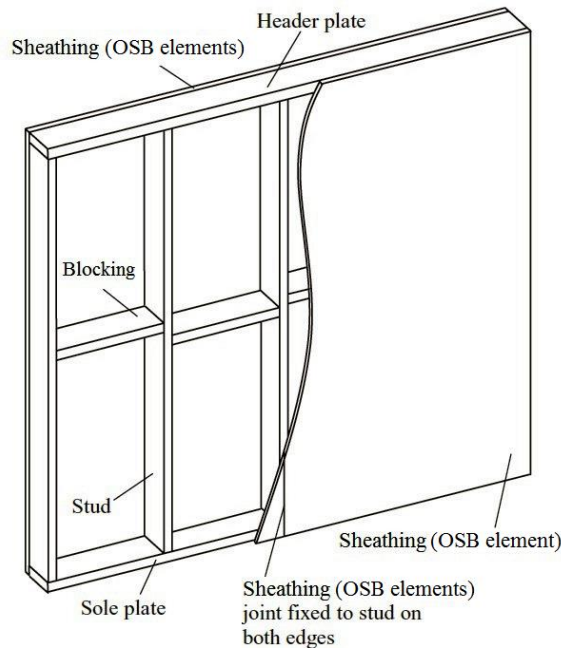
Figure 1. The structure of a prefabricated panel (insulation, breather membrane, etc. not shown) [8]

The studs of the prefabricated panel are placed at 600 mm (between the axes) and are made of fir, timber class C24. The exterior walls consist of 50 x 250 mm studs and they are boarded on the exterior face with 18 mm thick Oriented Strand Boards (OSB) which have a stiffening role. The interior walls consist of 50 x 200 mm studs and are boarded on both faces with 18 mm thick OSB elements. The OSB elements are nailed to the studs and to the blocking of the prefabricated panel.

The framing type slab (Figure 2) consists of timber joists of C24 class with the cross-section of 50 x 250 mm. On top of the slab, sheathings of 22 mm thick OSB elements are provided. The OSB elements are nailed to the joists and to the

blocking. This structure of the slab provides a diaphragm effect with respect to the lateral stiffness of the vertical elements.
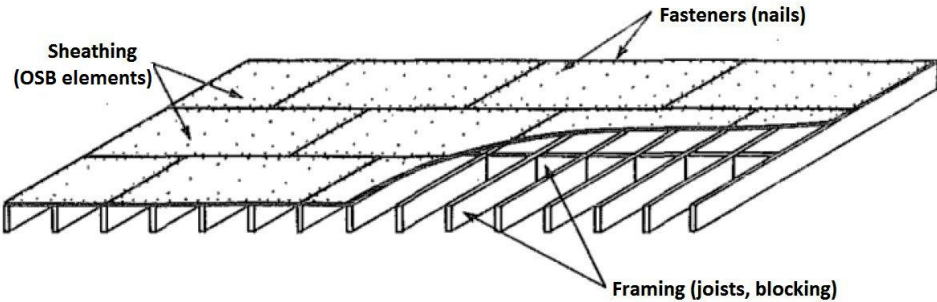
Figure 2. The structure of the framing type slab [9]

The framing type roof is a terrace and it is made by timber joists of C24 class, with the cross-section of 50 x 250 mm, covered with 44 mm thick OSB elements.

For thermal and acoustical isolation, straw bales were used for the exterior walls and the mineral wool is used for the interior walls and for the slabs.

Several hypotheses were used in order to define the structural model for the numerical analysis:
- the studs of the prefabricated panel were modelled using rib finite elements
- the structural OSB elements were modelled with shell elements;
- the connection between the studs and the structural board is rigid connection;
- the connection between the panels and the foundation is a rigid connection;
- the connection between the panels is continuous and assures both vertical and horizontal continuity of the walls;
- the slabs and the roof provide a diaphragm effect.

The loads acting on the structure are computed according to the norms for the specific site location (Iaşi City, Romania). After establishing the hypotheses and the load combinations, the structure will be meshed using a triangular finite element type (Figure 3).
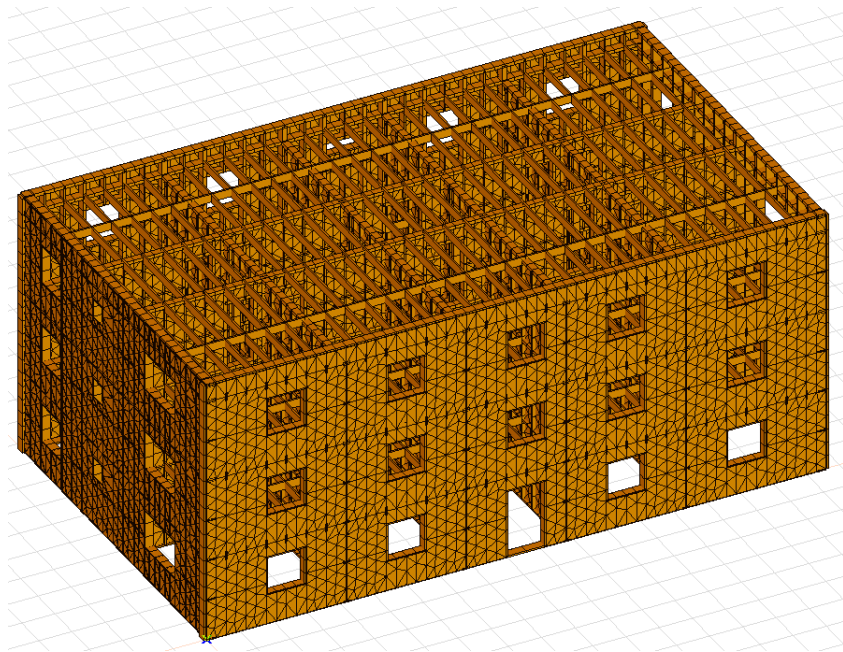
Figure 3. The mesh of the structure with triangular shell

2.2. Analysis results and discussion

From the modal analysis the next results can be observed (Table 1):

Table 1. Modal Analysis Results

Natural modes of vibration	Period [s]	Frequency [Hz]
Mode 1 of vibration	0.178	5.63
Mode 2 of vibration	0.157	6.38
Mode 3 of vibration	0.156	6.40

The first mode of vibration is a translation on X direction, the second mode is a translation on Y direction and the third one is torsion about Z axis.

After running the modal analysis, the seismic action can be computed according to P100-1/2013 for the site location (Iaşi City).

The main results obtained from static linear analysis are presented below. These results were used to design the structure.
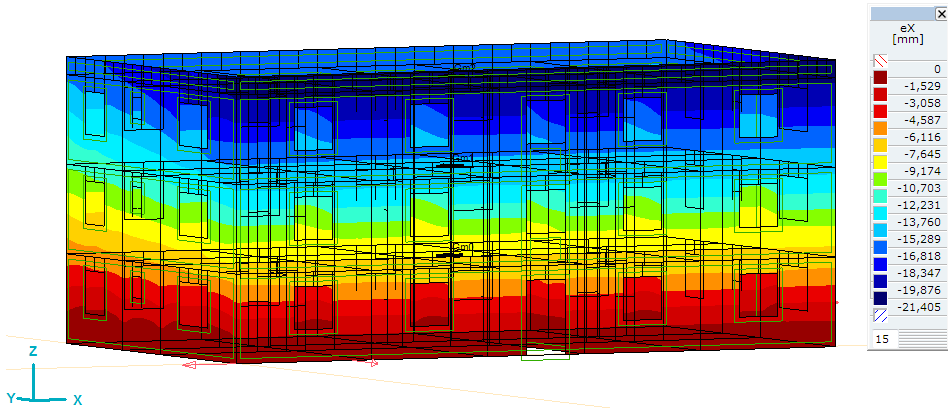
Figure 4. Maximum values of displacements on X direction
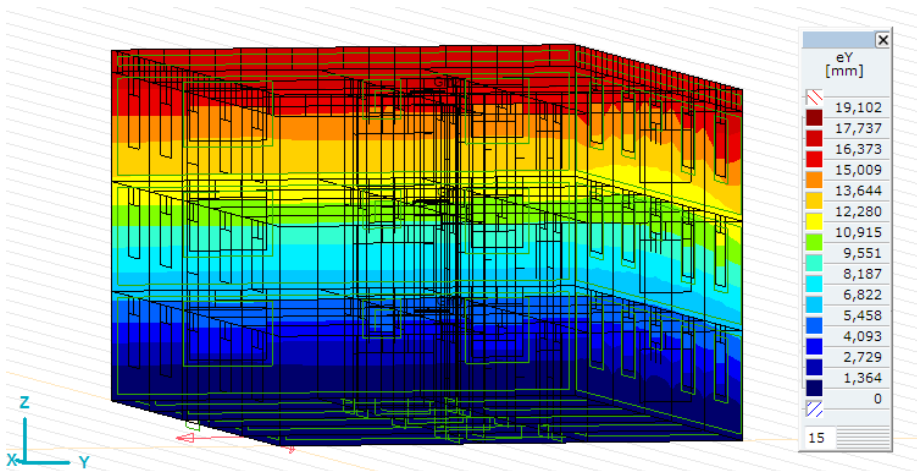
Figure 5. Maximum values of displacements on Y direction

The inter-storey drift check is done according to P100-1/2013, Annex E:

$$d_r^{SLS} = v \cdot q \cdot d_{re} < d_{r,a}^{SLS} \tag{1}$$

where: d_r^{SLS} is the inter-storey drift under the seismic action associated with SLS; d_{re} is the inter-storey drift, computed by elastic analysis under seismic design actions; v is the reduction factor accounting for the reduced recurrence interval of the seismic action associated with the SLS checks ($v = 0,5$); q is the behaviour

factor depending on the type of structure used for computing the seismic design forces $d_{r,a}^{SLS}$ is the admissible inter-storey drift.

Table 2. Inter-storey drift checks, X direction

Storey	d_r^{SLS} [mm]	$d_{r,a}^{SLS}$ [mm]	$d_r^{SLS} < d_{r,a}^{SLS}$ [mm]
Ground	10.4	21	OK
Level 1	10.9	21	OK
Level 2	8.9	21	OK

Table 3. Inter-storey drift checks, Y direction

Storey	d_r^{SLS} [mm]	$d_{r,a}^{SLS}$ [mm]	$d_r^{SLS} < d_{r,a}^{SLS}$ [mm]
Ground	8.9	21	OK
Level 1	9.2	21	OK
Level 2	7.4	21	OK

3. CONCLUSIONS

In this paper, it was numerically analysed the behaviour of a Platform Framing timber structure consisting of prefabricated panels, located in Iaşi City, having a regime height greater than the maximum recommended one.

The displacement results obtained from the numerical FEM analysis were checked according to P100-1/2013 [7]. It was concluded that the maximum value of the inter-storey drift is smaller than the admissible one.

References

1. MacKay, D.J.C., *Sustainable Energy — without the hot air,* UIT Cambridge Ltd., United Kingdom, 2009.
2. Stocker, T.F., Qin, D., Plattner, G.K., Tignor, M., Allen, S.K., Boschung, J., Nauels, A., Xia, Y., Bex, V., Midgley, P.M., *Contribution of Working Group I to the Fifth Assessment Report of the Intergovernmental Panel on Climate Change,* Climate Change 2013: The Physical Science Basis, IPCC, Cambridge University Press, United Kingdom and U.S.A., 2013.
3. Dodoo, A., Gustavsson, L., Sathre, R., *Lifecycle primary energy analysis of low-energy timber buildingsystems for multi-storey residential buildings,* Energy and Buildings, Vol. 81, Pp. 84–97, 2014.
4. Kubba, S., *Green Building Materials and Products,* Handbook of Green Building Design and Construction, Chapter 6, Pp. 227-311, 2012.
5. Mattila, T., Grönroos, J., Judl, J., Korhonen, M.R., *Is biochar or straw-bale construction a better carbon storage from a life cycle perspective?*, Process Safety and Environmental Protection, Vol. 90, Pp. 452–458, 2012.

6. Breyer, D.E., Fridley, K.J., Cobeen, K.E., Pollock, D.G., *Design of Wood Structures – ASD/LRFD*, Sixth Edition, McGraw-Hill, U.S.A., 2007.
7. P 100-1/2013, *Cod de proiectare seismică, Partea I: Prevederi de proiectare pentru clădiri,* Monitorul official al României, Bucureşti, 2013. (in Romanian)
8. Porteous, J., Kermani, A., *Structural Timber Design to Eurocode 5,* Blackwell Publishing Ltd., United Kingdom, 2007.
9. Hoekstra, T., *Multi-storey Timber-Frame Building - modelling the racking stiffness of timber-frame shear-walls,* MSc Thesis, Delft University of Technology, Munchen, 2012.

Carving joints for wood constructions.
Calculation models

Tudor-Andrei Leizeriuc, Dorina Nicolina Isopescu, Iulian-Daniel Zăpodeanu

"Gheorghe Asachi" Technical University of Iaşi, Faculty of Civil Engineering and Building Services

Abstract

 Romania is the only country in the world that has a large patrimony of wooden churches. These churches are historic monuments. Over the years, these buildings have been subjected to many actions that led to a degradation of structural elements and also to the degradation of joints between structural elements. Carving joints are predominant for this type of buildings. For the rehabilitation of this type of joints it is necessary to restore them and implicitly to know their behaviour and failure modes.

The article presents the evaluation of wood carving joints with simple threshold using analytical calculation and numerical modelling.

Keywords: carving joints, rehabilitation, analytical calculation, finite element.

1. INTRODUCTION

The wood is used from ancient times to the construction of bridges, houses, churches and many other applications in civil, industrial and agricultural structures. Wood can be easily used for resistance structures of tall buildings, over 7 or 8 floors, even 10 floors (ex. Residential building in Melbourne, Australia). In the future, large projects with buildings made of wood with 18 levels in hybrid system will be implemented.

In Romania an important activity is the restoration of numerous churches and residential buildings declared historical monuments, where wood is used as building material for the resistance structure. In Maramures County there are 93 wooden churches declared historic monuments. Eight of them were chosen to be part of UNESCO World Heritage, [5]. Some of these are: church "Sfantul Nicolae" from Budesti-Josani (year of construction: 1643), Figure 1, [6], church "Cuvioasa Parascheva" from Desesti (year of construction: 1717), Figure 2, [7], church "Sfanta Maria" from Ieud-Deal (year of construction: 1364), Figure 3, [8], church "Cuvioasa Parascheva" from Poienile Iezei (year of construction: 1602), Figure 4, [9].

Figure 1. Church "Sfantul Nicolae" from
Budesti-Josani

Figure 2. Church "Cuvioasa Parascheva"
from Desesti

Figure 3. Church "Sfanta Maria" from
Ieud-Deal

Figure 4. Church "Cuvioasa Parascheva"
from Poienile Iezei

Wooden buildings declared historical monuments can be made entirely of the wood
elements (columns, beams, rafters, ridge, props etc.) or with only the roof structure
made of the wood. These constructions are characterized by wooden joints
technique, and by achieving shingled roof, ornamental motifs visible on the surface
portals and frames made by chiselling or notching, Figure 5.
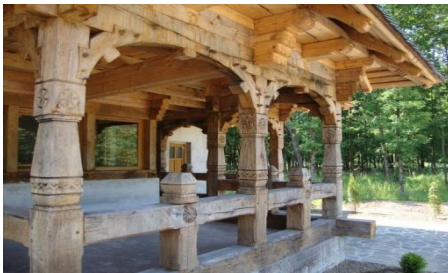
Figure 5. Wooden parts of church monuments

Wooden churches represent the spiritual roots of Romania. Preserving them requires, in most cases, trans-disciplinary knowledge that combines tradition expressed by sustainability, and a combination of advanced methods of calculation.

2. CARVING JOINTS TO WOOD CONSTRUCTIONS

2.1. Wood as a building material

Due to its properties as a building material and the possibilities of supplying and ease of processing, wood was in the past, the most utilized building material. Due to its multiple technical and constructive advantages, the wood is, and it has been, one of the traditional construction materials. The constructions of wooden structural frame are based on an advanced design technique which gives them certain advantages in terms of structural strength, human comfort and energy savings. Wood is durable over time with exceptional strength, and this is shown by the buildings from around the world, [10]. The main qualities of wood as a building material are:
  • Low characteristic density, 3.6 times less than steel.
  • Quite high mechanical resistance in tensile and compression, parallel to the fibers (grains), and for transverse loads which produce bending.
  • Coefficient of thermal expansion along the fibers is very small and, consequently, wooden structures do not require expansion joints.
  • Dry wood has a low thermal conductivity coefficient, [1].

2.2. Wood carving joints

The elements of a wood structure, (pillars, beams, rafters, props etc.) are connected together to form the structural frame. The joints may be of the following types: wood carving joints, joints with metal connectors, mechanically dowelled fasteners joints, or joints with adhesives. One type of joint, commonly used in old buildings, is the wood carving joint. Wood carving joints are found in most roof structures of the buildings made in 16-19 centuries. Over the years these buildings were subjected to numerous actions: service loads, wind, snow, earthquake, and they produced damages to structural elements and also degradation of the joints between structural elements. In many cases, it is necessary to strengthen the structure. Rehabilitation of wooden buildings declared as monuments must keep the same architecture and technology of execution so that significant values for history and culture of national civilization should not be altered. In strengthening of wooden constructions special problems occur in achieving specific traditional joints–carving, which are no longer found in modern manufacturing technologies, and

thus, in the technical regulations calculus. Restoring this type of connections require a deep analysis for sizing and load bearing capacities. Therefore it is actual the understanding and knowledge of these specific types of joints for old wooden buildings. Wood carving joints are the joints where the stress is directly transmitted from one element to another, without the use of intermediate connectors. The metal devices used in these joints (bolts, clamps, yokes etc.) play only a secondary role, preventing relative movement of the connected elements under the action of unforeseen loads calculations, either during installation or during operation.

3. MODELS FOR EVALUATING BEARING CAPACITY OF CARVING JOINTS WITH SIMPLE THRESHOLD AND ORTHOGONAL CUTTING

3.1 Description of the connection type

Simple threshold joints (Figure 6) are used in timber constructions, especially for joints of timber framed roof structures. In order to achieve an acceptable behaviour in service, for carving joints with simple threshold and orthogonal cutting, certain conditions are imposed, namely:
- If the cutting is made at end nodes, in order not to weaken the piece, the depth of the cut - h_c, should not exceed one third of the height - h of the element (for rectangular cross-section of wood elements) or one third of the diameter - d, (for round cross-section of wood elements);
- If the cutting is made at intermediate nodes, in order not to weaken piece, depth of cut - h_c, should not exceed one quarter of the height - h, of cutting element (for rectangular cross-section of wood elements) or one quarter of the diameter - d, (for round cross-section of wood elements);
- In all cases, h_c, must be at least 2 cm for rectangular cross-sections and 3 cm for round cross-sections;
- To avoid the cracking development due to shrinkage, the length of the shear plane, L_f, must be greater than twice the height - h, of the element and at least equal to ten times the depth of the cut - h_c;
- For a better connection, the elements (during assembly, transportation and installation) are connected together by a bolt that also acts as a safety element.
- To create a bearing surface for the washer bolt tight, in order not to make another cut in the beam, under the beam is installed an additional support which increases the load capacity of joints, [2].
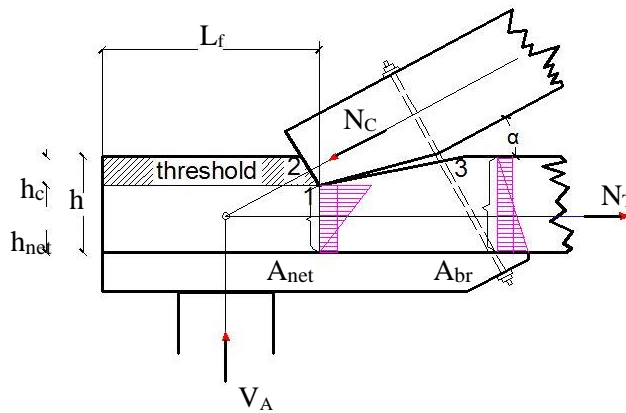
Figure 6. Carving joints with simple threshold and orthogonal cutting. Diagrams of normal stress distribution.

In Figure 6 it is seen how the crushing of the contact surfaces of the two elements takes place under the same angle (combination of equal resistance) and the axial force N_c of the compressed top beam (top chord of wooden truss) is taken both by surface 1-2 and by 1-3 also.

Figure 7 shows that the flow lines of stresses are developed in a single direction (linear stress development).
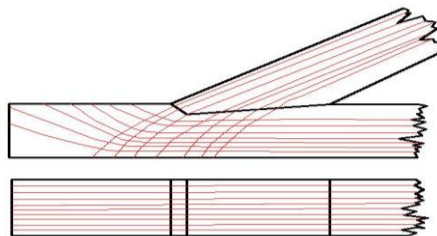
Figure 7. Isostatic flow stress lines for carving joints with simple threshold and orthogonal cutting

This represents an advantage compared to other types of connections where the flow lines of stresses are developed in two directions (plan stress development as in lateral carving joints or joints with spigots).

3.2 Analytical models to assess the load carrying capacity of carving joints with simple threshold and orthogonal cutting with limit states method

Carving joints with simple threshold and orthogonal cutting may lose load carrying capacity when one of the following limit states occurs:

1. Compression to an angle of the threshold
2. Development of slipping plan due to the shear stresses in the threshold
3. Failure of the bottom chord due to tensile stresses

Load carrying capacity of the joint is analytically determined according to European standard EN 1995-1 / 2004, [4].

3.2.1. Evaluation of load carrying capacity in compression

The strength condition is shown in equation 1:

$$N_s = N_c cos\alpha \leq m_c f_{c,\alpha,d} A_s \tag{1}$$

Where:
- N_s is the compression force acting to an angle;
- N_c is the compression force
- m_c is the factor for compression;
- A_s is the compression surface, calculated with the following relationship:

$$A_s = \frac{bh_c}{cos\alpha} \tag{2}$$

- $f_{c,\alpha,d}$ is the design resistance to compression to an angle α, determined according to the next relationship:

$$f_{c,\alpha,d} = \frac{C_{ri}Q_{ri}}{C_{ri}\sin + Q_{ri}\cos^2\alpha} \tag{3}$$

$$C_{ri} = f_{c,0,d}m_{TC} = k_{mod,c}\frac{f_{c,0,k}}{\gamma_M}m_{TC} \tag{4}$$

$$Q_{ri} = f_{c,90,d}m_{TC} = k_{mod,c}\frac{f_{c,90,k}}{\gamma_M}m_{TC} \tag{5}$$

where:

C_{ri} is the design tensile stress along the grain

Q_{ri} is the design tensile stress perpendicular to the grain

m_{TC} is the factor for tension;

$k_{mod,c}$ is the modification factor for duration of load and moisture content

$f_{c,0,d}$ is the design compressive strength along the grain

$f_{c,90,d}$ is the design compressive strength perpendicular to the grain

$f_{c,0,k}$ is the characteristic compressive strength along the grain

$f_{c,90,k}$ is the characteristic compressive strength perpendicular to grain;
γ_M is the Partial factor for material properties, also accounting for model uncertainties and dimensional variations.

3.2.2. Evaluation of load carrying capacity in shear

The strength condition is shown in equation 6:

$$N_s \leq m_f f_{v,d} A_f \tag{6}$$

where:
- N_s is the compression force acting to an angle;
- m_f is the shear coefficient for working conditions;
- A_f is the shear surface, $A_f = bL_f$;

- $f_{v,d}$ is the design shear resistance.

The distribution of the shear stresses is shown in Figure 8.
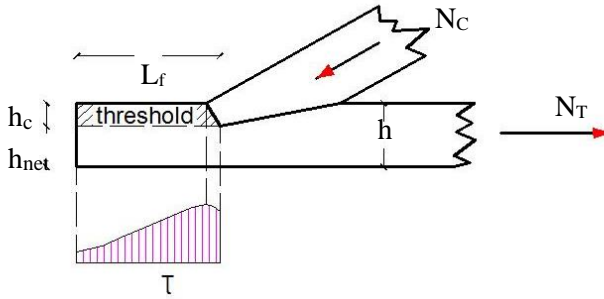
Figure 8. Diagrams of shear stresses in the shear plan

3.2.3. Evaluation of load carrying capacity in tension

- If the tensile force passes through the centroid of the net cross-section:

$$N_T \leq m_t f_{t,0,d} A_n \tag{7}$$

- If the tensile force doesn't pass through the centroid of the net cross-section:

$$\frac{N_T}{m_t A_n f_{t,0,d}} + \frac{N_T e_t}{m_m f_{m,d} W_n} \leq 1 \tag{8}$$

where:
- N_T is the tensile force;
- A_n is the net area;
- $f_{t,0,d}$ is the design tensile resistance;

- $f_{m,d}$ is the design bending resistance;
- m_t is the factor for tension;
- m_m is the factor for bending;
- W_n is the elastic section modulus.
- e_t is the offset distance of the load relative to the vertical portion of the element

3.3 Finite element numerical models for studying the behaviour of carving joints with simple threshold

The finite element analysis (FEA) has been made using the software program ANSYS-12. The models for the carving joint were developed in two situations:
- Case A: the two wooden bars of the carving joint have been defined as two distinct solid bodies, Figure 9;
- Case B: the two wooden bars of the carving joint have been defined as one solid body, Figure10.
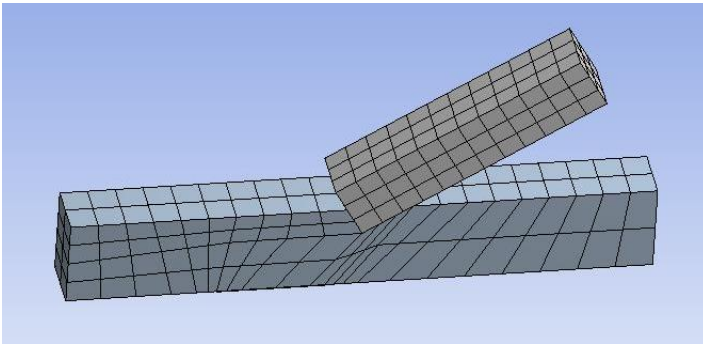
Figure 9. Case A, the two wooden bars of the carving joint with a contact area
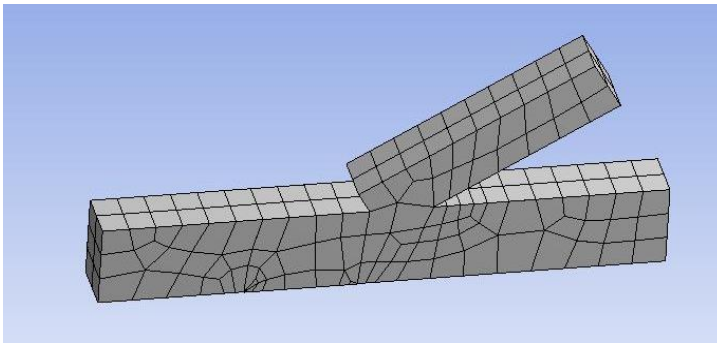
Figure 10. Case B, the two wooden bars of the carving joint defined as one solid body

4. STUDY CASE FOR THE ASSESSMENT OF THE LOAD CARRYING CAPACITY OF CARVING JOINTS WITH SIMPLE THRESHOLD AND ORTHOGONAL CUTTING

The study case presents the assessment of the carrying capacity of a carving joint from a roof truss made of wood elements, with the geometric scheme presented in Figure 11, having the following data:

- The span of the truss: 10.50 meters
- The height of the truss: 3.00 meters
- The truss bay: 3.00 meters
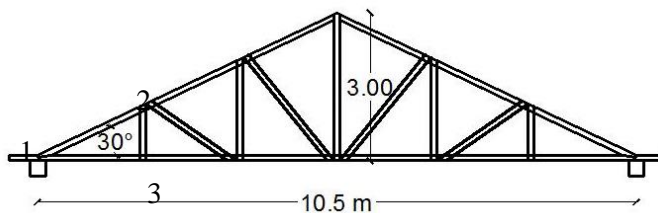
Figure 11. Geometric scheme of the wooden truss

The building is located in Iasi. According to the design code CR1-1-3-2012, "Snow action assessment for buildings", [3], characteristic values of snow load on the ground is $s_k = 2.5$ kN/m2, [3].

The structure is subject to the following loads: the dead load (roofing self-weight, and the weight of insulation, bracing, roof deck, etc.) and the snow load. It's analysed the end joint where the connection is made by carving joints as shown in Figure 6.

The beams connected in the joint are defined: 1-2 for the upper beam (top chord) and 1-3 for the lower beam (bottom chord). First, an analytical study has been performed.

Table 1 shows the values of the internal forces and the normal stresses. These values were determined by analytical calculation, for the previously considered loading scenario.

Table 1. The internal forces and the normal stresses

Beam	Cross section (mm x mm)	Axial forces (N)	Normal stresses (MPa)	Compression stresses to an angle (MPa)
1-2	100x100	-94000	-9.4	-18.8
1-3	200x100	87000	11.6	

The stresses obtained from analytical calculation are compared with the results provided by the finite element analysis performed with ANSYS-12 software. The results obtained for 3D models using the finite element analysis are presented in Figure 12 and Figure 13 for case A. For the analysis of case B the results are shown in Figure 14 and Figure 15.
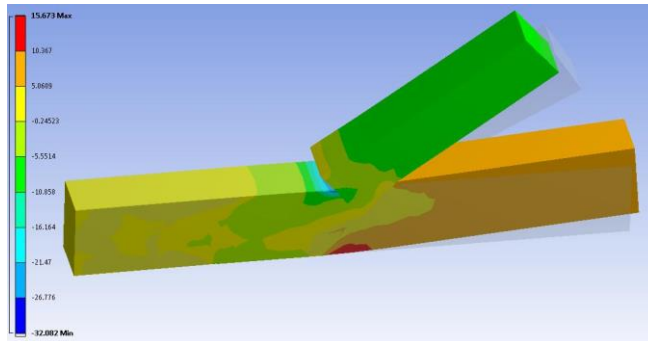
Figure 12. Normal stresses diagram for case A – FEA model
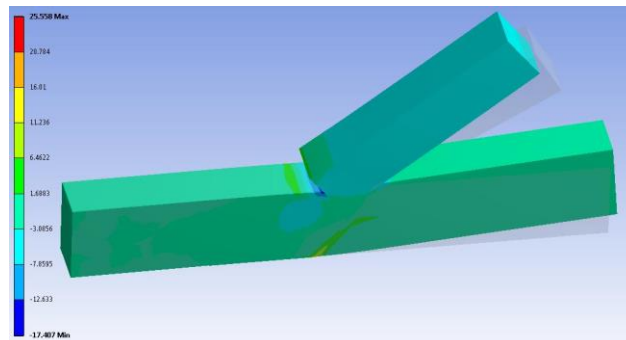
Figure 13. Shear stresses diagram for case A – FEA model
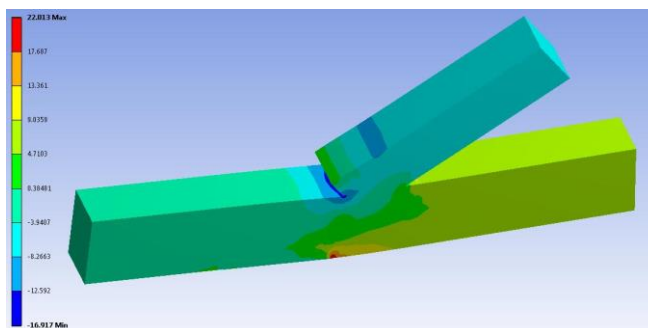
Figure 14. Normal stresses diagram for case B – FEA model
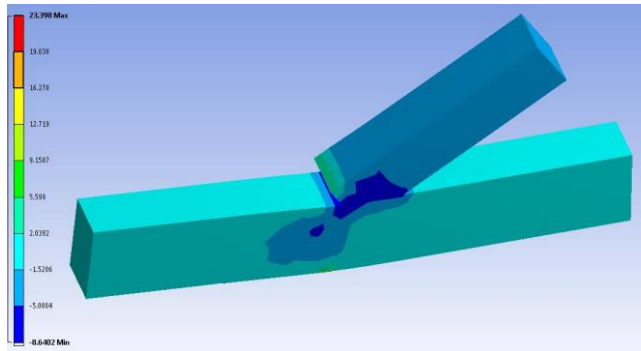
Figure 15. Shear stresses diagram for case B – FEA model

The resulted values from the finite element analyses, for the 3D models, are shown in Table 2.

Table2. Normal stresses and shear stresses for the modelled cases

Case	Maximum tensile stresses (MPa)	Maximum compression stresses (MPa)	Maximum shear stresses (MPa)
Case A	15.673	-32.082	25.558
Case B	22.013	-16.917	23.398

The results, obtained in FEM - case B, approached the analytical values, highlighting that the analytical model is based on the hypothesis of structural continuity between wood elements in carving joints.

In reality, the existence of imperfections in execution causes some gaps between the two wood elements, leading to the idea that FEM - case A is the model that could define the behaviour of the connection under loads, and also defines the development of stresses in the wood elements.

5. CONCLUSIONS

The carving joints are less used these days because they have disadvantages that influence choosing this type of joints. The joint technology reduces the section of elements, so it reduces the load carrying capacity of the element. The technology of fabrication is quite difficult, and it is time consuming and requires qualified workers.

Nowadays, there are many situations when the rehabilitation of joints is needed in buildings such as the historical monuments; therefore it is necessary, in order to strengthen them, to know how to evaluate rapidly the behaviour of structural elements and their joints for a correct sizing and for the strength checking.

The aim of the study was to present a comparative study case between the results of the analytical model and the finite element modelling cases for the evaluation of the carving joint with simple threshold. The comparative analysis of the obtained results highlights the following issues:

- The finite element modelling (FEM) of carving joints is possible.

- The fields of stresses obtained by FEM meet the isostatic flow lines of stresses for carving joints defined in classical theory for the assessment behaviour under loading conditions.

- Future research is required for refining the grid for FEA models and to validate the proper finite element model by experimental testing of the carving joints.

References

1. D. Isopescu, *Timber structures*, "Gh. Asachi" Publishing House Iaşi, 2002.
2. Vl. Gh. Boghian, *Timber construction* (in Romanian), Polytechnic Institute of Iasi, 284-305, 1970.
3. CR1-1-3-2012 - "*Design code. Snow action assessment for buildings*"
4. EN 1995-1 / 2004 – "*Design Code for Timber elements and structures*"
5. http://www.vacantesicalatorii.ro/modules/revista/articole/articol.php?artID=2329
6. http://www.lumeacredintei.com/reviste/...
7. http://www.ghiduri-turistice.info/...
8. http://necenzuratmm.ro/romania/...
9. http://www.ghiduri-turistice.info/...
10. http://casedinlemn.md/lemnul-ca-material-de-constructie

Development of Plastic Hinges in Steel and Composite Beams of Eccentrically Braced Frames

Mihai Senila[1] and Ioan Petran[1]

1Department of Structures, Faculty of Civil Engineering, Technical University of Cluj-Napoca, 400020, Romania

Summary

The frame structures with eccentrically braced frames (EBF) are used world-wide and represent the alternative to the concentrically braced frames (CBF). The dissipative elements of eccentrically braced frames are characterized by the forming of plastic hinges, situated at the extremities of frame elements, preferably in the beams, and only at limit states in columns. The strength and ductility of EBF is directly related to the strength and ductility of the links. The seismic energy is dissipated by means of elasto-plastic shear cycles (for the short link), bending cycles (for the long link) and shear and bending cycles (for the intermediate link).

This paper presents numerical studies with the objective to investigate the behaviour of 2D steel and composite eccentrically braced frames under seismic loading with active links which yield in bending,

KEYWORDS: plastic hinges, dissipative zones, composite sections, numerical analysis, eccentrically braced frames

1. INTRODUCTION

Steel and composite eccentrically braced frames (EBFs) are a very efficient type of structures for structural seismic response. The EBFs combine the advantages of both MRF (moment resistant frames) and CBF (concentrically braced frames), the ductility as the characteristic of moment resisting frames with the lateral stiffness associated with concentrically braced frames. [1]

In case of EBF's with composite beams, the current practice recommends a complete detachment between steel beam and concrete slab in the dissipative zones. The lack of connection between the concrete slab and the steel beam in dissipative areas does not lead to a behaviour similar with a pure steel beam. The presence of the reinforced concrete slab has an important influence on development of plastic hinges in beams. [2]

For a comparative analysis between the behaviour of eccentrically braced frames with steel sections and the ones with composite sections (without connection in dissipative zones), when are subjected to seismic loads, a series of nonlinear static analyses (pushover analyses) were carried out for both types of structures. The

design has been performed according to N2 method provided by SR EN 1998. The structures were modelled as 2D frames with 6 stories. The software SAP2000 was used to create the numerical model.

2. DESCRIPTION OF PUSHOVER AND N2 METHOD

The nonlinear static analysis (pushover) is a method used to evaluate the post-elastic capacity of structures. This type of analysis assumes incrementally imposed displacements up to the development of plastic hinges. As the displacements continue to increase, plastic hinges will be progressively developed until a failure mechanism will be reached (global or local). The recording of horizontal forces and top displacement of structure generate a graphic called capacity curve of structure or pushover curve. This curve is not associated with any earthquake, being a characteristic of structure. The capacity curve highlights different characteristic bending moments from post-elastic behaviour of structure and provides information about the resistance and ductility of structure. [3]

The N2 method implies determination of target displacement using a nonlinear static analysis. The procedure involves obtaining the base shear force – displacement capacity curve, with the characteristic points marked representing the requirements for displacement according to limit states. The requirements are determined by displacement spectra for inelastic seismic response. General safety condition is: demands ≤ capacity. [4]

3. MODELING PARAMETERS FOR THE STRUCTURES

The analyzed structure was located in Bucharest, characterized by the following features:
- Ground acceleration a_g=0,30g;
- Control period of design spectrum: Tc= 1,6s;
- Design snow load: $S_{0,k}$=2,00kN/m^2
- Design live load: Q=3,0kN/m^2.
- Design dead load: G=4,5kN/m^2.

The structural behaviour factor q = 6,0, which represents the energy dissipation capacity of structure is taken from Tab. 6.3 (P100-2013) for a high seismicity area (H): q = 5αu/α1, where αu/α1 =1,2 for EBF.

The reinforced concrete slab (C25/30, Ø12/15 - PC52) was modelled with steel multi-layered non-linear type of elements, which can be modelled the concrete in the slab, but also the reinforcement. For both materials a nonlinear behaviour has been defined.

Finer mesh was used in the potential plastic zones, where development of plastic hinges is expected. The type of mesh chosen for slab influences the result regarding the needed forces for development of plastic hinges. Different ways of meshing were studied until the optimum one, both in terms of results and analysis time.

The connection between the concrete slab and steel beam was modeled using link elements – available in software SAP2000. It has been chosen a version with fixed links, where the connection of concrete slab and steel beam is in centroid.
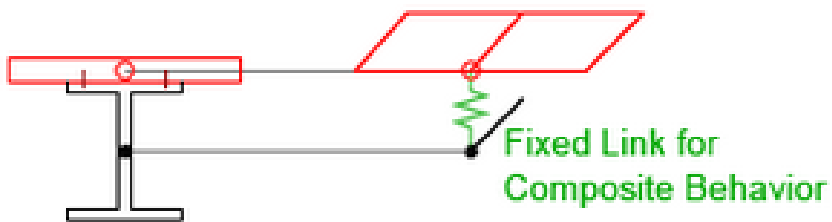
Fig. 1 Modelling of the composite beam – SAP2000 [3]

A distance of 30 cm between links was chosen taking into consideration different ways for layout of the links. A lower distance would increase the time for analysis, without difference in results.

Initial design was made with modal spectrum analysis (P100-2013), after which nonlinear static analyses – pushovers were performed, in order to evaluate the development of plastic hinges in dissipative zones and the capacity curve.

Two type EBF structures were analyzed: steel structure (S_4) and composite structure (C_4).
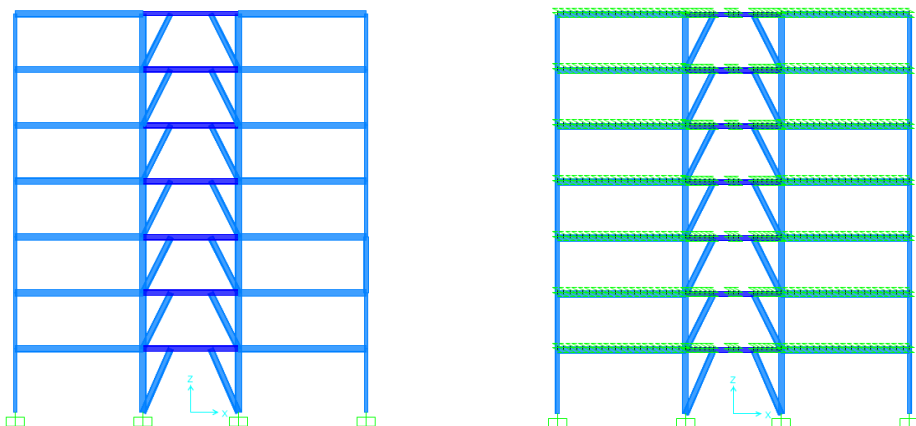
Fig. 2 EBF_S_6 (left) and   EBF_C_6 (right)

Table 1 Description of the structures P+6E

Type	Central columns	Marginal columns	Braces	Beams	EBF beam	Type of EBF beam
EBF_S_6	HEB400	HEB240	HEB340 HEB280	IPE400	HEB360 HEB340 HEB280	Steel
EBF_C_4	HEB400	HEB240	HEB340 HEB280	IPE400	HEB320 HEB280	composite

For the steel structure – EBF_S_6, the beams of the frame are as follows: HEB360 for the first three levels, HEB340 for levels 4, 5, 6, and HEB280 respectively for the last level.

For EBF_C_6, after performing the push-over analysis using the same sections as for steel structure EBF_S_6, in which was added the contribution of concrete slab, yield mechanism is formed in columns and braces at first level of the central frame. For this reason, the assure the formation of plastic hinges in the dissipative zones (links) it was necessary a reduction of composite section to HEB320 (exception - beam from the last level, which remain HEB280).

After performing the push-over analysis, the base shear force – displacement capacity curve (global force – top displacement) was obtained. From capacity curves the target displacements have been determined for both structures.

Next the results obtained in pushover analysis, the results for N2 method and the local and global checking for this method are presented.

The target displacements for both types of structures (with steel beam and composite beam) were determined for the following limit states:
- Serviceability limit state (SLS);
- Ultimate limit state (ULS);
- Collapse prevention limit state (CPLS).

4. RESULTS OF THE PUSHOVER ANALYSIS

The obtained target displacement values for structures with steel beam are: 12,9 cm for SLS, 28,5 cm for ULS, respectively 46,0 cm for CPLS.

For the frame with composite beams are: 7,99 cm for SLS, 18,3 cm for ULS, respectively 32,1 cm for CPLS.

The obtained values are presented in the following graphics:
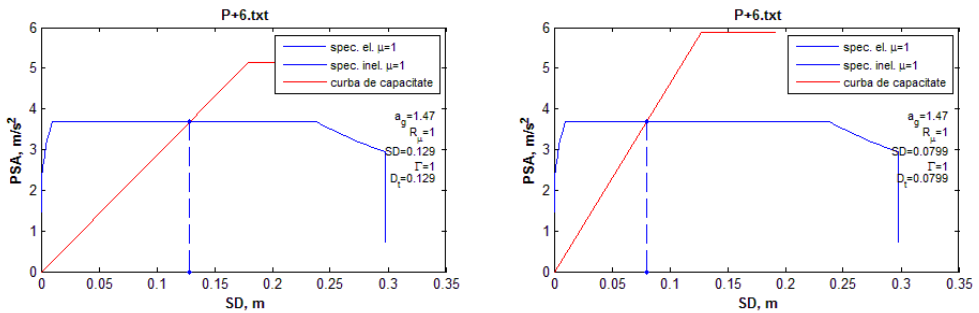
Fig. 3 Target displacements SLS – EBF_S_6 left, EBF_C_6 right
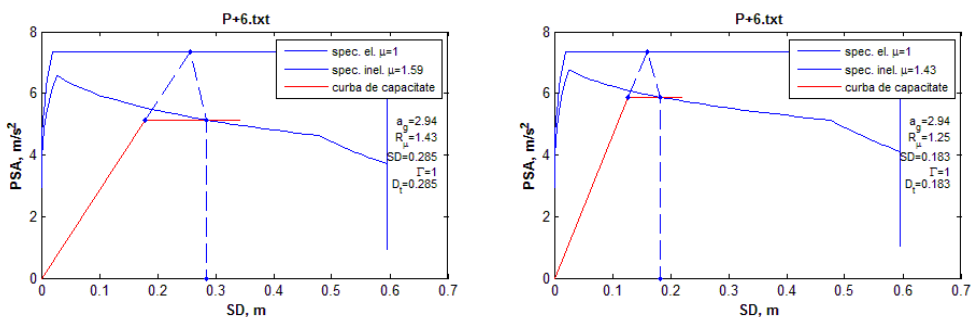
Fig. 4 Target displacements ULS – EBF_S_6 left, EBF_C_6 right
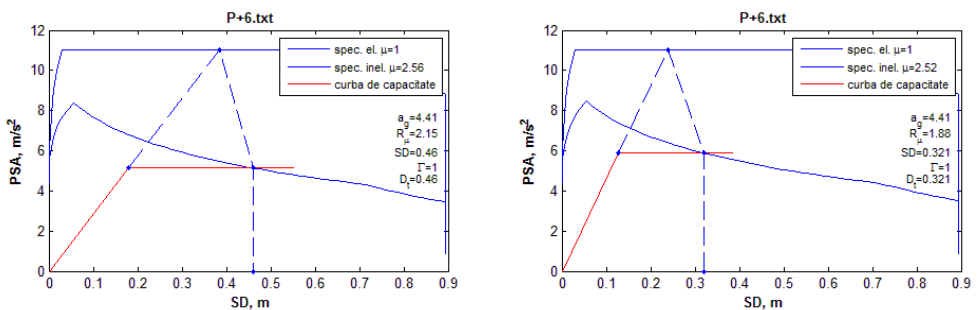
Fig. 5 Target displacements CPLS – EBF_S_6 left, EBF_C_6 right

From the graphics presented above it can be observed that the requirements for target displacements are higher for steel frames than for composite frames (12.9 cm vs, 7.99 cm for SLS, 28.5 cm vs. 18.3 cm for ULS, respectively 46 cm vs. 32.1 cm for CPLS)

The curves obtained from numerical analysis are shown in the next figure.
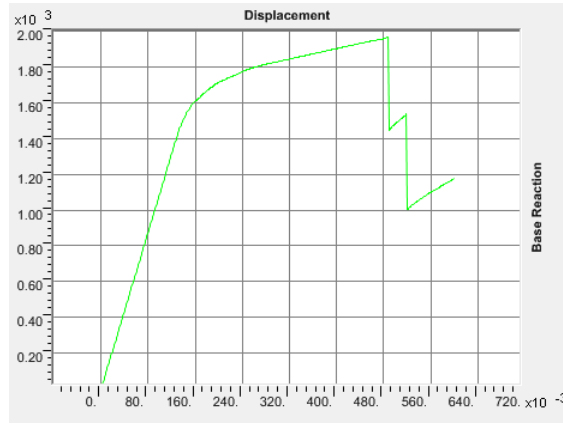
(a)
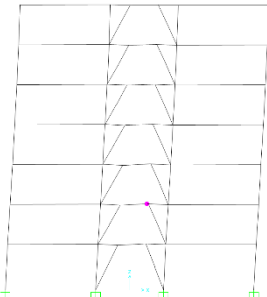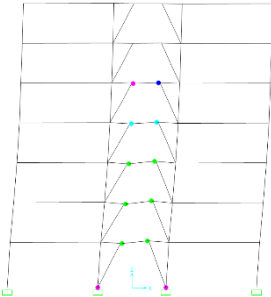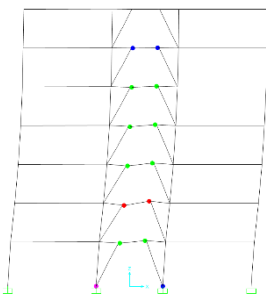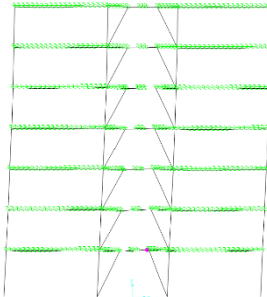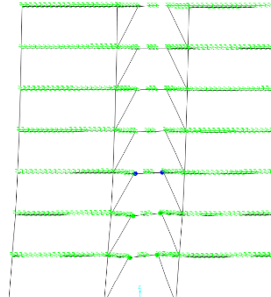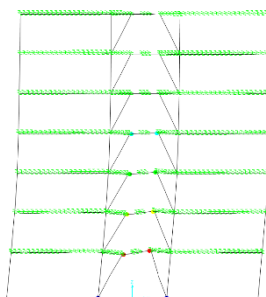
(b)

Fig. 6 Capacity curves for EBF_S_6 (a) and EBF_C_6 (b)

From these two force-displacement curves it can be observed that the contribution of concrete slab in case of EBF_C_6 is significant even if the dissipative zones are not provided with shear connectors. The maximum value of the force exceeds the value of 2900 kN for a 38 cm displacement compared with the steel frames, where the maximum value for the force is 2000 kN and the ultimate displacement is approx. 48 cm.

The following table presents the development of plastic hinges in the link .It was taken into consideration the following characteristic moments: development of first plastic hinge, the displacement for ultimate limit state (ULS) and the formation of failure mechanism.

Table 2 Development of plastic hinges

	Development of first PH	ULS	Collapse
EBF_S_6	$D_E=12.9$ cm$= D_{TSLS}$	$D_{ULS}=28.5$ cm	$D_U=48.9$ cm$> D_{TCPLS}$
EBF_C_6	$D_E=9.1$ cm $> D_{TSLS}$	$D_{ULS}=18.3$ cm	$D_U=39.2$ cm$> D_{TCPLS}$

The requirements for target displacement, calculated by using N2 method for all 3 limit states are reached for both types of structures (steel and composite).

In case of EBF_S_6 the first plastic hinge is developed approximately in the same time as achieving the requirements for serviceability limit state and plastic hinges are developed in links from the first five levels. For the requirements specific to ultimate state it can be observed that failure mechanism is formed in the link from the second level, by failure of both plastic hinges. The collapse mechanism occurs by failure of dissipative zone from beam of second level.

In case of composite frame EBF_C_6, the first plastic hinge is formed after reaching the requirements of SLS. For the requirements of ultimate limit state, the plastic hinges are developed in links of the first 3 levels. The collapse mechanism occurs by failure of dissipative zone from beam of the first level.

The obtained values for inter-story drift are presented in the following graphics:
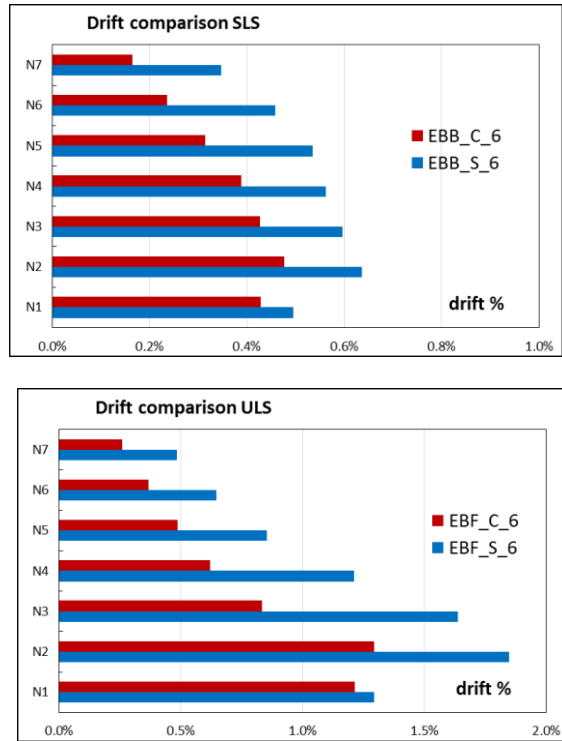
Fig. 7 Inter-story drift for EBF_S_6 and EBF_C_6 at SLS and ULS
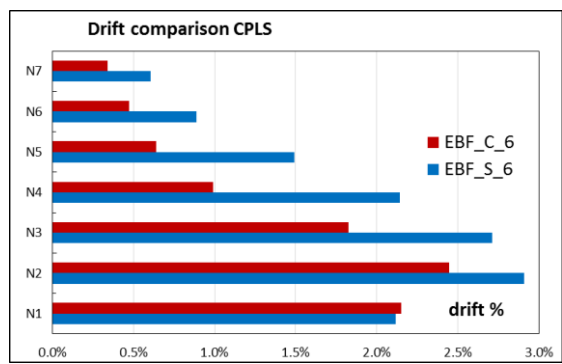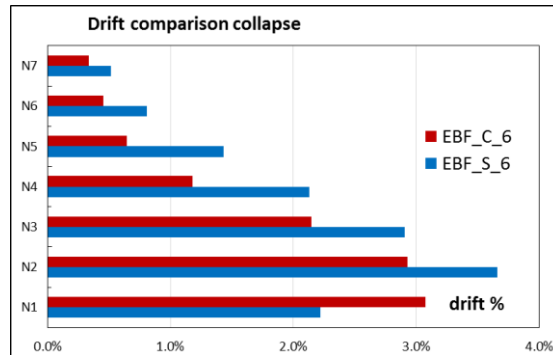
Fig. 8 Inter-story drift for EBF_S_6 and EBF_C_6 at CPLS and collapse

The values for the drift are within the values specified in the design norms in all the three limit states. There were taken into account the values from P100-2013, which provides a maximum value for the drift of 0.75% for SLS, 2.5% for ULS and 5% for CPLS provided by the FEMA356 (in P100-2013 does not exist requirements for CPLS).

The maximum value for the inter-story drift is reached to the second level for all the three limit states. (SLS, ULS, CPLS)

5. CONCLUSIONS.

The difference in behaviour between two types of eccentrically braced frames, steel and composite, has been studied. The contribution of the concrete slab is significant in regards to the global behaviour of structure, even in the situation when shear connectors are not present in the dissipative zones.

From the push-over analyses it can be observed that the requirements for target displacements are higher for steel frames than for composite frames. The energy dissipation is done through the development of plastic hinges for both types of structures.

The push-over analyses showed that in case of composite beams to lower values of the inter-story drift, plastic hinges are formed later, which leads to a stiffer structure. The values for inter-story drift are within the limit values provided by norms for both types of structures in all the three limit states.

In case of eccentrically braced frames with links that yield in bending, it will be recommend to use the composite beam solution because leads to a better seismic response than the pure steel beams.

Bibliography

1. [1] S.-H. Chao and S. C. Goel, "*Performance-based seismic design of EBF using target drift and yield mechanism as performance criteria*," Department of Civil and Environmental Engineering, The University of Michigan, 2005
2. [2] A. Ciutina, D. Dubina and G. Danku, "*Influence of steel-concrete interaction in dissipative zones of frames: I - Experimental study*" Steel and Composite Structures, Vol. 15, No. 3, 2013.
3. [3] S. v. CSI Berkeley, FAQ.
4. [4] P. Fajfar, ""*A nonlinear analysis method for performance-based seismic design*"," Earthquake Spectra, 16(3):573-92, 2000.
5. [5] SR EN1998-1:2004, *Design of structures for earthquake resistance - Part 1: General rules, seismic actions and rules for buildings.*
6. [6] SR EN1994-1-1, "*Design of Composite Steel and Concrete Structures. Part 1.1. General Rules and Rules for Buildings.* Brussels: CEN, European Committee for Standardisation".
7. [7] FEMA 356, "*Prestandard And Commentary For The Seismic Rehabilitation Of Buildings*" November, 2000.
8. [8] P100-1-2013, "*Cod de proiectare seismica*".

Computational Methods in Predicting the Elastic Engineering Constants for Multi-layered Composites

Iuliana Dupir (Hudişteanu), Vlad Lupăşteanu

Department of Civil and Industrial Engineering, Technical University "Gheorghe Asachi", Iasi, Zip code 700050, Romania

Summary

The paper presents the development of the computational equations which describe the elastic behaviour of multi-layered composites. The prediction of the elastic engineering constants is studied based on classical lamination theory, both for an orthotropic lamina and for a symmetric angle-ply laminate. The stiffening effect of stacking two or more laminas is demonstrated based on a case study, where two different types of composite material were analysed. Graphical distributions of the engineering constants with respect to different fibre volume fractions, for unidirectional off-axis laminas and symmetric angle-ply laminates, were represented. The influence of the fibre volume fractions on the elastic behaviour of composite laminates is also investigated.

KEYWORDS: classical lamination theory, orthotropic lamina, angle-ply laminate, composite laminate, fibre volume fraction, fibre orientation angle, engineering elastic constants.

1. INTRODUCTION

The classical lamination theory (CLT) derives from the classical plate theory proposed by Kirchhoff-Love [1] and it is the most commonly used theory for analysing composite laminates. The extension of this theory is valid for thin laminates, with small displacement in the transverse direction. The basic assumptions which govern the lamination theory are presented by Herakovich in [2], as it follows:
- Perfect bonding between the layers is assumed.
- Each ply is a homogeneous material with known effective properties.
- Each lamina is in a plate stress.
- The individual lamina can be isotropic, orthotropic or transversely isotropic.
- The laminate deforms according to the Kirchhoff-Love assumptions for bending and stretching.

Classical lamination theory presented in the paper is applicable to orthotropic continuous fibre laminated composites only.

The laminate engineering elastic constants are important in predicting the stiffening behaviour of a composite structure. Therefore, it is necessary to know the influencing parameters as the fibres and matrix properties and the ply microstructure, the shape and size of the fibres' cross-sections, fibre volume fraction, fibre orientation angles and stacking sequence.

2. GOVERNING EQUATIONS OF ENGINEERING CONSTANTS

2.1. Off-axis unidirectional lamina

A ply or lamina is the simplest element of a composite material and it is considered an elementary layer of unidirectional fibres embedded in a matrix [3]. The off-axis unidirectional lamina or the general orthotropic lamina shown in Fig. 1 is defined as a composite ply where the principal material axes 1(L) and 2(T) make a different angle with the global system of reference (x, y) [4].
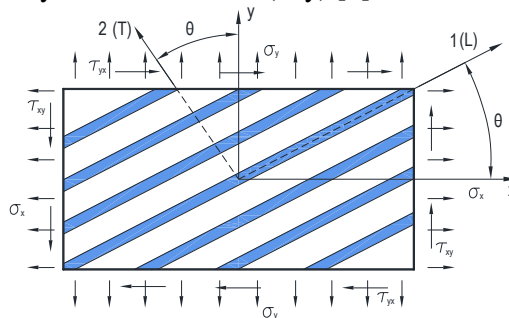
Figure 1. Off-axis unidirectional lamina

The effects of fibre orientation angles are studied with corresponding transformations between principal and global axes presented in Equation (1):

$$E_x = \frac{1}{\dfrac{1}{E_1}c^4 + \left(\dfrac{1}{G_{12}} - 2\dfrac{\nu_{12}}{E_1}\right)s^2c^2 + \dfrac{1}{E_2}s^4}$$

$$E_y = \frac{1}{\dfrac{1}{E_1}s^4 + \left(\dfrac{1}{G_{12}} - 2\dfrac{\nu_{12}}{E_1}\right)s^2c^2 + \dfrac{1}{E_2}c^4}$$

$$G_{xy} = \cfrac{1}{2\left(\cfrac{2}{E_1}+\cfrac{2}{E_2}+\cfrac{4v_{12}}{E_1}-\cfrac{1}{G_{12}}\right)s^2c^2 + \cfrac{1}{G_{12}}\left(s^4+c^4\right)} \tag{1}$$

$$v_{xy} = -\cfrac{\left[c^2s^2\left(1+\cfrac{E_1}{E_2}-\cfrac{E_1}{G_{12}}\right)-\left(c^4+s^4\right)v_{12}\right]}{\left[c^4+c^2s^2\left(-2v_{12}+\cfrac{E_1}{G_{12}}\right)+s^4\cfrac{E_1}{E_2}\right]}$$

$$v_{yx} = -\cfrac{\left[c^2s^2\left(1+\cfrac{E_1}{E_2}-\cfrac{E_1}{G_{12}}\right)-\left(c^4+s^4\right)v_{12}\right]}{\left[s^4+c^2s^2\left(-2v_{12}+\cfrac{E_1}{G_{12}}\right)+c^4\cfrac{E_1}{E_2}\right]}$$

where: E_1, E_2 and G_{12} are the axial and shear moduli with respect to the principal material axes, v_{12} and v_{21} are the Poisson's ratios and θ is the fibre orientation angle; $c = \cos\theta$, $c^2 = \cos^2\theta$, $c^4 = \cos^4\theta$; $s = \sin\theta$, $s^2 = \sin^2\theta$, $s^2 = \sin^2\theta$.

The in-plane engineering elastic constants with respect to the principal material directions are determined according to the micromechanics of fibre reinforced composites [4-6], as follows in Equation (2):

$$E_1 = E_f \cdot V_f + E_m \cdot V_m, \quad E_2 = \frac{E_f \cdot E_m}{V_f \cdot E_m + V_m \cdot E_f},$$

$$G_{12} = \frac{G_f \cdot G_m}{V_f \cdot G_m + V_m \cdot G_f} \tag{2}$$

$$v_{12} = v_f \cdot V_f + v_m \cdot V_m, \quad v_{21} = v_{12} \cdot \frac{E_2}{E_1},$$

where: E_f and E_m are the longitudinal Young's modulus of the fibre and matrix respectively; G_f and G_m are the shear modulus of the fibre and matrix; v_f and v_m are the Poisson's ratios of the fibre and matrix; V_f and V_m are the fibre and matrix volume fractions.

2.2. Angle-ply laminates

By definition, angle-ply laminates $\left[(\pm\theta)_n\right]_s$ are considered a special type of orthotropic laminates, having equal number of equal thickness layers at $+\theta$ and $-\theta$ fibre orientation angles. Symmetric angle-ply laminates are characterized by

symmetry with respect to the middle plane of the laminate, in terms of material, thickness and fibre orientation angles [6].
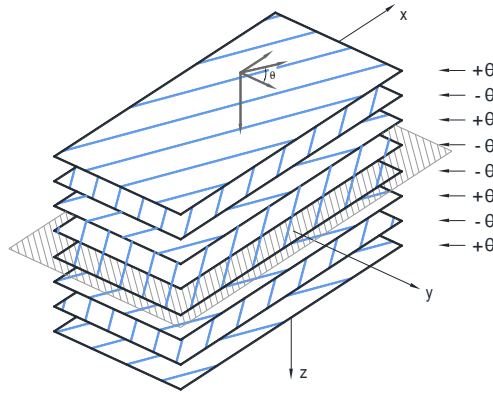
Figure 2. Angle-ply laminate $\left[(\pm\theta)_2\right]_s$

The computational equations which describe the stiffening behaviour of an angle-ply laminate are related to the elements of the laminate compliance $\left[a^*\right]$ and of the transformed reduced stiffness matrix $\left[\overline{Q}\right]$, as follows [4]:

$$E_x = \frac{1}{a_{11}^*} = \frac{\overline{Q}_{11}\overline{Q}_{22} - \overline{Q}_{12}\overline{Q}_{12}}{\overline{Q}_{22}}$$

$$E_y = \frac{1}{a_{22}^*} = \frac{\overline{Q}_{11}\overline{Q}_{22} - \overline{Q}_{12}\overline{Q}_{12}}{\overline{Q}_{11}}$$

$$G_{xy} = \frac{1}{a_{66}^*} = \overline{Q}_{66} \tag{3}$$

$$\nu_{xy} = -\frac{a_{12}^*}{a_{11}^*} = \frac{\overline{Q}_{12}}{\overline{Q}_{22}}$$

$$\nu_{yx} = -\frac{a_{12}^*}{a_{22}^*} = \frac{\overline{Q}_{12}}{\overline{Q}_{11}}$$

The elements of the transformed reduced stiffness matrix $\overline{Q}_{ij}$ are given by Equation (4) [4, 7]:

$$\overline{Q}_{11} = Q_{11}c^4 + 2(Q_{12} + 2Q_{66})c^2 s^2 + Q_{22}s^4$$
$$\overline{Q}_{12} = (Q_{11} + Q_{22} - 4Q_{66})c^2 s^2 + Q_{12}(s^4 + c^4)$$
$$\overline{Q}_{22} = Q_{11}s^4 + 2(Q_{12} + 2Q_{66})c^2 s^2 + Q_{22}c^4 \tag{4}$$

$$\overline{Q}_{16} = \left[\left(Q_{11} - Q_{12} - 2Q_{66} \right) c^2 + \left(Q_{12} - Q_{22} + 2Q_{66} \right) s^2 \right] cs$$

$$\overline{Q}_{26} = \left[\left(Q_{11} - Q_{12} - 2Q_{66} \right) s^2 + \left(Q_{12} - Q_{22} + 2Q_{66} \right) c^2 \right] cs$$

$$\overline{Q}_{66} = \left(Q_{11} + Q_{22} - 2Q_{12} - 2Q_{66} \right) c^2 s^2 + Q_{66} \left(c^4 + s^4 \right)$$

where: Q_{ij} represent the coefficients of the stiffness matrix, related to the in-plane engineering constants of the lamina, as follows:

$$Q_{11} = \frac{E_1}{1 - \nu_{12} \cdot \nu_{21}}$$

$$Q_{12} = \frac{\nu_{21} \cdot E_1}{1 - \nu_{12} \cdot \nu_{21}} = \frac{\nu_{12} \cdot E_2}{1 - \nu_{12} \cdot \nu_{21}}$$

$$Q_{22} = \frac{E_2}{1 - \nu_{12} \cdot \nu_{21}} \tag{5}$$

$$Q_{66} = G_{12}$$

3. CASE STUDY

The prediction of the elastic engineering constants for orthotropic laminas and symmetric angle-ply laminates is demonstrated based on a case study. Two different types of composite materials are chosen for the analysis, such as carbon fibre/epoxy resin and S glass/polyester resin, given in Table 1.

Table 1. Properties of materials [7]

Composite materials		Longitudinal Young's modulus [GPa]		Poisson's ratios		Shear modulus [GPa]	
Fibre	Matrix	E_f	E_m	ν_f	ν_m	G_f	G_m
carbon	epoxy	380	4.1	0.2	0.4	118.75	1.46
S glass	polyester	85.5	4	0.22	0.39	26.72	1.44

The variations of the elastic engineering constants with respect to the fibre volume fractions are shown in Figs. 3-7. Suggestive values for the fibre orientation angles were selected as to illustrate the stacking stiffening effect, but also the highest engineering constants obtained values for angle-ply laminates.
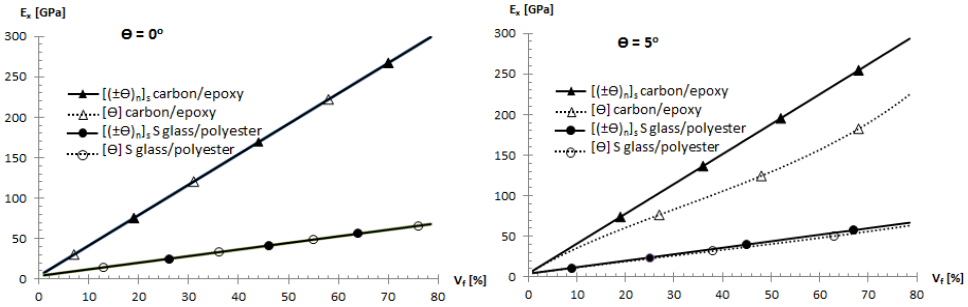
a). highest values for E_x
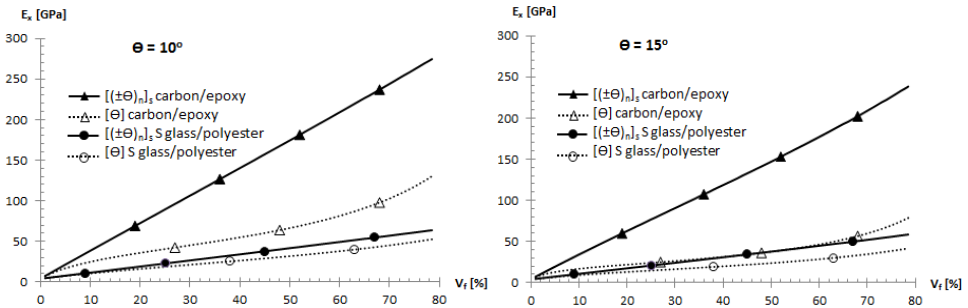
b). stacking stiffening effect

Figure 3. Variation of longitudinal modulus E_x

The longitudinal elastic modulus E_x reaches maximum values at $\theta = 0 - 5^o$, as shown in Fig. 3a. While increasing the fibre orientation angles, a gradual and continuous loss of stiffness appears. Moreover, the elastic properties for this interval are difficult to be distinguished for laminas compared with laminates, so the concept of an angle-ply laminate with low values of orientation angles is not feasible for design.

The stiffening effect is most clearly illustrated in Fig. 3b, for fibre orientation angles of $\theta = 10 - 15^o$, where significant differences can be observed between the orthotropic laminas and angle-ply laminates.

As expected, the graphical distributions shown in Fig. 4 for the transverse modulus E_y are identically with E_x, for complementary fibre orientation angles.
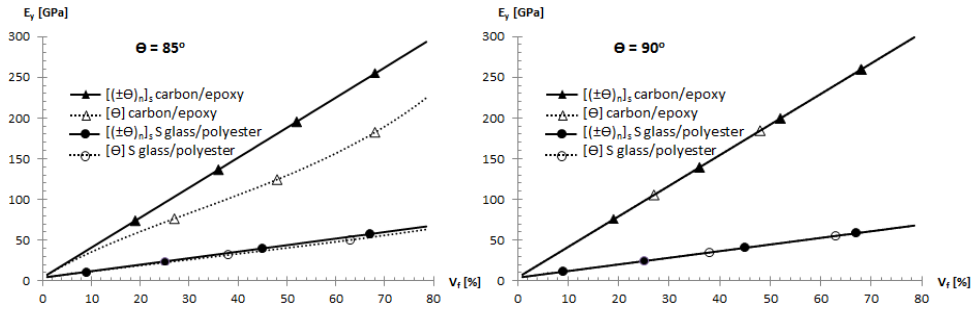
a). highest values for E_y
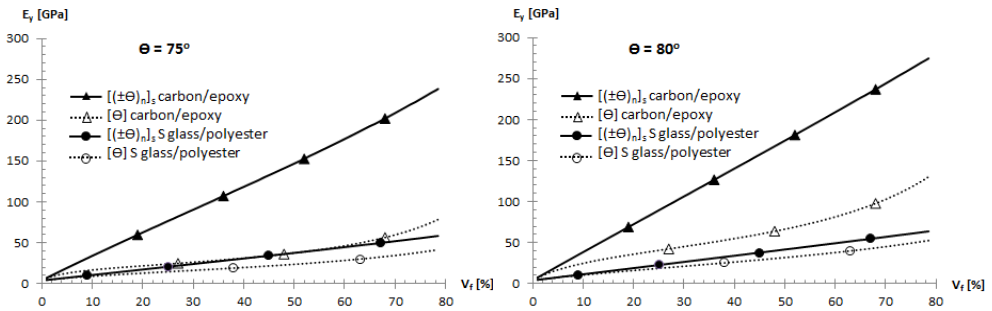
b). stacking stiffening effect

Figure 4. Variation of transverse modulus E_y

Comparison of the predictions for longitudinal modulus E_x and transverse modulus E_y shows that the fibre volume fractions influence the increasing of the analysed engineering constants.
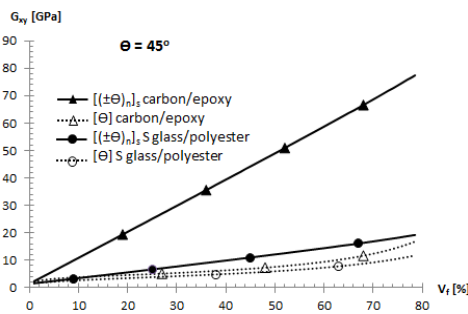
a). highest values for G_{xy} and stacking stiffening effect
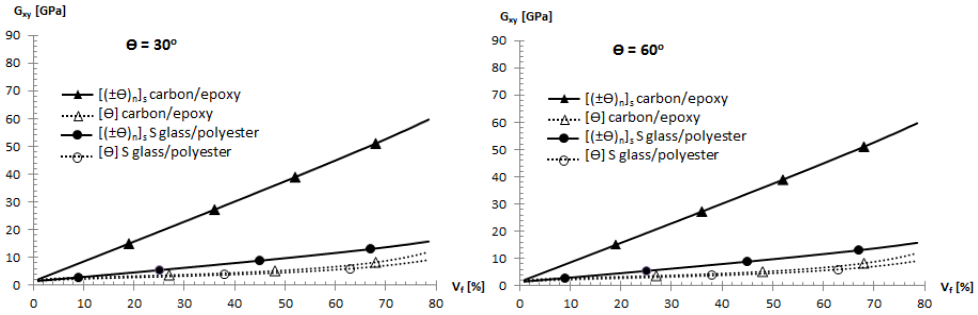
b). symmetry with respect to $\theta = 45^o$

Figure 5. Variation of shear modulus G_{xy}

The shear modulus G_{xy} reaches highest values and the stacking stiffening effect is the most clearly illustrated at a fibre orientation angle of $\theta = 45^o$ (Fig. 5a). The G_{xy} graphical distributions indicate a symmetry with respect to $\theta = 45^o$, showing increasing values for $\theta = 0 - 45^o$ and decreasing values for $\theta = 45 - 90^o$ (Fig. 5b).

The variations of the Poisson's Ratios v_{xy} and v_{yx} are illustrated in Figs. 6-7.
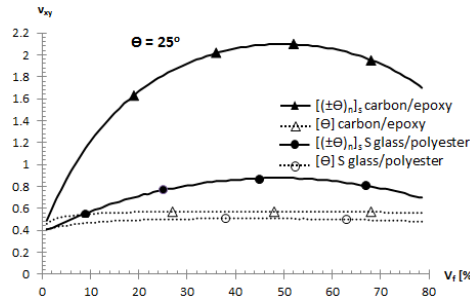
a). highest values for v_{xy} and stacking stiffening effect
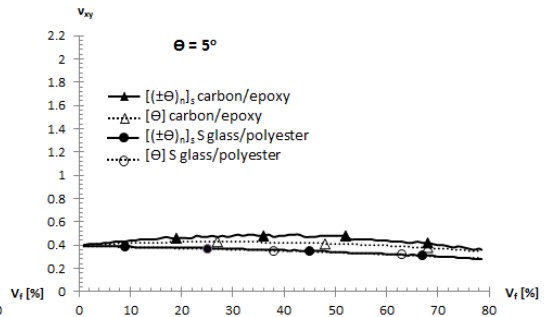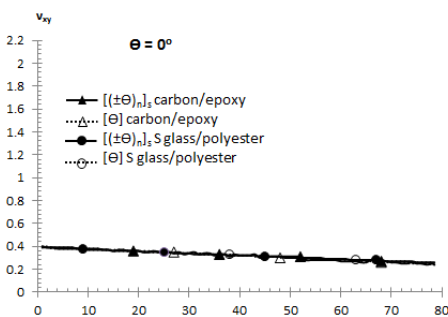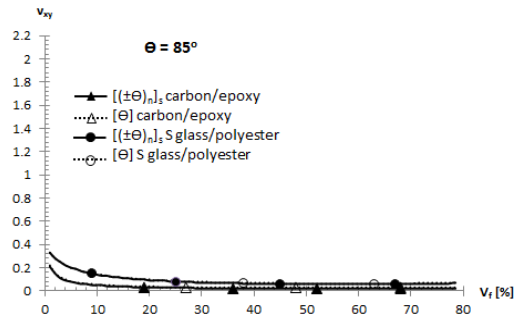
b). different slope distributions for ν_{xy}

Figure 6. Variation of Poisson's ratios ν_{xy}

The stacking stiffening effect and the highest reached values for the Poisson's ratios ν_{xy} and ν_{yx} are shown in Fig. 6a and Fig. 7b respectively. As expected again, the fibre orientation angles for the Poisson's ratios are complementary, so the graphical distributions of the engineering constants appear as in a mirror one to the other.
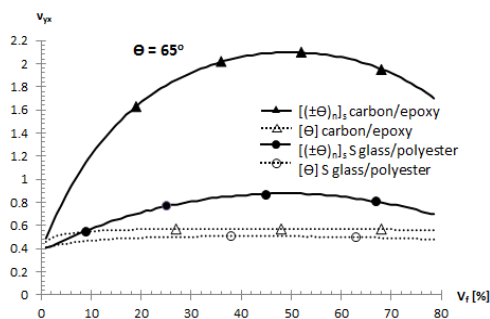
a). highest values for ν_{yx} and stiffening effect
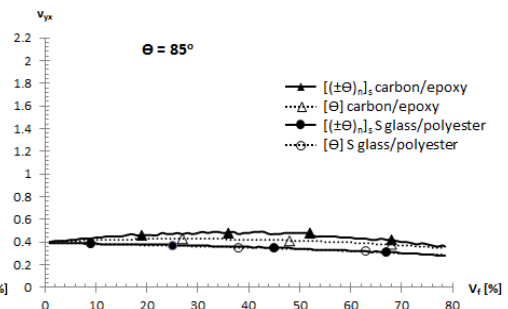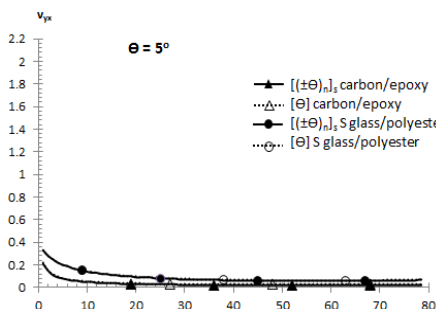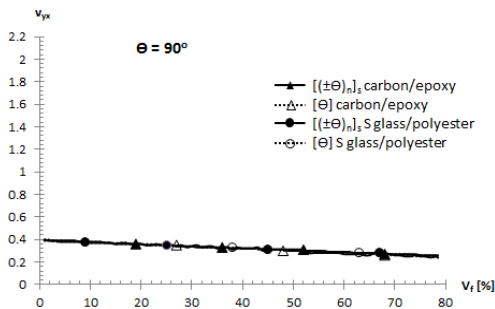
b). different slope distributions for ν_{yx}

Figure 7. Variation of Poisson's ratios ν_{yx}

The variation of Poisson's ratios is shown in Fig. 6b and Fig. 6a, for different fibre orientation angles. Different slope distributions are illustrated, suggesting a gradual loss or gain of stiffness once the fibre volume fractions or the fibre orientation angles are changed.

4. CONCLUSIONS

The influence of the fibre volume fractions on the elastic engineering constants of multi-layered composite was demonstrated. The presented graphical distributions indicate an increase on the elastic characteristics when higher percentages of fibre volume fractions are used. Even so, in the case of the Poisson's ratios, the increase is not proportional to the fibre volume fractions, neither to the fibre orientation angles.

Significant differences regarding the elastic characteristics and stiffening behaviour was observed between the two types of composite materials adopted for the case study. Therefore, when designing a composite laminate, all the previous discussed parameters have to be taken into account to fulfil the needed requirements.

References

1. Love, A.E.H., *On the small free vibrations and deformations of elastic shells*, Philosophical transactions, The Royal Society, London, Vol. serie A, No. 7, p. 491–549, 1888
2. Herakovich, C.T., *Mechanics of Fibrous Composites*, John Wiley & Sons, Inc., University of Virginia, 1998.
3. Vasiliev. V.V., Morozov E., *Advanced Mechanics of Composite Materials and Structural Elements, Third Edition*, Elsevier, 2013.
4. Ţăranu, N., Isopescu, D., *Structures made of composite materials*, Ed. Vesper, Iaşi, 1996.
5. Kaw, A.K., *Mechanics of Composite Materials. 2nd ed.*, CRC Press, Taylor & Francis Group, 2006.
6. Barbero, E.J., *Introduction to Composite Materials Design. 2nd ed*, CRC Press, 2011.
7. Ţăranu, N., Bejan, L., Cozmanciuc, R., Hohan, R., *Materiale şi elemente composite I. Prelegeri şi aplicaţii*, Ed. Politehnium, Iaşi, 2013.

Analytical Evaluation of the Flexural Capacity of Steel Beams Strengthened with Bonded CFRP Composite Strips

Vlad Lupășteanu, Lucian Soveja and Iuliana Hudișteanu

Faculty of Civil Engineering and Building Services, Gheorghe Asachi Technical University of Iaşi, 700050, Romania

Summary

Traditional strengthening solutions of steel beams usually consist in supplementing the base material in specific locations, for which, certain parameters are not fulfilled any more. For the most common cases, these strengthening solutions imply large consumptions of construction materials and high costs. Strengthening solutions based on carbon fibre reinforced polymer (CFRP) composites have gained much interest in the last years, because of the superior mechanical properties of the latter and due to their simple and rapid technique of application. This paper presents the analytical evaluations of the flexural capacity of a steel beam which has been strengthened using a (CFRP) strip.

KEYWORDS: steel beams, flexural capacity, adhesively bonded CFRP composite strips.

1. INTRODUCTION

Traditional strengthening schemes of steel beams consist in welding or mechanically fastening steel plates or profiles in those sections for which the resisting capacity is smaller than the effective applied forces. Other conventional solutions consist in encasing the steel element, either partially or totally, in concrete, or changing the static scheme of the element by introducing supplementary components, like bracings or props and even intermediate supports [1, 2, 3]. Also, for the cases in which the strength or the stiffness of the beam are affected due to local degradations, the strengthening solution my consist in replacing the damaged sections with new ones.

For most of the traditional solutions, the strengthening process implies large consumptions of materials, labour and costs. Moreover, the strengtheing process usually comes with the incapacity of using the building, which may amplify the financial impact of the project. Using composite materials in strengtheing processes of steel beams may turn into a feasable solution, first because of the great mechanical properties of these materials (high ratio between strength and specific weight) and second, because of the execution phase which can be done in a very short time with minimum impact upon the activities that are run inside the building.

Strengthening solutions of steel beams based on CFRP composite elements are among the newest methods, the first steel structure which has been strengthened with this technique is the Tickford Bridge from UK, in 1999 [4].

Steel beams flexurally strengthened with CFRP composite elements have been analysed by numerous research teams, by either analytical and numerical methods or experimental tests [5, 6, 7, 8]. The results of the experimental programs have confirmed the efficiency of this strengthening solution, the flexural capacities of the beams being improved from 15% up to 85%, depending on the amount and quality of the CFRP material that was used and being also influenced by the bonding agent. Also, in many cases, a good correlation between the analytical models and the experimental results has been confirmed [9].

2. DESIGN EXAMPLE

For a better illustration of the strengthening effect for a steel beam, a design example is presented in this section. Thus, a simply supported steal beam is considered, with geometrical characteristics being presented in Figure 1. The bottom flange has been strengthened with a CFRP composite strip bonded with an adhesive characterized by a non-linear bond-slip model presented in Figure 2. The mechanical properties of the materials are briefly inserted in Table 1. The beam is subjected to a concentrated force, in the midspan and in order to emphasise the effects of the strengthening scheme, the lateral buckling of the beam and the premature debonding failure of the adhesive are not taken into account.
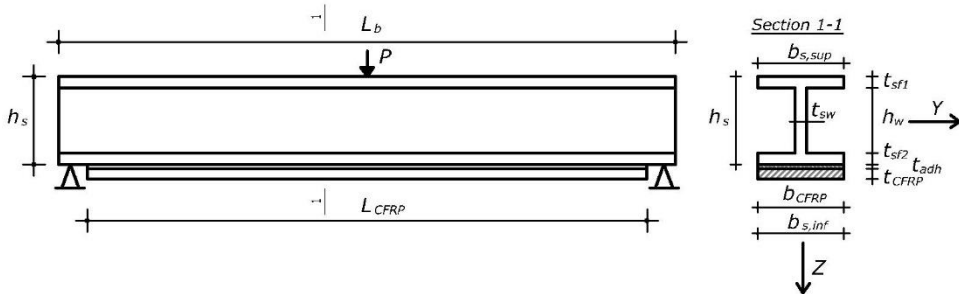
Figure 1. Layout of the FRP plated steel beam

Table 1. Geometrical and mechanical properties of the components

Property	Notation	Value	Unit
Steel beam			
Span	L_b	4100	mm
Height	h_s	270	mm
Top flange width	$b_{s,sup}$	150	mm
Bottom flange width	$b_{s,inf}$	150	mm

Thickness of the top flange	t_{sf1}	12	mm
Thickness of the bottom flange	t_{sf2}	12	mm
Thickness of the web	t_{sw}	10	mm
Height of the web	h_w	246	mm
Cross-sectional area	A_s	6060	mm^2
Yield strength	f_y	235	MPa
Young's modulus	E_s	200000	MPa
Yielding strain	ε_{sy}	0.001175	-
Safety factor	γ_s	1	-
Elastic modulus in Y direction	$W_{y,el}$	535974.66	mm^3
Plastic modulus in Y direction	$W_{y,pl}$	615689.94	mm^3
Capable elastic bending moment	$M_{y,el,cap}$	125.954	KNm
Capable plastic bending moment	$M_{y,pl,cap}$	144.687	KNm
Epoxy adhesive			
Thickness	t_{adh}	1	mm
Modulus of elasticity	E_{adh}	1750	MPa
Tensile strain energy	R	0.139	MPa mm/mm
Slip at the end of the elastic stage	δ_1	0.0163	mm
Slip at the end of the constant stage	δ_2	0.809	mm
Ultimate slip	δ_f	1.36	mm
Safety factor	γ_{adh}	1.25	-
CFRP composite strip			
Thickness	t_{cfrp}	1.4	mm
Length	L_{cfrp}	4000	mm
Width	b_{cfrp}	150	mm
Tensile strength	f_{cfrp}	2900	MPa
Modulus of elasticity	E_{cfrp}	170000	MPa
Safety factor	γ_{cfrp}	1.25	-
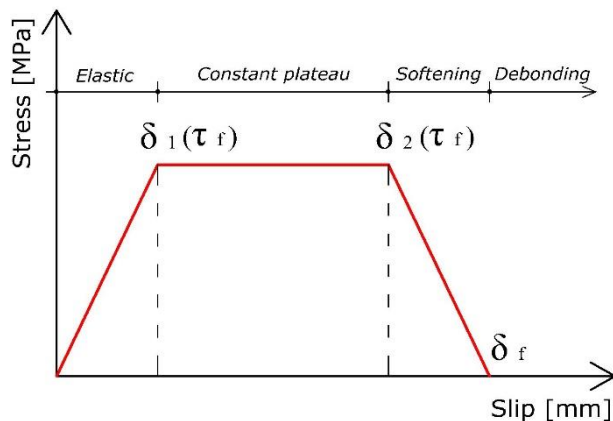
Figure 2. Bond-slip model for non-linear adhesive

2.1. Calculating the ultimate strain of the CFRP composite strip

$$\varepsilon_{cfrpl,d} = \min(\varepsilon_{cfrp,rup,d}; \varepsilon_{cfrp,l,d}) \tag{1}$$

where:

  - - $\varepsilon_{cfrpl,d}$ is the design ultimate strain of the CFRP composite strip;
  - - $\varepsilon_{cfrp,rup,d}$ is the design strain corresponding to the rupture of the CFRP composite strip;
  - - $\varepsilon_{cfrp,l,d}$ is the design strain corresponding to the intermediate debonding of the CFRP composite strip.

The design strain corresponding to the rupture of the CFRP composite strip is calculated with Equation 2.

$$\varepsilon_{cfrp,rup,d} = \frac{f_{CFRP}}{\gamma_{CFRP}E_{CFRP}} = 0.013647 \tag{2}$$

The design strain corresponding to the intermediate debonding of the CFRP composite strip is calculated with Equations 3 and 4.

$$\varepsilon_{cfrp,l,d} = \frac{1}{\gamma_{adh}}\sqrt{\frac{2G_f}{E_{CFRP}t_{CFRP}}} = 0.00807 \tag{3}$$

G_f is the interfacial fracture energy and is calculated with Equation 4.

$$G_f = 628t_{adh}^{0.5}R^2 = 12.1335 \text{ Nmm/mm}^2 \tag{4}$$

Equation 3 is valid only if the anchorage length of the CFRP strip (L_a) is greater than the effective one (L_e).

Because the critical section of the beam is at the mid-span, the anchorage length is calculated with Equation 5.

$$L_a = \frac{L_{CFRP}}{2} = 2000 \text{ mm} \tag{5}$$

The effective anchorage length (L_e) is calculated with Equation 6.

$$L_e = a_d + b_e + \frac{1}{\lambda_1}\ln\frac{1+C}{1-C} = 187.318 \text{ mm} \tag{6}$$

Factors λ, λ_1, λ_3, a_d, b_e and C are obtained with Equations 8, 9, 10, 11 and 12.

$$\lambda = \sqrt{\frac{\tau_{max}^2}{2G_f}(\frac{1}{E_{CFRP}t_{CFRP}} + \frac{b_{CFRP}}{E_S A_s})} = 0.00569 \text{ mm}^{-1} \tag{7}$$

where:

- $\tau_{max} = 0.9 f_{adh}$.

$$\lambda_1^2 = \frac{2G_f}{\tau_{max}\delta_1}\lambda^2 = 0.05985 \text{ mm}^{-1} \tag{8}$$

$$\lambda_3 = \sqrt{\lambda^2 \frac{2G_f}{\tau_{max}(\delta_f - \delta_2)}} = 0.01029 \text{ mm}^{-1} \tag{9}$$

$$a_d = \frac{1}{\lambda_1}\sqrt{((2\frac{\delta_2}{\delta_1} - 1) - 1)} = 148.910 \text{ mm} \tag{10}$$

$$b_e = \frac{1}{\lambda_3}\arcsin\left[\frac{\lambda_3\lambda}{0.97\delta_1\lambda_1^2}(\delta_f - \delta_2)\right] = 59.006 \text{ mm} \tag{11}$$

$$C = \frac{\lambda_3}{\lambda_1\delta_1}(\delta_f - \delta_2)\cot(\lambda_3 b_e) - \lambda_1 a_d = -0.5486 \text{ mm} \tag{12}$$

Since L_e is smaller than L_a, Equation 3 can be used and the design ultimate strain of the CFRP strip $\varepsilon_{cfrpl,d} = \varepsilon_{cfrp,l,d} = 0.00807$.

2.2. Determining the capable bending moment of the composite section

The capable bending moment of the composite sections can be obtained using the classical mechanical theories by imposing the assumption of total plasticization of the steel section. Still, for steel sections reinforced with CFRP strips, it has been observed that when the capable moment is reached, the steel section is not completely plasticized, the mid-part of the web being in elastic stage [1]. Figure 3 presents the variation of the stresses and strains on the composite cross-section.
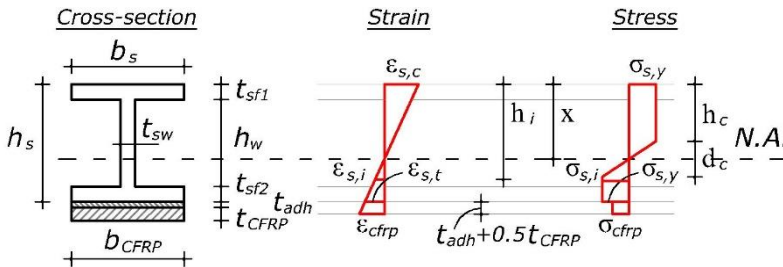
Figure 3. Variation of strains and stresses on the composite cross-section

where:

- - $\varepsilon_{s,c}$ is the strain at the limit of the compressed steel section;
- - $\varepsilon_{s,t}$ is the strain at the limit of the tensioned steel section;

- - ε_{cfrp} is the strain in the mid-section of the CFRP strip;

- - σ_{cfrp} is the average axial stress in the CFRP strip;

- - $\sigma_{s,y}$ is the yielding stress of the steel;

- - $\varepsilon_{s,i}$ is the strain in the steel at h_i height;

- - $\sigma_{s,i}$ is the stress in the steel at h_i height;

- - x is the depth of the neutral axis;
- - h_c is the height of the plasticized steel section;
- - d_e is the height of the elastic steel section;

The depth of the neutral axis is unknown and, for that reason, in the first stage, its value is imposed as x = 150mm. This value will be verified when the equilibrium conditions are check on the composite cross-section. Based on the design ultimate strain of the CFRP strip and on the depth of the neutral axis, the strains at the boundaries of the steel sections, $\varepsilon_{s,c}$ and $\varepsilon_{s,t}$, can be calculated, using Equations 13 and 14, respectively.

$$\varepsilon_{s,c} = \varepsilon_{cfrpl,d} \frac{-x}{h_s + t_{adh} + \dfrac{t_{cfrp}}{2} - x} = 0.0099 \text{ mm} \tag{13}$$

$$\varepsilon_{s,t} = \varepsilon_{cfrpl,d} \frac{h_s - x}{h_s + t_{adh} + \dfrac{t_{cfrp}}{2} - x} = \text{-}0.0079 \text{ mm} \tag{14}$$

The strain of the steel at h_i depth can be calculated with Equation 15.

$$\varepsilon_{s,i} = \varepsilon_{cfrpl,d} \frac{h_i - x}{h_s + t_{adh} + \dfrac{t_{cfrp}}{2} - x} \tag{15}$$

The height of the compressed zone, is obtained by assuming in Equation 15 that $\varepsilon_{s,i} = \varepsilon_{s,y}$.

$$h_c = \frac{\varepsilon_{s,y}(h_s + t_{adh} + t_{cfrp}/2 - x)}{\varepsilon_{cfrpl,d}} + x = 132.2982 \text{ mm} \tag{16}$$

The height of the elastic zone, is obtained with Equation 17.

$$d_e = 2(x - h_c) = 35.4036 \text{ mm} \tag{17}$$

The position of the neutral axis is checked by balancing Equation 18.

$$\int_0^h \sigma_{s,i} b_i dh_i + \sigma_{cfrp} b_{cfrp} t_{cfrp} = 0 \qquad (18)$$

which, in an explicit form, can be written as:

$$\frac{f_y}{\gamma_s} t_{sf1} b_{s,\sup} + \frac{f_y}{\gamma_s} (h_c - t_{sf1}) t_{sw} + \frac{f_y}{2\gamma_s} (x - h_c) t_{sw} - \frac{f_y}{2\gamma_s} (x - h_c) t_{sw} -$$
$$- \frac{f_y}{\gamma_s} (h_s - t_{sf2} - d_e - h_c) t_{sw} - \frac{f_y}{\gamma_s} t_{sf2} b_{s,\inf} - \varepsilon_{cfrp} E_{cfrp} b_{cfrp} t_{cfrp} = -217889.4339 \neq 0 \qquad (18^*)$$

Since the equilibrium of Equation 18 has not been achieved, the correct value of the depth is obtained using an iterative process, by applying successive values for x.

It has been found that, for x = 196.36, Equation 18 becomes:

$$\frac{f_y}{\gamma_s} t_{sf1} b_{s,\sup} + \frac{f_y}{\gamma_s} (h_c - t_{sf1}) t_{sw} + \frac{f_y}{2\gamma_s} (x - h_c) t_{sw} - \frac{f_y}{2\gamma_s} (x - h_c) t_{sw} -$$
$$- \frac{f_y}{\gamma_s} (h_s - t_{sf2} - d_e - h_c) t_{sw} - \frac{f_y}{\gamma_s} t_{sf2} b_{s,\inf} - \varepsilon_{cfrp} E_{cfrp} b_{cfrp} t_{cfrp} = 2.6131 \cong 0 \qquad (18^*)$$

where:
- - $\varepsilon_{s,c} = 0.02105$;
- - $\varepsilon_{s,t} = -0.00789$;
- - $h_c = 185.4014$ mm;
- - $d_e = 21.9170$ mm

The capable moment of the composite section is evaluated with Equation 19.

$$M_{ib,d} = \int_0^h \sigma_{s,i} b_{s,i} (\frac{h_s}{2} - h_i) dh_i + E_{cfrp} \varepsilon_{cfrp} b_{cfrp} t_{cfrp} (\frac{h_s}{2} + t_{adh} + \frac{t_{cfrp}}{2}) \qquad (19)$$

Which, in explicit form, can be written as:

$$M_{ib,d} = t_{sf1}b_{s,\text{sup}}\frac{f_y}{\gamma_s}(\frac{h_s}{2}-\frac{t_{sf1}}{2})+(h_c-t_{sf1})t_{sw}\frac{f_y}{\gamma_s}(\frac{h_s}{2}-(t_{sf1}+\frac{h_c-t_{sf1}}{2}))+$$

$$+\frac{d_e}{2}t_{sw}\frac{f_y}{2\gamma_s}(\frac{h_s}{2}-(t_{sf1}+(h_c-t_{sf1})+\frac{2}{3}\frac{d_e}{2}))+$$

$$+\frac{d_e}{2}t_{sw}(-\frac{f_y}{2\gamma_s})(\frac{h_s}{2}-(x+\frac{d_e}{2}\frac{1}{3}))+ \tag{19*}$$

$$+(h_s-h_c-d_e-t_{sf2})t_{sw}(-\frac{f_y}{2\gamma_s})(\frac{h_s}{2}-(x+\frac{d_e}{2}+(\frac{h_s-h_c-d_e-t_{sf2}}{2})))+$$

$$+t_{sf2}b_{s,\text{inf}}(-\frac{f_y}{2\gamma_s})(\frac{h_s}{2}-(h_s-\frac{t_{sf2}}{2}))+$$

$$+E_{cfrp}(-\varepsilon_{cfrp})b_{cfrp}t_{cfrp}(\frac{h_s}{2}-(h_s+t_{adh}+\frac{t_{cfrp}}{2}))=175.256\,\text{KNm}$$

3. CONCLUSIONS

The application of CFRP composite strips on the bottom flange of I-shaped steel beams subjected to bending, is an efficient strengthening solution. For the case st that has been presented in this paper, the 1.4 mm thick and 150 mm width CFRP composite strip that has been adhesively bonded to the bottom side of the steel beam, produced an increase of the capable bending moment of 21.13%.

References

1. Zhao, X-L. 2014. *FRP-Strengthening Metallic Structures*. CRC Press Taylor&Francis Group, Boca Raton.
2. Cadei, J.M.C., Stratford, T.J., Hollaway, L.C., and Duckett, W.H. 2004. C595 – *Strengthening metallic structures using externally bonded fibre-reinforced composites*. CIRIA. London.
3. Canning, L., Farmer, N., Luke, S., and Smith, I. 2006. *Recent developments in strengthening technology and the strengthening/reconstruction decision*. Railway Bridges Today and Tomorrow Conference, Bristiol.
4. Lane, I.R., and Ward, J.A. 2000. *Restoring Britain's bridge heritage. Institution of Civil Engineers* (Sout Wales Association).
5. Deng, J., and Lee, M.M.K. 2007. *Behavior under static loading of metallic beams reinforced with a bonded CFRP plate*. Composite Structures, 78(1).
6. Al-Saidy, A.H., Klaiber, F.W., and Wipf, T.J. 2004. *Repair of steel composite beams with carbon fiber-reinforced polymer plates*. Journal of Composite for Construction, 8(2).
7. Sayed-Ahmed, E.Y. 2006. *Numerical investigation into strengthening steel I-section beams using CFRP strips*. ASCE Structures Congress.
8. Yu, T., Fernando, D., Teng, J.G., and Zhao, X.L. 2012. *Experimental study on CFRP-to-steel bonded interfaces*. Composite Part B: Engineering, 43(5).
9. Colombi, P., and Poggi, C. 2005. *An experimental, analytical and numerical study of the static behavior of steel beams reinforced by pultruded CFRP strips*. Composites: Part B (37).
10. Fernando, D. 2010. *Bond behaviour and debonding failures in CFRP-strengthened steel members*. PhD thesis, Hong Kong Polytechnic University.

Modelling the Geometrical Characteristics of Fabric Reinforced Composites

Andrei Axinte

Faculty of Civil and Industrial Engineering, "Gheorghe Asachi" Technical University of Iaşi, RO

Summary

Some micro-mechanical models are in use today to accurately describe the shape of textile reinforced composite materials. Physically, the textile reinforced composites modelling is more demanding than those of traditional composite (unidirectional) materials, given the fact that their geometric architecture of wire connections is quite sophisticated. Refined and accurate models are required to analyse these complicated structures. The numerical modelling techniques can be broken down into three main categories: classical laminate theory (CLT), stiffness averaging method (SAM) and finite element method (FEM). Of all the methods, finite element method (FEM) is the most promising because it allows analysis of nonlinear systems with general boundary conditions and can be adapted to complex geometries. Each model is based on micro-mechanical analysis, because all mechanical properties are affected by microscopic variables (geometric lengths, areas and volumes) and their properties. This paper is an attempt to find an efficient method of modelling the geometry, by analytical/numerical means, in order to save time and costs associated with the analysis of these composites. The method used here is a compromise between the continuous and pure discrete approaches and is associated with a mesoscopic analysis of the repetitive unit cell (UC).

KEYWORDS: composite material, woven composite, repetitive unit cell.

1. INTRODUCTION

In order to minimize the cost of analytical/numerical modelling of a woven composite material, only a small representative cell, the so-called unit cell (*UC*), that repeats itself along the entire material, is analysed. One of the first geometric patterns, extremely idealized, of the unit cell of a plain weave fabric was presented by Peirce [1]. Peirce's model (Fig. 1a) is based on a circular cross-section and incompressible wire. Kemp [2] modified Peirce's model, using elliptical wire cross sections (Fig. 1b), thereby achieving a more realistic representation of the geometry of the fabric.

a. Pierce model (1937)   b. Kemp model (1958)   c. Shanahan and Hearle
                                                      model (1978)

d. Ning and Chou model   e. Searles, Odegard and   f. Hofstee and van Keulen
        (1998)   Kumosa model (2001)   model (2001)
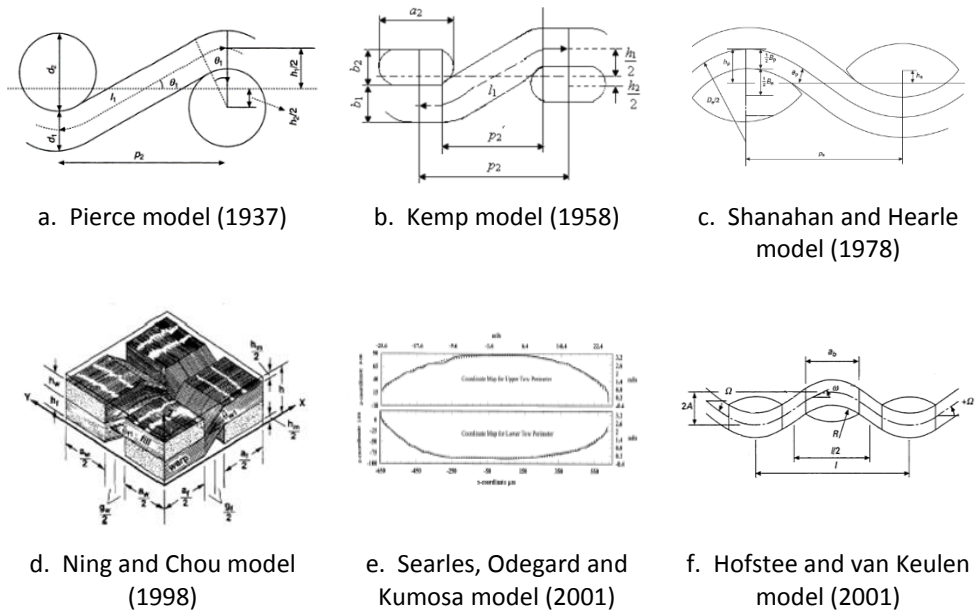
Fig. 1 The unit cell modelling evolution

Shanahan and Hearle [3] presented a geometric pattern using wire cross-section of lenticular shape (Fig. 1c) and introduced energy calculation methods. Ning and Chou [4] have developed a model with a more idealized unit cell (Fig. 1d) to estimate the effective plan thermal conductivity of the composite. Another representation of the wires was proposed by Searles [5], which introduced new procedures to characterize the upper and lower half of the cross section of the wires, relative to the centre of gravity (Fig. 1e). Hofstee and Van Keulen [6] proposed a geometric model of unit cells based on woven wire variable section (Fig. 1f).

An important feature of the available models is that they are all developed with certain textile architecture in mind. There is a need for a generalized model of fabric, in which one of the parameters should be the fabric pattern itself [7]. Also, the correlations between geometric parameters have not been fully investigated in published studies, in order to determine accurately how the change in a parameter affects the other design parameters [8].

2. MODELLING THE SATIN REINFORCED COMPOSITES

The micromechanical study was performed on an epoxy lamina, reinforced with satin fabric. The method adopted is a hybrid method, which was proposed by Barbero [9] and is a good compromise between the accuracy of finite element methods and

the simplicity of analytical methods. To find the elastic constants of the material, in-depth characterization of lamina geometry was necessary, pursuing the need to make an accurate estimation of both these constants and the factors influencing them. Due to the complexity of geometry, calculus become complicated and require the use of a computer backed-up by an appropriate programming language. Thus, all functions that describe the fabric geometry and equations for determining various parameters of the composite may be implemented in a MATLAB® like environment.

The *UC* is used for geometric and mechanical analysis and it is the smallest part of the fabric (2D) that contains all the features necessary to define the composite material. Therefore, the entire element can be rebuild by replicating the *UC* along the fill and warp pathways. Fig. 2 shows the *UC* of satin fabric 5/2/1. Fibres exposure on material faces is unbalanced, thus being dominated by fill or warp on opposite sides.
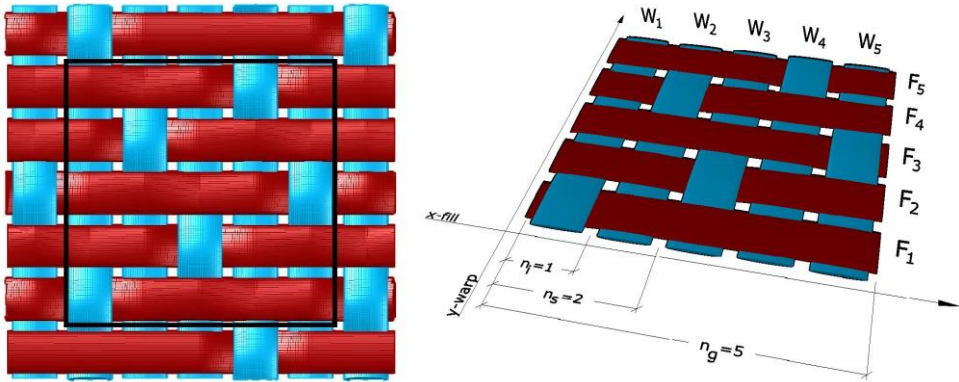
Fig. 2 The *UC* of satin fabric 5/2/1 and geometrical parameters n_g, n_s, n_i

To identify the *UC*, three geometric parameters are introduced to facilitate the modelling and implementation of specific geometry in software. These parameters are n_g, n_s, n_i, defined as follows (Fig. 2):
- n_g is the number of subcells along one direction of the UC (harness). In case of 5/2/1 satin, n_g=5;
- n_s is the number of subcells between consecutive interlacing regions (shift). For 5/2/1 satin, n_s=2;
- n_i is the number of subcells in the interlacing region (interlacing). For satin 5/2/1, $n_i = 1$.

These parameters are proposed and used as a new coding system for 2D fabrics (biaxial orthogonal). Under this scheme, any style of fabric is described by combining the three parameters $n_g/n_s/n_i$, with no need to generate special geometric descriptions for individual cases.

The satin fabric is made by fill (x axis), and warp (y axis). They are described by the following geometric parameters, as seen on Fig. 3:

- tow width for fill a_f and warp a_w;
- tow height for fill h_f and warp h_w;
- gap between two consecutive tows for fill g_f or warp g_w;
- neat-matrix thickness h_m.
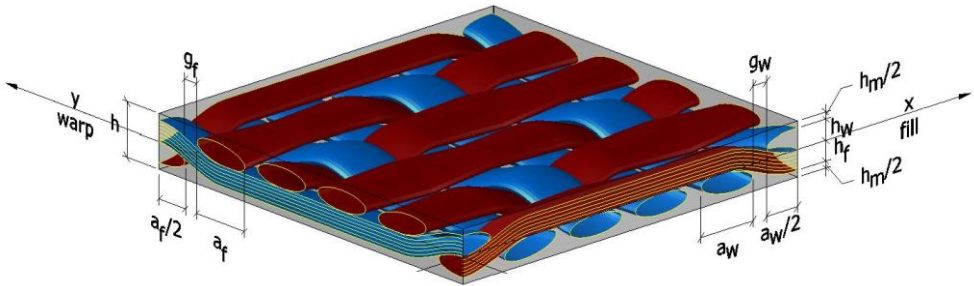
Fig. 3 Geometrical parameters of the *UC*

In the first step, the *UC* is split along the (x, y) plane in 2D smaller units subcells, in order to better consider the influence of curling wires. As the number of subcells is higher, the results are more accurate, but computing power needed increases with a quadratic rate (Fig. 4).
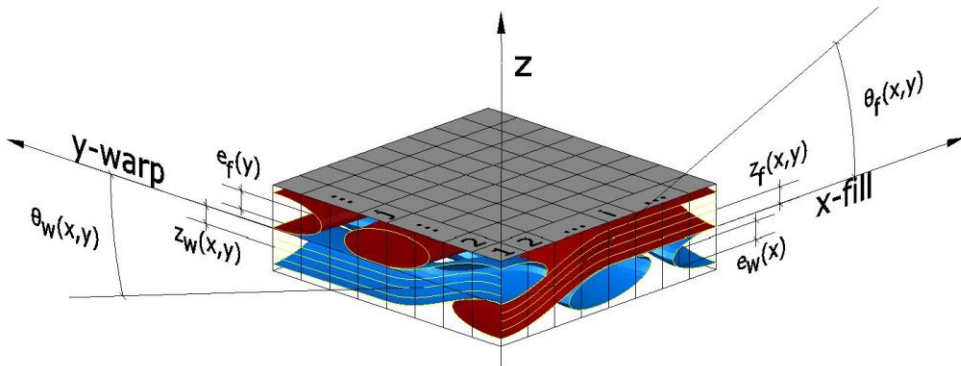
Fig. 4 Intermediate geometrical parameters of the woven textile

For each subcell, thus for each location (x, y), the geometry of the two tows (fill and warp) may be depicted by the complex functions. It starts from undulation along the wires, taking into account the space between them g_f and g_w, which is expressed in terms of z coordinate of midpoint of the tow thickness. For example, in the case of the satin type fabric, the undulation of the fill $z_f(x, y, j)$ is given by Eq. 1 and for the

warp by Eq. 2, where $i \ and \ j \in [1, n_g]$ are the interlacing positions for the warp and fill:

$z_f(x, y, j) =$

$$
\begin{cases}
\textbf{if} \ (j-1)w_f + \frac{g_f}{2} \leq y \ \leq j w_f - \frac{g_f}{2} \\
\quad \textbf{for} \ k \in 1 \dots \textbf{trunc} \left[\frac{n_s(j-1)+1}{n_g} \right] + 1 \\
\qquad \begin{cases}
(-1)^{(kn_g+1)} \frac{h_f}{2} \sin\left[\frac{\pi x}{w_w} + n_s(j-1)\pi \right], \ \textbf{if} \ \left[n_s(j-1) - \frac{1}{2} - kn_g \right] w_w \leq x \leq \left[n_s(j-1) + \frac{3}{2} - kn_g \right] w_w \\
\frac{h_f}{2}, \qquad \textbf{if} \ (k-1) \geq 1 \ \textbf{and} \ \left[n_s(j-1) + \frac{3}{2} - kn_g \right] w_w < x < \left[n_s(j-1) - \frac{1}{2} - (k-1)n_g \right] w_w
\end{cases} \\
\frac{-h_f}{2} \sin\left[\frac{\pi x}{w_w} + n_s(j-1)\pi \right], \qquad \textbf{if} \ \left[n_s(j-1) - \frac{1}{2} \right] w_w \leq x \leq \left[n_s(j-1) + \frac{3}{2} \right] w_w \\
(-1)^{(n_g+1)} \frac{h_f}{2} \sin\left[\frac{\pi x}{w_w} + n_s(j-1)\pi \right], \qquad \textbf{if} \ \left[n_s(j-1) - \frac{1}{2} + n_g \right] w_w \leq x \leq \left[n_s(j-1) + \frac{3}{2} + n_g \right] w_w \\
\frac{h_f}{2}, \qquad \textbf{if} \ \left[n_s(j-1) + \frac{3}{2} - n_g \right] w_w < x < \left[n_s(j-1) - \frac{1}{2} \right] w_w \ \textbf{or} \\
\qquad \left[n_s(j-1) + \frac{3}{2} \right] w_w < x < \left[n_s(j-1) - \frac{1}{2} + n_g \right] w_w \\
0, \qquad \textbf{if} \ \left[(j-1)w_f \leq y < (j-1)w_f + \frac{g_f}{2} \ \textbf{or} \ j w_f - \frac{g_f}{2} < y \leq j w_f \right] \ \textbf{and} \ g_f \neq 0
\end{cases}
\tag{1}
$$

$z_w(x, y, i) =$

$$
\begin{cases}
\textbf{if} \ (i-1)w_w \leq x \ \leq i w_w \\
\quad \textbf{for} \ k \in 1 \dots \textbf{fix} \left[\frac{(n_g - n_s)(i-1)+1}{n_g} \right] + 1 \\
\qquad \begin{cases}
(-1)^{(kn_g+1)} \frac{h_w}{2} \sin\left[\frac{\pi y}{w_f} + (n_g - n_s)(i-1)\pi \right], \qquad \textbf{if} \ \left[(n_g - n_s)(i-1) - \frac{1}{2} - kn_g \right] w_f \leq y \ \textbf{and} \\
\qquad \qquad y \leq \left[(n_g - n_s)(i-1) + \frac{3}{2} - kn_g \right] w_f \\
\frac{-h_w}{2}, \qquad \textbf{if} \ (k-1) \geq 1 \ \textbf{and} \ \left[(n_g - n_s)(i-1) + \frac{3}{2} - kn_g \right] w_f < y \ \textbf{and} \\
\qquad \qquad y < \left[(n_g - n_s)(i-1) - \frac{1}{2} - (k-1)n_g \right] w_f
\end{cases} \\
\frac{h_w}{2} \sin\left[\frac{\pi y}{w_f} + (n_g - n_s)(i-1)\pi \right], \qquad \textbf{if} \ \left[(n_g - n_s)(i-1) - \frac{1}{2} \right] w_f \leq y \ \textbf{and} \\
\qquad \qquad y \leq \left[(n_g - n_s)(i-1) + \frac{3}{2} \right] w_f \\
-(-1)^{(n_g+1)} \frac{h_w}{2} \sin\left[\frac{\pi y}{w_f} + (n_g - n_s)(i-1)\pi \right], \qquad \textbf{if} \ \left[(n_g - n_s)(i-1) - \frac{1}{2} + n_g \right] w_f \leq y \ \textbf{and} \\
\qquad \qquad y \leq \left[(n_g - n_s)(i-1) + \frac{3}{2} + n_g \right] w_f \\
\frac{-h_w}{2}, \qquad \textbf{if} \ \left[(n_g - n_s)(i-1) + \frac{3}{2} - n_g \right] w_f < y < \left[(n_g - n_s)(i-1) - \frac{1}{2} \right] w_f \ \textbf{or} \\
\qquad \left[(n_g - n_s)(i-1) + \frac{3}{2} \right] w_f < y < \left[(n_g - n_s)(i-1) - \frac{1}{2} + n_g \right] w_f \\
0, \qquad \textbf{if} \ \left[(i-1)w_w \leq x < (i-1)w_w + \frac{g_w}{2} \ \textbf{or} \ i w_w - \frac{g_w}{2} < x \leq i w_w \right] \ \textbf{and} \ g_w \neq 0
\end{cases}
\tag{2}
$$

where:
- $w_f = a_f + g_f$ - the distance between two consecutive fill tows;
- $w_w = a_w + g_w$ - the distance between two consecutive warp tows.

The thickness of the cross section for the fill and warp tows is specified in the Eq. 3 and Eq. 4).

$$e_f(y,j) = \begin{cases} \left| h_f \sin \frac{\pi \left(-(j-1)w_f + y - \frac{g_f}{2} \right)}{a_f} \right|, & \textbf{\textit{if}} \ (j-1)w_f + \frac{g_f}{2} \le y \le jw_f - \frac{g_f}{2} \\ 0, & \textbf{\textit{if}} \ (j-1)w_f \le y < (j-1)w_f + \frac{g_f}{2} \ \textbf{\textit{or}} \ jw_f - \frac{g_f}{2} < y \le jw_f \end{cases} \tag{3}$$

$$e_w(x,i) = \begin{cases} \left| h_w \sin \frac{\pi \left(-(i-1)w_w + x - \frac{g_w}{2} \right)}{a_w} \right|, & \textbf{\textit{if}} \ (i-1)w_w + \frac{g_w}{2} \le x \le iw_w - \frac{g_w}{2} \\ 0, & \textbf{\textit{if}} \ (i-1)w_w \le x < (i-1)w_w + \frac{g_w}{2} \ \textbf{\textit{or}} \ iw_w - \frac{g_w}{2} < x \le iw_w \end{cases} \tag{4}$$

Given the above parameters, undulation and cross-sectional thickness of the wires for the entire *UC* can be computed (Eq. 5, 6).

$$\textbf{\textit{if}} \ (j-1)w_f \le y \le jw_f \rightarrow \begin{cases} z_f(x,y) = z_f(x,y,j) \\ e_f(y) = e_f(y,j) \end{cases} \tag{5}$$

$$\textbf{\textit{if}} \ (i-1)w_w \le x \le iw_w \rightarrow \begin{cases} z_w(x,y) = z_w(x,y,i) \\ e_w(x) = e_w(x,i) \end{cases} \tag{6}$$

The upper and lower surface boundaries of the fill and warp yarns can be evaluated using Eq. 7, 8.

$$\begin{cases} z_f^{top}(x,y) = z_f(x,y) + \frac{1}{2}e_f(y) \\ z_f^{bot}(x,y) = z_f(x,y) - \frac{1}{2}e_f(y) \end{cases} \tag{7}$$

$$\begin{cases} z_w^{top}(x,y) = z_w(x,y) + \frac{1}{2}e_w(x) \\ z_w^{bot}(x,y) = z_w(x,y) - \frac{1}{2}e_w(x) \end{cases} \tag{8}$$

Undulation angle of the tows θ (Fig. 5), is then calculated with Eq. 9.

$$\theta_f(x,y) = \arctan\left(\frac{\partial}{dx} z_f(x,y) \right)$$

$$\theta_w(x,y) = \arctan\left(\frac{\partial}{dy} z_w(x,y) \right) \tag{9}$$
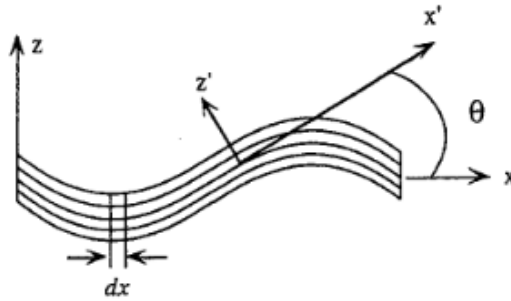
Fig. 5 Undulation angle θ of the fill and warp tows

Cross sectional area of the fill and warp tows of *UC* can be estimated by Eq. 10.

$$A_f = \int_0^{w_f} e_f(y)dy$$
$$A_w = \int_0^{w_w} e_w(x)dx$$

(10)

Wire length is determined in *UC* using the description of undulation (Eq. 11):

$$L_f = \int_0^{n_g \cdot w_w} \sqrt{1 + \left(\frac{\partial}{\partial x} z_f(x,y)\right)^2} \, dx$$

(11)

$$L_w = \int_0^{n_g \cdot w_f} \sqrt{1 + \left(\frac{\partial}{\partial y} z_w(x,y)\right)^2} \, dy$$

Based on the above relationships, the volume of the fill tows is $v_f = n_g A_f L_f$ and that of the warp tows is $v_w = n_g A_w L_w$.

The mechanical characteristics of the composite are determined by the properties of the matrix and those of the fill and the warp tows. The mechanical properties of the yarns (i.e. E_1, F_{1t}, etc.) are calculated based on the apparent resistance of the constituent material (fibre and matrix), taking into account the volume fractions of the fibres in the yarns.

3. CONCLUSIONS

Mechanical performance of the textile composites can be determined either experimentally or through simulations (modelling); the latter is the less expensive approach, commonly used when calculating the mechanical properties of fabrics. In order to minimize the cost of analytical/numerical modelling of a woven composite material, only a small representative cell, the so-called unit cell (*UC*), that repeats itself along the entire material, is analysed.

The micromechanical study was performed on an epoxy lamina, reinforced with satin fabric. The method adopted is a hybrid method and is a good compromise between the accuracy of finite element methods and the simplicity of analytical methods. To find the elastic constants of the material, in-depth characterization of lamina geometry was necessary, pursuing the need to make an accurate estimation of both these constants and the factors influencing them. Due to the complexity of geometry, calculus become complicated and require the use of a computer backed-up by an appropriate programming language. Thus, all functions that describe the fabric geometry and equations for determining various parameters of the composite may be implemented in a MATLAB® like environment.

References

1. Peirce, F. T., (1937), *The geometry of cloth structure*. Journal of the Textile Institute Transactions, 28(3): T45-T96
2. Kemp, A., (1958), *An extension of Peirce's cloth geometry to the treatment of non-circular threads*. Journal of the Textile Institute Transactions, 49(1): T44-T48
3. Shanahan, W. J., Hearle, J. W. S., (1978), *An energy method for calculations in fabric mechanics part ii: examples of application of the method to woven fabrics*. Journal of the Textile Institute, 69(4): pp.92-100
4. Ning, Q. G., Chou, T. W., (1998), *A general analytical model for predicting the transverse effective thermal conductivities of woven fabric composites.* Composites Part A: Applied Science and Manufacturing (Incorporating Composites and Composites Manufacturing), 29(3): pp.315-322
5. Searles, K., Odegard, G., Kumosa, M., (2001), *Micro and mesomechanics of 8-harness satin woven fabric composites: I-evaluation of elastic behavior*. Composites Part A: Applied Science and Manufacturing, 32(11), pp. 1627- 1655
6. Hofstee, J., van Keulen, F., (2001), *3-D geometric modeling of a draped woven fabric*. Composite Structures, 54, pp.179 195
7. Lomov, S., Verpoest, I., Peeters, T., Roose, D., Zako, M., (2003). *Nesting in textile laminates: geometrical modeling of the laminate*. Composites Science and Technology, 63:993–1007
8. Lee, S., Byun, J., Hyung, S., (2003), *Effect of fiber geometry on the elastic constants of the plain woven fabric reinforced aluminum matrix composites*. Materials Science and Engineering: A, 347:346–358
9. Barbero E, (2011), *Introduction to composite materials design - SE*, CRC Press, New York

Stress Analysis of Masonry Walls in Case of Limited Excavation for Foundation Underpinning

Maria Solonaru[1] Irina Lungu[2] and Mihai Budescu[1]

[1]*Department of Structural Mechanics, "Gheorghe Asachi" Technical University of Iaşi, Iaşi, 700050, Romania*
[2]*Department of Transportation Infrastructure and Foundations, "Gheorghe Asachi" Technical University of Iaşi, Iaşi, 700050, Romania*

Summary

The assessment of safety and structural integrity of existing buildings is often an intricate task regarding the optimum structural intervention measures on superstructure, infrastructure or both. When the cause of structural deterioration is related to the geotechnical condition unfit for the new load regime, a widely used method for the rehabilitation of infrastructure is the underpinning of foundations.

This paper is focused on the analysis of the stresses developing into a masonry wall when excavating in segmented areas with limited lengths under and on both sides of the continuous foundation. In this respect, a linear elastic analysis for a three-dimensional model was carried out by using finite element software ANSYS.

The case study refers to a layered soil profile, consisting of 1.00 m of clayey silt, 2.70 m of clay, 1.50 m of clays with sand inclusions, 2.10 m of silty clay and 2.70 m of clay, with the relevant geotechnical parameters considered constant during service. The structure is considered a brick masonry wall, 3 m high, 10 m long and 0.375 m thickness, supported by a 0.60 m width stone masonry continuous foundation, extended to 0.60 m depth (insufficient at present to satisfy the frost depth restriction). During service, the material aging and climate influence within the wall is regarded by a slow decrease of the elastic modulus (E), from 4000 MPa to only 1200 MPa.

The excavation for the underpinning is assumed to start from the middle of the wall, with variable lengths, from 0.60 m increasing with a rate of 0.10 m, up to 1.00 m. The depth of the excavation is considered constant, as 0.60 m under the foundation, to exceed the frost depth by a final value of the foundation depth of 1.20 m.

The model of the wall, foundation and soil was developed with ANSYS interface for all excavation ranges, considering a frictionless contact between foundation and soil and the program run for all modulus variations and excavation geometries. The results are given in diagrams correlating the E modulus versus in-plane and vertical stress for all the excavation geometries.

KEYWORDS: ANSYS software, finite element modelling, excavation, underpinning, stress analysis.

1. INTRODUCTION

The underpinning is a traditional method used to strengthen and develop higher bearing capacity of the soil beneath the extended foundations.

The structural rehabilitation can be accomplished with different technical solutions depending on many factors, so the right method should be thoroughly appraised.

In case of shallow foundations, the traditional underpinning consists in segmented excavations of the soil beneath the foundation and replace it with concrete with or without a lateral enlargement of the foundation, thus obtaining an increase of the bearing capacity.

Excavation of the soil underneath the foundation may develop some considerable risks concerning the safety of the structural elements within the superstructure and/or the infrastructure of the building, particularly when dealing with historical buildings [2].

In other cases, the underpinning can be supplemented with the addition of concrete beams or using micro-piles, the loads being transferred to the soil through the mixed system: existing footings and new added elements.

2. THE FINITE ELEMENT APPROACH

A 3D static structural analysis in Workbench platform of the ANSYS software has been performed in order to calculate stresses in the investigated masonry wall when excavating a section underneath its continuous foundation with the purpose of underpinning.

More than 685000 nodes and 108000 elements resulted with the discretization of the model geometries.

As a frictionless (non-linear) contact between the continuous foundation and the soil was used, over 190 spring elements (COMBIN14, which is an uniaxial tension-compression element [6]) were automatically added to stabilize the model and to achieve convergence and a reasonable numerical solution.

The soil, foundation and the wall have been meshed with SOLID186, a higher order 3-D 20-node solid element that exhibits quadratic displacement behavior [6] with isotropic material properties.

CONTA174 and TARGE170 have been used to represent the contact with sliding between 3-D target surfaces of the foundation and the deformable surfaces of the soil layer [6].

3. PARAMETRIC STUDY

In this paper the integrated wall-foundation-soil system has been analyzed with the finite element software ANSYS, based on direct method of soil-structure interaction (SSI) assuming linear elastic behavior of all materials [5], [1], and [3]. The 3D model was used to analyze the influence of in-plane and vertical tension and compression stresses (Figure 3, nodes A and B) under a vertical load applied on the wall for a variety of elastic modulus of the brick masonry wall for a no excavation hypothesis and for a variation of the excavation length between 0.6 and 1 m with a rate of 0.1 m.

3.1. Input data for the model geometry and construction materials

The input model geometry consists of a brick masonry wall 10 m long and 3 m high and a stone masonry continuous foundation with the same length and 0.6 m depth (Figure 1, 2) with the specific isotropic material properties as presented within Table 2.

The foundation is considered located on a layered half-space with the geometries and soil isotropic properties assumed in Figure 1 and Table 1.
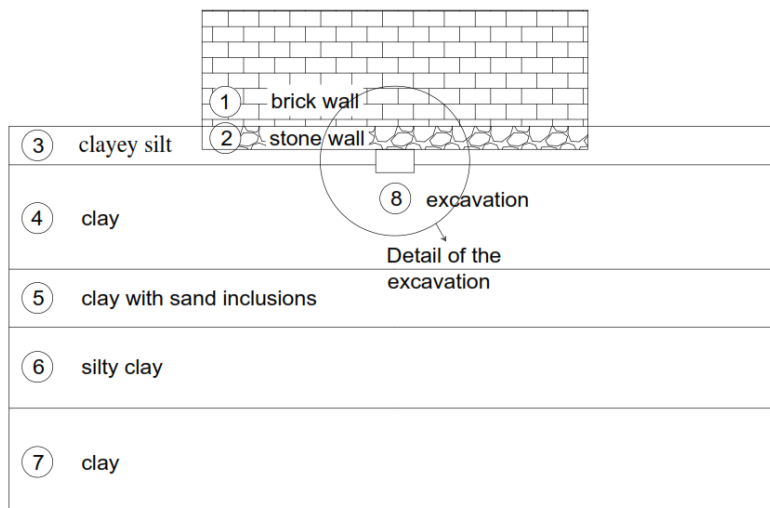
Figure 1. The model geometry – lateral view
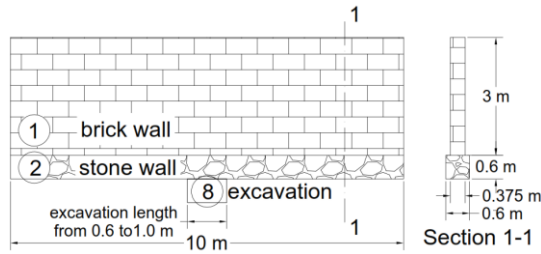
Figure 2. Detail of the excavation, with the wall and corresponding foundation

The stresses developed into the wall have been analyzed for different excavation lengths as presented in Table 3. The initial model considers no excavation, as an assessment of the existing in situ situation. Then, a variation for the length of the excavation has been analyzed and tension and compression stresses for the brick masonry wall have been observed whilst the elastic modulus of the masonry wall, due to the material aging, decreased from 4000 to 1200 MPa with a 400 MPa rate.

Table 1. Characteristics of the soil layers

Soil type	Thickness of the layer [m]	Young's Modulus [MPa]	Poisson's Ratio	Density [kg/m^3]
clayey silt	1.00	10	0.35	1900
clay	2.70	16.362	0.42	2170
clay with sand inclusions	1.50	16.667	0.42	2080
silty clay	2.10	13.076	0.35	1980
clay	2.70	18.000	0.42	2070

Table 2. Characteristics of the structural elements

Element	B x L x H [m]	Young's Modulus [MPa]	Poisson's Ratio	Density [kg/m^3]
Stone masonry foundation	0.6x10x0.6	6000	0.2	2200
Brick masonry wall	0.375x10x3	1200÷4000	0.2	1800

Table 3. Dimensions for the excavations

Depth [m] (constant)	Length [m] (variable)	Width [m] (constant)
0.6	0.0	2.6
0.6	0.6	2.6
0.6	0.7	2.6
0.6	0.8	2.6
0.6	0.9	2.6
0.6	1.0	2.6

3.2. Analysis set-up

The bottom surface of the 3D model geometry is restrained against displacement in all directions and the vertical sides are free to move in-plane, but confined to move out-of-plane (Figure 3). Due to the symmetry of the model, symmetrical boundary conditions have been applied in order to reduce the computing time. The symmetry condition prevent any nodes from moving through the symmetry plane during the analysis.

The stone masonry foundation, as well as the brick masonry wall have been modelled based on the assumptions of the macro-modelling strategies which consider the masonry as a homogeneous continuum able to replicate the masonry behavior. This assumption is applicable when analyzing bigger parts of a structure or an entire building, the amount of computational time being reduced [4].
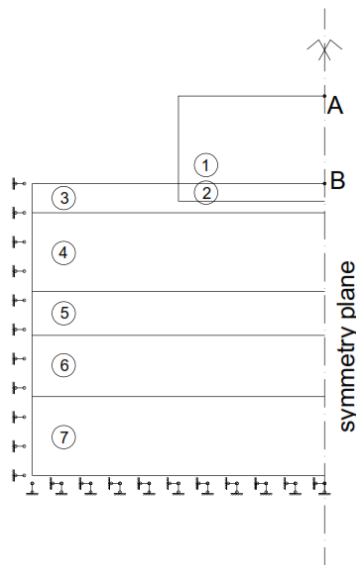
Figure 3. Applied symmetry on the wall - foundation system with restrains against displacements

A frictionless contact between the foundation and the soil has been considered in order to allow free sliding of the bodies, gaps being allowed to develop depending on the intensity of the load.

The upper part of the model geometry has been meshed with 0.1 m sizing elements and the bottom part with 1 m sizing elements (Figure 4).

A load of 2000 KN has been applied on the upper surface of the brick masonry wall for the symmetrical model.
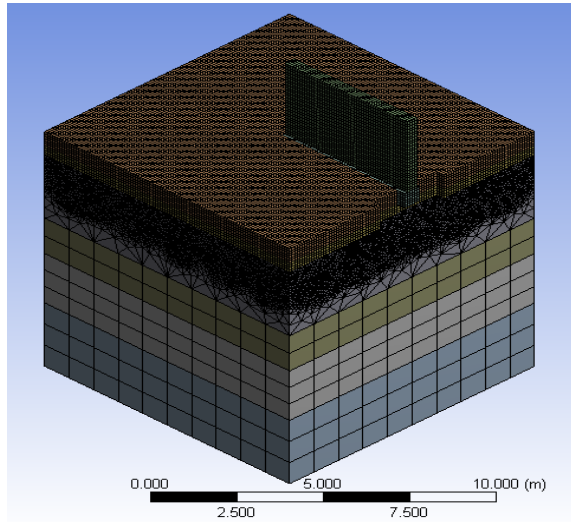
Figure 4. 3D mesh pattern for the symmetrical geometry of the wall-foundation-soil system
- the excavation with 1 m length

4. RESULTS AND DISCUSSION

The output was focused on the in-plane and vertical normal stresses resulted in
nodes A and B represented in Figure 3, as mid points at the top and base surfaces
of the wall.
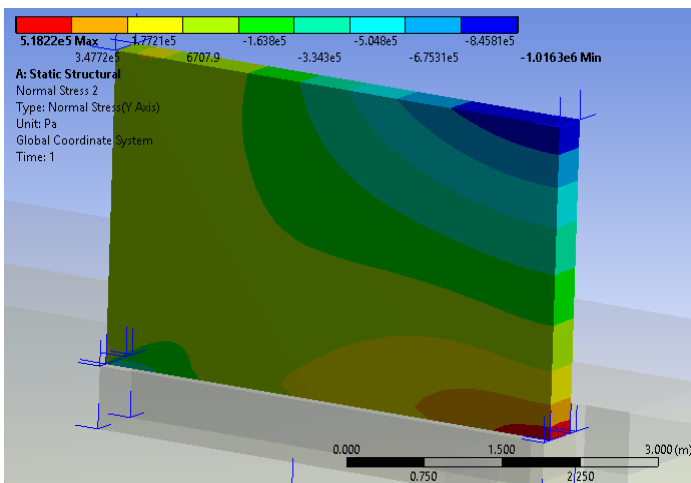
Figure 5. Typical in-plane stresses within the symmetrical model for the brick masonry wall
– the excavation with 1 m length

Results of the in-plane tension and compressive stresses for nodes A and B are reported with the graphic representation within Figure 7, for all excavation lengths corresponding to the entire range of the elastic modulus variations of the brick masonry wall.

A display of the resulted contours for in-plane normal stresses for one of the geometry model is given in Figure 5 (excavation length of 1 m).
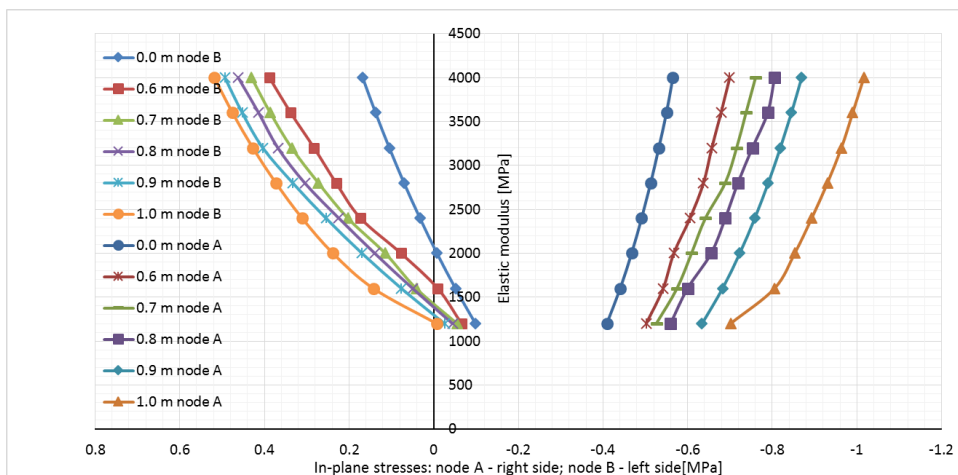
Figure 6. The evolution of the in-plane stresses correlated with the variation of the elastic modulus of the masonry wall for all the excavation lengths
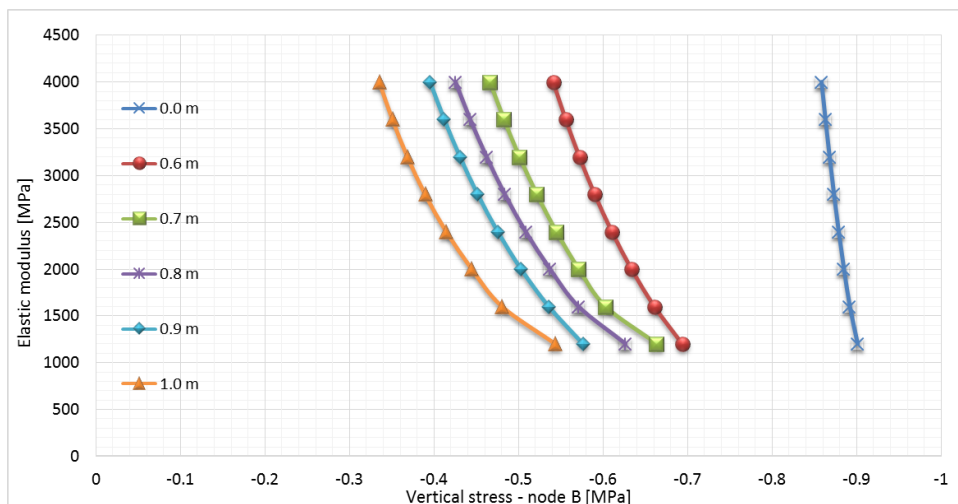
Figure 7. The evolution of the vertical stresses correlated with the variation of the elastic modulus of the masonry wall for all the excavation lengths

As seen in Figure 6, the upper part of the wall (node A) is subjected only to compression, as for the lower part of the wall (node B), it withstands compression stresses for the smallest values of the elastic modulus, then tension stresses develop as the values for the elastic modulus and the excavation lengths increase gradually.

The vertical stresses (Figure 7) in the wall (node B) amplify their values with the increase of both the excavation length and the elastic modulus of the brick masonry wall.

5. CONCLUSIONS

The stress related behavior of an existing brick masonry wall, as part of a historical building has been analyzed for the case of limited excavation under a stone masonry foundation anticipating its underpinning and simultaneously for the degradation related to the elastic properties of the brick masonry wall. For higher excavation lengths, the values for the normal stresses increase. Thus, the excavation sections should be chosen as not to exceed the strength of the structural materials and avoid damages of the existing elements.

In case of the in-plane stresses recorded in node A, as against the no-excavation model, there is an increase of the stress values of 22.78% for the 0.6 m excavation length for 1200 MPa elastic modulus and 23.79% for the same excavation, but for 4000 MPa as the value for the brick masonry wall. For the 1.0 m excavation length, the stress values grew with 71.50% for the 1200 MPa elastic modulus and 79.90% for the 4000 MPa. Following the same comparisons, for the stress values in node B, it is noted a significant increase of 33.56% for 1200 MPa up to 131.27% for 4000 MPa, for the 0.6 m excavation length and an increase of 93.18% for 1200 MPa up to 208.76% for 4000 MPa, for 1.0 m excavation length.

References

1. Malekova, V., Jendzelovsky, N., An analysis of contact elements of foundation structures, *Machines, Technologies, Materials*, vol. 7, 2012.
2. Betti, M., Galano, L., Seismic analysis of historic masonry buildings: The Vicarious Palace in Pescia (Italy), *Buildings*, vol. 2, 2012.
3. Srilakshmi, G., Rekha, B., Analysis of mat foundation using finite element method, *International Journal of Earth Sciences and Engineering*, Vol. 04, 2011.
4. Soveja, L., Budescu, M., Gosav, I., Modelling methods for unreinforced masonry structures, *Buletinul Institutului Politehnic din Iași*, Tomul LIX (LXIII), Fasc. 6, 2013.
5. Potts, D.M., Zdravkovic, L., *Finite element analysis in geotechnical engineering - Theory*, Thomas Telford Publishing, London, 1999.
6. ANSYS Release, Documentation for ANSYS.

Dynamic Behavior of Road Structures

Gabriela Cioarba[1], Ciprian Costescu[2] and Adrian Dogariu[3]

[1]SC MGM Design SRL, Timisoara, 300109, Romania
[2]Department CCTFC, University Politehnica Timisoara, Timisoara, 300244, Romania
[3]Department CMMC, University Politehnica Timisoara, Timisoara, 300244, Romania

Summary

The present paper deals with dynamic effect induced by traffic loads in flexible pavements. The dynamic effect is not accounted by current design approaches. This fact is due the high complexity of the dynamic analysis and the difficulty of assessing the real behavioral parameters. In order to obtain confident results, one should use advanced numerical tools such as dedicated finite element software. The numerical software should be able to perform dynamic analysis and to model as accurate as possible the traffic loading conditions.

In the framework of this study will be summarized the main design demands and design methods for pavements according with the actual national and European prescriptions. In the same time will be described the possibility to use advanced mathematical procedures based on finite element analysis with the help of ABAQUS code. One pavement flexible system will be comparatively analysis presenting in detail the main steps and introduced parameters such as: defining the traffic loading conditions, modeling of the pavement structures, constrains, contact interactions, boundary conditions, material laws etc.

KEYWORDS: flexible pavement, numerical model, finite element, dynamic analysis, ABAQUS.

1. INTRODUCTION

1.1 The importance of road networks

The purpose of having road networks is to ensure safe and cost effective transportation for goods and persons, which is so necessary for the development and progress of any society. Even since the dawn of civilization, people realized the importance of roads and invested in the realization of road networks. The technological progress brought about the development of the construction and composition solutions trying to answer optimally and with minimum costs the design requirements. These requirements include the consideration of the location, ground and weather conditions, the different traffic levels, both in intensity and

frequency, as well as the prognosis of the future conditions as traffic, weather, and materials behavior in time and maintenance.

1.2 Design methods of road pavements

The road pavements are made up of different layers and materials aiming at supporting the traffic. The composing materials respond differently to the interaction with the vehicles in motion. The response of the road pavement to the loading resulting from the interaction between the wearing course and the tire of the vehicle depends on the time. Reasons such as: insufficient calculation power, uncontrollable modeling and input data, determined the analysis of the road pavements in the current design practice with the help of a static analysis, where the loading is considered constant and the response of the pavement not depending on time. Lately, many research have concentrated on the study of the dynamic response of the pavement under the traffic.

Although there are methods for the dynamic analysis of pavements, they are not necessary perfect and easy to use. There are a lot of limitations regarding the characterization of the loading brought by the tire, the material patterns, its ability or lack of ability to model nonsymmetrical loading conditions and the determination of the mechanical features of the materials. Presently, there is worldwide the requirement to find and develop methodologies to practically approach the dynamic analysis of road pavements under the action of loadings with their real characteristics [2].

The impact of vehicles on the road pavements has been studied and presented in several scientific papers, underlining the fact that they do not bring a constant loading on the road surface, on the contrary, a dynamic loading. The intensity of this loading depends on several factors such as the profile of the structure, the type of tire and the characteristics of the suspensions, the speed of the vehicle. The optimal dimensioning and design require the determination of these factors, the follow-up and quantification, through analysis, of their effects on the answer and performances of the road pavement. The exact quantification of these parameters makes the real analysis of the pavements extremely complicated. The simplifying hypotheses concerning the traffic (namely the static loading) and the behavior of the materials (namely linear elastic) lead to analysis errors that alter the exact assessment of the road pavement performances, having direct effects on the initial design cost and on the subsequent maintenance cost.

1.3 Purpose of the paper

The paper will present the analysis of a road pavement under the dynamic action of vehicles through models and analysis methods. The calculation standards for road

pavements in Romania will be also presented. Different factors with impact upon the dynamic transient response of the pavement will be shown. The vehicle action may be considered as follows [2]:

- *Static loading* (IS) when the loading intensity depends neither on the position nor on the time and the application point is fixed;
- *Dynamic loading* (ID) when the loading intensity does not depend on the position but is variable in time, and the application point is fixed;
- *Constant mobile loading* (IMC) when the loading intensity depends neither on the position nor on the time, but the application point is mobile;
- *Dynamic mobile loading* (IMD) when the intensity of the loading depends on the position and on the time, and the application point is mobile.

The present study deals with the differences occurring in the first two approaches (IS vs. ID), in a pavement chosen as case study, depending on the specific stresses and strains and the settlement occurring in the foundation ground and in the pavement layers. In order to study the transient response of the road pavement, the numerical analysis has to take into consideration the vehicle speed, the inertia of the road pavement and its damping. The paper will describe largely the used numerical models.

2. DESCRIPTION OF THE CHOSEN PAVEMENT

2.1 Types of road pavements

The road pavements are characterized by a large diversity in composition, determined by the development in time of the conception concerning the role played by the different composing layers and certainly by the technological progress. The diversity of materials (such as: soils, natural aggregates, binders) and construction technologies determine the existence of distinct and varied types of road layers. Their operation behavior under dynamic stress from traffic and alteration of the weather conditions needs to be assessed correctly with the help of specific dimensioning methods. From this point of view, the types of layers and pavements in operation need to be classified according to well-structured principles. Each typology of road pavement is associated to a specific design method correlated to its response under stresses [3].

Based on their composition and operation behavior, the road pavements can be:

- *flexible* – an ensemble of layers made up of non-cohesive materials stabilized mechanically and/or with hydrocarbon binders, the pavement and base course made up of asphalt mixtures;

- *rigid* – an ensemble of layers stabilized or not with binders, on top of which a cement concrete pavement is realized;
- *semirigid* – layers in natural aggregates stabilized mechanically and with hydraulic of pozzolanic binders, in which contraction cracking occurs in time, and the pavement and maybe the base course are bituminous layers.

2.2 Road layers of the analyzed pavement

The numerical investigation of a flexible road pavement (in operation on DN59C [3]) response will be described. It is made up of the following road layers, according to STAS 6400 [6] (see Figure 1):

- road pavement – wearing course and capping layer – 7cm asphalt mixture;
- base course – 15cm gravel;
- foundation layer (layers), resistance layer – 10cm well-graded aggregate;

7 cm asphalt mixture

15 cm gravel

10 cm old well-graded aggregate
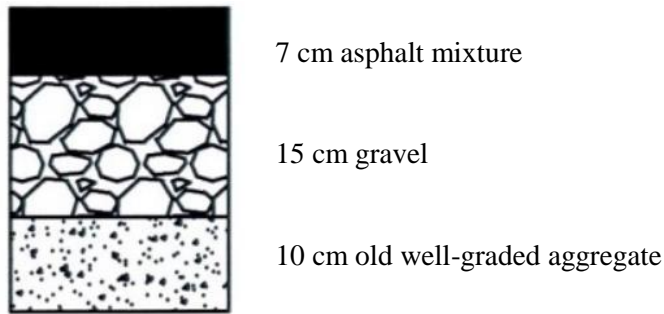
Figure 1. Composition of the studied road pavement [3]

It is worth pointing out that the flexible road pavements require intense maintenance works, fact explained by the relatively reduced initial investment in comparison to the other types of road structures [3]. In the case of flexible road pavements, the distribution of the internal forces is realized on a relatively reduced area, and the internal forces are also felt at the level of the inferior layers, the level of the earthworks active area include. Figure 2 shows the distribution of the traffic generated stresses on rigid road pavements, and flexible or semirigid pavements respectively.

The reason for choosing a flexible road pavement as a case study is the relatively reduced rigidity of these structures. This condition impacts negatively on their bearing capacity under the variation of the design factors.

(a) Rigid   (b) Flexible
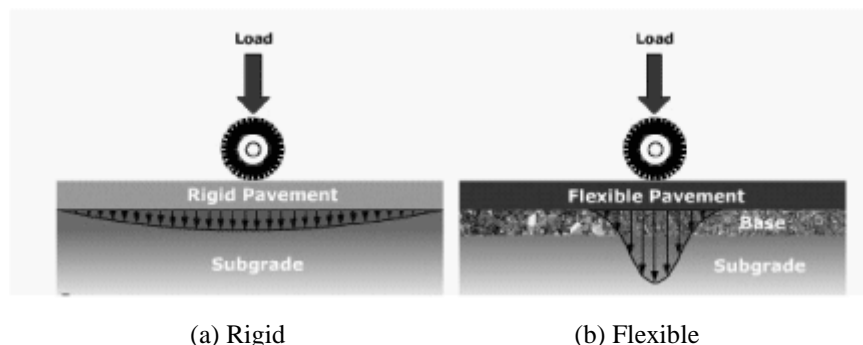
Figure 2. The effect of traffic stresses on rigid (a) and flexible (b) road pavements [8]

3. DESIGN AND DIMENSIONING OF FLEXIBLE ROAD PAVEMENTS

3.1 European design standards

The dimensioning models of the flexible road pavements used in Europe are analytical and empirical methods [3]. The dimensioning criteria used by analytical methods are similar and based on the assessment of the specific elongation strain admissible at the bottom of the bituminous layers or the specific compression strain admissible at the road formation level. The dimensioning is based on the linear elasticity theory in order to calculate the values of tensions and specific strains in the critical points of the road pavement. The road pavements are considered horizontally infinite layers, on a semi-infinitely thick foundation ground. These layers are considered homogeneous, isotropic and having elastic behavior. The answer of the road pavement under traffic stress is based on the theory of multilayer modeling, which, due to significant simplifications concerning the mechanic behavior of the layers, shows some drawbacks: the materials in the road layers are considered elastic, homogeneous, continuous and isotropic; the layers are considered horizontally infinite, of constant thickness, making it impossible to take into consideration possible local discontinuities; it neglects the viscous-elastic behavior of bituminous materials and the vehicle-induced dynamic effects generated by the unevenness of the road surface [3].

In Romania, a standard vehicle is considered; the standard axle was defined in 1985. This is characterized by the type, number of wheels, 115kN axle loading, 57.5kN on double wheels, 0.625MPa tire-pavement contact pressure, 17.1cm - radius of the equivalent circular contact area [4].

4. TRANSIENT RESPONSE OF THE PAVEMENT

If the road pavement, regarded as a physical system, is subjected to external action, resulted from traffic, it will respond in a way determined by its composition. In our case, the physical system is made up of geometrically defined (by shape and position) road layers, their links and composition materials.

The response of the structure depends on the nature of the traffic stress. As described above, the traffic has a dynamic character through the intensity variation in time (considered in the previous study), as well as through the shifting of the application point. Knowing the response of the structure implies the determination of the behavior of the loaded structure. The behavior is quantified by the calculation of unitary efforts, specific strains, and settlements respectively.

The determination of the response, in this case, is realized with the help of a theoretical model, based on the modeling of the structure with finite elements, model which replaces the scheme of the structure with mathematical expressions describing its behavior.

A very important issue, is the case of using mathematical and numerical models, is whether the response obtained is plausible from the quality point of view and accurate enough from the quantity point of view. The first question can be answered by using intuitive models to indicate if what was obtained through calculation is in accordance with the intuition and the engineering common sense. The second question is very difficult to answer and requires advanced calculation procedures.

The determination of the pavement behavior is realized for a pavement scheme and not for a real structure. The scheme of the structure keeps only the essential features, adopting a series of simplifying hypotheses. The lower the number of simplifying hypotheses, the more complex the structure and the greater the solving difficulty, but the solution is closer to the accurate one. Generally these hypotheses refer to materials behavior, geometrical dimensions and shapes, boundary condition, element interactions etc.

5. MATHEMATICAL MODELING OF ROAD PAVEMENTS

Numerous disadvantages of the designing methods, based on analytical methods of the elasticity theory, introduced due to the simplifications can be, even if partially, removed by using advanced structural calculation instruments based on the method of the finite element. This approach allows the close to reality modeling of the stress and response conditions, by eliminating certain simplifications.

5.1 Description of the calculation program

The present paper proposes a mathematical modeling to investigate the dynamic response of road pavements. The mathematical model is built with the help of the ABAQUS program. Lately, several studies in the scientific literature have used the numeric modeling of road pavements with the ABAQUS program, validating the results of the numeric simulations by those determined experimentally. This is a commercial program based on the method of finite elements. The ABAQUS program offers numerous advantages in road pavement analysis through a bi-dimensional or tridimensional calculation, allowing both the linear modeling and the non-linear, elastic, viscous-elastic and viscous-plastic modeling of road layers considering different yielding criteria depending on the material type. The program allows the application of the loading both statically and dynamically by considering the dynamic characteristics of the response of the road pavement. If, in the case of analytical methods in the theory of elasticity, the space is considered continuous, in the modeling with contact finite elements the real characteristics of the interfaces between the road layers can be taken into consideration [7].

The ABAQUS program allows, through its two products, namely ABAQUS/Standard and ABAQUS/Explicit the solution of the analyses through an implicit, respectively explicit approach.

5.2 Geometrical modeling

Through the nature of the road pavement, the necessity to consider the foundation ground as a component of its response, the geometric modeling should consider the tridimensional character of massive structure with all the three dimensions of comparable size. This is done either through a modeling with spatial geometry elements, or through a bi-dimensional axis-symmetrical modeling (Figure 3). The spatial modeling results in a large dimension of the numerical problem and a very long time. The axis-symmetrical approach allows the a decrease of the problem dimension without neglecting the spatiality, but it is limited to symmetrical problems, symmetrical tests and obviously a fixed application point. In order to consider the mobile character of the traffic induced stresses, a plane strip can be taken into consideration (plane condition of strains) along the longitudinal axis of the road, loaded in its plane.

The modeling of the geometry will be realized so that the depth of the model is larger than the active area. Even so, an accurate modeling of the reality requires the use of infinite elements.

Foundation ground	
Gravel	
Well-graded aggregate	
Asphalt mixture	
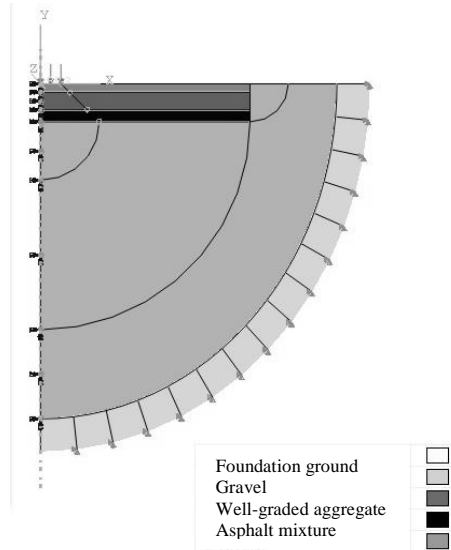
Figure 3. Axis-symmetrical model of the road pavement

Gravel – aggregate contact	
Asphalt – gravel contact	
Pavement – soil contact	
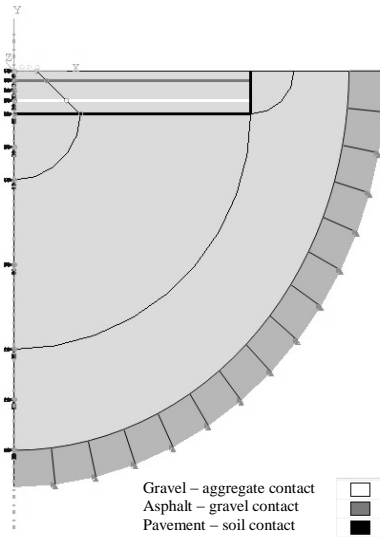
Figure 4. Definition of the contact areas [1]

5.3 Behavior laws of materials

The analytical models, available to the designer, have the disadvantage of considering certain simplified material models - linear elastic, but the composing materials of road layers have a much more complex behavior. The use of the

ABAQUS program allows the input of behavior characteristics close to the real ones.

The materials become deformed under stress. The deformation mode and its characteristics define the type of material. The deformations can be: elastic, plastic and viscous. For each of these patterns, the specialized literature describes analogous behavior patterns – Hooke patterns (elastic), Saint Venant patterns (plastic), and Newton patterns (viscous).

The elastic characteristics of the layers are shown in Table 1. In the present paper, only the elastic characteristics of the materials have been used.

Table 1 Elastic characteristics of the composing materials [3]

Name of layer	Longitudinal elasticity modulus E [N/mm2]	Poisson's coefficient	Density [N s2/mm4]
Asphalt mixture	3000	0.35	2.2 E-09
Gravel layer	760	0.27	1.8 E-09
Well-graded aggregate layer	350	0.27	1.6 E-09
Foundation ground	65	0.3	1.2 E-09

5.4 Consideration of loadings and connections

The traffic loading was modeled according to the provisions of the design standard PD177-2001 [4]. The "disadvantage" of the axis-symmetrical patterns is that they allow only the input of loadings distributed on circular areas. But this does not contravene the provisions of the standard which recommend a circular print with a 171 mm radius, on which a pressure of 0.625MPa acts uniformly. The loading was modeled as constant static loading as well as a dynamic loading whose intensity depends on time (Figure 6 / Intensity of loading).

The issue of road pavement modeling is reduced to the multilayer analysis of the infinite semi-plan. In the case of dynamic modeling, the modeling of a substructure (active area) and the introduction if retainers to prevent totally the freedom degrees can have negative effects. These effects show by overlapping the direct vibration waves, resulting from the direct action, and the reflected ones from the fixed edges (retainers). These can be removed by introducing infinite elements. They are also called "silent boundaries" (silent edge conditions) since they eliminate the reflected waves. Along the symmetry axis the perpendicular shifting and the circling in the modeled plan (xOy) were blocked, respecting the symmetry.

The contacts between the road pavement layers and the road pavement and the foundation ground were modeled. It was considered that the foundation ground cannot take over the stretching stresses (contact-1), and any relative sliding cannot occur between the road layers (Figure 4).

5.5 Structure model

The mathematical model was discretized using finite elements characteristic for the simulations on axis-symmetrical geometries, as follows: the layers of the road pavement with CAX3, CAX4R, the foundation ground with CAX8R, and the geometry of the infinite "semi-plan" with CINAX5R. The dimension of the finite elements is smaller, realizing a finer network of mesh in the vicinity of the loading (Figure 5).
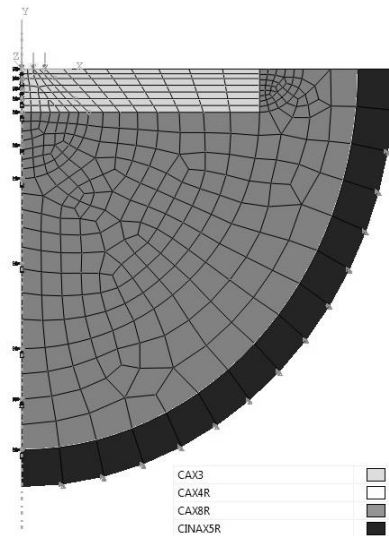
Figure 5. Meshing – shape and type of finite elements [1]

5.6 Types of analyses

In order to study the dynamic effect of the loading on the response of the studied pavement, the loading was introduced independent of time (constant intensity), in a first numerical simulation and dependent on time as a pulse (Figure 6), to reproduce the dynamic character.

6. RESULTS OF THE NUMERICAL SIMULATIONS AND CONCLUSIONS OF THE ANALYSIS

Figure 6 shows the graph of variation for the maximum settlement of the point in the symmetry axis of the wearing course, resulted from the numerical analyses. An increase by 1.39 is noticed in the case of the dynamic analysis. Table 2 presents the

specific stretching strain at the bottom of the bituminous layers (ε_{xx}) and the specific compression strain at the formation level (ε_{yy}).

Table 2 Specific strains [1]

Specific strain	Static analysis	Dynamic analysis	Difference [%]
ε_{xx}	1,29E-05	1,67E-05	1,29
ε_{yy}	-5,16E-04	-6,05E-04	1,17

These results have made it clear that a simple static analysis considering a constant impact factor ([5] recommended the use a factor 1.2 for rigid road pavements) does not offer a correct answer for all the design criteria stipulated in the calculation standards.
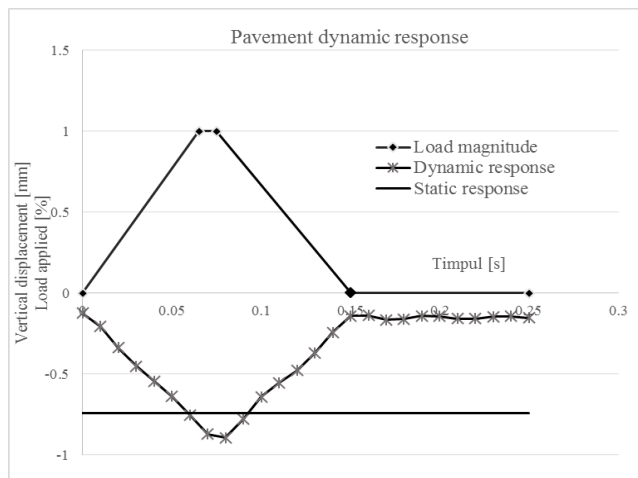
Figure 6. Results of the numerical analysis on the studied road pavement [1]
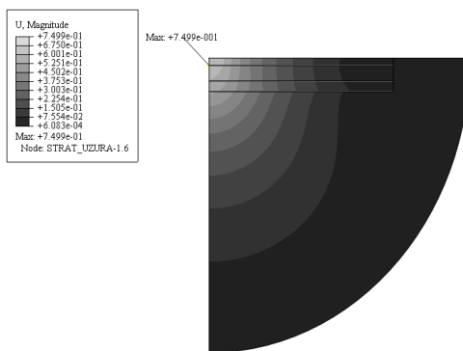
Figure 7. Diagram of the settlement resulted from the static calculation [1]

Acknowledgements

References

1. Cioarba, G., *Comportarea in exploatare a complexelor rutiere la solicitări dinamice prin modelare matematica (Operational behavior of road complexes under dynamic stress through mathematical modeling)*, Dissertation, University Politehnica Timişoara, June 2014 . (in Romanian)
2. Steyn W.J.M., *Consideration of Vehicle-Pavement Interaction for Pavement Design*, PhD Thesis, Faculty of Engineering, Build Environment and Information Technology, University of Pretoria, January 2001.
3. Costescu, C., *Contribuţii la studiul unor factori de influenţă asupra stării tehnice a drumurilor din zona Banatului (Contributions To the study of certain factors influencing the technical condition of the roads in the Banat area),* University Politehnica Timişoara, June 2010. (in Romanian)
4. *Normativ pentru dimensionarea sistemelor rutiere suple şi semirigide (Metoda analitică) (Dimensioning standard for the flexible and semirigid road pavements (Analytical method) Indicative PD 177 – 2001*, MTCT, 2003 . (in Romanian)
5. *Normativ de dimensionare a structurilor rutiere rigide (Dimensioning standard for rigid road pavements) Indicative NP 081-2002; MTCT*, (in Romanian)
6. *STAS 6400-84, Straturi de baza si de fundaţie (Base and foundation courses),* Romanian Standardization Institute, 1984. (in Romanian)
7. Costescu C., Dogariu A. *Studies regarding operation behavior of road pavements based on numerical modeling*, Scientific Bulletin of Mineral Resources and Environment Faculty of the North University of Baia Mare, Volume XXIV no.1/2010;
8. E. J. Yoder, M. W. Witczak *Principles of Pavement Design,* John Wiley & Sons, ISBN O-471-97780-2 1975

Numerical Study of Stress Intensity in Flexible Pavement Under Airplane Loading

Mohammad Javad Akhavan Bahabadi[1], Mohammad Mehdi Khabiri[2] and Alireza Fotouhi Firouzabadi[3]

[1,2]*Civil Engineering Group, Yazd University, Yazd, 8915818411, Iran*
[3]*Mechanical Engineering Group, Yazd University, Yazd, 8915818411, Iran*

Summary

Stress in the pavement structure leads to all types of failures in road and runway surface. Pavement stress from foreign indicators of failure that the cause of loading, environmental factors, poor construction or a set of them pavement failure can be structural or functional. Structural failure requires detailed analysis of failure mechanisms and layers are contributing in pavement failure. Repairs are generally very expensive and runway pavement may require reconstruction. One of the common methods for studying of cracks derived from fatigues is fracture mechanics method. In this study, to evaluate the development of sample crack, the airport pavement was modelling by finite element software and the amounts of stress were measured at the crack tip. The results show that, by increasing the thickness of the layer of asphalt, the stresses and displacements are reduced.

KEYWORDS: Numerical study, Runway cracking, fatigues, Crack initiation, Crack growth, Asphalt pavement.

1. INTRODUCTION

Ground facilities are an integral part of the airport which the most important ones are runway pavements. Since the airplane wheels is opened directly on the pavement system, the behaviour and status of pavement has an effective impact on the performance of pavement traffic. Therefore, having a good road system is essential affairs due to consider all design conditions [1].

One of the problems and failures of the pavement is cracking. Cracking is damages in flexible pavement, seen in most flying areas. There are several factors that cause pavement lead to cracking which traffic loads on the pavement that play most important role. On the other hand, the periodic nature of loading pavement causes appearance of a phenomenon known as fatigues in asphalt layer [2].

The phenomenon of fatigue in the pavement is the failure of pavement due to repeated load, temperature fluctuations or a combination of those two. This phenomenon appeared as cracks in pavement and it is the major events of asphalt

pavements in Iran and other countries of the world, especially in cold and temperate regions.

Failure due to fatigue is the most important issues in the airport pavement design that has been under periodic loading. The occurrence of failure due to fatigue can be started from a small crack and crack growth continues somewhat, it will lead to failure. During the crack growth process from initial to final length can be express as fatigue crack propagation (FCP), that was numerically examined in this papers [3,4].

The fatigue cracking is one of the major problems in the long-term performance of asphalt. Nowadays, many researchers have been done to study the fatigue behaviour of asphalt pavement. There are various methods of fatigue analysis, which many of them are using now, and many do not provide accurate results in predicting the fatigue performance of pavements. As a result, the predicting of fatigue cracking continues as a main concern for engineers. The process involved parameters that a number of fracture mechanic and other related material are obtained by laboratory methods [5, 6].

In this paper, we examine the numerical growth of fatigue cracks in the runway due to airplane wheel loading, by finite element software. Finite element method is one of numerical methods for linear and nonlinear problems. This method has many advantages over other methods of numerical solution.

Analytical solution for the many problems that have complex differential equations, special boundary conditions or non-linear terms is very hard, so the use of numerical methods increase very much the quality of the results. According to the previous content and the importance of cracks in the pavement airport from the safety perspective, this article reviews the results of previous studies and conducted with numerical analysis by the help of finite element software method has been examined from stress concentration in the cracking pavement runway.

2. REVIEW OF LITERATURE

Until now, many studies have been done to investigate the damages on the airport pavement and the effect of different types of airplane. Also in 2004, Kim and Tutumluer have carried out many experiments on the basis of passenger airplane and a few sample of military airplane in the studies lasting deformations pavement airport [7].

In 2005, Wang and Chia-Pei based on field research results in the Chiang Kai Sheck Taiwan international airport and generalize the results in three-dimensional environment finite element software, showed that the characteristics of the main wheels of the airplane on the amount of damage pavement has an important role

and it is effective on the useful lifetime of pavement and the thickness of the concrete pavement slab is effective [8].

In 2006, a study has been done by Joel on the some software of US aviation department, including LEDFAA and FEDFAA by using the formers researches on the analysis, designing airport in the world and the required development or progress for future wide-body airplane, the following results were presented: It is required to predict the status of runway pavement in the future, by considering new generations of wide-body airplane and damage through each of them with above software in two and three-dimensional environment of finite element, as regards, the next generation of air plane are more heavy and larger. The number of wheels and their arrangements has more important with increasing total weight of the next generation airplane and the need to select the best type of geometric arrangement of the wheels by producers [9].

In 1999, the America Aviation department used field test with real scale and through related facilities to real simulation of the airplane movement. Different types of airplane in terms of arrangement of wheels, their weights and simulate the effects of each other on the pavement [10].

3. RESEARCH METHODOLOGY

3.1. Introducing research place

Early studies for the establishment of Kerman airport commenced in 1925, building construction activity has started in 1956. Start transferring passengers and carrying cargo occurred from 1970 with two flights from DC6 kind during a week between Tehran and Kerman and return.

Kerman airport terminal has initial area of 600 square meters and length of the main runway 2,600 meters with a width of 45 meters and 2,000-meter secondary runway with width 45 meters. In 1981, lengthening operations and the cover of main runway has improved with a length of 3845 meters, a width of 60 meters in which it has obtained in 1366 and delivered certainly in 1990. The current situation of airport pavement can be seen in the figure 1.

3.2. Introducing modelling software

ABAQUS software is used extensively in the automobile industry, aerospace and industry of manufacturing industrial goods. Also, this software packages due to extensive capabilities in modelling for various materials, as well as the ability to

customize it by programming, it is very popular in academic research area. Primarily, ABAQUS is designed for non-linear physical behaviour [11]. Overview of model has brought in Figure 2 after definition of crack and the manner of stress distribution.

Figure 1. Overview of cracks in the Kerman Airport runway

Mechanical and geometrical specifications for runway pavement layer were selected base on the table (1), it has been tried that they were close to realities of Kerman runway airport. Modelling has been done like three-dimensional and made model to prevent in the vertical and horizontal movement floor bed layer is completely closed. Crack like circle shape with length 40 cm were selected and with dimensions of 3 x 2.5 cm was chosen and for loading, wheeled Airbus A-320 was used which has the most number of flights in Kerman airport. Analysis was considered with assumption linear elastic behaviour, materials of pavement layers and loading in static (non-dynamic).

Table 1. Specifications of materials and geometry of pavement layer for flight runway

The type of used materials	Sub-base	Base	Asphalt	Bed
Density(kg/m^3)	2200	2250	2300	1900
E -Modulus of Elasticity (MPa)	470	1250	12500	155
Poisson's ratio(v)	0.35	0.35	0.3	0.45
Thickness(cm)	45	30	20-30	200
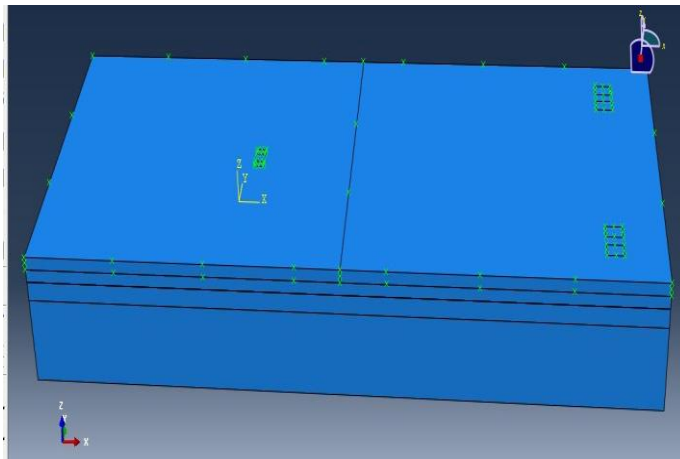
a)
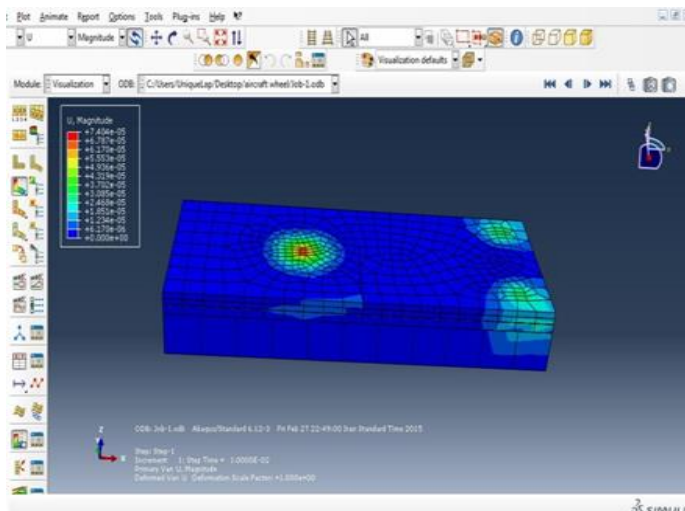
b)

Figure 2. Cracks width modelling on the airport's asphalt runway and the manner of stresses intensity in uploading

4. THE SIMULATION'S RESULTS

4.1. Analysis model by changing the thickness of the pavement layer

On the designed model, to determine the effect of pavement layer thickness that

this thickness is changed by covers frequent asphalt layer, the thickness of the asphalt's layer once 30 and once 20 cm was considered (Figure 3) changes of tension was shown in this layer, the stress reduced from 7.34×105 to 5.22×105(Pa).

4.2. Analysis model by changing the location of cracks in the surface layer

To determine the effect of changes for cracks occurrence on the rate of the stress concentration, was evaluated in two issues, crack in the latter manner was located between the wheels of the plane. The manner of changing the level of tension is considered which is displayed in Figure 4.

a)   b)
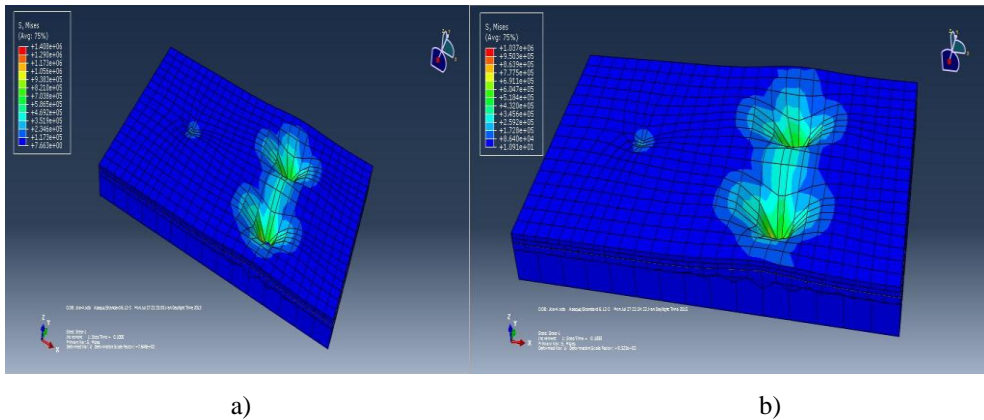
Figure 3. Changing of stresses

a) 20 cm asphalt's thickness   b) 30 cm asphalt's thickness
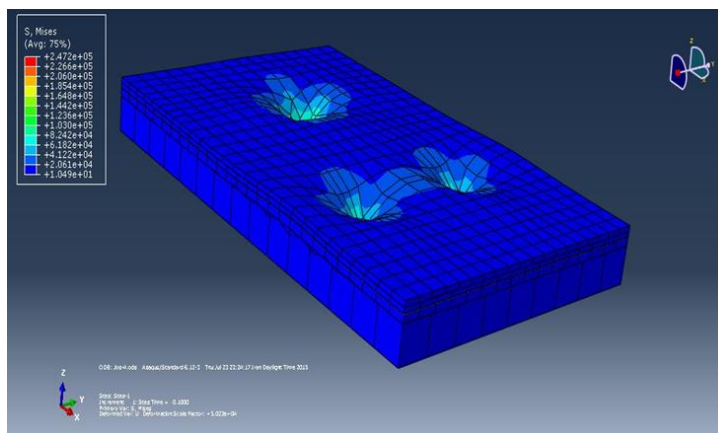
Figure 4. Changes intensity stresses with change location of cracking

5. CONCLUSIONS

In this research was studied the aircraft wheel loading effect on stress at the fatigue crack by the finite element software. For compliance with real condition, crash data of the Kerman airport pavement actual was examined. Results show:

1. According to adapt the results of modelling runways and loading airplane was determined, the model and conditions of work has been properly treated;
2. In the first case, the thickness of the asphalt has changed, it can be seen that by increasing the asphalt's thickness, displacement and stress levels was reduced with about 30%;
3. In the second case, the crack displacement does not have effect on stress and moving.
4. Continuous assessment of airport pavement and identification the rate of damage in the airport pavement, particularly cracks predicted the possibility of damage growth and reduction the life chances.

It is necessary to mention that the results of this part of these studies include special case of a plane load and for different loading and the wheel movement is required to apply different load and the structural conditions in the software.

Acknowledgements

References

1. Navneet Garg, *Introduction to FAA's national airport pavement test facility (NAPTF), workshop – accelerated pavement testing for airport pavements and its impact on pavement design for new generation aircraft*, Presented to 3rd Intl. Conf. on APT, Madrid, Spain, September 30, 2008.
2. M. Willis, D. Johnson and B. Sukumaran, *Three –Dimensional Finite Element Analyses of Flexible Airport Pavement for the Next Generation of Aircrafts*, Minnesota Department of Transportation, USA, 2006.
3. Gopalakrishnan, K. and Thompson. M. R. , *Rutting Study of NAPTF Flexible Pavement Test Sections*, *In Proceedings of the 2003 ASCE Airfield Specialty Conference,* Las Vegas, 2003.
4. Gopalakrishnan, K., *Evaluation of accelerated deterioration in NAPTF flexible test pavement*, Journal of Zhejiang University *SCIENCE A*, May 4 2008.
5. Paris, P. and Erdogan, F., *A critical analysis of crack propagation laws,* Journal of Basic Engineering, Transactions of the American Society of Mechanical Engineers, December, pp. 528-534, 1963 .
6. Schorsh, M., Chang.C.M. and Baladi.G.Y. *Effect of Segregation on the Initiation and Propogation of Top-Down Cracks*, Proc.82th Transportation Research Board Annual Meeting Washington D.C., January 2003.
7. Erol Tutumluer & In Tai Kim, *Permanent Deformation Behaviour of Airport Pavement Base and Subbase Courses*, University of Illinois, Urbana-Champaign, November 9, 2004.

8. Chia-Pei & Shih-Ying Wang., *The Development and Application of Finite Element Model in the Chiang Kai-Shek International Airport*, Proceedings the 8th International Conference on Concrete Pavements, August 10-12, Colorado, USA,2005.
9. Rodney N. Joel, FAA Rigid Pavement and Tools Design Philosophy, Northwest Region Airports Conference, April 10, 2006.
10. Walter Perlongo and Gaetano Bosurgi., *Numerical Analysis of Fatigue Cracks Growth in Flexible Pavements with the Elastoplastic Fracture Mechanics Method*, 2013.
11. Darvishi M. M. and TarazJamshidi, U, *Comprehensive Guide Mechanical Analysis By Software Abaqus*, book collection orange triangle, Second Edition, Fall, page 400,2013.

A Review of the Application of Computational-Probabilistic Chain Markov Method in Predicting the Deterioration of Pavement

Behzad Kazemi and Mohammad Mehdi Khabiri

Civil Engineering Group, Yazd University, Yazd, 8915818411, Iran

Summary

Pavement naturally are deteriorating and eroding due to many traffics and environmental conditions. The prediction of pavement performance has an important role in efficiency of pavement management system. By understanding the process and the manner of reduction of pavement service can predict the necessary resources and arrangements to avoid accelerating process of degradation and deterioration. The deteriorated models are tools for predicting the future failure of pavement based on the current status, the causes of failure and the effect of different techniques of repair and rehabilitation for maintaining the level of performance and the status of its structure. In this paper, after stating the concepts of performance and deterioration of road surface, studies has been done in the past decade researches in the world, about Computational-Probabilistic Markov models, transition probability matrix extraction techniques, predictive models and their application in management of the road surface.

KEYWORDS: computational chain Markov, deterioration of road, probabilistic predicting models, pavement maintenance management, semi-Markov model.

1. INTRODUCTION

Pavement naturally are deteriorating and eroding due to many traffics and environmental conditions. Doubtless, without adequate and timely maintenance, highways and roads in city and suburban severely will be declined and deteriorate. A good pavement management system requires a predictive model, an accurate and effective performance pavement [1]. By understanding the process and the manner of reduction of the pavement service can predict the necessary resources and arrangements to prevent from the accelerate degradation and deterioration. The mean of deterioration can be the type of changes for the status of pavement or changes in surface roughness or an indicator of a particular kind of damages such as during time.

After the construction and implementation of the road surface, several factors depending on the type and severity of the effect, began to destroy and to decrease its ability to provide service. These factors can be divided in two general categories: load

(loads of traffic) and the environment conditions (weather and drainage conditions). The factors related to the design and implementation of road surfaces, including the type of materials, the correct design, methods and quality of implementation, also have considerable effects in accelerated pavement deterioration [2].

2. APPLICATION MODELS OF PAVEMENT DETERIORATION PREDICTION

The most important part of pavement management represent the exact prediction of pavement failures during the pavement life cycle analysis; therefore, prediction failure of road procedures is a key factor in pavement management system [3].

The prediction rate of the road surfaces deterioration due to complexity identify the rate of pavement status or difficulty of collecting accurate data, especially in the absence of sophisticated equipment or highly skilled technical force, is very difficult. Various pavement maintenance systems are used around the world but, unfortunately, all these systems do not use a systematic method to determine the rate of pavement condition or determined experimentally the probabilities of transition state pavement [4].

A pavement performance prediction model has the different types which depending on management objectives, the richness of database and ease of use. Three main categories of these models include certain models, probabilistic and easy computational. The deterioration processes of pavement generally result from five parameters: pavement structure, traffic load, weather, modification history and quality construction. Many of these parameters are changed randomly and are not predictable; on the other hand, the interaction between these factors is uncertain, so the deterioration of pavement is completely random phenomenon and the probability [5].

Accurate models of predicted pavement performance and optimization models that properly designed are the key elements in a successful management at the network level. For the proper schedule in maintenance of road surfaces need to identify the behaviour of pavement & it's vanish model and predict the pavement condition. So the level of network management, predictive models of pavement status to schedule inspections, life cycle costing, analysis, benefit / cost and budget planning and optimization are used and requires less accuracy [6].

3. THE APPLICATION OF MARKOV PROBABILITY COMPUTATIONAL MODEL IN THE DECADE 2004-14

Some people related the start discussion of pavement management to tests of Osho,

in 1956 to 1960 that led to providing the concept of performance and capability of serving road surface. Halbrok and Vanhokov in 1974 measure and predict the performance of welded structural concrete pavement performance in the 128 projects with performance more than 15 years in Michigan State, used a variety of techniques such as Markov model. They concluded that the Markov chain approach has the best correlation with field data and in general not only for wide cracks but also for pavement of suture concrete is also a suitable method [7].

Dong Yang and Chang in 2004 on the basis of the analysis and data the status pavement highway, Shin-da China, Markov probability predicting techniques and the use of regression analysis was used to predict pavement performance. They concluded that the exponential function, pavement performance decreases with time and Markov's predicting possible model has the range of application and specific limitations [8]. T.John and Pytalka in 2005 with a review of a 1000 km hypothetical networks and predict the future state of pavement base on Markov probability model and solve equation AX = B, with a deviation of 5.5 to 6.10 per cent (Figure 1) was obtained. The following figure shows differences between the values of the current pavement status and the predicted status.
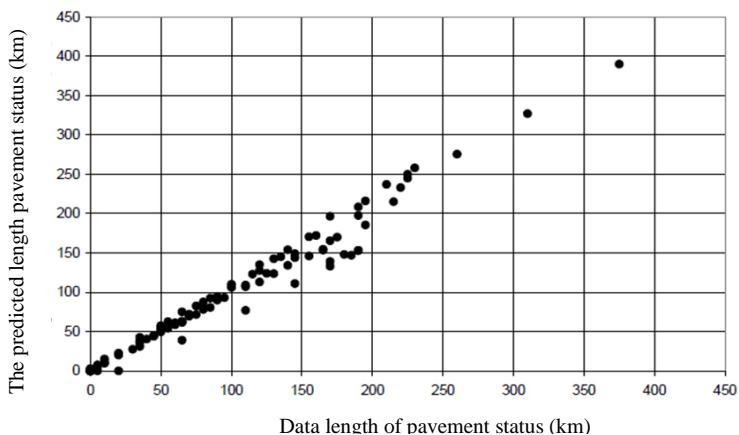
Figure 1. The real length and predicted the pavement status [10]

Ortiz Garcia and Associates extracts the transition probability matrix of the data bank in 2006, proposed three nonlinear optimization problem and they asses by the six special artificial data bases: the first method assumes that the past data of pavement status for each part of the network are readily available [9].

The second methods uses regression curve derived from the original data and a third method assumes that annual distributions of pavement status are available. In this method, the aim of minimizing the difference between the actual distributions of cases derived from the recorded data with predicted modes by possibilities Transfer Matrix.

Minimize $z = \sum_t \sum_i [a_t(i) - a'_t(i)]^2$ subject to:

$$\begin{cases} 0 \leq P_{ij} \leq 1 \text{ for } i, j = 1, \dots, n \\ \sum_{j=1}^{n} P_{ij} = 1 \text{ for } i = 1, \dots, n \end{cases} \tag{1}$$

where

$a_t(i)$: the predicted state vector by transition probability matrix and

$a'_t(i)$: actual state vector obtained of the recorded data at time t [10].

Chow and colleagues in 2008 compared with predictive models pavement conditions, by comparing the predicted conditions with observed actual conditions for a period of 5 years (2001-05) and use the database Ohio Department of Transportation, they concluded that Markov model has the highest prediction accuracy compared to other assessed models in addition to it can predict the amounts of PCR (the rate of pavement condition), damage road surfaces in the future.

Figure 2 shows the difference between the predicted values of PCR (which is derived from the Markov model) and show real PCR values.
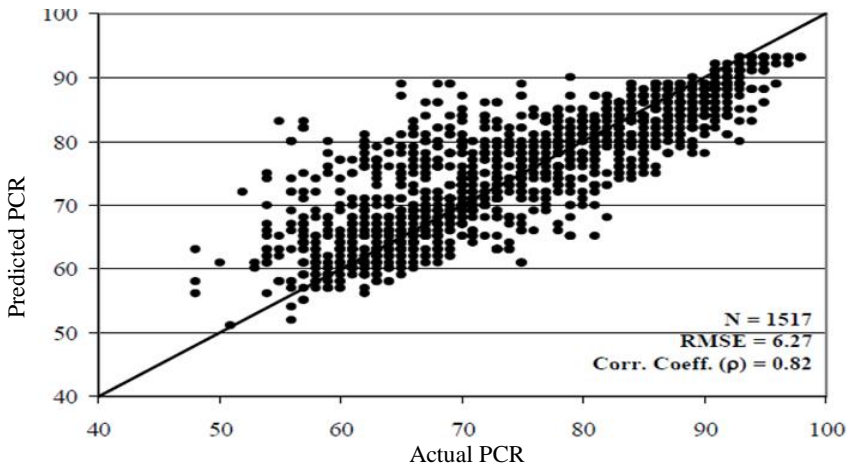
Figure 2. The predicted PCR and PCRA real value (2002-06) [11]

The accuracy of model has expressed by the root mean square error (RMSE) and coefficient expressed. RMSE is defined as follows:

$$RMSE = \sqrt{\frac{\sum_{i=1}^{n}(PCR_P - PCR_A)^2}{n}} \tag{2}$$

where PCRP the predicted value of PCR, PCRA real value of PCR and *n* is the number of observations. The Smaller values of RMSE indicate more accurately model. The correlation coefficient indicates the rate of compliance between actual and predicted the PCR. Full compliance has the coefficient of correlation [11].

Abazai in 2011 with a case study on low-traffic roads, use Markov model to predict the failure rate road surfaces in the future as well as predict the required thickness of flexible road surfaces [12]. Lthan and Eddie in 2012 with an experimental study and by using real data in the world, use the hidden Markov models for modelling deterioration hide pavement (deterioration that is not directly measurable) used [13].

Uchwuat and MacLeod, in 2012 with comparisons between regression models and Markov chains in modelling the performance of road surface, achieved the following results:

1. Advantage Markov models are that it can be calculated with a minimum of 2 years of pavement condition data while regression models need more data.
2. Markov models have the possibility that the expert's opinion or Bayesian methods used in the development of pavement performance curves.
3. The predicted data analysis with the actual performance data of pavement during the period of 6, 9, 13, 19 and 23 years showed that Markov models estimate the lower pavement performance. This issue is well shown in the figure (3) [13].
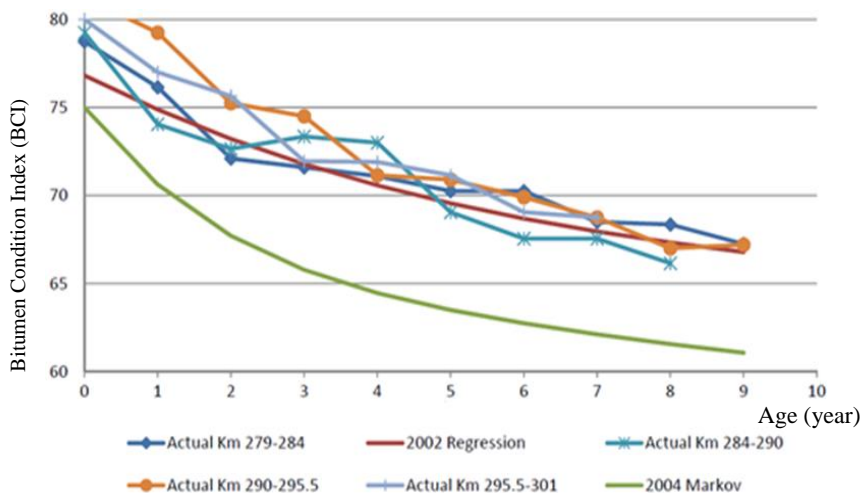
Figure 3. Comparison of Markov models and Regression by real data [13]

Wang and colleagues in 2013 developed and implemented a network-level optimization model into a pavement management data system for the Ohio Department of Transportation as well as they predicted future status pavement based on past data and Markov's transition probability model. This combined the optimized model, linear programming model and Markov's transition probability model and has the following features [14]:

1. Calculating the needed minimum funds to achieve the desired level of network status road surface,
2. The creation of maximum improvement in the status of pavement network of

the allocated budge t, and
3. Identify the relationship between optimized development policy and allocated budget. They concluded that the highway agencies can use this model as a decision support tool used to manage network-level road surface.

Suman and Sinha in 2013, Markov chains and application of pavement quality index (OPQI) were used to predict the future state of road surfaces. The index is obtained based on a theoretical concept that includes all conditions process of the road surface:

$$OPQI_k = 10 \sum_{i=1}^{i=n} \left[1 - (1 - \frac{CI_i}{10}) * W_{i,k} \right] \qquad (3)$$

where $OPQI_k$ - indicator of the overall quality of the pavement with a scale of 1 to 10, CI - status indicator or malfunction indicator with a scale of 1 to 10, K -index of the pavement performance, k mi,- index of status or failure of I, Out of the total number. n -Status Indicator = the total number of different types of failures or status indicators which is on the performance index, and W_i, k - the weight of any damage or index of status.

Comparing the observed rate of status in 2011, with the predicted status rate in the same year was used for validating the model which is obtained by the developed failure model. The figure (4) demonstrates this problem.
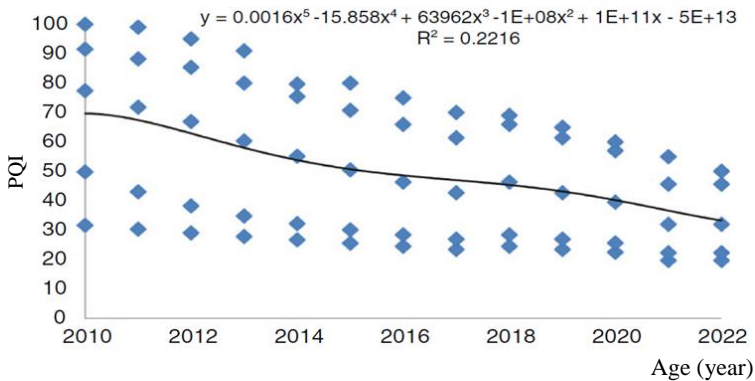
Figure 4. A performance of pavement predictive model [15]

In 2011, the rate of pavement status was 8.6 that the observed value is 1.6 for the same year. This result shows that the developed model has the ability to predict the rate of future state of the pavement with an acceptable degree of accuracy [15].
Surendra Kumar & assoc. use the Markov possible process to develop a decision support system to predict future situation of pavement in 2013. They use Poisson method to calculate consecutive transition matrices and x2 inference test to assess the rate of compliance. Finally they conclude that the possible process of Markov is a tool for finding the manners of future pavement conditions in any given year, and it will help to find the optimal maintenance policy (due to budget constraints and the

current state of the road surface) [4].

4. CONCLUSIONS

A good pavement management system requires a predictive model and accurate & effective performance of road surface. By understanding the process and the manner of reduction the pavement service can predict the necessary arrangements and resources to prevent the accelerated process of degradation and deterioration. The deteriorated models are tool for predicting future pavement failure base on the present status, the cause of failure and the effect of different techniques of repair and maintenance to maintain the performance level of structural condition the road surface. By reducing forecast error of deteriorate road surface, organizations can save the cost of a lifetime with intervention and careful planning. So the accurate models to predict deteriorate are very valuable tool for the road departments and organizations related to pavement maintenance. Some of results of this research are presented as below:

- Since many researchers are interested in predicting the status of piece and to acquire the deteriorate process of special piece, in addition to innovation in the network should be analysed the length of road including many pieces of different indices, and the prediction process by Forecasting the desired length lead in the future. Accordingly, the analysis of cost of future repair and maintenance is also easily done.
- Markov transition probability matrix is assumed to be constant over time that the assumption on the pavement does not conform to reality (homogeneous matrix). Therefore it is suggested to use the heterogeneous matrix with the ability to change over time due to the limitations of homogeneous Markov method, offered by the network is divided into different parts and defines the time zone for each of these segments and time intervals (period), extract matrix separately and combine them together to use to remove this limitation of the homogenization Markov method. Since the semi-Markov model, pavement repair operations also considered that it would be more compatible with the actual situation of road surfaces, the use of this model is recommended for future research.

References

1. Butt, A. A., Shahin, M. Y., Carpenter, S. H and Feighan, K. J, *Pavement performance prediction model using the Markov process*. Transportation Research Record, Journal of the Transportation Research Board, No.1123, pp.12-19, 1987.

2. Carnahan, J. V., Davis, W. J., Shahin, M. Y., Keane, P. L and Wu, M. *Optimal Maintenance Decisions For Pavement Management*. Journal of Transportation Engineering, Vol. 113, No. 5, pages 554÷572, 1998.

3. Tabatabaii S.A. and Khorani,H., *Transfer matrix method in predicting future state Markov pavement using MATLAB*, Quarterly Transportation Technology Journal,No.18, Road and urban ministry of Iran,2013[in Persian].

4. Surendrakumar, Katkar., Prashant, Nagrale and Mayuresh, Patil, *Application Of Markovian Probabilistic Process To Develop A Decision Support System For Pavement* Maintenance Management, International Journal of Scientific & Technology Research Volume 2, Issue 8, pages 295÷303, 2013.

5. Ziadi M. ,Tabatabaii, N. and Aqajani,R. *Markov probability transition matrix update road networks in developing countries using Bayesian inference, and considering the uncertainty parameters*, 9th International Congress of Civil Engineering, Isfahan University of Technology, 2013 [in Persian].

6. Holbrook, L. F and Kuo, Wen-Hou, *General Evaluation of Current Concrete Pavement Performance In Michigan.* Final Report on A Highway Planning and Research Investigation Conducted in Cooperation with the U.S. Department of Transportation, federal highway administration, No. R-905, 1974.

7. Dong-Yang, FU and Chang-bin, HU, *Markov probability forecasting of performance of asphalt pavement in expressway*. Journal of Fuzhou University (Natural Sciences Edition), 2005.

8. Tjan, A. and Pitaloka, D., *Future prediction of pavement condition using Markov probability transition matrix*. Parahyangan catholic university, Proceedings of the Eastern Asia Society for Transportation Studies, vol. 5, pp. 772 – 782, 2005.

9. Ortiz-García, J., Costello, B.,Seósamh S. and Snaith, M, *Derivation of Transition Probability Matrices for Pavement Deterioration Modeling*. Journal of Transportation Engineering., vol. 132, no. 2, 2006.

10. Y. Chou, Eddie, Pulugurta, Haricharan and Datta, Debargha, *Pavement forecasting models*. FHWA/OH-2008/3, University of Toledo Department of Civil Engineering mail stop 307 Toledo, OH 43606-3390,Ohio Department of Transportation, Columbus, Ohio 432, 2008.

11. Abaza, Khaled, Stochastic Approach for Design of Flexible Pavement. Road Materials and Pavement Design, Volume 12, No. 3, pages 663 to 685, 2011.

12. Lethanh, Nam and T.Adey, Bryan,A *Hidden Markov Model for Modelling Pavement Deterioration under Incomplete Monitoring Data*. International Journal of Civil and Environmental Engineering, 2012.

13. Uchwat, Chris and MacLeod, *Case studies of regression and Markov chain models*. Paper prepared for presentation at the pavement performance case studies, Session of the 2012 Conference of the Transportation Association of Canada Fredericton, New Brunswick, 2012.

14. Wang, Shuo., Y. Chou, Eddie and Williams, Andrew, *Development and Implementation of A Network-Level Pavement Optimization Model For Ohio Department Of Transportation*. TRB 2013 Annual Meeting, 2013.

15. Suman, S.K and Sinha, S, *Pavement Performance Modelling Using Markov Chain*. Proceedings of the International Symposium on Engineering under Uncertainty: Safety Assessment and Management (ISEUSAM), pp. 619÷627, 2013.

Modelling in A. L.W.T. the Dynamic Characteristics of the Wind in Mixed Climates

Carmen Elena Teleman[1], Georgeta Băetu[1], Elena Axinte[1], Victoria Elena Roşca[1], Radu Silion[2]

[1]Department of Civil Engineering, Faculty of Civil Engineering and Building Service, Technical University "Gheorghe Asachi" Iasi, Romania
[2]Department of Computer Science, Faculty of Automatic Control and Computer Engineering, Technical University "Gheorghe Asachi" Iasi, Romania

Summary

The climate behaviour suffers important changes as result of the impact with a rapid extension of the anthropic space. The abrupt modification of season temperature and severe wind storms are put in evidence now all over the world.

Simulation of the dynamic effects of wind action upon the built environment in laboratory is a process of scaling at reduced dimensions of a complex combination of factors insuring similarity between the natural phenomenon and the one artificially reproduced.

Usually, the design wind dynamic action on structures is identified with the so-called extra-tropical depressions, specific for middle global latitudes; the atmosphere is considered neutrally stratified, the vertical profile is in equilibrium with the terrain roughness in A.B.L. The simulations of wind speeds and pressures in the boundary layer of the air moving at the surface of the earth are based on vertical profile of the mean speeds, turbulence intensity, spectral power and histograms of the recorded values. The analysis of data is based on the model of the wind speed in A.B.L. fairly considered as a random, stationary, Gaussian process.

Lately, the observations put in evidence the fact that it is the strong winds associated with thunder storms along with the so called gust fronts that affect the built environment and that they are not stationary and Gaussian processes. The paper presents the analysis of series of measured speeds in the wind tunnel SECO 2 at different time intervals, different sampling rates in different types of boundary layers, analyzing the possibility of reproducing some of the characteristics of the wind speed in a non-neutrally stratified boundary layer.

KEYWORDS: wind tunnel simulations, wind profile in A.B.L., statistic distributions of wind speed

1. INTRODUCTION

It is rational to think that, by improving the quality of the research background, the results of laboratory studies will increase in precision; this would further result in the coherence of the theoretical concepts. Almost all the studies developed by scale modelling of different structures in atmospheric boundary layer wind tunnels are based on the theories developed in the years of 1960 on the character of the dynamic action of the wind in the proximity of the ground surface. The formulation introduced by Davenport [1] on the design wind velocity acting on structures uses a time interval of averaging between 10 minutes and 1 hour, based on the representation of van der Hoven spectrum which points out the spectral gap separating the macro- and micro-meteorological peaks; the process is approached on statistical bases as a random, stationary, Gaussian process and the atmosphere is considered neutrally stratified, the velocity vertical profile being in equilibrium with the terrain roughness. Consequently, the intensity of the design wind velocity is established in a probabilistic framework, by safely assuming for the mean wind velocity a suitable return period. This whole theory is valid for the usually atmospheric conditions identified with extra-tropical depressions typical of temperate countries at mid-latitudes.

The development of modern infrastructure of our society faces unpredicted confrontations with natural violent manifestations and the engineers' awareness is increasing on the fact that thunderstorms and strong winds must play a key role on wind actions and effects on structures [2], because their extreme effects might not be estimated correctly in the first place.

It seems that a more accurate definition is necessary, based on long and short time periods of observation of the interaction between the wind in the atmospheric boundary layer and the structures placed on the ground. Indeed, which is called now as "mixed climate" refers to "a climatology in which wind phenomena of different nature coexist" [3].

The most aggressive frequent manifestations, thunderstorms, are phenomena of convective nature and by the rapid air downburst directed to the ground level, radial outflows of air are directed all around and generating burst of different size, macro and micro. It is obvious and already stated in published research papers that these events are characterized by a random process of velocity which is non-stationary and non-Gaussian; in particular, the vertical profile of the velocity is nearly independent of the terrain roughness and has a typical nose shape fully different from the shape that characterizes extra-tropical depressions. It is now widely recognized that wind phenomena with a return period greater than 10–20 years are often associated with thunderstorms.

Recent studies show in addition to extra-tropical depressions and thunderstorms, another wind phenomena of intermediate properties, also called "gust fronts" [4],

[5], for which the wind velocity tends to be stationary but not Gaussian. For this kind of manifestations of wind action, the mean velocity is rather limited but turbulence is very high and causes peaks of relevant intensity, the velocity records showing high atmospheric instability.

The basic study of wind velocity and the structural response in these combined situations is dependent on the huge amount of data available up to now, obtained from atmospheric neutral stable phenomena with regard to extra-tropical depressions and disregards by quasi total lack of information the later observed phenomena, associated with the instable atmospheric conditions.

If the studies in boundary layer wind tunnels regarding wind effects on structures will admit the mixed climate existence, then appropriate simulations should be taken into account. Knowledge on this respect must have in view the characteristics of the wind action in instable atmosphere along with all the implications included. The basic studied feature of the wind velocity random process would in this case be the possibility of associating it with the statistic attributes.

UPDATES IN WIND SPEED MEASUREMENTS

2.1 Wind velocity measurements at site

The raw data regarding wind speed and directions of action are obtained through standard methods. Anemometers placed in open fields, quite frequently in the proximity of airports are able to gather wind velocity values averaged from seconds to 1 hour simultaneously with the direction of action at 10 meters high above the ground. The recorded raw data are further transmitted and afterwards transformed into more datasets associated with different wind phenomena.

The wind velocity characteristics measured at site are:
- the fundamental reference speed, which is a mean value obtained by averaging over 10 minutes period the values obtained from the anemometer, without considering the direction of action and the season and determined at 10 meters above the ground level on a standard terrain of II category of roughness, [6] and [7] ;
- correction factors because of the variation of the wind intensity with the direction and also with the season;
- the correction factor that takes into account the annual probability of exceeding the mean speed obtained from averaging the measured data over 10 minutes, determined with [7]:

$$c_{prob} = \left(\frac{1 - 0.2 \cdot \ln(-\ln(1-p))}{1 - 0.2 \cdot \ln(-\ln(0.98))} \right)^{0.5} \qquad (1)$$

All the data concerning the reference values of the wind speed and pressure for different particular sites are presented in Eurocode and in the annex to Eurocode referring to national specific values. And although these data contain sets of maxima values during 10 minutes records, daily, annual or even the absolute maximum from the period of observation (in Romania being between 20 to 50 years), they do not include information concerning the synoptic nature of the event that covers the period when these values are determined [7].

The modern trend of analysis of the wind maxima manifestations based on observations gathered at meteorological stations, discards the events into three families of properties, all being specific for the random processes, likewise:
- - events characterized by stationary and Gaussian nature for which the common features are the relative large values of the mean speed and small values of gust factors; they are extra-tropical depressions, related to neutral atmospheric conditions (no significant transitions occur inside the boundary layer);
- - non-stationary and non-Gaussian events, like the typical thunderstorms or strong winds for which the mean speed values are small but the peak values of the velocities and the gust factors are large;
- - events situated between these two mentioned above, called gust fronts accompanying the unstable atmospheric conditions; they are stationary but non Gaussian.

The definition of a stationary event refers to time periods from 10 minutes to 1 hour. The normal or Gaussian distribution of the wind speed data is adopted in connection with other processes that define the random nature of climate actions in particular and in general within the study of the safety design of structures based on the semi-probabilistic model.

It must however be mentioned here that while the data recorded by the anemometers could be analysed with the help of the Gaussian distribution, the reference or characteristic values of the wind speed provided by the codes for practice for the structural design are given in terms of maxima values, that may not be described by a Gaussian distribution, but typically by a Gumbel distribution.

The internal structure of the random process of wind speeds at site is usually studied starting with the histogram of the wind speed measures, compared with the ideal Gaussian density matching the mean wind speed and the standard deviation. As already mentioned above, it then is important to adjust the data obtained via at site measurements which are represented by the maxima values and analyzed by Gumbel maxima functions of distributions.

The analysis of similar recordings at site data, like the prodigious work of Solari and al. [2] are facing similar situations and they are not clearly statistically defined.

New methods of analysis are elaborated based on Cook's observations on storms, [8] trying to isolate the heterogeneous events from statistical monotonic data; it resulted into series of observations of wind speeds that exceed particular values of speed (threshold speeds) over specific subsequent time periods, for ex. 10 hours. This period marks an increase or a drop down of wind speed values and two sequential drop-down periods mark clearly a period during which a windstorm occurs, for example the threshold speed values that mark a lull are chosen as to take into account almost 100 storms per year; further analysis of the consequences are not developed yet.

The specific case of at site measurements on which we rely here is a set of raw data obtained from the National Meteorology Agency (A.N.M.H.) and concerns 10 years period of observation, from 1997 to 2006 in a standard II category of terrain, the airport of Iasi.

There are two types of data: averaged values from 10 minutes velocities recorded daily every 6 hours and peak velocities (the maximum successively recorded on 3 seconds intervals, a final maximum for a 10 minutes interval being chosen). Part of these data were already processed during a research program [9] and some of the results published [10], but further analyses must be developed regarding aspects related to the subject discussed here.

Table 1. Distribution and classification of maximum speed values over the period of observation

Year	Mean speed V_m	STD, σ	Maximum value, V_{max}	Minimum value, V_{min}	Gust factor, $G= V_{max/} V_m$	Skew	Kurtosis
1997	15.8333	4.03801	24	10	1.515789	1.177681	1.103828
1998	13.8333	1.90758	18	12	1.301205	0.853621	-0.01385
1999	15.3333	2.21108	20	12	1.304348	0.787296	-0.05455
2000	13	1.73205	18	12	1.384615	2.211083	5.323457
2001	13.4793	2.88942	24	10	1.780502	1.389032	1.991126
2002	13.3065	2.97817	25	10	1.878771	1.269169	1.925171
2003	13.3885	2.63360	22	10	1.643202	1.090796	1.930703
2004	13.1377	2.73249	22	10	1.674572	1.032397	0.617493
2005	12.9593	3.14008	24	0	1.851944	0.599442	3.183838
2006	12.7863	3.00129	28	6	2.189850	1.214529	4.229297

Some important knowledge must be mentioned:
- the Romanian code recommendations NP-082-2004 previous to the release of Eurocode 1, EN 1991-1-4/2004 gives the statistical description of the wind speeds based on 27 successive years of observations in terms of 1 minute wind speed, 1 absolute maximum value/year, the mean of yearly maxima

values and the skew coefficient of the Gumbel distribution; also, the characteristic value (probability of not being exceeded of 0.98) for a standard return period, T = 50 years;

- the correlation of the skew and kurtosis coefficients of the yearly maxima on the Romanian territory corresponds to a period of time of 20….50 years.

The analysis of the distributions of yearly wind maxima speeds along the period of observation provided the values for the statistic indicators (Table 1):

The graphical representation of the distributions of measured data per year confirmed the Gumbel shape for maxima type of distribution (Figure 1 a, b):

a   b
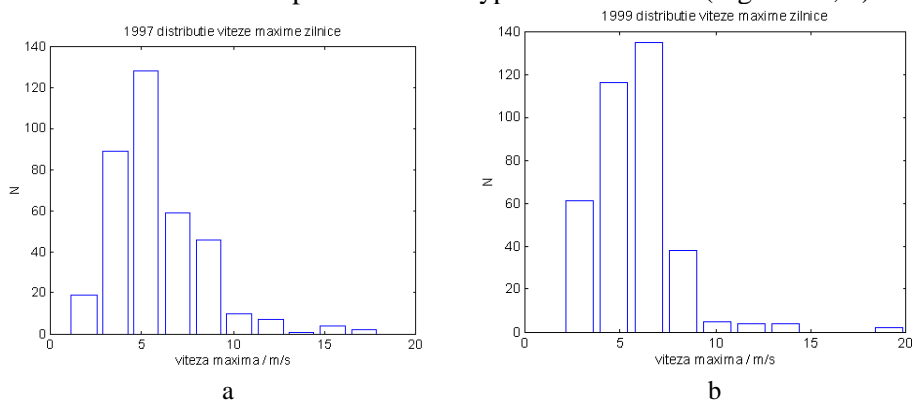
Fig 1. Distributions of daily maxima speeds at site (Iasi) per year of observation:
a- 1997; b- 1999

The distributions of mean speeds are presented in Table 2.

Table 2 Statistical data of the standard mean speed data measured at natural scale (Iasi airport) on 10 minutes period of averaging

Year	Mean speed V_m	STD,σ	Maximum value, V_{max}	Minimum value, V_{min}	Gust factor, $G= V_{max}/ V_m$	Skew	Kurtosis
1997	3.0	1.8912	11.5	0.0	3.833	1.2670	2.3521
1998	2.8	1.7256	12.0	0.0	4.285	1.2149	2.5898
1999	2.7	1.6757	12.3	0.3	4.555	1.3939	3.5870
2000	3.0	1.6488	13.5	0.3	4.5	1.3780	4.1562
2001	2.9	1.2708	10.0	0.8	3.448	1.5205	4.0408
2002	2.8	1.2716	9.5	0.3	3.393	1.7498	5.1074
2003	2.9	1.2060	9.0	0.5	3.103	0.9302	1.4403
2004	2.8	1.3250	9.5	0.3	3.393	1.4729	3.1467
2005	2.7	1.2782	8.0	0.5	2.963	1.2322	1.6540
2006	2.6	1.1855	7.5	0.3	2.884	1.0477	1.4864

A graphical representation of the processed data brings to light some peculiar distributions that may be considered as anomalies, like the mean speeds presented below; being random values, we may admit that there are always possibilities of

not obtaining the expected distribution, usually due to the lack of sufficient number of data. But similar results of the analysis developed in the succeeding year might motivate a second thought (Figure 2 a, b); inside the observation period the successive periods of lulls are separated by a storm and the whole interval becomes non stochastic and non-stationary.

The conclusion is that these data do not correspond to the same conditions from atmospheric or synoptic point of view; more clearly, they do not characterize a neutral stable atmospheric event.

a   b
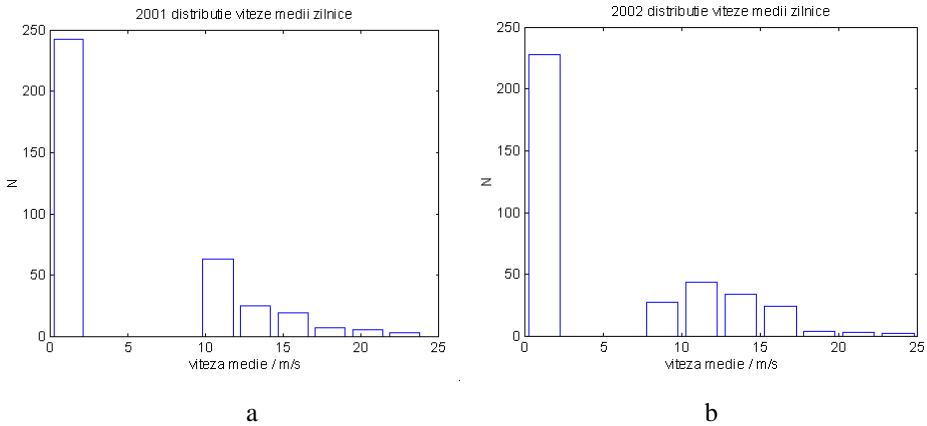
Fig. 2. Distribution of the mean speed data per year: a- year 2001; b-year 2002

2.2. Wind velocity components

Wind manifestation in neutral stable atmosphere is described by the in-wind dynamic velocity u of the turbulent flow at a certain height; it is expressed by a relationship between the time varying mean velocity, $\bar{v}(t)$ and the fluctuating component of $v, \tilde{v}(t)$ respectively:

$$v(t) = \bar{v}(t) + v'(t) \tag{2}$$

Although a random process, the fluctuating velocity has a quasi-deterministic nature being driven by the mean value at large scale; the quantity linked to the atmospheric turbulence, is a small scale random function:

$$v(t) = \bar{v}(t)\left[1 + I_v(t) \cdot \tilde{u}(t)\right] \tag{3}$$

where I_v is referred to as the time-varying turbulence intensity:

$$I_v(t) = \frac{\sigma_v(t)}{\bar{v}(t)}$$

(4)

The basis of the analysis of wind speeds in the three different kinds of manifestations relies on this decomposition because:

- in the case of neutral stable flow the mean wind velocity, the standard deviation and the turbulence intensity I_v are referred to a time interval T = 10 minutes and, on such interval, they are constant quantities and the reduced fluctuating wind velocity is a random stationary Gaussian process;
- however, in the case of thunderstorms, the mean value averaged over a 10 minutes interval is not representative.

In the modern literature scientists operate with time varying mean velocity values and moving average period T [11], for ex. 20 seconds between two extreme situations; if too large, it may be influenced by the general trend of the mean value, if too small the mean part of the velocity is contaminated by the turbulence fluctuations at small scale.

- in the case of gust fronts the mean velocity, standard deviation and turbulence intensity extracted from 10 minutes averaging interval are also constant but due to the imbalanced wind flow momentum.

Differently from extra-tropical depressions and also from thunderstorms, however, the reduced fluctuating wind velocity is a random stationary but non-Gaussian process.

3. STUDIES IN ATMOSPHERIC LAYER WIND TUNNEL AND RESULTS

3.1 Simulation of wind velocities in wind tunnel

The simulations of wind flow in atmospheric boundary layer at reduced scale are always a difficult task and it seems that they raise endless subjects of study. In reverse, there are several advantages in modelling at small scale and between them one of the most relevant is that we may fully control the characteristics of the flow inside the tunnel.

The events that reproduce the wind action at small scale in tunnel are theoretically based on the status of relative equilibrium of the dynamic pressure inside, defining the neutral stable atmosphere; in the neutral stable atmosphere a quasi-stationary flow is characterized by quasi deterministic values of the mean speed and of the turbulence intensity. Still, even for a specific constant roughness, constant values of the wind velocity are not expected, the process remaining random.

The most important aspect in modelling is perhaps the sampling rate since the scale depends on the relationship between the in space geometry and the time:

$$L_M = V_M \cdot T_M = \frac{L_P}{s} = \frac{V_P \cdot T_P}{s} \tag{5}$$

where $L_{M(P)}$, $V_{M(P)}$, $T_{M(P)}$ and s are the relevant geometric dimension, the speed and the time of the model and of the prototype and s is the scale ratio. While the geometry and the speed limits depend on the possibilities of the tunnel, the time may be adjusted as to fit the scale.

As both geometric dimensions (length scale) and the period of time associated with an event are reduced to fit the model scale (for ex. from 1/50 to more than 1/400) then adjusting to this scale means to increase the frequency of data acquisition.

Based on the assumptions previously stated regarding the Gaussian distribution of the stationary wind velocity, there are conversion relationships of speeds for different averaging time intervals [7]:

$$1.05 \cdot V_{ref}^{1h} = V_{ref}^{10\min} = 0.84 \cdot V_{ref}^{1\min} = 0.67 \cdot V_{ref}^{3\sec} \tag{6}$$

As stated before, data acquisition in the wind tunnel laboratory is mandatory and depends on the characteristics of the equipment which converts the speed or pressure signal into analogue data. The analogue data are transformed into digital data, these processes being electric signals.

The frequency of data acquisition in the laboratory corresponds to the possibilities of measuring electrical signals and high frequencies are the most usual. A consequence of the sensitivity of the measuring equipment to higher frequencies consists in reducing the time of acquisition, which is consistent with the principles of scale modelling; indeed, the time of observation is contracted in the wind tunnel in comparison with the periods of observation at natural scales, in order to fit the scale criteria. Another consequence is that, in reducing the time of acquisition in the tunnel, we practically induce the probability of producing sequential events which will not replicate themselves integrally, reflecting the character of random process although characterized by expected ("deterministic") values of mean velocity and gust values, the result of the expected turbulence and roughness length, respectively.

Still, experiments in wind tunnel rely on expected values of wind speed and pressures; they are the keystone of a reliable wind action reproduced at scale and consequently, should satisfy all the criteria imposed by both theoretical (scientific) concepts and practical experience.

The experience in these directions shows that although higher frequencies of acquisition are necessary, longer periods of acquisition are nevertheless desirable because they offer more realistic values of the statistic descriptors.

In the context of extending the knowledge for modelling different modes of manifestation of the wind action in wind tunnel, the time of acquisition and the frequency of sampling have their key role to play. Modelling the wind speed at small scale is mandatory and the calibration of the measured data is based on the reference values of full scale speed and pressure; the standard reference is to fit the scaled speed to the mean wind speed at 10 m above the ground level on a II category of roughness terrain.

According to the method adopted by Solari on data obtained from the anemometers [2], a prior splitting the samples in time intervals scaled to 10 minutes in nature followed by the statistical processing these data on these successive intervals is a possibility to put in evidence the parts of the event which are stationary and the non-stationary part as well. Although the phenomena that determines the manifestations of storms or of gust fronts are mainly of convective nature and air convection is difficult to be modelled in wind tunnel, their effects observed at natural scale may be artificially reproduced in wind tunnel in the conditions of similar model of wind action random manifestations.

3.2 Experiment and Results

The study presented herein is developed in the boundary layer wind tunnel SECO 2 belonging to the Laboratory of Building Aerodynamics of the Faculty of Civil Engineering and Building Services. It refers to the simulation of the wind flow over a terrain with moderate roughness, corresponding to a mean speed profile with the power law exponent $\alpha = 0.28$ (see Figure 4) and the acquisition of sets of along wind speeds with the specific equipment.
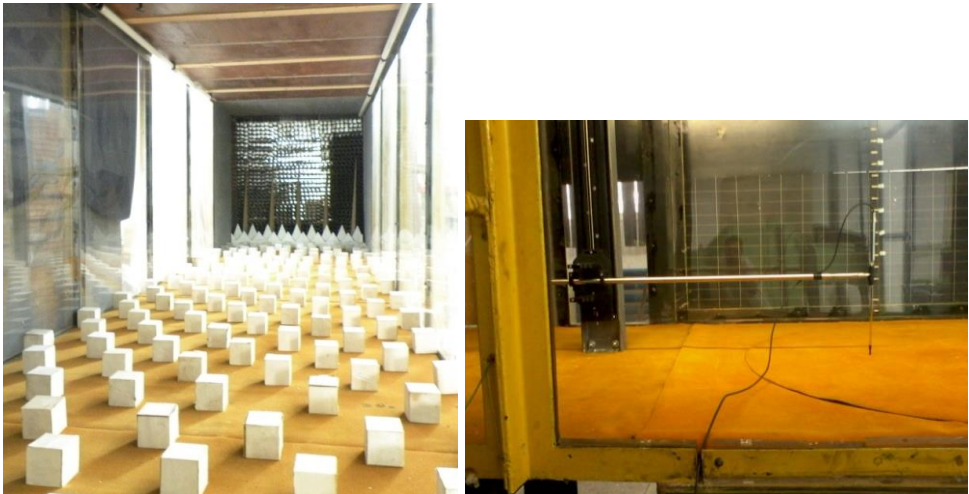
Fig. 3 View inside the BLWT: a) system for generating the turbulence of the flow over an II category of terrain; b) equipment for acquisition of wind velocity

The characteristics of the wind flow in the simulated boundary layer are presented in the figure above, being in concordance with the reference natural conditions, exponent of the mean wind speed profile and the turbulence intensity.

The acquisition of the wind speed is run at the reference height in laboratory for a time period of 2 minutes with a sampling rate of 1/sec, depending on the performance of the equipment, but also because we had in view the statistic distribution, not necessary the maxima values of the velocity. Data were processed over the total period of time, respectively over sequential 10 sec. time intervals. The 10 seconds extension of the periods was decided with respect to a 1/200…1/300 reduced scale of the time, corresponding to the hourly mean speed but also by knowing that the 10 minutes reference period at full scale would correspond to a period of 1…2 sec, reducing the number of sampled velocities to no more than 1 or two samples.

(a)

(b)
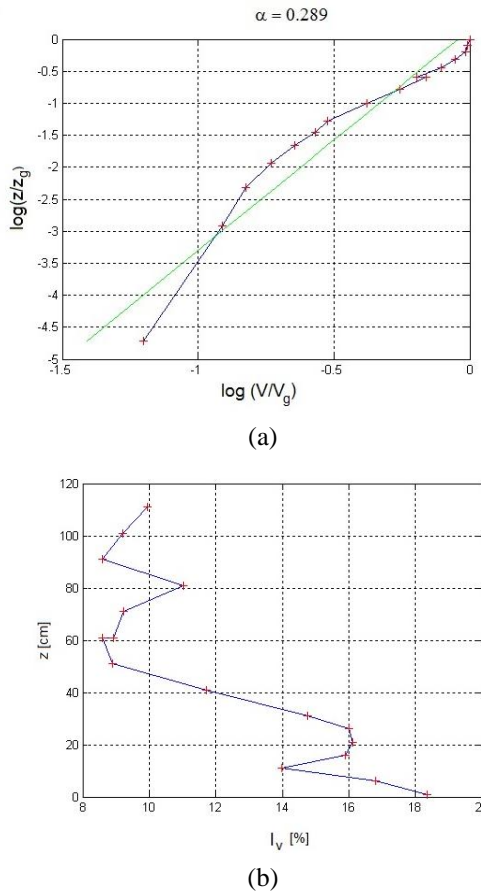
Fig. 4 Characteristics of the simulated wind profile in wind tunnel: a) in-wind mean speed profile (exponential law); b) in wind turbulence intensity, I_v

At this point it has to be mentioned that for a representative model of the peak values recorded in nature at intervals of 10 minutes or less, the frequencies of data acquisition must be much higher than 1 Hz.

The results of the statistic processing of the data are presented in Figure 5; the first two records are the random values of the velocity v{t} during 120 seconds at heights that correspond to the full scale reference height (10 m) for the reduced scales of modelling common to the wind tunnel SECO 2 (1/200…1/400).

The records in Fig. 6 are obtained after processing the velocities measured closely to the top part of the tunnel; the turbulence of the flow in that part is under 10%, the flow becoming close to laminar, in concordance with the models of turbulence in boundary layer wind tunnels.
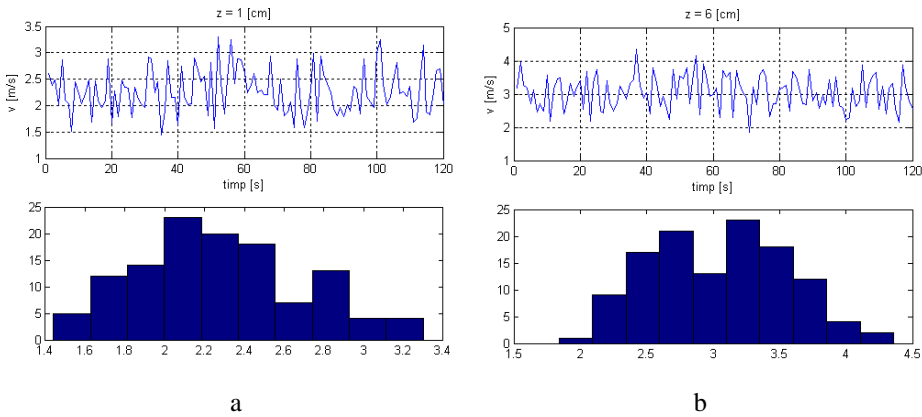
Fig. 5. Recorded values of the velocity in the wind tunnel and the statistic distributions: a) - at 1 cm height; b) - at 6 cm height

A synthetic analysis of the statistical processing of the velocities measured in laboratory was developed. It was meant to put in evidence the statistic descriptors: mean values, standard deviation, ratio of maxima related to mean values (gust factors), skew and kurtosis.
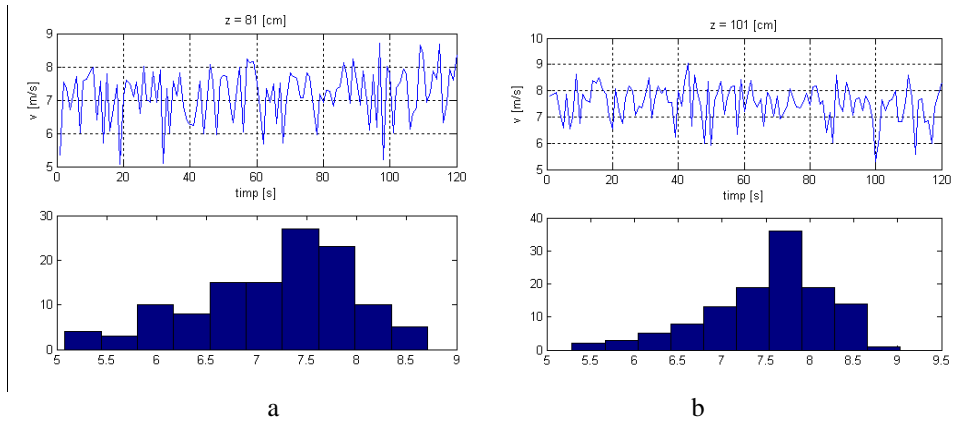
Fig. 6 Recorded values of the velocity in the top part of the wind tunnel and the statistic
distributions: a) - at 70% of the total height of the tunnel; b) - at 85% of the total height

For a comparison between the standard velocities measured at full scale and the
velocities measured in wind tunnel, the values obtained at a reference height (at 10
above the ground in nature) are presented in Table 3 below.

Table 3 Analysis of speeds measured at reference heights in nature (10 m) at time intervals
corresponding to 1 hour (about 10 sec in laboratory)

| Crt. Int.	Mean speed $V_{mean,10}$ (m/s)/10 sec time interval		Peak speed value, $V_{peak,10}$ (m/s)/10 sec time interval		Gust factor, $G=V_{peak,10}/V_{mean,10}$		Skew		Kurtosis	
	1cm	6cm	1cm	6cm	1cm	6cm	1cm	6cm	1cm	h=6cm
1	2.40	3.40	3.15	4.42	1.3086	1.2984	0.7946	1.0209	-0.0084	1.7747
2	2.51	3.45	3.1	4.44	1.2335	1.2843	0.0734	0.7684	-0.2338	0.3655
3	2.41	2.86	3.1	3.36	1.2841	1.1715	0.6370	0.2247	-0.4754	-1.1955
4	2.41	3.09	3.15	4.38	1.3070	1.4174	0.6500	1.2859	0.40294	0.8822
5	2.66	3.07	3.1	3.73	1.1627	1.2165	-0.7597	0.0766	-0.1078	-0.8996
6	2.21	3.16	2.66	4.29	1.2014	1.3558	-0.0446	0.8394	-1.7390	-0.7096
7	2.40	3.08	2.9	3.82	1.2043	1.2378	0.3754	-0.2352	0.7633	0.5111
8	2.25	3.16	3.3	3.61	1.4679	1.1431	1.5821	0.6924	1.4010	-1.201
9	2.37	3.22	3.15	3.57	1.3291	1.1076	1.5821	-0.779	1.4010	-0.667
10	2.32	3.24	2.94	3.57	1.2694	1.3277	0.1530	0.5911	0.9335	0.3243
11	2.46	2.95	3.13	4.04	1.2713	1.3681	0.4791	1.1148	-1.1672	0.5482
12	2.49	3.27	3	3.86	1.2057	1.1782	1.039	0.1953	0.4373	-1.571

4. CONCLUSIONS

Solari's work is based on continuous measurements with modern anemometers and an extensive acquisition [2]. A typical 1-hour sample of a stationary and Gaussian event recorded by the anemometer displays relatively high mean wind velocity (mean velocity averaged on one hour is 12.94 m/s and a 1 second gust peak is 20.40 m/s), the turbulence intensity 0.16 corresponds to a standard II category terrain and the gust factor, G of 1.58 is typical of neutral atmospheric conditions; the value of the skewness over one hour record is -0.08 and the kurtosis is 3.25 confirming the Gaussian distribution.

Records of thunderstorms displays lower mean velocities high peak values and gust factors of more than 2…3 and a non-Gaussian distribution; in the case of gust fronts the same low mean values, high gust factors but skewness and kurtosis denote a moderate non Gaussian distribution.

Finally, a very important aspect is that the turbulence intensity varies with the intensity of the event, increasing in the case of the thunderstorms and the gust fronts.

The raw data from Iasi airport are not the result of continuously records; the result consist in successive separate events with mean and maxima values of very different level of intensity of the whole measured values during a specific event, the identification of certain specific characteristics is possible.

NP 082 presents the following data for Iasi, by artificially extension of the observation period: maximum speed of 40 m/s, which is also the characteristic value for 0.98 probability of non-exceeding, mean of maximum speeds/year, 22 m/s and skewness 0.3.

From the data gathered at site and averaged on 3 sec periods, presented in Table 1, it is not possible to put in evidence these standard data; still the similarity with the data presented by Solari is evident, mainly the G values, the skewness and kurtosis. In Figure 1 a, b typical Gumbel maxima distributions may be observed. The statistical descriptors in Table 2 show the random process of the wind speed; the low mean values and high maxima values, the gust factors of more than 2, up to 4.5 are not uncommon, these values being associated with wind pressure local or global coefficients in the codes of design to wind action [6]. But these values show that whether continuous observations were developed, similar values to the ones reported by Solari and associated with wind manifestations other than those developed in neutral stable atmosphere. In this case steps for identification the thunderstorms and the gust fronts must be done by site observations at natural scale.

A mixt climate at small scale in laboratory may be identified if the statistic descriptors that characterize it are known with a relying degree of accuracy. The

simulation described in par.3 displays a general aspect of a Gaussian event, being described as stationary and stochastic. The values of the gust factor G of about 1.5 close to the reported values of the maxima wind velocity distributions and the shapes of the distributions presented in Figure 5 a, b show the asymmetry of Gumbel distributions. But the asymmetry varies at least with respect to the position on the height of the tunnel, being both on left and on right side; sometimes the process is symmetric.

In the study however, the analysis of the wind velocities recorded in fix positions in the wind tunnel (at 1 cm and 6 cm height, respectively) was developed by separating the period of observation in time intervals in order to observe the succession of the events. From Table 3 it may be seen from the II and III order moments of the statistical distribution, the skewness and the kurtosis, that the processes have alternative asymmetries left and right. During the time intervals quite symmetric distributions are put in evidence, the statistic indicators of skewness and kurtosis showing a Gaussian process which characterize neutral stable events; but they alternate in time with asymmetrical processes. Although the nature of these events in the wind tunnel is not the same as the one that governs the synoptic dynamics, it is important to understand there meaning and their possible role of alteration of the simulation.

On the other hand, if more extensive data acquisition is available describing non neutral stable atmosphere events, the simulations can take into account this fact by modelling the process in the wind tunnel by adjusting the time intervals when measuring the speed and the turbulence scales.

More accurate statistical processing of the simulated events is a step further in modelling the natural events that affect in a most unfavourable way the built habitat.

References

1.   Davenport, A.G., *The application of statistical concepts to the wind loading of structures*, Proceedings of the Institute of Civil Engineers, 19, 449-472, 1961
2.   Solari G., De Gaetano, P., Pia Repeto, M., *Wind Loading and Response of Structures in Mixed Climates*, Proceedings of the Eight Asia Pacific Conference on Wind Engineering, dec 10-14, 2013, Chennai, India, Research Publishing Services, ISBN 978-981-8012-8, DOI: 10.380/978-981-07-8012-8_Key-03
3.   Gomez, L., Vickery, B.J., *Extreme wind speeds in mixed climates*, J.W.E.I.A., 2, 331-344, 1977/1978
4.   Kasperski, M., *A new wind zone map of Germany*, JW.E.I.A., 90, 1271-1287, 2002
5.   De Gaetano, P., Solari, G., *Thunderstorm wind velocity decomposition and moving average period*, Proceedings of the Eight Asia Pacific Conference on Wind Engineering, dec 10-14, 2013, Chennai, India
6.   EN 1991-1-4, Eurocode 1. *Actions on structures - General actions*, Part 1-4, Wind actions, 2005
7.   NP-082-04, *Cod de proiectare. Bazele proiectarii si actiuni asupra constructiilot. Actiunea vantului*, 2005
8.   Cook, N.J., *Towards better estimation of extreme winds*, J.W.E.I.A., 9, 295-323, 1982

9.   Grant tip A CNCSIS cod 265/2007-2008, „*Dezvoltarea tehnicilor de evaluare a acţiunii vântului în tunel aerodinamic pe suprafaţa clădirilor înalte în vederea optimizării proiectării şi reducerii riscului în exploatare*", Contract GR 33/2007, tema 27/2007, ", Contract GR. 77/2008, tema 39/2008, director de proiect Teleman C.
10. Teleman, C., Silion, R., Axinte, E., Ţăranu, N. *Local full scale wind speed measurements used in parallel with wind tunnel modelling*, Proceedings of the 4th International Conference on Dynamics of Civil Engineering and Transport Structures and Wind Engineering DYNWIND'2008, mai 2008, EDIS Zilina University publisher, first edition, ISBN 978-80-8070-827-6, Slovacia, pp. 38-41
11. Chen, L, Letchford, C.W.*, A deterministic –stochastic hybrid mode of downbursts and its impact on a cantilevered structure*, Engineering Structures, 26(5), 619-629

Benefits and Drawbacks of Using on-line Assessments of Student Learning in Construction Education

Cristina Cosma

Department of Construction Management, Wentworth Institute of Technology, Boston, MA, 02115, USA

Summary

Assessment of student learning is a critical step for achieving a quality learning environment in construction/civil engineering education. Proper assessment strategies are also significant drivers of the paradigm shift from instruction based education to learning based education. Additionally, accreditation requirements call for programs to "implement and support a systematic and broad-based approach to the assessment of student learning".

The paper will review and compare the two major points of view on student learning: the constructivist instructional reform and the measurement/technical quality approach. The two methods of measuring student learning (summative evaluation and formative evaluation) will be described.

Even if on-line assessments of student learning use typical summative evaluation tools like tests, quizzes and surveys, they can also be categorized as formative when used constantly during the semester (i.e. practice tests or quizzes).

For the past three years the author has been the principal instructor for CONM150 "Heavy Construction Equipment" class which is taught to Construction Management (CM) freshmen. After two years of using traditional assessment techniques, in spring 2015 the instructor adopted Blackboard Learn (BB) as a course management software. Class assessments were exclusively offered through BB. The paper will cover the way in which assessments on BB were designed. A list of lessons learned will be presented based on grade comparison and also on the students' feedback and comments.

KEYWORDS: Instructional Paradigm, Learning Paradigm, Accreditation, Quality Learning Environment, Student Assessment, Blackboard Learn.

1. INTRODUCTION

Higher education in the 21st century is characterized by a dramatic change from the "instruction paradigm", where the mission of the college is to deliver (50-min) instruction to students, to a new "learning paradigm" which envisions the institution itself as a learner-over time [2]. The ultimate goal of this transformation is to improve

efficiency and effectiveness of learning through the change in emphasis from objective-based/input-based education to outcome-based education [4].

The growing importance of transparency and accountability that characterizes the new paradigm has led to increased demands for colleges and universities to engage in outcomes assessment [13]. Institutions of higher learning started to design new program structures, identify desired learning outcomes, determine ways to align and attain their outcomes through revising course content, provide pedagogical training for faculty, adopt a variety of teaching and learning methods, and devise appropriate assessment criteria and methods [4].

Another important driving force towards the design and implementation of a proper assessment system in US (engineering) education was the Accreditation Board for Engineering and Technology (ABET) which specifically requires the education institutions to set in place "an assessment and evaluation process that periodically documents and demonstrates the degree to which the program outcomes are attained" [1]. The data and evidence accumulated through assessment practices will further be interpreted and will result in and evaluation process whose final goal is to determine the extent to which program outcomes or educational objectives are being reached; the end result of this process will be decisions and actions taken to improve the program and achieve higher quality education.

As far as assessment history is concerned, four major components influenced assessment practice in the past century: psychometrics (the measurement of skills and knowledge, abilities, attitudes, personality traits, and educational achievement), theories of cognition, the nature of curriculum, and the sociopolitical context of education [10]. Consequently assessments were directed towards checking whether students can perform according to certain predefined measurements of appropriate responses and were routinely carried out to estimate the strengths and weaknesses of students. In the 21st century these type of assessments show little effectiveness in contributing to improve the educational outcome.

2. CONSTRUCTIVIST VS TRADITIONAL APPROACH

Two main teaching approaches are coexisting in the 21st century academic system: the traditional (instructor centered) teaching and the progressive (student centered) constructivist approach. Present pedagogical approaches make use of a mixture of both systems depending on the requirements and configuration of a particular class, on the subject taught, on the instructor's own beliefs and also on the administrative policy of the college itself.

2.1. The traditional approach in teaching

The most common approach at university level remains the traditional teaching approach that is using the lecture method (Figure 1a). Traditional instruction is based on a theory of learning that suggests that students will learn facts, concepts, and understandings by absorbing the content of their teacher's explanations or by reading explanations from a text and answering related questions [11].

This approach has been criticized lately for the unilateral transfer of information from instructor to the (passive) students. In the traditional approach instruction is strictly based on a fixed curriculum, curriculum which will rely mainly on textbooks. The approach is instructor centered showing reduced level of student choice, involvement and/or interaction. The instructor has total authority and decision power on the selection of subject matter (based on the Syllabus), structure presentation, teaching methods and pace.

2.2. The constructivist approach in teaching

The constructivist approach (Figure 1b) is based on a theory of learning that suggests that understanding arises only through prolonged engagement of the learner in relating new ideas and explanations to the learners' own prior beliefs [11].
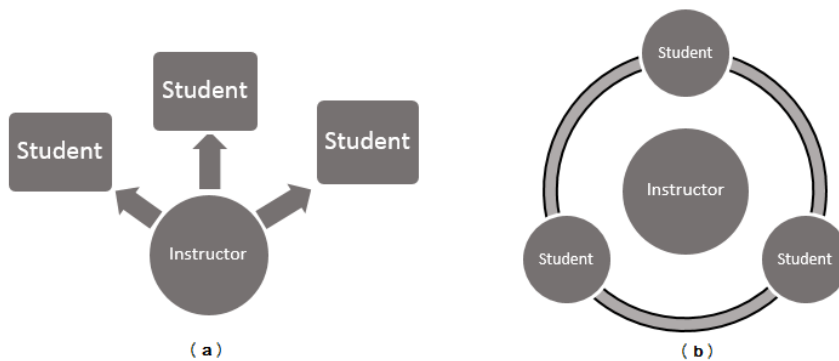
Figure 1. Traditional teaching approach (a) vs constructivist approach (b)

Some distinctive characteristics of constructivist teaching according to Kim [7] are:
- Students are encouraged to engage in free discussion, ask questions, share and test own ideas and be innovative;
- Students are invited to generate ideas even before any instructional material is presented to them;
- Students are encouraged to challenge and/or use different concepts and ideas after a thorough reflection and analysis;
- Instructional strategies are changed to enhance students' thought, experience and interests.

2.3. Teaching Approach in (Construction) Engineering

Student success can be achieved if the teaching style will match the students' learning styles. From the 32 student learning styles identified by researchers, the usual methods of engineering education tries to address five main categories: intuitive, auditory, deductive, reflective, and sequential.

Most engineering courses will favor the intuitive learners by emphasizing concepts rather than facts and through using primarily lectures and readings (words, symbols) to transmit information. But the majority of engineering students are sensors (hands-on, practical learners), suggesting a serious learning/teaching style mismatch in most engineering courses which might result in low test grades, unresponsive classes, poor attendance and dropouts [6].

Some of the teaching techniques recommended to be used in engineering in order to address all learning styles and enhance student education according to Felder are [6]:
- Motivate learning;
- Balance concrete information and abstract concepts;
- Balance practical-problem solving methods with fundamental understanding;
- Provide explicit illustrations of intuitive patterns and sensing patterns;
- Follow scientific method in presenting theoretical material;
- Use pictures, schematics, graphs and show films;
- Use computer assisted instruction.

3. TYPES OF ASSESSMENTS

3.1. The need for assessment

Assessment of student learning is an intrinsic part of the learning process as a whole and one of the most powerful tools used both for feedback and for advancement of instruction. In tandem with the paradigm shift in education the approach on assessment has also evolved from the traditional assessment *of* learning towards the assessment *for* learning. Assessment is also an influential tool that drives student learning as students allow assessment define and prioritize what is important to learn, and ultimately how they spend their time learning it [9].

Figure 2 below shows the four eras of progressive evolution of learning assessment in US [12] driven towards the newly expressed demand for a culture of evidence of student learning.
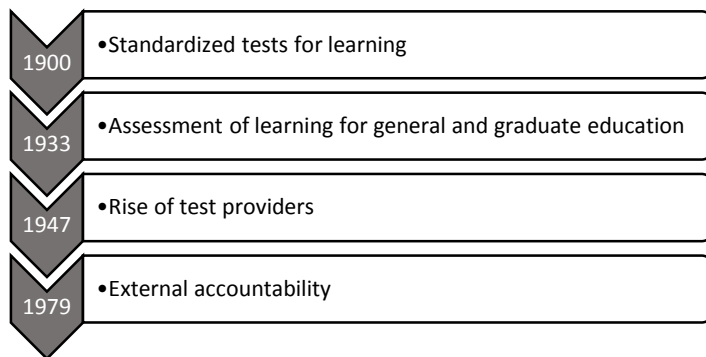
Figure 2. The evolution of assessment in US

Before the beginning of the 20th century assessment had already developed into the forms and procedures that still characterize it today [14]. Alternatively there is new attention to developing creative ways to assess student learning. The new approach is trying to align assessment tasks with real life processes of problem-solving as the traditional examinations are believed not to resemble the work and life situations the graduates will have to face. The new technological possibilities are also a major source of innovation, with universities actively exploring the potential of computer-based assessment to assess learning and provide students with rapid and informative feedback [8].

Two main types of assessment practices have emerged in time and are widely used in academia: formative assessment and summative assessment.

3.2. Formative assessment

Formative assessment, is actually used as practice for the student and as a check for their understanding during the learning process. It provides feedback to the student on their learning and also allows students to make revisions and provides them with the opportunity to improve. Additionally the formative assessment process guides instructors in making decisions about future instruction. Homework, observations, conferences, Q&A sessions and other periodical in-class activities are specific examples of formative assessments.

3.3. Summative assessment

Summative assessment is assessment that is used to measure student performance and contribute to a student's grade in a course, module, level or degree. Summative assessments are cumulative and are scheduled at the end of a significant part of the course (Quizzes), half way through the course (Midterm Tests) and/or at the end of a course (Final Exam). Term papers, projects, portfolios and student evaluation of teaching effectiveness are other examples of summative assessments.

The biggest difference between summative and formative assessments is that the summative assessments are product-oriented (learning achieved) while the formative assessments focus on the process toward completing the learning. Another difference is that once completed, no further revisions can be made on the summative assessments which will end up with a grade as a measure of student learning. If students are allowed to make revisions, the summative assessment becomes formative.

3.4. On-line assessment

The need to improve assessment techniques and strategies increased in tandem with the technological advances and transformations in the delivery of instruction. One of the most often used tools for offering on-line summative assessments is Blackboard.

Blackboard offers a wide variety of formats for questions used in assessments (Figure 3) and offers the advantage of providing the instructor with automatic grade calculation.

Blackboard also gives to the instructor the ability to administer quizzes 24/7 with safeguards such as random questions for each student, timed tests, password protection and adaptive release of quizzes. Using a variety of formats addresses multiple learning styles, and using pools of questions with random blocks for tests mitigates against student collaboration on tests.

A major concern is whether computer-based testing meets the needs of all students equally and whether some are advantaged while others are disadvantaged by the methodology [5].

Create Question ⌄
- Calculated Formula
- Calculated Numeric
- Either/Or
- Essay
- File Response
- Fill in Multiple Blanks
- Fill in the Blank
- Hot Spot
- Jumbled Sentence
- Matching
- Multiple Answer
- Multiple Choice
- Opinion Scale/Likert
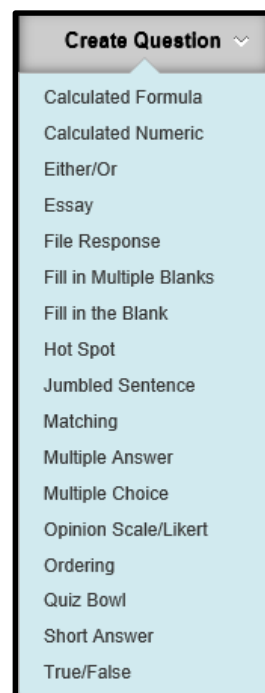- Ordering
- Quiz Bowl
- Short Answer
- True/False

Figure 3. Question types

Among the main advantages of on-line administration of assessments are [3]:
- Immediate feedback for students;
- Objective grading by eliminating human error
- Easy to update and edit
- Increased accessibility (anytime/anywhere)
- Item analysis helps instructor identify areas for improvement

4. DEVELOPING ASSESSMENTS FOR CONM150

CONM150 "Heavy Construction Equipment" is offered every spring semester to the Construction Management (CM) freshmen class. The course introduces students to current methods and equipment used in heavy construction projects including highways, tunnels, bridges, dams, storm drains, and sanitary sewers. Formative assessments (weekly quizzes) and summative assessments (midterm and final tests) constitute 60% of students' final grade.

In 2013 student learning in CONM150 was assessed by using constructed-response (CR), 'traditional" open-ended problems. In 2013 tests scheduled during the semester contained mainly open-ended problems while the final exam consisted mostly of multiple choice (MC) questions. In spring 2015 all tests were offered on Blackboard Learn and consisted primarily of MC, true/false (TF), fill in the blank and matching type of questions. A dramatic difference was noticed in students' final grades (Table 1) with a constant increase in final scores as the dominance of MC questions in tests increased too.

Table 1. CONM150 (average) final grades

	2013 (CR)	2014 (CR & MC)	2015 (MC)
Average Final Letter Grade (Average Final Grade)	C- (72)	C (77)	B (87)

The design of the MC questions in 2015 included choosing distractors or wrong answers based on the most common mistakes and misconceptions identified in 2013/2014 CR problems. In order to reduce errors and increase performance, a fixed number of 4 alternatives was used in the 2015 MC tests. Wrong answers received a grade of 0 (zero), which definitely encouraged guessing.

Students were asked to comment on the effectiveness and clarity of the on-line tests when they were filling the class evaluations at the end of the semester. From their written and sometimes verbal comments, and also from the instructor's own observations some lessons were learned as follows (Table 2):

Table 2. Students' comments on on-line assessment

Positive comments	Negative comments
• Guessing is helpful • Instant grading is appreciated • Less time consuming • Easy	• TF questions are more confusing than MR • Fill in the blank created problems with following format requirements • The lack of partial credit is disappointing and unfair • Would prefer "not to know so fast how (bad) I did" • Pictures/graphs should be in paper format • Concerns regarding cheating • "I hate Blackboard"

5. CONCLUSIONS

Recent developments in computer based technologies have a dramatic impact on teaching and assessment practices. On-line assessments are gaining more ground than ever due to undisputable advantages like time efficiency and accessibility (anytime/anywhere). Disadvantages in the area of connectivity issues, answer formatting and cheating can be handled through proper network development, student training and appropriate test design approaches.

Implementation of on-line assessments equally impacts students and instructors. Both test taking strategies and test development strategies must change accordingly while both students and instructor need training into taking/offering tests administered on Blackboard.

Comparison of traditional paper-based summative testing versus on-line testing in a CM freshmen class undoubtedly revealed the positive impact Blackboard administered test had on average class grades.

References

1. ABET, *Criteria for Accrediting Engineering Programs*, 2007, www.abet.org.
2. Barr, R., Tagg, J., From Teaching to Learning - A New Paradigm for Undergraduate Education, *Change Magazine*, Vol. 27(6), Taylor & Francis Group, Philadelphia, 1995, http://www.maine.edu/pdf/BarrandTagg.pdf.
3. Boyles, P.C., Maximizing Learning Using Online Student Assessment, *Online Journal of Distance Leaning Administration,* vol.14, 2011, http://www.westga.edu/.
4. Chung, C., Changing Engineering Curriculum in the Globalized World, *New Horizons in Education*, Vol. 59(3), Hong Kong, 2011, http://files.eric.ed.gov/fulltext/EJ955545.pdf
5. Erstad, O., Changing assessment practices and the role of IT, *International handbook of information technology in primary and secondary education*, Vol. 1, New York: Springer, 2008.
6. Felder, R.M., Silverman, L.K., Learning and teaching Styles in Engineering Education, *Engr. Education*, Vol. 78(7), 1988, http://www4.ncsu.edu/unity/felder/public/Papers/LS-1988.pdf
7. Kim, J.S., The Effects of a Constructivist Teaching Approach on Student Academic Achievement, Self-concept, and Learning Strategies, *Asia Pacific Education Review*, Vol. 6, No. 1, 2005, http://files.eric.ed.gov/fulltext/EJ728823.pdf.
8. McInnis, J.R., Devlin, M., *Assessing Learning in Australian Universities*, Centre for the Study of Higher Education, Canberra, Australia, 2002.
9. O'Farrell, C., *Enhancing Student Learning through Assessment – A Toolkit Approach*, 2005, http://www.tcd.ie.
10. Pellegrino, J. W., The Evolution of Educational Assessment: Considering the Past and Imagining the Future, *The sixth annual William H. Angoff Memorial Lecture,* Princeton, NJ, 1999, https://www.ets.org.
11. Ravitz, J.L., Becker, H.J., Wong, Y., *Constructivist-Compatible beliefs and Practices among U.S.Teachers*, NSF Grant #REC-9600614, 2000, http://www.crito.uci.edu/tlc/html/findings.html.
12. Shavelson, R. J., *A Brief History of Student Learning Assessment*, The Association of American Colleges and Universities, Washington DC, 2007, http://cae.org/.
13. Tremblay, K., Lalancette, D., Roseveare, D., *Assessment of Higher Education Learning Outcomes, Feasibility Study Report*, Vol. 1, OECD, 2012, www.oecd.org/edu/ahelo.
14. Wilbrink, B., Assessment in historical perspective, *Studies in Educational Evaluation,* 31-48, 1997, http://cae.org.

Maple Program for Studying Physics Phenomena with Applications in Civil Engineering

Irina Radinschi[1], Gabriela Covatariu[2] and Marius-Mihai Cazacu[3]

[1]*Department of Physics, "Gheorghe Asachi" Technical University, Iasi, 700050, Romania*
[2]*Department of Structural Mechanics, "Gheorghe Asachi" Technical University, Iasi, 700050, Romania*
[3]*Department of Physics, "Gheorghe Asachi" Technical University, Iasi, 700050, Romania*

Summary

Nowadays, students need adequate software to study Physics in universities and to have high levels of educational achievement and decent test scores. As our experience has demonstrated along the years, the combination of the experimental physics and computational methods motivates students to explore deeper the world of physics phenomena in a modern way. Also, they test their knowledge showing what they have learned.

This paper presents how physics phenomena are really well understood by the students because of using of a powerful algebra system like Maple 17. Also, the Maple 17 program it is a useful tool for solving physics problems. The Graphics package of Maple 17 program has been used for the applications at the laboratories and the seminars of the Physics I and Physics II courses that are designated to the first and second semesters, respectively at the Faculty of Civil Engineering and Building Services of "Gheorghe Asachi" Technical University.

The versatility and the wide range of applications of Maple 17 make it a powerful tool in assisting the students for solving problems and drawing graphs. This algebra system also provides many applications in engineering. Also, a platform as Maple presents advantages like speed, flexibility and many graphical facilities. For this reasons we consider the Maple program to be a reliable tool for teaching and learning physics.

In our work we present some examples of plotting the displacement and speed for damped systems. The plot command that creates a two-dimensional plot and the plots[animate] command that generates an animation are both used for making the graphs in the case of overdamped, critically damped and underdamped systems, respectively. Using this powerful algebra system the students will work faster and a deeper understanding of the differences between the three cases of damped systems will be developed.

KEYWORDS: Maple 17, Physics, Civil Engineering, physics phenomena, damped oscillations.

1. INTRODUCTION

Computational instruments are more and more widely used and many teachers deal with them to improve the teaching-learning process [1]-[5]. The experience in this area demonstrated that traditional methods in Physics and engineering together with computational physics are an important tool that gives to the students a deeper understanding of the physical phenomena and engineering studies [6]-[10]. These tools motivate and enable the students to improve their learning process and obtain better results to the exams. A plethora of programs like Maple, Mathematica and Matlab [11]-[13] are used for teaching Physics.

The authors use Maple 17 [11] to improve Civil Engineering physics teaching-learning. Among other many useful commands the software provides the commands used to perform calculations, to solve differential equations, to solve equations, to make plots and to produce plots with animations.

We have implemented both Maple and Mathematica programs in the Physics course, laboratories and seminars. Regularly, we improve our computational methods using the newest versions of these algebra systems. Also, the students can work in campus and achieve a better understanding of the physics phenomena and change ideas.

In this paper we focus our attention to the use of Maple 17 program for plotting some examples of physics phenomena that are studied in the chapter Damped Oscillations. We present the plots and plots[animate] commands for the cases of overdamped, critically damped and underdamped systems. The graphs of displacement and speed are plotted.

2. MAPLE 17 APPLICATIONS FOR DAMPED OSCILLATIONS

2.1. Applications of Maple 17 for damped systems – the plots for the displacement and speed

Because in the last decade we have gained experience in using several computational programs and developing simulations of physics phenomena [14]-[17] we decided to implement the newest algebra systems in the Physics course, laboratories and seminars.

As we pointed out above, the students are motivated to use the Maple 17 program because it provides them a high-level programming language plots and animations. They have used the program also for other calculations. Maple 17 allows to perform Numeric and Symbolic Computations, Visualizations, Matrix

Computations, Differential Equations, Control Systems Design, Dictionary of Math and Engineering, Units and Tolerances, Maplets and MapleNet, Smart Documents, Special Functions, Optimization, Statistics, Programming, Code Generation, and OpenMaple and Education and Assessment.

2.2.1. Plotting 2D of the displacement for damped oscillations

Firstly, we briefly present the theory for damped oscillations. In this case upon the oscillator act the elastic force and the friction. Writing the second law of dynamics and solving the differential equation for the displacement three different cases are obtained, the case of overdamped systems, critically damped systems and underdamped oscillations, respectively.

The second order linear differential equation with constant coefficients is given by

$$\frac{d^2 x}{dt^2} + 2\delta \frac{dx}{dt} + \omega_0^2 x = 0, \tag{1}$$

where $\frac{\gamma}{m} = 2\delta$ and $\omega_0^2 = \frac{k}{m}$ and with γ the damping constant, k the spring constant and ω_0 the natural frequency that represents the frequency at which the oscillator oscillates in the absence of any friction. The case of oscillation without friction is the case of harmonic oscillations. In the presence of damping the solution of equation (1) which is the displacement will behave differently depending on the size of γ (δ^2) relative to ω_0^2. Solving the characteristic equation

$$r^2 + 2\delta r + \omega_0^2 = 0, \tag{2}$$

the solutions are

$$r_{1,2} = -\delta \pm \sqrt{\delta^2 - \omega_0^2}. \tag{3}$$

There are three cases:

1. Overdamped system $\delta > \omega_0$, the roots of the characteristic equation (2) are real and negative and the displacement is

$$x(t) = C_1 e^{r_1 t} + C_2 e^{r_2 t}, \tag{4}$$

where C_1 and C_2 are two arbitrary constants that are determined from the initial conditions (displacement and speed at $t = 0$). This is the case of aperiodic motion and the mass crosses equilibrium position at most once. There are no oscillations.

2. Critically damped system $\delta = \omega_0$ in this case the roots of the characteristic equation (2) are equal and the displacement is

$$x(t) = C\,e^{-\delta t}. \tag{5}$$

This is an incomplete mathematical solution because the solution of (1) must have two arbitrary constant. Physically, these constants allow the setting of the initial conditions ($x(t)$ and $v(t)$ at $t = 0$). The complete solution of equation (1) is

$$x(t) = (C_1 + C_2\,t)\,e^{-\delta t}. \tag{6}$$

This is the case of critically aperiodic motion and the mass also crosses equilibrium position at most once. There are no oscillations, the body tends towards the equilibrium position without oscillates around it.

3. Underdamped oscillations $\delta < \omega_0$, the characteristic equation (2) has two complex conjugate roots and the displacement is

$$x(t) = A_0 e^{-\delta t}\sin(\omega t + \varphi), \tag{7}$$

with the amplitude $A(t) = A_0 e^{-\delta t}$ decreasing exponentially overtime. The system oscillates quasi periodic with the quasi frequency $\omega = \sqrt{\omega_0^2 - \delta^2}$. The mass can cross the equilibrium position infinitely often (excepting the zero solution).

In the following, we present the plots for the displacement in the cases of the overdamped, critically damped and underdamped systems, respectively.

In the case of the overdamped system the equation (1) has the expression $\dfrac{d^2 x}{dt^2} + 10\dfrac{dx}{dt} + 9\,x = 0$. The initial conditions for the displacement and for the speed are $x(0) = 1$ and $\dfrac{dx}{dt}(0) = 3$. Solving the characteristic equation and applying the initial conditions the constants C_1 and C_2 are determined. Their values are $C_1 = \dfrac{3}{2}$ and $C_2 = -\dfrac{1}{2}$.

The solution is given by

$$x(t) = \frac{3}{2}e^{-t} - \frac{1}{2}e^{-9t}. \tag{8}$$

The Maple commands for plotting 2D are with(plots); plot($\frac{3}{2}e^{-t} - \frac{1}{2}e^{-9t}$, t=0..10).

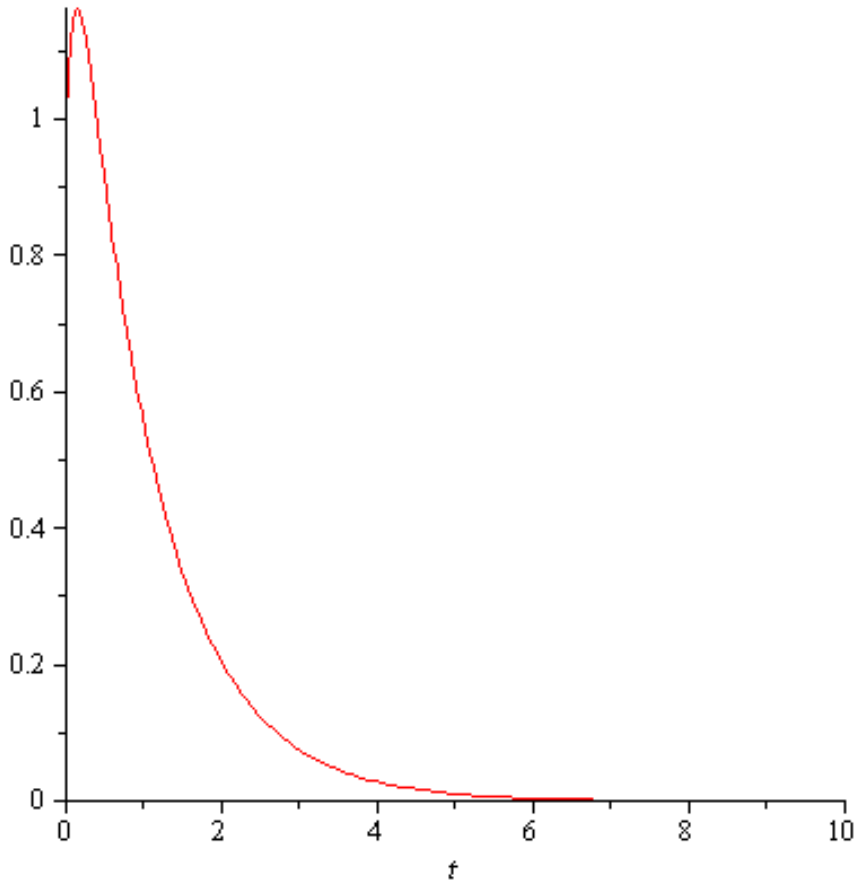The graph is given in Figure 1.

Figure 1. Displacement of an overdamped system

In the case of the critically damped system the equation (1) has the expression $\dfrac{d^2 x}{dt^2} + 4\dfrac{dx}{dt} + 4x = 0$. The initial conditions are expressed by $x(0) = 2$ and $\dfrac{dx}{dt}(0) = 5$. In this case, also solving the characteristic equation and with the aid of the initial conditions the constants C_1 and C_2 are $C_1 = 2$ and $C_2 = 9$. The displacement is given by

$$x(t) = (2 + 9t)e^{-2t}. \tag{9}$$

The commands are with(plots); plot((2+9t)e^{-2t} , t=0..10) and the plot is given in Figure 2.
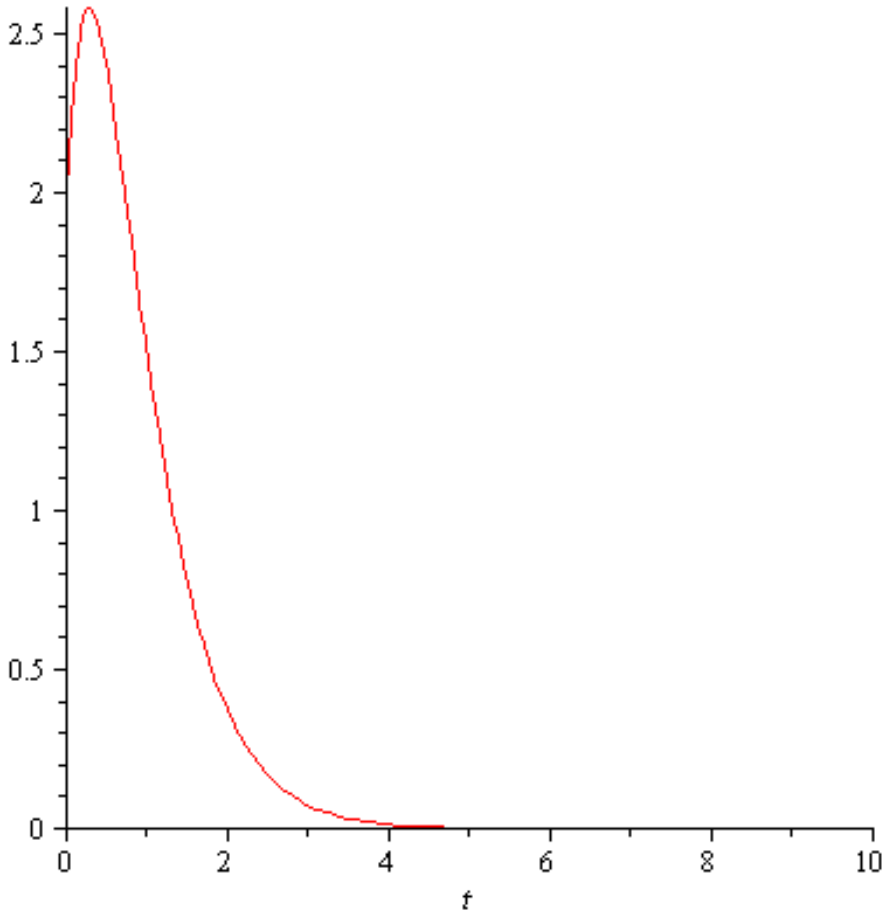
Figure 2. Displacement of a critically damped system

In Figure 3 is given the graph of displacement for the underdamped oscillations. In this case, for the equation (7) that is given by the expression $x(t) = A_0 e^{-\delta t} \sin(\omega t + \varphi)$ the expressions of A_0, φ, a and b are given by

$$A_0 = \sqrt{a^2 + b^2}, \quad tg\varphi = \frac{a}{b}, \quad A_0 \sin\varphi = a, \quad A_0 \cos\varphi = b. \quad \text{In this case}$$

A_0 represents the constant value of the amplitude and φ the initial phase.

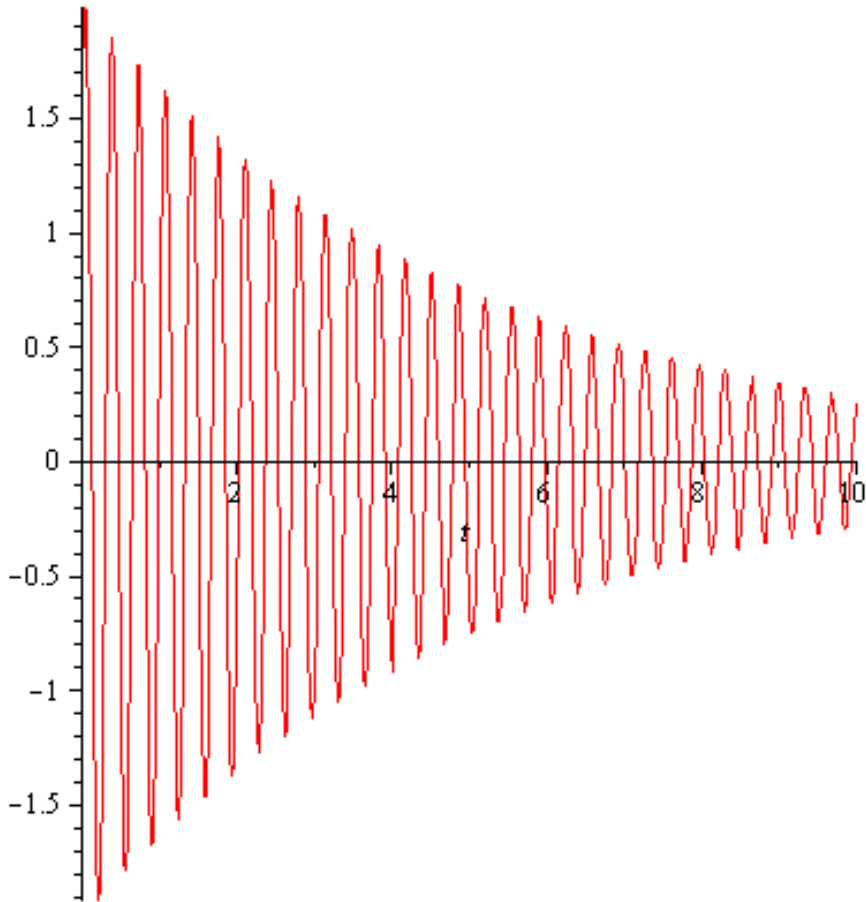The values obtained after the calculations for A_0 and φ are $A_0 = 2$ and $\varphi = \dfrac{\pi}{4}$.

Figure 3. Displacement of underdamped oscillations

The displacement is given by

$$x(t) = 2e^{-0.194t} \sin(18.25t + \frac{\pi}{4}).$$ (10)

The Maple commands for underdamped oscillations are with (plots); plot($2e^{-0.194t} \sin(18.25t + \frac{\pi}{4})$,t=0..10).

In Figure 4 we make the plots of the displacement for all the three cases of the overdamped system, the critically damped system and the underdamped oscillations on the same graph, respectively.

The Maple commands are with (plots); $f := \dfrac{3}{2}e^{-t} - \dfrac{1}{2}e^{-9t}$; $g := (2 + 9t)e^{-2t}$;

$h := 2e^{-0.194t} \sin(18.25t + \dfrac{\pi}{4})$; plot$\{ f(t), g(t), h(t), t=0..10\}$.
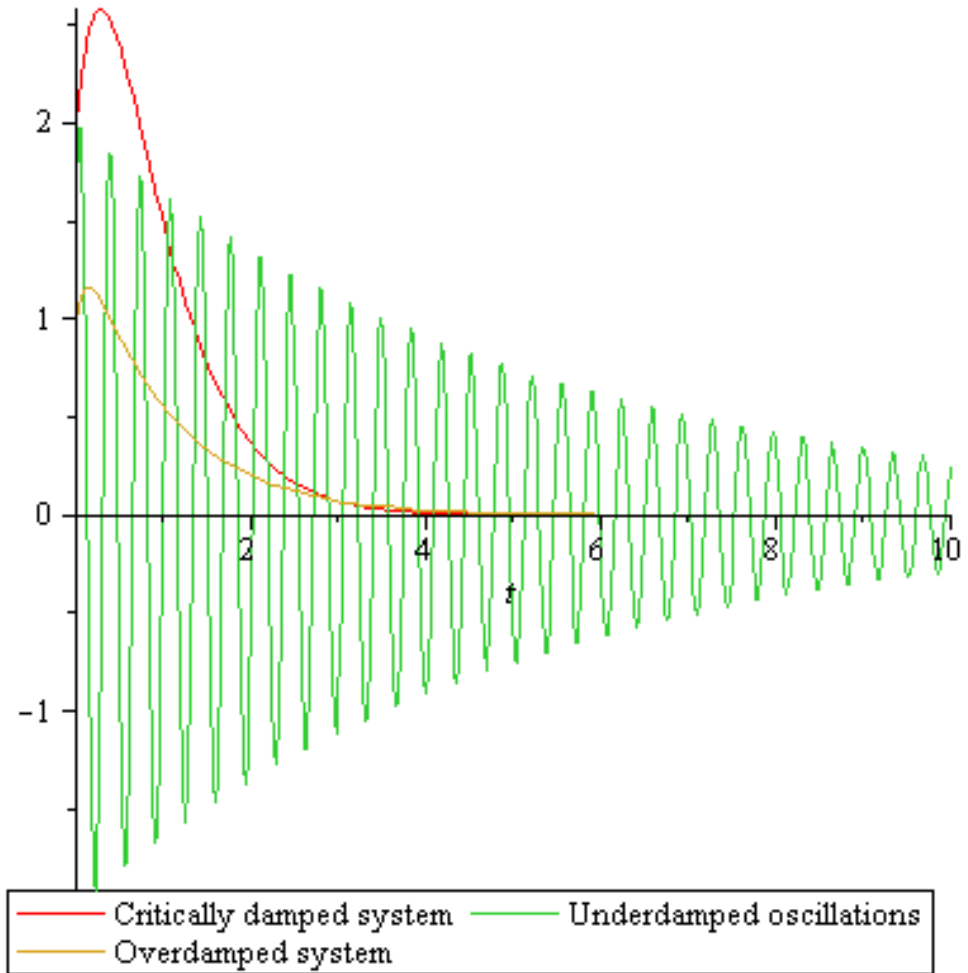

Figure 4. Displacements for the overdamped system, the critically damped system and the underdamped oscillations

In the case of the underdamped oscillations the larger the damping factor the quasi frequency becomes smaller. The quasi-period becomes longer. If the damping

factor becomes smaller for its zero value the case of harmonic oscillations is reached.

Using the command animate, after this click on Animation and Play we have the possibility to modify the values of the damping constant. In Figure 5 we present the case of underdamped oscillations. The commands are with(plots); animate (plot,[$2e^{-bt}\sin(18.25t + \dfrac{\pi}{4})$, t=0..10],b=0..10).
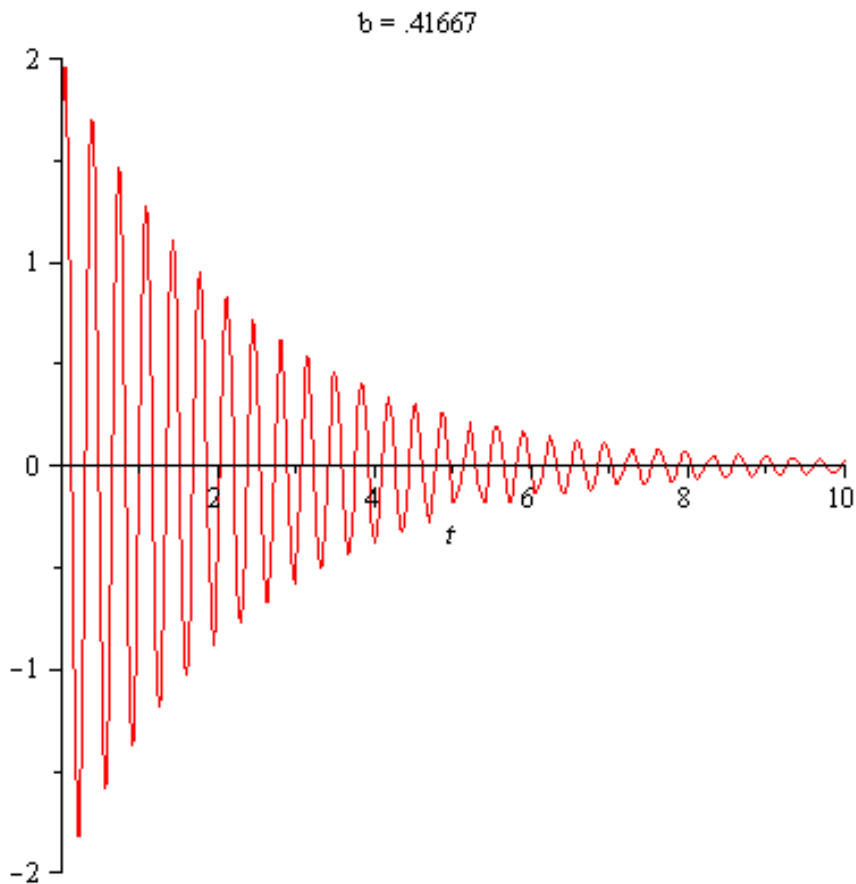

Figure 5. Displacement of underdamped oscillations with animation

2.2.2. *Plotting 2D of the speed for damped oscillations*

We plot the speed in the case of the underdamped oscillations given by equation (10).

The expression for the speed in the case of the underdamped oscillations is

$$v(t) = \omega A_0 e^{-\delta t}[-\frac{\delta}{\omega}\sin(\omega t + \varphi) + \cos(\omega t + \varphi)]. \tag{11}$$

For $\dfrac{\delta}{\omega} \ll 1$ the first term from equation (11) can be neglected and we obtain for the speed

$$v(t) = \omega A_0 e^{-\delta t}\cos(\omega t + \varphi). \tag{12}$$

The graph of the speed is given in Figure 6. The Maple commands are with(plots); plot($36.5e^{-0.194t}\cos(18.25t + \dfrac{\pi}{4})$,t=0..10).
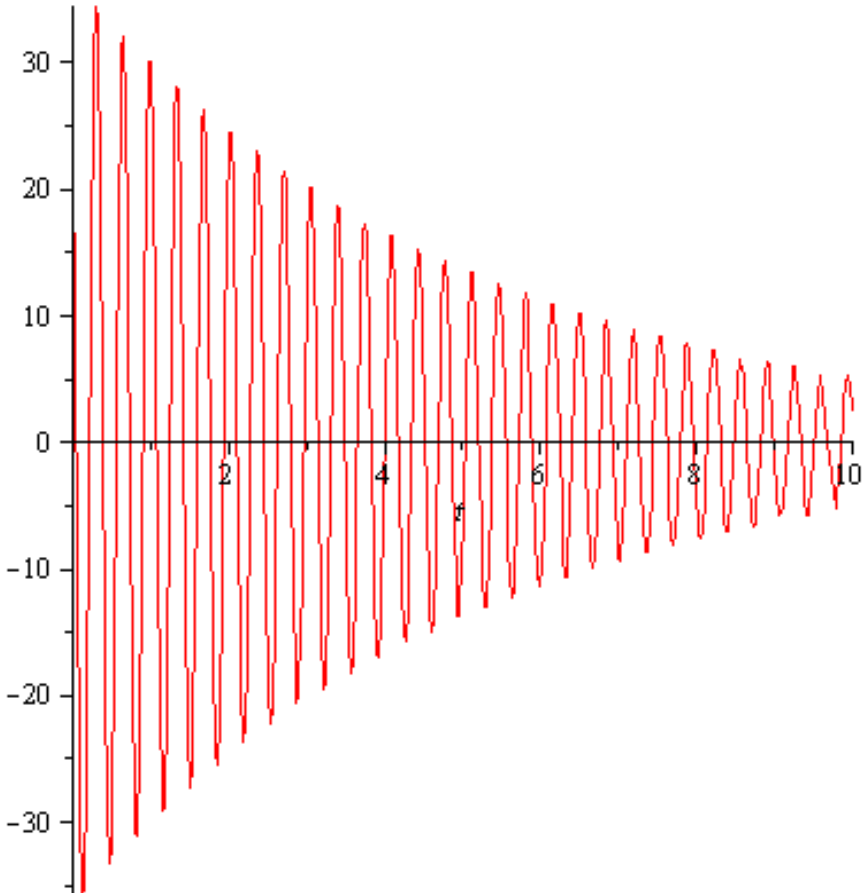

Figure 6. Speed of an underdamped oscillation

3. CONCLUSIONS

The Maple 17 provides new functions and packages presenting in this way many advantages. Very important are the facilities for calculus, plotting and animation. We present some examples for an important chapter of Physics the one of damped oscillations. In all oscillatory systems there is damping. As applications of damping we notice that all the vibrating systems are connected to damping because they are dissipative systems [18]. A small damping has a little influence on the natural frequencies, but the damping play an important role in limiting the amplitude of the oscillator at resonance. Structural engineering is based on damping, in earthquake areas or on structural components that are exposed to wind gusts. In the case of tall buildings that are placed in regions with seismic risk some damping systems are built in to help protect the buildings. For the cable-stayed bridges, in order to prevent the oscillations produced by wind with high speeds, hydraulic dampers have to be installed at the end of the cables.

We consider that working at Physics laboratories and solving problems with the aid of computer programs is a main part of the teaching-learning process and our students should understand the computational process. In this view, we point out that the students are more and more interested in the algebra computer systems for learning. Using Maple 17 the students will improve their abilities of working at a high-level at Physics laboratories and seminars. They can also take advantage of the computing programs and use the computers in campus for plotting and solve problems. As an immediate perspective, we want to introduce more applications of the Maple program and in this way to provide to the students the environment to work in the best conditions.

References

1. http://phet.colorado.edu, http://wildcat.phys.northwestern.edu
2. www.myphysicslab.com, http://virlab.virginia.edu
3. http://www.java.com/en
4. adobe.com/products/flash
5. Covatariu, G., Covatariu, D., *Development of Information Technology in Civil Engineering*, Acta Technica Napocensis: Civil Engineering & Architecture, Volume 51, Number 1, pp. 105 - 114, Proceedings of the International Conference Constructions 9-10 May 2008 Cluj-Napoca, ISSN 1221-5848, 2008.
6. Smith, P.R., Pollard, D*., The role of computer simulations in engineering education*, Computers & Education, Vol. 10, No. 3, pp. 335-340, July 1986.
7. Jones, A., Issroff, K., *Learning technologies: Affective and social issues in computer supported collaborative learning, Computers & Education*, Vol. 44, No. 4, pp. 395-408, 2005.
8. Andaloro, G., Donzelli, V., Sperandeo-Mineo, R.M., Modelling in Physics teaching: the role of computer simulation, *International Journal of Science Education*, Vol. 13, No. 3, pp. 243-254, 1991.
9. Wisman, R.F., Forinash, K., *Science in your pocket*, Proc. of the 5th International Conference on Hands-on Science Formal and Informal Science Education, HSCI 2008, Espaço Ciência, Olinda-Recife, Brasil, pp. 180-187, 2008.

10. Gould, H., Tobochnik, J., Christian, W., *An Introduction to Computer Simulations Methods: Applications to Physical Systems*, 3rd. ed., Addison-Wesley, 2007.

11. http://www.maplesoft.com/

12. www.wolfram.com

13. http://www.mathworks.com/products/matlab/index-b.html

14. Radinschi, I., Damoc, C., Cehan, A., Cehan, V., *Computer simulations of physics phenomena using Flash*, Proc. of the 5th International Conference on Hands-on Science Formal and Informal Science Education, HSCI 2008, Espaço Ciência, Olinda-Recife, Brasil, pp. 147-152, 2008.

15. Radinschi, I., Damoc, C., *Computer simulations for physics laboratory*, Proc. of the Sixth International Symposium „Computational Civil Engineering 2008", CCE 2008, pp. 441-447, 2008.

16. Radinschi, I., Frunza, M.D., Ciobanu, B., *Online virtual model for testing the knowledge*, Proc. of INTED 2007, Valencia, Spain, pp. 42-47, 2007.

17. Radinschi, I., Aignatoaie, B., *Efficiency of Using a Virtual Physics Laboratory*, Bulletin of the Polytechnic Institute of Iasi, Romania, LVI (LX), Fasc. 4, Section Mathematics. Theoretical Mechanics, Physics, pp. 141-146, 2010.

18. Stefan, D., *Dinamica structurilor şi inginerie seismică*, Editura Tehnică, Ştiinţifică şi Didactică, CERMI, Iaşi, ISBN 973-667- 018-x, 2003. (in Romanian)